

# **STRESS EVALUATION TECHNIQUE OF HELICAL SPRING WITH MODIFIED DESIGN PARAMETERS**

## **THESIS**

*submitted in fulfillment of the requirement of the degree of*

**DOCTOR OF PHILOSOPHY**

*to*

**J. C. BOSE UNIVERSITY OF SCIENCE & TECHNOLOGY, YMCA**

*by*

**SURESH KUMAR**

**YMCAUST/Ph37/2K12**

*Under the Supervision of*

**Dr. M.L Aggarwal, Professor (Supervisor)**

**Dr. Lakhwinder Singh, Professor (Co-Supervisor)**



**DEPARTMENT OF MECHANICAL ENGINEERING**

**FACULTY OF ENGINEERING & TECHNOLOGY**

**J C BOSE UNIVERSITY OF SCIENCE & TECHNOLOGY, YMCA**

**SECTOR-6, MATHURA ROAD, FARIDABAD, HARYANA, INDIA**

**September, 2021**

## DECLARATION

I hereby declare that this thesis report entitles “**STRESS EVALUATION TECHNIQUE OF HELICAL SPRING WITH MODIFIED DESIGN PARAMETERS**” by **SURESH KUMAR**, being submitted in fulfillment of the requirement for the Doctor of Philosophy in Mechanical Engineering (Design) of YMCA University of Science & Tech., Faridabad, during the period 2013- 2020, is a bonafide record of my original work carried out under guidance and supervision of **Dr. M.L. Aggarwal (Professor), Dr. Lakhwinder Singh (Professor), Department of Mechanical Engineering** and has not been presented elsewhere.

I further declare that the thesis work report does not contain any part of any work which has been submitted for the award of any degree either in this university or in any other university.

SURESH KUMAR

I.D. No.: YMCAUST/Ph37/2K12

## CERTIFICATE

This is to certify that this thesis report of entitled “**STRESS EVALUATION TECHNIQUE OF HELICAL SPRING WITH MODIFIED DESIGN PARAMETERS**” by **SURESH KUMAR** submitted in fulfillment of the requirement for the Doctor of Philosophy in **Mechanical Engineering** of YMCA University of Science & Technology Faridabad, during the period 2013- 2020, is a bonafide record of work carried out under my guidance and supervision.

I further declare that to the best of my knowledge, the thesis report does not contain any part of any work which has been submitted for the award of any degree either in this university or in any other university.

Dr. M.L. Aggarwal

Professor

Department of Mechanical Engineering

JCBUST YMCA Faridabad

Dr. Lakhwinder Singh

Professor

Department of Mechanical Engineering

JCBUST YMCA Faridabad

Dated: September, 2021

## ACKNOWLEDGEMENT

I would like to express my sincere gratitude firstly to my Supervisor **Dr. M.L Aggarwal** & Co-supervisor **Dr. lakhwinder Singh** for allowing me the opportunity to work in this area. Secondly to **Mr. Jagdish Sagar**, **Mr. Jaipal**, and **Mr. Inder Saini** for providing electronic equipment and functioning of them, it would never be possible for me to take this thesis report to this level without innovative ideas and relentless support and encouragement of mentioned personalities.

SURESH KUMAR

I.D. No.: YMCAUST/Ph37/2K12

## ABSTRACT

Last 10 years, developments of shape memory alloys (SMA's) based on new type of equipment/devices have taken place in pharmaceutical engineering, aerospace industry, biomedical industry, robotics field and other several fields of sciences & engineering. Shape memory alloy (SMA) actuators have drawn much attention and interest in recent decades due to their unique properties and are expected to be increasingly integrated commercially within several fields of science and engineering, pharmaceutical, aerospace, biomedical/medical, civil-structure, automotive, and robotics industry applications. The developments of NiTi-based shape memory alloys equipment/devices have taken place by researchers in many fields with helix-shaped springs. NiTi-based SMA's devices or equipment are depended on commonly terms 'displacement moves' or 'load capability done' by the actuator materials. The work presented the stress evaluation techniques represents a development of NiTi SMA's based equipment/device by utilizing forces/load capacities produced within their actuation at various preset conditions. This dissertation includes the development of NiTi-based mechanical model/equipment as a major application (Smart Fork-Lift; including physical-loaded helical springs preparation, design, simulation & fatigue life) and development of NiTi-based mechanical model/device as the minor application (A simple solenoid valve). This work also included the preparation of NiTi based intelligent SMA helical springs by the application of various fixture tools and clamping/holding devices and heat treatment processes. The basic actuation parameters and modified or exploring them for NiTi-based SMA helical springs by the development of a physical model for various working parameters (up to 20Kg) also done. This work considered the effect of slender-wires diameters, metallurgical & mechanical fatigue properties of NiTi wires. The methodology adopted by experimental set-up comprising following equipment have been utilized as muffle furnace, sensors and load-cells, thermocouple and electronic measuring instruments, DPM's based on operational amplifiers, soldering m/c and TIG welding m/c, workshops tools, basic electrical-electronic components, electronic scanning microscope for metallurgical properties. In the presented work, Ni-Ti SMA's helical springs, modified design of helical spring, and CAD Analysis: For its design, fatigue: 'Solid works' designer (Version-2017) are used.

# TABLE OF CONTENTS

Acknowledgement.....	IV
Abstract.....	V
List of tables.....	X
List of figures/graphs.....	XIII
List of abbreviations.....	XVIII
Chapter 1 Introduction.....	1
1.1 Background.....	1
1.2 Ni-Ti based SMA's.....	2
1.2.1 Manufacturing.....	3
1.2.2 Properties.....	4
1.3 Ni-Ti phase diagram.....	5
1.4 Mechanism of Ni-Ti.....	6
1.5 Ni-Ti SMA's based equipment/devices systems.....	8
1.6 Objectives and organization of proposed thesis.....	10
Chapter 2 Literature Review.....	12
2.1 Overview.....	12
2.2 Thin film (MEMS base) shapes of SMA's.....	13
2.3 Coil/helix shapes of SMA's.....	15
2.4 Gripping/holding shapes of SMA's.....	18
2.5 Shapes of SMA's as embedded/composite form.....	20
2.6 Cryofit (coupling/fascinating) shapes of SMA's.....	23
2.7 Design/fatigue of physically loaded spring.....	26
2.8 For metallurgical & true-fatigue properties.....	28
2.9 Research gaps.....	31
Chapter 3 Manufacturing and experimental set-up of SMA intelligent helical springs....	33
3.1 Introduction.....	33
3.2 Material description.....	34
3.3 Preparation of one-way smart intelligent SMA helical springs.....	35
3.3.1 Design statement.....	36
3.3.2 Preparation of 1.0mm NiTi-based SMA spring.....	38

3.3.3 Preparation of 0.5mm NiTi-based SMA Spring.....	40
3.3.4 Preparation of 0.2mm & 0.1mm NiTi-based SMA springs.....	42
3.4 Arrangement/set-up.....	44
3.5 Observations of basic parameters for various constant temperatures	
Conditions.....	47
3.6 Summary.....	52
Chapter 4 Estimation of various parameters of SMA intelligent helical springs.....	54
4.1 Introduction.....	54
4.1 Basic parameters.....	55
4.2 Results and discussion with basic parameters.....	55
4.3.1 Experimental results and discussion of 1.0mm SMA at	
530°C.....	56
4.3.2 Experimental results and discussion of 0.1mm SMA at	
550°C.....	57
4.3.3 Experimental results and discussion of 0.1mm SMA at	
330°C.....	60
4.3.4 Experimental results and discussion of 0.5mm SMA at	
430°C.....	60
4.4 Modeling of SMA's based helical springs on constant temperature	
Conditions.....	63
4.5 Summary.....	64
Chapter 5 Design of NiTi SMA for actuating helical spring.....	65
5.1 Introduction.....	65
5.2 Main components/parts.....	66
5.3 Material & manufacturing of SMA helical spring.....	73
5.4 Experimental setup and observation data.....	74
5.5 Results and discussion.....	76
5.8 Summary.....	81
Chapter 6 Load-carrying capacity of SMA springs.....	82
6.1 Introduction.....	82
6.2 Material description.....	83

6.3	Experimentation of 0.1mm and 0.2mm NiTi-based SMA's.....	84
6.4	Illustration with 0.5 SMA-based the solenoid valve.....	96
6.7	Summary.....	101
Chapter 7	Smart fork-lift actuator using NiTi one way helical spring.....	102
7.1	Introduction.....	102
7.2	Model preparation.....	103
7.3	Material & SMA helical spring.....	112
7.4	Experimental setup.....	113
7.5	Results and discussion.....	114
7.6	Summary.....	118
Chapter 8	Stability and stiffness analysis of helical springs.....	119
8.1	Introduction.....	119
8.2	Purpose.....	119
8.3	Material and specifications.....	120
8.4	Manufacturing of helical and conical shaped helical springs.....	121
8.5	Experimental setup and observation.....	124
8.6	Results and discussion.....	131
8.7	Summary.....	136
Chapter 9	Fatigue design of helical springs.....	137
9.1	Introduction.....	137
9.2	Design of helical springs of various positioning.....	138
9.3	Simulation of helical spring.....	141
9.4	Result and discussion.....	145
9.6	Summary.....	146
Chapter 10	Metallurgical & fatigue properties of SMA wires.....	147
10.1	Introduction.....	147
10.2	Metallurgical property.....	148
10.2.1.	Preparation of SMA's specimens.....	148
10.2.2	Polishing of specimens of SMA's.....	151
10.2.3	Etching Process.....	154
10.2.4	Microstructures of SMA's wires.....	156



10.3 Mechanical fatigue or true-fatigue.....	158
10.3.1 Preparation of specimens with slender SMA wires.....	159
10.3.2 Set-up for Specimens of Slender SMA wires.....	162
10.3.3 Results and discussion.....	163
10.4 Summary.....	165
Chapter 11 Conclusions and scope for future work.....	166
11.1 Results and discussion.....	166
11.2 Conclusions.....	176
11.3 Limitations and scope for future work.....	178
References.....	179
List of Publications out of thesis.....	194
Appendix A.....	196
Appendix B.....	197
Appendix C.....	198
Appendix D.....	199

## LIST OF TABLES

Table 2.1 NiTi based SMA's description.....	32
Table 3.1 Nitinol / Flexinol wires description.....	34
Table 3.2 Parameters obtained at 430°C for 0.5mm SMA (Compression to expansion).....	48
Table 3.3 Parameters obtained at 430°C for 0.5mm SMA (Expansion to compression).....	48
Table 3.4 Parameters obtained at 530°C for 1.0mm SMA (Compression to expansion).....	49
Table 3.5 Parameters obtained at 530°C for 1.0mm SMA (Expansion to compression).....	49
Table 3.6 Parameters obtained at 550°C for 0.1mm SMA (Expansion to compression).....	50
Table 3.7 Parameters obtained at 530°C for 1.0mm SMA (Compression to expansion).....	50
Table 4.1 SMA spring (1.0mm) in compression to expansion.....	55
Table 4.2 SMA spring (1.0mm) in expansion to compression.....	57
Table 4.3 SMA spring (0.1mm) in compression to expansion.....	58
Table 4.4 SMA spring (0.1mm) in expansion to compression.....	59
Table 4.5 SMA spring (0.5mm) in compression to expansion.....	61
Table 4.6 SMA spring (0.5mm) in expansion to compression.....	62
Table 4.7 Observations of 0.1mm, 0.5mm, 1.0mm and 0.1mm SMA's.....	64
Table 5.1 Load cell for 0-20 kg of pressure specifications as-received.....	68
Table 5.2 specifications as-received for Temperature Sensor (LM35).....	69
Table 5.3 Average scale value for 1.0mm NiTi SMA Spring.....	74
Table 5.4 Observation data for 1.0mm deformed SMA.....	75
Table 5.5 Minimum value to Maximum value of $W_t$ , $A_s$ .....	76
Table 5.6 Data considered for Average current & GF value.....	77
Table 5.7 Data considered for voltage and spring-load values.....	78
Table 5.8 Data considered for V & $W_t$ for minimum to median value.....	79

Table 5.9 Data considered for V & W <sub>t</sub> for maximum to median value.....	80
Table 6.1 Specification as-received for 0.1 mm, 0.2mm, and 0.5mm slender wires.....	83
Table 6.2 Average scale value for ‘One’ gram of wires.....	89
Table 6.3 Observation data obtained for 0.1mm SMA.....	91
Table 6.4 Observation data obtained for 0.2mm SMA.....	92
Table 6.5 Data considered for 0.1mm SMA.....	93
Table 6.6 Data considered for 0.2mm SMA.....	94
Table 6.7 Observation data for 0.5mm SMA-based.....	99
Table 7.1 Specification as-received for bearings.....	103
Table 7.2 Specification as-received for load cell.....	106
Table 7.3 Average scale value of 1gm for 0.040" NiTi-based SMA Spring.....	114
Table 7.4 Observation data for 0.040"/ 1.0mm NiTi SMA Spring.....	115
Table 8.1 Composition of spring steel ASTM A227 wire.....	120
Table 8.2 Average scale value i.e. ‘1’ reading of strain equal to ‘10.512gm’.....	125
Table 8.3 Parameters for stage first (cylindrical/conical).....	126
Table 8.4 Data obtained for stage first (conical shape helical spring).....	127
Table 8.5 Data obtained for stage first (cylindrical shape helical spring).....	128
Table 8.6 Parameters for stage second (cylindrical/ conical).....	129
Table 8.7 Data obtained for second stage (cylindrical shape helical spring).....	130
Table 8.8 Data obtained for second stage (conical shape helical spring).....	130
Table 8.9 Spring Rate (K <sub>c</sub> ) of conical spring for stage first.....	131
Table 8.10 Spring Rate (K <sub>c</sub> ) of helical spring for stage first.....	132
Table 8.11 Spring Rate (K <sub>c</sub> ) of conical spring for stage second.....	134
Table 8.12 Spring Rate (K <sub>c</sub> ) of helical spring for stage second.....	135
Table 9.1 Units for solid model.....	137
Table 9.2 Material Properties.....	142
Table 9.3 Mesh information.....	143
Table 9.4 Reaction forces.....	144
Table 9.5 Reaction Moments.....	144
Table 9.6 Loading Options.....	145
Table 10.1 Observation data for mechanical fatigue/ true-fatigue.....	163

Table 11.1 Data obtained for 0.1mm, 0.5mm, 1.0mm and 0.1mm SMA's.....	167
Table 11.2 Data obtained for 0.1mm SMA.....	169
Table 11.3 Data obtained for 0.2mm SMA.....	170
Table 11.4 Data obtained for 1.0mm SMA.....	171
Table 11.5 Obsevation data for conical shape helical spring.....	174
Table 11.6 Obsevation data for cylindrical shape helical spring.....	174
Table 11.7 Table 11.7 Observation data for fatigue results.....	176

## LIST OF FIGURES/GRAPHS

Figure 1.1 Timeline describing the history of the discovery after 1950 of numerous shape memory alloy systems.....	2
Figure 1.2 Phase diagram of Ni-Ti alloy system.....	6
Figure 1.3 One way memory Effect.....	7
Figure 1.4 Chapter wise organization of proposed thesis.....	11
Figure 2.1 Classification of literature review.....	12
Figure 3.1 Figure 3.1 Muffle Furnace with a) digital infrared sensor b) handle tong .....	35
Figure 3.2 Preparation arrangement of 1.0mm SMA involves a) threaded screw and MS hollow part b) end restraints (Cu) and MS fixture c) sample before HT processes d) final SMA spring (1.0mm).....	39
Figure 3.3 Preparation arrangement of 0.5mm SMA involves a) fixture-cum-spring tool b) clamping wire (soften mild steel) c) hollow straight holder d) final SMA spring (0.5mm).....	41
Figure 3.4 Preparation arrangement of 0.2mm and 0.1mm SMA's involves a) fixture-cum-spring tool (pre-final) b) Final SMA's springs of 0.1mm and 0.2mm.....	42
Figure 3.5 Experimental Set-up (separated form) to observing the basic parameters of deformed SMA's.....	45
Figure 3.6 Experimental Setup (combined form) to observing the basic parameters of deformed SMA's.....	46
Figure 3.7 Constant temperatures conditions of various NiTi based includes a) 0.1mm SMA at 550°C and 0.1mm SMA at 330°C b) 0.5mm SMA at 430°C c) 1.0mm SMA at 530°C.....	47
Figure 3.8 Experimental Setup for physical-loading springs.....	51
Figure 3.9 Spring Load Stiffness Tester.....	52
Figure 4.1 Temperature and length of 1.0mm SMA in compression to expansion.....	56
Figure 4.2 Temperature and length of 1.0mm SMA in expansion to compression.....	57
Figure 4.3 Temperature and length of 0.1mm SMA in compression to expansion.....	58
Figure 4.4 Temperature and length of 0.1mm SMA in expansion to compression.....	59

Figure 4.5 Temperature and length of 0.5mm SMA in compression to expansion.....	61
Figure 4.6 Temperature and length of 0.5mm SMA in expansion to compression.....	63
Figure 5.1 Iron Stand a) captured photo b) base plate and vertical column c) adjustable lower plate with locking.....	66
Figure 5.2 Load Cell (0 to 20 Kg).....	68
Figure 5.3 Temperature Sensor (LM35).....	69
Figure 5.4 Amplifier circuit (Operational type).....	70
Figure 5.5 IC 7107.....	70
Figure 5.6 DC supply with CV and CC display.....	72
Figure 5.7 Setup with deformed 0.1mm NiTi testing approach.....	74
Figure 5.8 Minimum values to maximum value of $W_t$ , $A_s$ .....	76
Figure 5.9 Variation of GF values V/s Average currents.....	78
Figure 5.10 Variation of $L_s$ w.r.t applied voltage.....	79
Figure 5.11 Variation of $W_t$ for minimum to median value.....	80
Figure 5.12 Variation of $W_t$ for maximum to median value.....	81
Figure 6.1 Mild steel round bar.....	84
Figure 6.2 Electric cutter with buffing wheel and cutter.....	85
Figure 6.3 Drill-Machine (230V/2200rpm).....	85
Figure 6.4 Threading Tool.....	86
Figure 6.5 Spring-tools making involves a) long threaded part b) TP of various sizes c) drill bits of 0.8, 0.9, 1.0, 1.5mm d) fixture-cum-spring tool (pre-final) e) specimens before HT processes.....	87
Figure 6.6 Preparation of one way helical SMA springs includes a) combined final SMA springs b) 0.008” / 0.2mm SMA spring c) 0.004” / 0.1mm SMA spring.....	87
Figure 6.7 SMA (0.1mm) testing approach.....	89
Figure 6.8 SMA (0.2mm) testing approach.....	90
Figure 6.9 Variations of $I_A$ & $V$ , $I_A$ , & $L_s$ for 0.1mm SMA.....	93
Figure 6.10 Variations of $I_A$ & $V$ , $I_A$ & $L_s$ for 0.2mm SMA.....	95
Figure 6.11 Acrylic box (sketched by AutoCAD 2017).....	96
Figure 6.12: Sliding part.....	97
Figure 6.13 Final SMA Spring (showing (a) Muffle furnace (b) fixture holder).....	98

Figure 6.14 A simple solenoid valve 0.5mm SMA-based.....	99
Figure 6.15 Variations of V, Ia and Tav <sub>g</sub> .....	100
Figure 6.16 Variations of Ia & V, Tav <sub>g</sub> and Ia for 0.5mm SMA.....	101
Figure 7.1 Alloy steel 4-bearings.....	103
Figure 7.2 Stainless steel round rods.....	104
Figure 7.3 Channels (Fe / Al based).....	104
Figure 7.4 Compression-springs of spring steel.....	105
Figure 7.5 Load cell (0 to 3Kg).....	106
Figure 7.6: Temperature sensor LM35 (with small Al-plate).....	107
Figure 7.7 Transparent acrylic box (for loading).....	107
Figure 7.8 Power supply circuit.....	108
Figure 7.9 Operational amplifier circuit with digital panel meter.....	109
Figure 7.10 Pulley and supports.....	109
Figure 7.11 Socket terminal connectors.....	110
Figure 7.12 Final 0.040" NiTi-based SMA helical spring.....	112
Figure 7.13 Smart fork-lift setup included a) deformed 9.8cm SMA b) SMA testing approach c) fork-lift testing model / equipment.....	113
Figure 7.14 Core-constraints of smart fork-lift.....	116
Figure 7.15 Load lifted V/s Voltage applied.....	117
Figure 7.16 Load lifted V/s working SMA Temperature.....	117
Figure 8.1 Tempering of wire.....	121
Figure 8.2 Fixture- cum-spring-tools.....	121
Figure 8.3 Wrapping Steel Wire.....	122
Figure 8.4 Muffle Furnace operating at 860 deg C.....	122
Figure 8.5 Oil-dip tool-fixtures with springs (after quenching).....	123
Figure 8.6 Separation of spring included a) clamping wires b) cylindrical shape helical spring c) conical shape helical spring.....	123
Figure 8.7 Pre-final and final specimens a) for acrylic base and b) for 'four' supports c) For initial specimens d) for final specimens.....	124
Figure 8.8 ADC based amplifier circuit and smart fork-lift loading box.....	125
Figure 8.9 specimens for first stage.....	126

Figure 8.10 Final specimens for second stage observations.....	129
Figure 8.11 Vertical scale reading or Deflection V/s load variation for conical spring (Stage first).....	132
Figure 8.12 Vertical scale reading or Deflection V/s load variation for helical spring (Stage first).....	133
Figure 8.13 Spring Load V/s Vertical scale for conical spring (stage second).....	134
Figure 8.14 Vertical scale reading or Deflection V/s load variation for helical spring (Stage second).....	135
Figure 8.15 Combined spring rate variation for a) stage first b) stage second.....	136
Figure 9.1 Single helical a) Single spring-steel b) Single alloy-steel.....	139
Figure 9.2 Dual helical a) Alloy-steel springs b) Spring-steel springs.....	139
Figure 9.3 Triple helical a) Spring-steel springs b) Alloy-steel springs.....	140
Figure 9.4: Model Information.....	141
Figure 9.5 Loads and fixtures.....	142
Figure 9.6 Contact-information.....	143
Figure 9.7 Simulation result.....	144
Figure 9.8 Material properties with model reference.....	145
Figure 9.9 Study results (First and Second).....	146
Figure 10.1 Two steel pieces a) AutoCAD Drawing's b) Actual images.....	148
Figure 10.2 a) SMA's specimen before implementing as an actuators/drawn conditioned b) SMA's specimen after implementing as an actuators/smart intelligent springs c) Final specimens with SMA's wire pieces d) Separated final SMA's specimens.....	151
Figure 10.3 Work-pieces after Hand Files (fine & coarse).....	151
Figure 10.4 a) After emery paper up to '100-180' grit size b) After emery paper up to '180-280' grit size.....	152
Figure 10.5 a) distilled water (95ml) b) nitric acid (2.5ml) c) hydrochloric acid (1.5ml) d) hydrofluoric acid (1.0ml).....	154
Figure 10.6 NiTi-based SMA's specimens (After Etching reagent).....	155



Figure 10.7 Arrangement / Set-up for Specimens of SMA's wires (showing scanning electron microscope).....	156
Figure 10.8 a) 0.2mm wire (B/200X) b) 0.2mm wire (A/200X) c) 0.5mm wire (B/200X) d) 0.5mm wire (A/200X).....	157
Figure 10.9 Center Lathe (Horizontal bed type).....	159
Figure 10.10 Buffering wheel (wire based).....	160
Figure 10.11 a) Mild steel piece with axis face hole (2.00mm) b) Mild steel piece with turning side hole (3.4mm, Tap size i.e. M4x0.75) c) Final SMA-based specimens with 0.1mm NiTi wire d) Final SMA-based specimens with 0.2mm NiTi wire.....	161
Figure 10.12 Arrangement /Set-up for Specimens of Slender SMA wires (showing fatigue testing machine and specimen testing approach).....	162
Figure 10.13 Eccentric-load and No. of Cycles with 'D'.....	164
Figure 10.14 Eccentric-load V/s No. of Cycles.....	164
Figure 11.1 Combined average currents ( $I_A$ ) variations with applied voltage (V).....	172
Figure 11.2 Fatigue results.....	173
Figure 11.3 i) 0.2mm wire (B/200X) ii) 0.2mm wire (A/200X) iii) 0.5mm wire (B/200X) iv) 0.5mm wire (A/200X).....	175

## **LIST OF ABBREVIATIONS**

SMA's - Shape memory alloys  
SME - Shape memory effect  
MEMS - Micro-electro-mechanical system  
PSM - Personnel status monitor system  
USNOL - United States naval ordnance laboratory  
VIM - Vacuum induction melting  
VAR - Vacuum arc remelting  
OWSME - One-way shape memory alloy  
TWSME - Two-way shape memory alloy  
TTT - Time-temperature-transformation  
TME - Temperature memory effect  
TFN - Thin film nitinol  
STFN - Superhydrophilic thin film Nitinol  
DSC - Digital scanning correlation  
IR - Infrared  
VSC - Variable structure control  
FEA - Finite element analysis  
UTM - universal testing machine  
AF – Ausforming  
DC - Direct current  
M/c – Machine  
Atm – Atmospheric  
Avg/Temp – Average/Temperature  
CAD - Computer aided design  
GF - Gauge factor  
SF - Strain Factor  
RTD's - Resistance temperature detectors  
T/C - Thermocouple  
ICs - Integrated circuits  
DPM - Digital panel meter

GND - Grounded  
ADC - Analogue to digital converter  
CV - Current voltage  
PID - Proportional integral derivative  
K<sub>c</sub> - Conical spring rate  
K<sub>h</sub> - Helical spring rate  
GFRP - Glass fiber reinforced plastic  
NBG - Nano bioactive glass  
TEM - Transmission electron microscopy  
LSSA - Load shifting SMA actuator  
LCF - Low cycle fatigue digital image correlation  
SEM - Scanning electron microscope  
DIC - Digital image correlation  
UTFN - Untreated thin film nitinol  
FEM - Finite element method  
CC – Current  
BJT - Bipolar junction transistor  
MOSFET - Metal oxide silicon field effect transistor  
HT - Heat transducer  
T<sub>A</sub> - Average temperature  
DPM's - Digital panel meters  
I<sub>A</sub> - Average current  
PMMA - Poly-methyl-methacrylate  
L<sub>S</sub> - Spring load  
TIG - Tungsten inert gas  
L<sub>f</sub> - Free Length  
NEMS - Nano-electro-mechanical system  
T<sub>avg</sub> - Average temperature  
CF - Coarse to fine finish  
MF - Medium to fine finish  
FM - Fine to micro finish

# CHAPTER 1

## INTRODUCTION

### 1.1 BACKGROUND

In the last 10 years, shape memory alloys (SMAs) have been implemented in several high-performance applications requiring high work densities, large recoverable deformations, high stresses, and good biocompatibility. The shape memory effect was first noticed in 1932 by Olander in gold-cadmium samples and in 1938 by Greninger and Mooradian in their study of brass alloys/copper-zinc. In 1951, Chang and Read observed the shape recovery effect during an experimental study. Both were also working on gold-cadmium alloys material. William J. Buehler and his team at the Naval Ordnance Laboratory established the shape memory effect in nickel-titanium alloy in 1962. It was named NiTiNOL by nickel-titanium Naval Ordnance Laboratory [1-3, 8, 14].

Smart materials, devices, and structures /systems are familiar staples to the scientific community, researchers, and industry, and in other commercial sectors; however, they are considered futuristic or even magical by most of the medical community, and in particular by the busy practicing surgeon micro-electromechanical system (MEMS), personnel status monitor system (PSM) [37]. Yet, only two systems have been provided substantial commercial attention as copper-based systems and Nickel-Titanium systems. The SMA's deformation recovery-related in shape memory effect, pseudoelastic/super-elastic notion of behavior may be in tension, compression, torsion, or flexion and is well beyond the elastic limit in a non-linear manner. The remembering and restoring the original shape, alloys perform the mechanical work against the environment, this ability to self-act has reputational advantage smart material or metallic compound or metal of magic has distinguished them from all conventional metal alloys [17]. When the shape memory alloy is heated /cooled, it goes through solid-solid transformations. In the austenite/martensite phases, the memory metal "remembers" the shape it had before it was deformed /conditioned. Shape memory alloys (SMAs) are a unique type of smart materials that can be deformed at low temperature/martensite phase and regains to its original undeformed configuration when heated to a higher temperature phase/austenite phase also known as an inter-metallic compound [113].

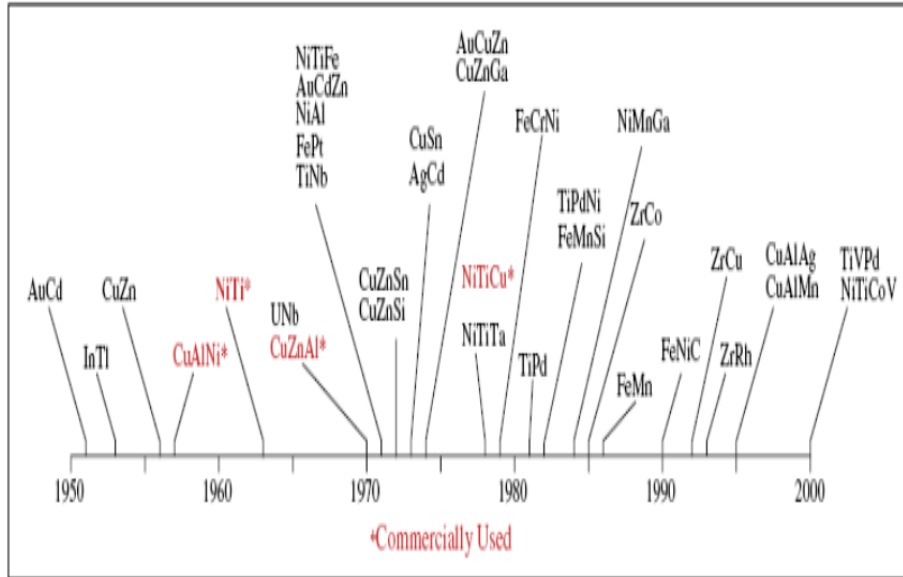


Figure 1.1 Timeline describing the history of the discovery after 1950 of numerous shape memory alloy systems (from Nicole Latrice [7])

Figure 1.1 shows a timeline describing the history of SMA's. Three types of SMA are currently popular CuZnAl, CuAlNi, and NiTi among the various SMA's as Ag-Cd, AuCd, FeMn Cu-Zn-Si, Cu-Zn-Sn, Au-Cu-Zn, Ti-Nb, Ln-Ti, Cu-Zn, Ni-Al, Cu-Zn-Ga, Cu-Sn, Ti-Pd-Ni, U-Nb, Fe-Pt, and Fe-Mn-Si due to commercially availability [15].

## 1.2 Ni-Ti BASED SMA'S

Today Ni-Ti is the most common commercially available shape memory alloy and for good reason. The maximum strain that can be obtained from this kind of alloy reaches 8%. This is a high number under SMA standards since most of the alloys only achieve between 2 to 4% strain [79]. Its biocompatibility makes them attractive for vast applications. NiTi-based shape memory alloys are a unique class of metallic materials that exhibit the shape memory effect i.e. previously deformed, usually at a low temperature or room temperature, and are capable of returning to their original/parent shape or form when exposed to the appropriate thermal or stress procedure. The nickel-titanium alloys (SMA) were first developed in 1962 by the United States naval ordnance laboratory (USNOL) and commercialized under the trade name as 'Nitinol'. Their remarkable properties were discovered by accident. A sample that was bent out of shape many times was presented at a laboratory management meeting by associate technical directors.

The NiTi system is often preferred due to its large shape memory strain, environment-friendly, thermal stability, excellent corrosion resistance, high biocompatibility, high ductility, considerable work per unit mass, and attractive transformation temperature. The commercial Ni-Ti shape memory physical properties such as corrosion resistance, density, electrical-resistivity, specific heat, thermal-conductivity, thermal-expansion coefficient, young's modulus, yield strength, etc. are shown in 'Appendix B' with symbols, units, and values of martensite/austenite. Applications for Nitinol as free recovery, constrained recovery, superelasticity/psyudoelasticity, work production, etc. The one-way shape memory effect is the result of a phase transition. The phase transition occurs during a hearing process at a certain temperature [7].

### **1.2.1 Manufacturing**

Ni-Ti alloys are exceedingly difficult to make, due to the exceptionally tight compositional control required and the tremendous reactivity of titanium. These are specialized techniques used to keep impurities in the alloy to a minimum and ensure the metals are well mixed. The ingot is then hot rolled into longer sections and then drawn to turn it into wire. Every atom of titanium that combines with oxygen or carbon is an atom that is robbed from the NiTi lattice, thus shifting the composition and making the transformation temperature that much lower. Manufacturing of these alloys is typically made by casting; two major casting methods of melting are commonly used i.e. VIM / VAR. The manufacturing of Ni-Ti alloy or Nitinol by either method is similar and they both provide suitable material as per requirement [3].

**Vacuum Induction Melting (VIM):** This is done by striking an electrical arc between the raw material and a water-cooled copper strike plate. Melting is done in a high vacuum, and the mold itself is water-cooled copper. VIM involves melting in a graphite crucible under vacuum or an inert gas atmosphere for the simultaneous melting of all raw materials, NiTi melts dissolve carbon, and TiC particles form during solidification [1].

**Vacuum Arc Remelting (VAR):** This method is classified into two types with regard to the heating system. The first type uses a non-consumable electrode and the second is a consumable electrode consisting of materials to be melted. The first method is preferred in laboratories because it is applicable to many kinds of alloys.

VAR is done by using alternating magnetic fields to heat the raw materials in a crucible usually carbon. It is also done in a high vacuum. Both methods have specific advantages, one research reported about VIM that to leading to higher fatigue resistance. Other research reported about VAR that to an improved fatigue behavior. Other methods are also used on a boutique scale, including plasma arc melting, e-beam melting, induction skull melting, etc. [3].

### **1.2.2 Properties**

Ni-Ti or Nitinol alloys exhibit various closely related and unique properties such as SME or constrained recovery, work production, and superelasticity/pseudoelasticity [7]. Phase transformation temperatures of NiTi material form hysteresis curve in which constrained recovery and pseudoelasticity are very much related unique properties in which solid-solid two faces transformations i.e. martensite soft face and austenite hard phase. Unique properties or characteristics discussed as: -

**Shape memory effect (SME):** It is a phenomenon, in which a material recovers to its original size and shape when heated above a certain characteristic transformation temperature i.e. to remember or memorize its pre-deformed shape when heated/cooled. A shape-memory alloy is also called memory metal, memory alloy, smart metal, smart alloy, or muscle wire due to this special property. In one-way shape memory alloy (OWSMA): retains a deformed state after the removal of an external force, and then recovers to its original shape upon heating only (one direction). For OWSMA;  $A_s$  is found by the alloy type, composition, the loading conditions, and variable temperature between  $-50^{\circ}\text{C}$ , and  $150^{\circ}\text{C}$  [75].

**Two-way shape memory effect:** Two-way shape memory effect, the material remembers two different shapes at different and shape-memory effect is seen in both cases, i.e., heating and cooling. The material behaves so differently in different situation is that a shape memory can "learn" to act in a various way [80].

**Work production:** Here the alloy is allowed to recover, but to do so it must act against a force (thus doing work). Thermal efficiency is defined as the ratio of total amount of mechanical work done ( $W$ ) to shape memory alloy related to change of strain due to the temperature differences [3].

### 1.3 Ni-Ti PHASE DIAGRAM

The phase diagram is important for heat-treatments of the alloys and improvement of material properties. The thermo-mechanical properties such as shape memory effect (SME)/pseudoelasticity of the near equi-atomic composition of Ni and Ti are muscally dependent on stoichiometry and thermal/mechanical treatments [91]. At elevated temperatures, NiTi or Nitinol assumes an interpenetrating simple cubic structure referred to as austenite (Parent phase with the elastic modulus (75-83GPa) and yield strength: 195-690 MPa). At low temperatures, NiTi spontaneously transforms to a more complicated monoclinic crystal structure as martensite (daughter phase) and variation of 0.1 atomic% in the Ni content is shown to shift the transformation temperature up to 10<sup>0</sup>C [1, 7]. Impurities such as nitrogen and carbon should also be avoided since the transformation temperatures, hysteresis loop, impact loading, strength, and ductility of the material are very sensitive to these impurities. This diagram illustrates the Ni-Ti binary equilibrium phase diagram according to which thermodynamically exist in the proximity of equiatomic percentages of Ni / Ti stable phase. For shape memory properties, the research interests are focused on the central region bounded by the NiTi<sub>2</sub> and Ni<sub>3</sub>Ti phases. In the middle, there is the NiTi phase, which is associated with the shape memory effect. The boundary of the NiTi phase region is almost vertical on the Ti-rich side, but there is some solubility on the Ni-rich side at high temperatures.

Figure 1.2 shows the phase diagram of Ni-Ti alloy system in which phase transformation of Ti-50.8% Ni wire shows the Ni-Ti phase region becomes very narrow at temperatures below 650<sup>0</sup>C. To achieve the balance between the driving force and diffusion rate required for phase transformation, for all curves with different temperatures ( $A_f$ ), the maximum precipitation rate occurs at about 400-500<sup>0</sup>C, which is the best temperature for aging [6]. On the other hand, the higher  $A_f$  temperature, the wider the area of temperature hysteresis between austenite and martensite phases. Based on this fact, it is possible to obtain totally martensite microstructure in samples with high  $A_f$  temperatures easier and in lower cooling rates. Nevertheless, above 500 <sup>0</sup>C, a higher diffusion rate takes place and therefore the time required for transformation to be finished decreases may verify in the conventional time-temperature-transformation (TTT) diagram for NiTi wire with initial  $A_f = 11^0\text{C}$  [Appendix 'C'].



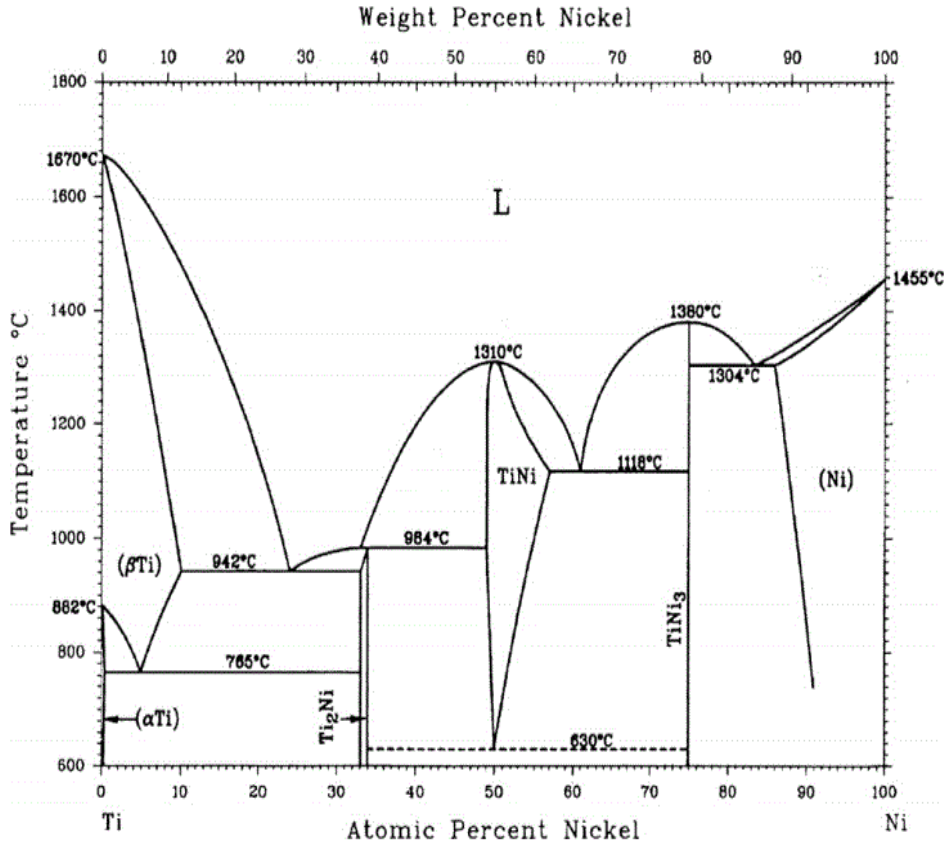


Figure 1.2 Phase diagram of Ni-Ti alloy system

(From Mohammad H. Elahinia [1] )

The heat treatments are applied (as per required properties) on SMA's as annealing, normalizing, and solution treatment, etc. The aging can have significant effects on types of microstructural phases in the final products and also on thermo-mechanical properties (i.e. shape memory effect/super-elasticity) of NiTi -based devices/equipment.

#### 1.4 MECHANISM OF Ni-Ti (ACTUATOR-ROOT)

Nitinol's extraordinary properties are derived from a reversible solid-state phase transformation as a martensitic transformation between two-crystal phases required 10,000-20,000 psi or 69MPa -138MPa of mechanical stress [6]. The mechanism of the Ni-Ti as the austenite phase (high-temperature region/very hard) starts to transform to martensite at Ms (starting temperature) during cooling. At low temperatures, Nitinol spontaneously transforms to a more complicated monoclinic crystal structure known as martensite. Since this (low-temperature region/soft) phase has lower symmetry than the austenite phase, martensites with the same structure but in different crystallographic orientations/variants of martensite can be formed.

The  $M_s$ ,  $M_f$  is the temperatures at which the transition to  $M_s$  (starting temperature) completes and accordingly, during heating  $A_s$  and  $A_f$  are the temperatures at which the transformation from martensite to austenite starts and finishes [6]. At high temperatures, nitinol assumes an interpenetrating simple cubic structure referred to as austenite. So, there are four transition temperatures associated with the austenite-to-martensite and martensite-to-austenite transformations. For the point of NiTi, cubic to monoclinic (B2 to B19') transformation alloy as many as 12 correspondence variants can be formed. NiTi formation of  $M_s$  (starting temperature) in the parent phase will cause a large strain up to 8% [79]. The combination of two or four variants may form in tandem to reduce strain i.e. self-accommodation. When stress is functional twins introduced upon martensitic transformation can act as a deformation mode of NiTi, as the twin boundary in Ni-Ti is movable. This process is called de-twinning i.e. a favorably oriented variant grows at the expense of other less favorable ones. The deformation remains after the stress/load is released which is applied at low temperature. In heating, the  $M_s$  (starting temperature) variants revert to their parent orientations in the austenite phase so that the original shape is restored.

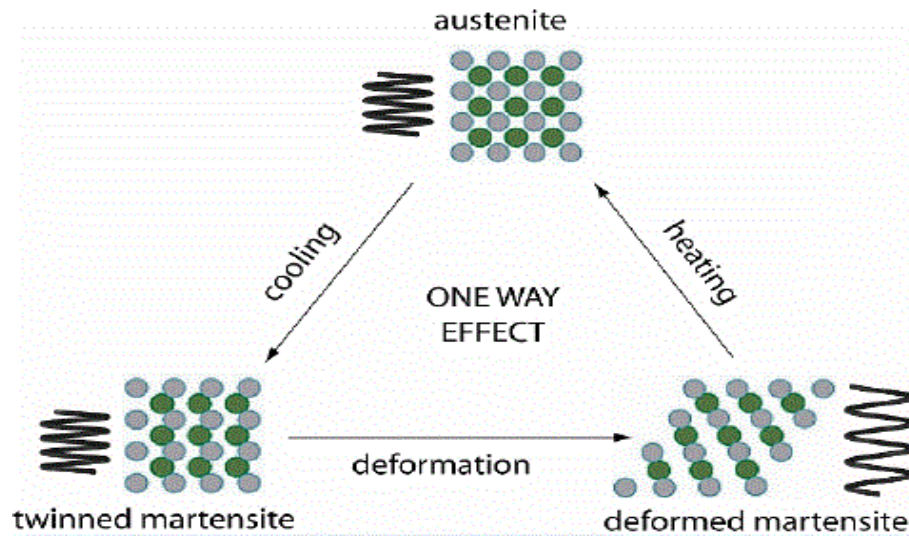


Figure 1.3 One-way memory effects

(Figure taken from <https://shape memory alloy/NiTi/images>)

In Figure 1.3; the NiTi-based shape memory alloy ordinarily the shape memory effect is one-way as only the shape of the austenite phase is memorized represented 2-D view of Nitinol's crystalline structure during cooling/heating cycle.

Thermal hysteresis of Ni-Ti phase transformation (cooling/heating cycle shows thermal hysteresis) in which properties are two key aspects of this transformation. The transformation is "reversible", meaning that heating above the transformation temperature will return the crystal structure to the simpler austenite phase. The other point is that the transformation in both directions is instantaneous as per requirement or conditioned applied. Thus the name "shape memory" refers to the fact that the shape of the high-temperature austenite phase is "remembered," even though the alloy is severely deformed at a lower temperature [80]. (This One-way phenomenon is used as an actuator for Ni-Ti shape memory alloy which is further applied for the development of a smart equipment/device as an actuator-root, or basis of the actuator)

### **1.5 Ni-Ti SMA'S BASED EQUIPMENT/DEVICES/SYSTEMS**

In the last 10 years, developments of shape memory alloys (SMA's) based new equipment/devices have taken place in several fields of science and engineering, pharmaceutical engineering, aerospace industry, biomedical industry/medical industry, civil-structure industry, automotive industry, and robotics industry, etc [7, 10, 13, 56 72, 73, 77]. SMA's based devices/equipment are depended on commonly terms 'displacement moves' or 'load capability done' by the actuating materials. The stress evaluation techniques represent a development of SMA's based equipment by utilizing forces/load capacities/displacement moves produced within the materials during their actuation. Due to these forces or load capacities in SMA's recovery, the predefined shape i.e displacement moves. These 'forces' either defined the displacement or load capability as per the applicability of SMA's. In fact, 'displacement moves' represents the change of parameter i.e. length and 'forces' represents the actuation load capacities of shape memory alloys [74, 91]. This stress evaluation is also called the shape memory effect (SME). The shape memory effect has been found in many alloys, but NiTi is the most common ones employed due to its features as high corrosion resistance, high ductility, high recoverable deformation, high biocompatibility, etc [75]. The model example of NiTi based: G. Machado (2014), presented new properties of nickel-titanium SMA for engineering applications [39]. Similarly, nonlinear hysteresis identification and compensation based on the discrete Preisach model of an aircraft morphing wing device by a NiTi based SMA actuator represented by Yuchen Chen (2018).

The conception of aircraft morphing wings thrives in aeronautics since the appearance of shape memory alloys (SMAs), it is manipulated by NiTi-based SMA actuator [81].

The stress evaluation techniques or development of SMA's based on types of equipment, mainly focus on designs or shapes of SMA's. The various shapes of NiTi SMA's as thin film (MEMS-based), gripping/holding, embedded/composite, coiled/helix shapes, and cryofit (for coupling & fasteners), etc. are used by researchers as per requirements or applications for the developments of equipment in the different field; includes such as aerospace, pharmaceutical, medical, robotics, aerospace, and biomedical, etc[20, 75]. The design or shape of NiTi SMA's depend upon the types of fixtures applied, types of clamping devices used types of the heat treatment process (fixed-temperature based) applied as annealing, normalizing, and various pre-defined parameters (for drawn condition depending on the alloying or the loading condition) [79]. The designs or shapes of NiTi-based SMA's (represents helix form as a spring) for the developing instruments/equipment are limited. The basic actuation parameters on which the shapes are dependent as actuation temperatures, actuating currents & voltages, elongation (length in compression and expansion), working loads, and atmospheric working temperatures [91]. The various researches worked with these parameters for its shapes or designs but little bit used modified parameters for the same shape. The modified actuation parameters introduced by changing the types of fixtures applied, types of clamping devices used, and types of heat treatment process used (fixed temperature-based), resulted as different actuation-temperature, different actuating currents & voltages, different working-loads and different atmospheric working temperatures for the same NiTi SMA's. The experimental results will provide helical SMA actuator designers a better understanding of how each parameter affects the actuator's resultant reaction times and strokes. Involved increases or decreases in shear stress; i.e., the wire diameter, spring diameter, and bias force investigations; a common theme of stroke convergence was observed [5, 18].

The Nitinol/flexinol alloy (one-way) is utilized for producing smart actuator equipment from non-conventional materials because of their interesting mechanical properties.

The NiTi-based shape memory alloy is initially shaped or designed into helix form mainly helical spring (cylindrical/conical), then calculates the various working parameters in equipment/instrument.

Further, the present work discussed separately the Metallurgical properties of NiTi SMA's (before/after heat treatments) and design, fatigue life for physical-loaded helix springs which applied at various stages. Helical springs find wide applications in mechanical engineering equipment, in the present work; modified design of helical spring and shape memory alloy (SMA) helical springs are used.

## **1.6 OBJECTIVES AND ORGANIZATION OF PROPOSED THESIS**

### **1.6.1 Research objectives**

The research on NiTi-Based shape memory alloys actuator-model as mechanical equipment/device was initiated over the last decade when various shapes such as thin-film shapes (MEMS-based), gripping/holding shapes, embedded/composite shapes, coiled/helix shapes, and cryofit shapes (for coupling & fasteners), etc. These shapes are rapidly developed and started to be widely used in many engineering applications of technology engineering, pharmaceutical engineering, aerospace industry, biomedical industry / medical industry, civil-structure industry, automotive industry, and robotics industry, etc [7, 10, 13, 56 72, 73, 77]. Researchers are also exploring actuator-model / techniques for NiTi-based preferred helix shapes mainly. The objective of the current work is to gain some insights into those issues. By carrying out this research with a number of benefits like: -

- ✓ To find basic actuation parameters in an organized manner
- ✓ Estimation of basic parameters
- ✓ Model applicability to check actuation parameters
- ✓ To find the 'load capability'
- ✓ Check the 'stability and stiffness'
- ✓ Actuator applicability as a mechanical equipment/device
- ✓ Software applicability as fatigue design
- ✓ To check metallurgical properties
- ✓ To find true-fatigue properties

**The methodology adopted for achieving the objectives**, experimental set-up comprising following equipment have been utilized as muffle furnace, sensors and load-cells, thermocouple and electronic measuring instruments, digital panel meters based on operational amplifiers, soldering m/c and TIG welding M/c, workshops tools, basic electrical-electronic components, electronic-scanning-microscope for metallurgical properties and CAD analysis for its design and fatigue design using ‘Solid works’ designer Version-2017.

### 1.6.2 Organization of the proposed thesis

The current work has been planned in 11 chapters. The chapter-wise organization of the research work has been epitomized in Figure 1.4 as mentioned below:

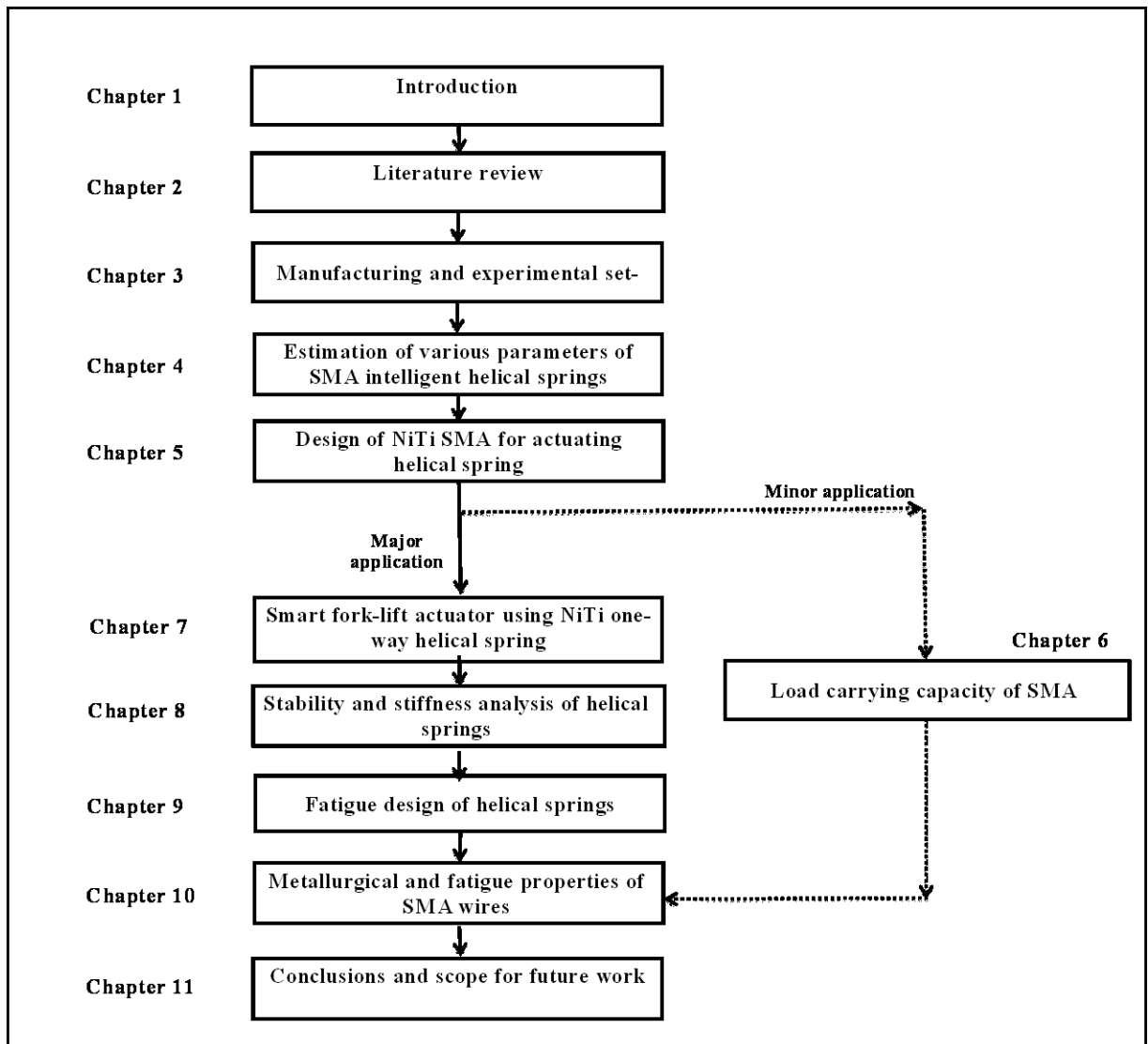


Figure 1.4 Chapter wise organization of a proposed thesis

# CHAPTER 2

## LITERATURE REVIEW

### 2.1 OVERVIEW

The nature of shape memory alloys-based actuator model development as mechanical equipment/ device requires a researcher to have a vast understanding of the subject. The role of this review is to provide the user with a commonly accepted environment about the SMA's & developments of shape memory alloys (SMA's) based equipment/devices that relate to various shapes such as thin-film shapes (MEMS-based), gripping/holding shapes, embedded/composite shapes, coiled/helix shapes, and cryofit shapes (for coupling & fasteners) of SMA's. A review of current actuator-based equipment/devices is similar to the one proposed. Particular areas of interest for literature search were grouped into different categories related to the shape, design, development, simulation, fatigue, and application of shape memory alloys (SMA's) based equipment/devices as shown in Figure 2.1.

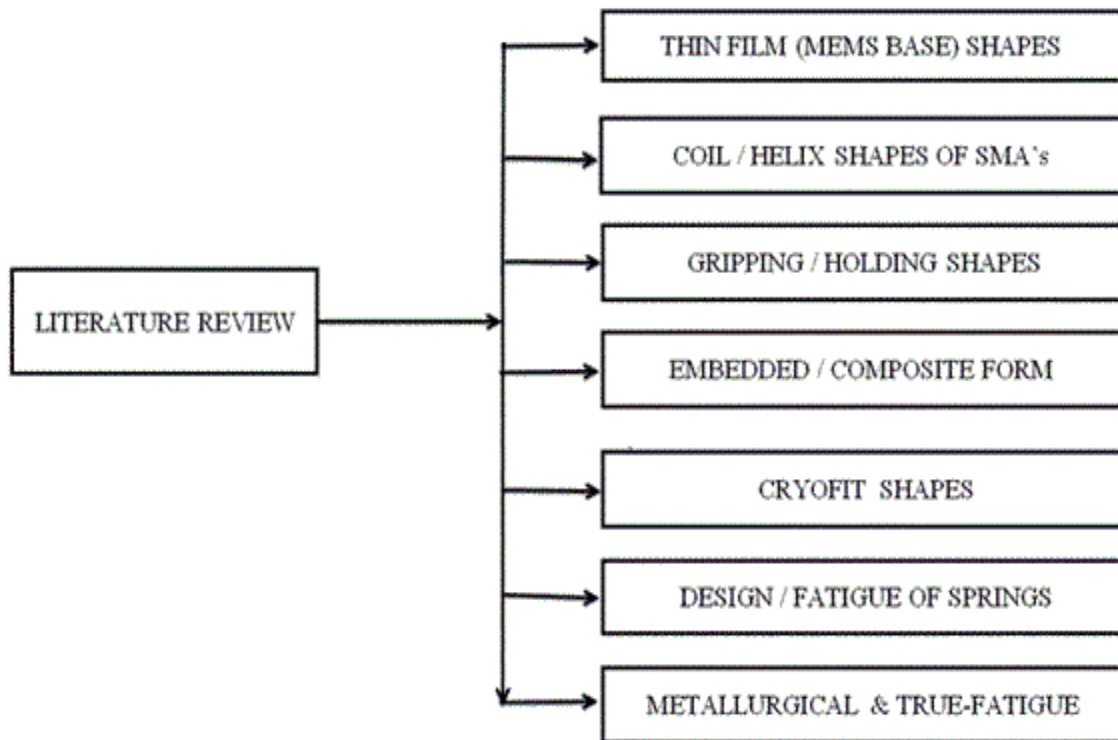


Figure 2.1 Classification of Literature Review

Finally, gaps were identified based on the literature survey which provided the platform for this dissertation work in the field of developments of shape memory alloys (SMA's) based equipment/devices.

## **2.2 THIN FILM (MEMS BASE) SHAPES OF SMA'S**

This included the fabrication of thin films with SMA's, manufacture of bulk SMA and the most common method used to deposit thin-film SMA is sputtering deposition. Other methods included flash evaporation, pulsed laser deposition, filtered arc deposition, cluster beam deposition, and cathodic arc plasma ion plating; including preparation and characterization, residual stress and adhesion, frequency improvement, fatigue and stability, modeling of behaviors of SMA's.

**Christoph Bechtold and Christoph Chluba, et al. (2019)[115]** characterized NiTi-based films with thicknesses of 20-25  $\mu\text{m}$ . The freestanding films from binary NiTi, ternary NiTiCu, and NiTiHf were fabricated by DC magnetron sputtering and their properties. NiTiCu shows high cyclic stability: all NiTiCu samples tested reached the  $10^7$  cycles test run out and cycle numbers  $>10^8$  are possible.

**Shahabeddin Ahmadi and Kiran Jacob, et al. (2018)[125]** presented shape memory alloy film damping for smart miniature systems which involved a dynamic analysis of the free and forced vibration of a free-standing bridge of super-elastic shape memory alloy TiNiCuCo film with ultra-low fatigue properties and evaluated its versatility for novel miniature scale damping applications.

**Christoph Bechtold and Rodrigo Lima et al. (2016)[114]** presented a method for fabricating miniaturized NiTi self-expandable thin film devices i.e. a novel approach to fabricate self-expandable medical components from NiTi with increased radiopacity. The combination of Ta and NiTi seems to be uncritical since the multilayer show good corrosion resistance and both NiTi and Ta are biocompatible.

**M Kabla, E Ben-David, and D Shilo, et al. (2016)[26]** described a novel concept for in-plane actuators based on a thin free-standing shape memory alloy (SMA) film. A prototype actuator demonstrated a displacement of  $45\mu\text{m}$  related to 4.5% of the SMA film length.



And a force of up to 115 mN related to a stress of 230 MPa in the SMA film without plastic deformations. Integration of the stress with respect to the strain showed that the demonstrated actuator provided a work per volume of  $8 \times 10^6 \text{ J m}^{-3}$ .

**Yongqing Fu (2004)[4]; Mehrshad Mehrpouya et al., (2016)[13]**, described the TiNi-based thin films in MEMS applications: a review in which preparation of high-performance shape memory TiNi films using sputtering methods and their MEMS applications were involved. In their review paper, some critical issues and problems in the development of TiNi thin films were discussed; Different types of TiNi thin-film-based micro-devices, such as micro-switches, micro-valves, and micro-sensors, etc. are also described and discussed.

**Md.AmriZainal (2015)[12]** explained micro-machined SMA micro-actuators and their application in biomedical devices. They included fabrication of thin films, manufacture of bulk SMA and the most common method used to deposit thin-film SMA is sputtering deposition. It was shown that Ti-rich films exhibit a transformation temperature near to or above ambient temperature. They also considered the different compositions of NiTi thin-film shape memory alloys (SMAs) and bulk micro-machined SMA actuation methods.

**Nicole Latrice Harris Odum et al. (2010)[7]** described NiTi thin film processing and characterization techniques in his dissertation. NiTi thin film '1'  $\mu\text{m}$  thick was produced using sputter deposition techniques. Substrate-bound thin films were deposited to analyze the surface using scanning electron microscopy.

**Y.Q. Fu et. al. (2009)[111]** discussed the micro-electro-mechanical system (MEMS) applications by thin film shape memory alloys and micro-actuators. They focused on crystal nucleation and growth during annealing, film thickness effect, film texture, stress-induced surface relief, wrinkling, and trenches as well as temperature memory effect (TME). They also considered micro-cage for biological application (TiNi/DLC bimorph micro-cage structure), micro-mirror for optical application (cantilever-based micro-mirror structure), and data storage using nanoindentation method.

**T. Shahrabi and S. Sanjabi, et al. (2008)[126]; Rodrigo Lima de Miranda, et al. (2016)[137]; C. Chluba and H. Ossmer, et al. (2016)[127]** the first one discussed the specific applications in the thin film as extremely high pitting resistance of NiTi SMA thin film in simulated body fluids.

The second one by Christoph Bechtold and presented a novel approach to fabricate self-expandable medical components from NiTi with increased radiopacity in which a common strategy to increase the radiopacity of NiTi devices is the addition of radiopaque markers by micro-riveting or micro-welding. Another application by as ultra-low fatigue quaternary TiNi-based films for elastocaloric cooling as an elastocaloric in which cooling agent, transformation temperature adjustment was necessary.

**David Rigberg (2009)[138]; C.P. Kealey, et al. (2010)[135]**, described ‘in vitro hemocompatibility’ of thin-film Nitinol in stenotic flow conditions (Thin-film nitinol (TFN) is ideally suited for use in the construction of endovascular devices) in which developed a surface treatment for TFN designed to minimize platelet adhesion by creating a super-hydrophilic surface. The hemo-compatibility of expanded poly-tetrafluoro-ethylene (ePTFE), untreated thin film nitinol (UTFN), and a surface-treated super-hydrophilic thin film nitinol (STFN) were compared using an in vitro circulation model. Similarly, performed feasibility study of thin-film NiTi (Nitinol) could be used as a covering for stent-grafts ranging from 16 mm to 40 mm in diameter.

**Xi Wang (2007)[113]** performed a crystallization study in which amorphous films were annealed by a scanning laser (experimentally and numerically). The nucleation and growth mechanisms in the laser annealing process were found to be the same as for furnace annealing. Uniform microstructure and shape memory properties were locally introduced in the films by the laser. A 3-D thermal model was developed to simulate the crystallization behavior of the laser annealing process of amorphous Ni-Ti thin films.

**Francisco M. Braz Fernandes and Rui Martins, et al. (2002)[136]** also discussed the structural characterization of NiTi film shape memory alloys.

### **2.3 COIL/HELIX SHAPES OF SMA'S**

In helical SMA actuator behavior with coil/ helix shapes included various wires of spring coil diameter. This shape is applied in one-way and two-way memory effects of SMA coil springs.

**Pierre-Antoine Gédouin (2019)[19]** described the stress analysis effect of the two-way memory effect of SMA coil springs.

**Ranjith Pillai Ra et al. (2018)[82]** developed two DOF flexible parallel platforms which consist of a triangular top and base plate connected by a universal joint at its centroid. The SMA springs were connected between the top and base plate on all three vertices of the platform. The top plate provides desired orientation to the base plate on SMA actuation. Two separate models, one to understand the kinematics/dynamics of the platform, and the other to understand the dynamics of the SMA spring actuator had been developed.

**Je-sung Koh (2018)[9]** described the two-state model of the SMA spring actuator, spring design procedure through experimental investigation.

**Samuel de Oliveira et al. (2015)[27]** discussed the prediction of the change of elastic force of a helical spring of a shape memory alloy NiTi using a recursive neural network was performed. For this study, the coil spring NiTi was heated by Joule effect with a controlled and a load cell was determined that the force being generated electric current. Prediction results of tensile strength are presented.

**R. B. Barjibhe (2015)[55]** evaluated the performance of SMA helical spring through experimentation to control the structural vibration in a cantilever beam. The close-coil helical springs were used for conducting the experiment and the result demonstrated that the single SMA spring was more effective than 2 or 3 springs connected in series in vibration control. Work included the various plots for frequency V/s acceleration for conventional spring and frequency V/s acceleration for 3 SMA springs.

**Shane J. et al. (2013)[142]** described a mechanical actuator in a coil shape. Shane J. Yates performed an experimental study of SMA actuators and analyzed the effects of various parameters on temperature changes.

**Mohammad Mahdi Kheirikhah et al. (2011)[56]** discussed the robotic applications as a two-way linear actuator using SMA spring and silicone bellows had been applied to the micro-robot for a first application, second application involved the locomotive principle of the proposed microrobot. Other robotic applications included circular soft robot jumping i.e. jumper robot, movement of stem and flower petal (flower robot), fish robot, locomotion of rigid gecko robot (walker robots), and bio-mimetic robotic hands.

**A Hadi and M Elahinia (2011)[55]; Esuff Khan et al. 2011)[83]** developed a one-degree-of-freedom differential actuator using SMA springs as the internal actuators, found the actuator demonstrates a good positioning accuracy in addition to a higher level of stiffness control and design parameters were analyzed with the consideration of transformation strains in the design of SMA actuator springs. The linear approach, proposed nonlinear approach, stress distribution over the wire cross-section, torque v/s angle of twist, variation of diameter (d) with respect to total strain in martensite phase were also estimated.

**Andrea Spaggiari (2010)[54]** focused on adopting for the actuator a telescopic multi-stage architecture and using SMA helical springs with hollow cross-section to power the stages. The use of the hollow spring construction and the telescopic architecture leads to excellent performances i.e. hollow geometry leads to reduced axial size.

**Sergio Puértolas et al. (2010)[94]** proposed splints based on the NiTi alloy in coiled form for the correction of joint deformities in the fingers; A new model of splint based on NiTi alloy had been designed, simulated, and tested comparing its behavior with two of the most regularly used splints.

**Sangbae Kim and Elliot Hawkes et al. (2009)[85]** introduced micro-muscle fiber crafted from shape memory alloy (NiTi) coiled springs. The fiber was 400 $\mu$ m in diameter and 0.5m in length exhibiting 50% contraction and 1226 J/kg of energy density with 40g of force. By changing the geometry of the spring, force-displacement characteristics are tuned. They compared experiment data and model using equation and described a manufacturing process and characterization for micro-scale NiTi coil actuators in various annealing temperatures.

**Vinicius Piccirillo et al. (2008)[93]** analyzed the influence of SMA spring on a non-ideal system during the passage through the resonance. The torque generated by a DC motor was limited and, according to the classical Kononenko theory, assumed as a straight line. Angular velocity, Lyapunov exponent, Frequency-response curves, phase portrait, and phase diagram are also estimated.

**Young Pyo Lee and Byungkyu Kim (2004)[84]** introduced a novel bio-mimetic microrobot with a simple mechanism using shape memory alloy (SMA) to generate earthworm-like locomotive motion without electric cable.

This had an adverse effect on the mobility of the microrobot and the proposed microrobot system was composed of an actuator with SMA spring and silicone bellows, wireless control system, wireless power supply (battery), and body frames.

**Dieter Stoeckel et al. (1990)[76]** included potential applications of shape memory thermal actuators in automobiles: radiator shutter, fan clutch, fuel management, climate control, engine control, brake ventilation, transmission control/rattling noise reduction and suspension adjustment, etc. The electrical actuators such as fog lamp with shape memory electrical actuator, a windshield wiper with shape memory pressure actuator, and door locking mechanism with shape memory springs are also considered.

## **2.4 GRIPPING/HOLDING SHAPES OF SMA'S**

The effect of loading history, gripping force, gripping range of different linear and nonlinear model systems based on the transformation conditions of the shape memory alloys are considered. The various different ways applicability and applications are also included.

**Zahra Khalid (2018)[58]** compared the mean change of tooth movement in canine retraction between an elastic module and NiTi coil spring. Thirty-two patients were inducted. The pre and post-retraction measurements was recorded. The mean rate of tooth movement in the NiTi coil group and in the elastomeric module group was 1.1 mm and 0.7 mm in one month, respectively ( $p = 0.05$ ). And found the rate of tooth movement was more rapid with the NiTi coil spring than with the elastomeric module.

**Chavan Madhura (2017)[139]** discussed the design and development of a robotic gripper actuated by shape memory alloy. NiTi wires were experimentally investigated to evaluate the effect of loading history on the transformation start conditions of the shape memory alloys. The actuation mechanism was designed using a combination of torsion spring and Shape Memory Alloy spring. The results showed the grippers were able to track the position rapidly and precisely.

**K.C. Munasinghe et al. (2016)[105]** proposed a MEMS gripper system for object manipulation and micro assembling with the overall size of  $2730 \mu\text{m} \times 1500 \mu\text{m} \times 50 \mu\text{m}$ . It had a gripping range of 1-120  $\mu\text{m}$ . The simulation results showed that Ti-Ni can be used as an effective method of actuating the gripper and eigenfrequencies seems to be very high hence minimizing failure due to resonance.

**Amin Jamalimehr and Hossein Ravanbakhsh (2016)[57]** studied a simple tensile test of SMA by considering stress concentration caused by the grippers. This pre-stress was utilized in the simulation of SMAs under uniaxial tension by applying the finite element method. Brinson's 1-D constitutive model was used and found that the pre-stress leads to a non-uniform distribution of uniaxial stress as well as martensite volume fraction throughout a wire.

**Mohammad H. Elahinia (et al. 2015)[61]** designed an extended Kalman filter for a rotary SMA actuated manipulator and has been tested through simulations. The model included nonlinear dynamics of the manipulator, a constitutive model of the shape memory alloy, and the electrical and heat transfer behavior of SMA wire.

**Sundara sathiyam (et al. 2015)[18]** told by the use of shape memory alloy spring, the mechanical gripper is able to pick an object of the small size of 98mm diameter and weight less than 200g. This mechanical gripper can be automatically activated by the supply of heat and also it can be used in high-temperature environments such as robotic applications, chemical industries, laboratories, nuclear power plants.

**Z.W. Zhong and S.Y. Chan (2007)[141]; SC Mishra et al. (2015)[20]**, both discussed fabrication and actuation mechanism of gripping device actuated by shape memory alloy (SMA) wire and applications. An SMA wire was used to close the gripper during operation and a torsion spring was integrated to open the gripper when the SMA wire relaxed. SMA wire diameter and the number of coils the SMA wire was wound had significant effects on the gripping device's performance. The gripping force was adjustable by changing the driving current. The gripping device using one coil of  $\varnothing$  100  $\mu$ m SMA wire with a music wire spring produced a good performance and the gripping device could withstand over 1.175 million opening and closing cycles without any deterioration in its performance.

**Yanhong Ma and Qicheng Zhang (et al. 2014)[60]** described the forced excitation tests that have been performed to identify the static and dynamic stiffness and the damping capacity of the shape memory alloy metal rubber support. This particular metal rubber damper showed variable stiffness and damping versus temperature frequency and amplitude.

**Alaa AbuZaiter et al. (2014)[103]** performed experimental characterizations of the developed micromanipulator when the micromanipulator was actuated in its three DOF.

A laser displacement sensor was used to measure the displacement ranges, while an infrared (IR) camera measured the temperature of the links, and gripper fingers showed the relationship between the displacement and the temperature.

**Ehsan Tarkesh Esfahani et al. (2010)[86]** proposed an adaptive PID controller to control an experimental model of an ankle-foot orthosis device actuated by SMAs. Experimental and simulation results showed the advantage of using this controller in comparison with a PID controller. The robustness of the controller was also demonstrated by testing the controller in presence of a different source of disturbance such as external force, increasing the mass, and changing the temperature of the wire. The block diagram, phase transformation diagram, ankle moment V/s ankle angle plots were also considered [86].

**Ahmed M. El Kady and Ahmed E. Mahfouz (et al. 2010)[102]** described SMA as a mechanical design for an anthropomorphic prosthetic hand, one of the main components of upper limb prosthesis. The design included the pathways for the finger flexing cables which actuated using shape memory alloy (SMA) wires.

**Luciano G. Machado (2007)[59]** evaluated the nonlinear dynamics of passive vibration isolation and damping (PVID) devices through numerical simulations and experimental correlations. The device, a mass connected to a frame through two SMA wires, was subjected to a series of continuous acceleration functions in the form of a sine sweep.

**Han Zhang and Etienne Burdet (2002)[109]; N. Grassi et al. (2012)[110]** described biomedical applications first one an integrated approach to design and fabricate scaffold/cell constructs for tissue engineering as and building a scaffold/cell constructed by robotic micro-assembly of microscopic polymer building blocks. This paper introduced a 3D contact FEM simulation to study the forces and involved scaffold elements and micro-gripper during assembly. The second one ‘The Italian colon-ring register’ (or ‘Registro Italiano Colon Ring’) has recently been created in order to collect and process the experience of Italian surgeons who perform biodynamic compression anastomosis of the colon-rectum with the use of this device.

## **2.5 SHAPES OF SMA’S AS EMBEDDED/COMPOSITE FORM**

The dimensions, varying lengths, position, volume fractions, compatibility of SMA wires with fibers and matrix, NiTi fiber diameter, bonding properties, optimization process of the flexural stiffness, weight, and damping capacity of the hybrid composite are considered. The various different ways applicability and applications are also included.

**Danish Mahmood Baitab (2018)[16]; Michele Guida et al. (2019)[90]** discussed the behavior of thermoplastic composites and shape memory alloy hybrid composites (SMAHCs) for aeronautical applications. is analyzed and compared by means of findings from numerical analyses and experimental tests. The applied embedding of SMA wires in composites involved factors such as dimensions/position of SMA wire, actuating temperature of SMA wires, and composite curing method. SMA wires can be embedded in between layers of laminates of composites, can be directly embedded in a matrix as reinforcement, and can be embedded as woven structure depending on properties.

**Nicholas G. Garafolo 2017)[121]** presented a composite application of performance mapping of an aluminum-nitinol composite vibrating beam. Another application of aerospace described by **H. Asadi and M. Bodaghi (et al. 2013)[117]** on the free vibration of thermally pre/post-buckled shear deformable SMA hybrid composite beams.

**Bethany Gordon (2015)[62]** tested the flexural strength and self-centering properties of NiTi fiber-reinforced mortar at varying lengths and volume fractions and found when SMA fibers are embedded in concrete or mortar, the pseudo-elasticity of the fibers translates to a self-centering property that allows structures to recover from deformation after being exposed to strong cyclic loads.

**Xiang Chen and Adam Hehr et al. (2015)[130]** also discussed the deformation mechanisms in NiTi-Al composites fabricated by ultrasonic additive manufacturing. Similarly, **Zariff Chaudhury et al. (2011)[87]** prepared composites with a significant difference in NiTi fiber diameter (127 / 51 $\mu$ m) and found that 51 $\mu$ m NiTi fibers were better bonded with the Al matrix; de-bonding had seldom been observed. There was better micro-structural compatibility i.e. fiber diameter was of the same order as the Al matrix grain size for this case.

**Kin-Tak Lau (2002)[65]; Rameshwar S. Ingalkar et al. (2014)[66]** presented SMAs in the form of wires and strips and showed a pre-strained level of the SMA wires is lower than 8%.



The review of rehabilitation techniques of building and bridges by using shape memory alloy included seismic damper, seismic damper with composite NiTi-wires, SMA restrainer used at intermediate hinges of the bridge, and seismic damper with wrapped NiTi-wires were discussed. By using shape memory alloys in seismic dampers one may reduce plastic deformation in the structure and at the same time dissipate energy. The study also using SMAs in bridges created an energy dissipation device and designed to take the load only in bending.

**H. Asadi, Y. Kiani and M. Shakeri, et al. 2014)[99]** projected post-buckling behavior of shape memory alloy (SMA) hybrid composite laminated beams under uniform heating and found SMA fibers possess the great ability to delay the thermal bifurcation in beam-like structures, any increase in the volume fraction of fibers or fibers pre-strain results in higher buckling temperatures.

**M. Bocciolone (et al. 2013)[63]** discussed passive damping of GFRP (glass fiber reinforced plastic) laminated composite. The SMA had been embedded as reinforcement in the GFRP laminated composite and an SMA/GFRP hybrid composite was obtained. The pattern of the thin SMA sheets proved to be a key feature in the optimization process of the flexural stiffness, weight, and damping capacity of the hybrid composite. The application of the proposed hybrid composite for a new design of a GFRP lateral horn of a railway pantograph has been proposed.

**M Parlinska (2000)[112]; Jan Schrooten, et al. (2002)[40]** described the thermo-mechanical behavior of SMA wires with a simple force balance, the resulting composite behavior including interfacial quality, internal stress distribution, and reproducibility of the behavior were addressed. The following major steps are examined as selection and characterization of the material constituents, development of manufacturing processes for the production of composites with pre-strained SMA wires, analysis, and modeling of the action of the SMA wires in the composite, the contribution of the SMA-resin interface.

**Mojtaba Nasr-Esfahani (2011)[64]** proposed a titania network encapsulating nano bioactive glass 58s (NBG) particulate phase as a bio-ceramic composite coating. The grain size of NBG particles was uniform and its nanoscale (50-60 nm) was confirmed with transmission electron microscopy (TEM). These bands can increase the ability of NBG-Titania film to develop and induce the formation of HCA particles.

**Luana B. Pe´rtille (2008)[100]** described the development of a homemade device for in vivo human electrochemical properties of a NiTi-based alloy (Nitinol) used for minimally invasive implants i.e. the OCP to which a NiTi-based alloy was subjected upon contact with bloodstream had been assessed in vivo in six human patients.

**J A Balta (et al. 2005)[122]** described the embedded application as smart composites with embedded SMA actuators and fiber Bragg grating sensors: activation and control, journal of smart materials and structures.

**Gangbing Song and Brain Kelly et al. (1999)[123]; Romulo Pierre Batista Dos Reis et al. (2010)[124]** first presented the application of composite beams and vibration attenuation in an epoxy smart composite beam with embedded NiTi shape memory wires.

## **2.6 CRYOFIT (COUPLING/FASCINATING) SHAPES OF SMA’S**

The design, implementation, testing of various SMA’s based applications such as wing flap assembly, beam structures, buildings, bone fixation, and vibration isolation system, etc. are discussed.

**Rosario Pecora (2013)[81]; Yuchen Chen et al. (2019)[108]** presented the advanced application in aeronautics, first one identified the intrinsic hysteresis in an aircraft morphing wing device through the implementation of a discrete array of equal-distance points partitioning the Preisach plane. Preisach densities were hence derived from the forces. The second one is projected as an actuator device based on SMA, and a wing flap assembly fitted with such an actuator device (United States Patent). A wing-flap includes a flap made of a plurality of flap sections, in which each flap section is connected to the preceding one in a rotatable manner and one or more actuator devices adapted to control the rotation of flap sections.

**Iqra Zubair Awan (2018)[30]** given a brief review of the fascinating shape memory alloys and found wide usage in hydraulic, pneumatic, and motor-based systems. They discussed three variants of martensite in a cubic to tetragonal transformation, deformation twins in a polycrystalline zirconium specimen, and change of shape associated with deformation twinning is a simple shear. Physical phenomena and their applications are also discussed.

**Donatello Cardone (2012)[25]; M. Tazarv et al. (2018)[96]** discussed buildings applications in which the use of SMA in many forms such as longitudinal and transverse reinforcement and fibers in concrete. The experimental evaluation of a device prototype based on shape memory alloys for the retrofit of historical buildings by a post-tensioned system based on the super-elastic properties of Ni-Ti shape memory alloys for improving the structural performances of traditional metallic tie-rods. They represented the SMA-reinforced ECC column damage at 10% drift ratio, force-drift relationship for SMA-reinforced ECC and CIP columns.

**Mauro Dolce et al. (2000)[98]** projected memory alloys for new seismic isolation devices aimed at exploiting the great potential of SMAs in the field of passive seismic protection of structures, through comprehensive experimental and theoretical studies. It has lead to the conceptual design, implementation, and testing of two families of energy dissipating/re-centering devices for seismic isolation of buildings and bridges and for braces of framed structures. The overall performances of the SMA-based obtained better than currently used devices, not only for their mechanical behavior but also for their high durability and fatigue resistance.

**S. Ballandras (1997)[70]; Huilong Hou et al. (2016)[97]** discussed fabricating NiTi alloys which included a novel thin film deposition technique to NiTi alloy nanowires and micro stereophotolitho-graphy and shape memory alloy for the fabrication of miniaturized actuators. The length (100-1000  $\mu\text{m}$ ) and width (200, 90, 70, and 50 nm) with a fixed thickness of 800 nm of the nanowires were controlled by a cutting/sectioning process and free of oxygen impurities. These exhibited a high aspect ratio of length to cross-sectional dimensions. Similarity schematic process of nanoskiving to generate nanowires from BTIBD NiTi thin films, optical images, and bright-field TEM images also estimated.

**Hyuk-Soo Han (2011)[30]; Hyuk-Soo Han et al. (2016)[33]** discussed how to increase the frequency of femur fractures. The conventional treatment utilizes a bone fixation plate and screw system. This work presents the design of shape-memory-alloy fixation grip for femoral fracture, femur model and measurement of femur cross-section, simplified femur fracture model, and compressive analysis of boundary conditions.

In their study, the feasibility of a fixation grip which is composed of a shape memory alloy was investigated to resolve the disadvantages of bone fixation plates and screws by compressive and torsional analysis.

**Vaibhav Chaturvedi and Rituparna Data (2014)[69]** discussed a vibration isolation system comprising four-bar linkage mechanism along with SMA wire was proposed for space-related applications. Experimental investigation of the proposed system was carried out to examine the transmissibility of SMA wire. The passive vibration isolation with SMA wire included simulation and modeling of box stiffener, finite element analysis, and genetic algorithms also.

**Xiaoyong Zhang (2014)[77]** proposed a design concept for a separation device actuated by a load-shifting SMA actuator. The LSSA design methodology was developed to design the separation device. Four prototypes of the separation device were fabricated and tested and applied a folded solar array simulator. The LSSA design methodology can produce a reasonable design for a separation device under a certain output displacement and force safety factor. The separation device could release a design load of 2400N within 0.24s with a power consumption of 48.3W.

**J.M. McNaney (2003)[67]; Vishal.B.Wani et al. (2008)[68]** demonstrated tension-torsion experiments on thin-walled super-elastic Nitinol tubes that have a rich mechanical behavior involving significantly different characteristics in each of the two loading axes. The observed behavior provides important insights to the stress-induced phase transformation under multi-axial loading commonly encountered in a wide array of engineering applications involving super-elastic materials due to excellent biocompatibility and large pseudo-elasticity and discussed hydraulic tube couplings, blood-clot filter, and temperature-actuated switch.

**I. Dutta (2006)[106]** described microelectronic solder joints which are exposed to aggressive thermo-mechanical cycling (TMC) during service, resulting in strain localization near solder/bond-pad interfaces, which eventually leads to low-cycle fatigue (LCF) failure of the joint. In order to mitigate these strain concentrations, a “smart solder” reinforced with a martensitic NiTi-based shape-memory alloy (SMA) has been proposed.

Finite element modeling found NiTi particulate reinforcements can reduce inelastic strain levels in the solder via shape recovery associated with the B199/B2 transformation.

**Nagahiko Shinjo (2004)[107]** presented the preliminary design of a biologically inspired propulsive system incorporating internal mechanisms of swimming locomotion. The use of elastic systems in the scombrid propulsion system was investigated with NiTi SMA. The properties of scombrid propulsive systems, bending mechanisms of scombrid, oblique wire arrangement, and preliminary design of an SMA-based oscillating propulsive system are also considered.

**H. Fischer (1999)** demonstrated by the experiments performed up to a flexible distal end for the accommodation of the modular endoscopic camera unit can be fabricated from varying material thickness. Tube with guiding sleeves and Bowden wire, welding and cutting the structure of the tube with Nd-YAG laser, various bending moment characteristics also considered.

## **2.7 DESIGN/FATIGUE OF PHYSICALLY LOADED SPRINGS**

The physically loaded helical compression springs undergo fluctuating loading over the whole span of service life. The distribution analysis, maximum displacement, and different modes of failure of these springs have been discussed with the various case study.

**Gajendra Singh Rathore (2013)[49]; Noshirwaan Aibada, et al. (2018)[52]** discussed the detailed review of studies on helical compression springs with a perspective of material, methods, and failure. The promoted failure can be due to excessive loads, adverse environmental conditions, or fatigue. But the majority of the springs failed due to fatigue failure, crack initiation in the cross-section of the wire and intensifications was one of the significant modes of failure, improper manufacturing, and imbalance in the composition may also cause failure.

**Donghai Qiu et al. (2018)[116]** also described tuned nonlinear energy sink with conical spring: design theory and sensitivity analysis. The design theory and sensitivity analysis of a tuned NES attached to a harmonically forced linear oscillator were investigated. Firstly, a design criterion intended to find the tuned parameter of nonlinear stiffness for a given primary system specification was proposed.

**H. B. Pawar and D.D. Desale et al. (2018)[78]** discussed the optimization of three wheeler front suspension coil spring. As per design, the springs were made of material IS- 4454 and they found feed wire length required for modified spring new design II reduced by 10%. Due to the reduction in feed wire length, the mass of new design II was reduced by 10%. Due to the change in stiffness, the load-carrying capacity of the modified spring was increased by 7%. FEM analysis, UTM testing, load V/s deflection, load V/s acceleration curves were also estimated.

**Ronak B. Chaudhari and Dr. I. Navale et al. (2017)[29]** focused on the effect of change in parameters like material, wire diameter, pitch on fatigue life of helical spring used in stamping machine. The spring was designed and modeled using CAD software. This further evaluated using FEA software for static, fatigue analysis for cyclic loading and produces the best suitable compression spring.

**Niranjan Singh (2013)[23]; Vishal Chaudhari et al. (2016)[35]** had the theoretical results obtained by the shear stress equation and Finite Element Analysis (FEM) of springs and provided the better solution of the problems that arise in the existing design of the mechanical spring.

**Goran Vukelica and Marino Brcicb et al. (2016)[24]** discussed the frequent failures of coil springs on a specific type of motor vehicle and performed detailed scanning electron microscopy (SEM) examination at suitable magnifications then employed to characterize the fine microstructure of the fractured surface and reveal flaws that served as crack initiation points. They suggested that this was an example of corrosion fatigue failure. In their examination, they found protective paint layer of the wire was damaged as pits appearance. These pits served as crack initiation points from which fracture. They also used the image of optical magnification of fracture surface around crack initiation point and SEM image of fracture surface around crack initiation point.

**Supriya Rahul Burgul et al. (2015)[22]** discussed the fatigue analysis for helical compression spring for determining design alternatives for enhanced life and performance. In the IC engine; found percentage ratio of premature fatigue failure of an exhaust valve spring of a constant speed is more and applied tetrahedral mesh model zoom view, rigid and solid element connectivity, boundary condition, the maximum deflection of spring, and maximum von mises stress in the spring.

**Rahul M. Gupta (2015)[119]; Pratik Sharma et al. (2018)[120]** discussed conical springs analysis as heat transfer enhancement and friction factor analysis in a tube using conical spring insert and design and analysis of conical spring for performance enhancement of mirror assembly using a hybrid approach.

**Satbeer Singh Bhatia (2014)[31]; Youli Zhu et al. (2014)[118]** first one focused on the design of helical compression spring is first analyzed for the conventional steel material (IS 4454 Grade 3) and then compared with that of for the composites used as spring materials study their behaviors at the two loading conditions. The second one focused on the failure analysis of a helical compression spring for a heavy vehicle's suspension system by considering a case study and found fractured at the transition position from the bearing coil to the active coil (first) in service.

**Rinaldo Puff et al. (2010)[34]**, described the design, fatigue analysis of helical suspension springs for reciprocating compressors. They also discussed stress analysis by FEM results of stress distributions in the contact zone, showed plotting between loads with stresses, and loads with deformations.

## **2.8 FOR METALLURGICAL & TRUE-FATIGUE PROPERTIES**

The characteristic of NiTi fiber-reinforced structure, mechanical properties at ambient temperature, wire volume fraction, equivalent damping, energy dissipation, re-centering capability and strain recovery/stress gradients over forward, and reverse transformations are discussed. The mechanical fatigue behavior in the cyclic loading to assess their potential concentration of stress for tensile test was also considered.

**Nubailah Ab. Hamid and Azmi Ibrahim (2018)[101]** described experimentally the cyclic properties of pseudoelastic NiTi shape memory alloys bar to distinguish the cyclic loading number. The tensile cyclic test obtained demonstrated a rounded loading curve based on a 0.2% offset. NiTi bar exhibited superior pseudo-elastic behavior with narrow hysteresis through repeated cycling without significant degradation or permanent deformation and in good agreement with their re-centering capability but, decreasing in energy dissipation.

**S. Hahn (2016)[89]; Shuyong Jiang and Junbo Yu et al. (2017)[128]** considered microstructural & mechanical properties of small-scale NiTi samples (produced by PVD processes) and investigation on deformation mechanisms of NiTi SMA tube under radial loading. Special emphasis was placed on typical challenges while handling and analyzing these small-scale samples by DSC measurements, XRD analysis, electron microscopy, and tensile testing. Work demonstrated the special significance of high-resolution equipment.

**Yingying Zhu (2016)[92]** investigated the effects of a high-velocity impact on the microstructure, phase transformation, mechanical property of aged Ti<sub>49</sub>Ni<sub>51</sub> alloy, and found generation of stress-induced martensitic transformation is due to the concentration of stress in the grain boundary, under the shock waves. The DSC curves, various TEM micrographs and SAED patterns, micro-hardness distribution along crater in aged also considered.

**E. Hornbogen (1999)[21]** defined three temperatures ranges i.e. stable austenite ( $\beta$ ), transforming  $\beta \leftrightarrow \alpha$ , fully transformed martensite ( $\alpha$ ). This work included the evolution of lattice and surface defects in single/poly-crystals, stages of mechanical fatigue, nucleation/propagation of cracks, thermal cycling, effects, training/fatigue of one-way, two-way effects, and aging effects of NiTi alloy.

**Claire Morin et al. (2011)[51]** introduced tensile-compressive asymmetry and strong thermo-mechanical coupling ZM models. Secondly, the stabilized state was computed using an extension of the direct cyclic method. Third, the fatigue lifetime of the structure was determined with an energy-based criterion accounting for the influence of the hydrostatic pressure. This work also considered the influence of geometry, heat boundary conditions, dissipation, and numerical computation of the stabilized cycle/validation of the coupled model.

**Saidjafarzoda Ilhom (2018)[41]; Saidjafarzoda Ilhom (2019)[40]** obtained micro-indenters on Ni<sub>50</sub>Ti<sub>50</sub> SMAs with 1064 nm wavelength at 10 Hz. Time evolution of laser-induced shock wave and temperature were also simulated, in which pressure wave closely follows the laser pulse rise time and attenuates as time advances.



Illustration of laser shockwave imprinting on SMA substrate, SEM images of hexagonal square copper mesh grid after irradiation with laser energy of  $6.4 \text{ J/cm}^2$ , indent depth and, recovery ratio of patterns on NiTi shape memory alloys at different laser fluencies also were included. Secondly, the shape the recovery of the as-generated patterns by the laser direct-scribing of the NiTi SMA was realized. The depth of the patterns for Ni50Ti50 samples was represented to increase with laser energy density.

**Yousef Payandeh (2012)[43]** investigated the mechanical behavior of the NiTi–epoxy composite using a standard tensile test. The effect of different types of wire, test temperature, and wire volume fraction was studied. They found martensitic transformation in the wire can occur simultaneously in several points which results in a regular deboned / un-deboned pattern.

**M.J. Mahtabi (2015)[44]; O. Tyc et al. (2016)[47]** found classical fatigue models for the effects of mean strain/stress such as Goodman and Smith-Watson-Topper are not directly applicable to the super-elastic nitinol. The volume fraction of the stress-induced martensite was found to be a key parameter affecting the fatigue behavior of the super-elastic Nitinol. 4-Cyclic stress-strain response of Nitinol at different cycles of loading various strain ratios and SEM images under fatigue test also estimated. Another one considered thin super-elastic NiTi wires having a different cold work and heat treatments were investigated by uniaxial tensile fatigue tests at a constant temperature.

**Francesca Berti et al. (2018)[45];** This study performed a numerical analysis aimed at inspecting different multi-axial loads combinations and mimicking the FPA environment for Nickel-Titanium (NiTi) alloys exploit a typical super-elastic behavior. Four different fatigue criteria were implemented to give an interpretation of the severity of the conditions according to different indices.

**Bashir S. Shariat (2013)[46]** explained the geometrically graded NiTi strips with linear and parabolic sides have been fabricated by means of tension experiments and computational finite element modeling. By geometrically grading the NiTi plates, positive stress gradients were created over forward and reverse transformations, providing enlarged stress windows over transformation strain. The deformation behavior, effect of width ratio, numerical modeling of pseudoelastic behavior of concave NiTi strip, normal stress field, and normal strain field also were included.

**S. Kucharski et al. (2015)[48]** investigated parameters of NiTi shape memory alloy subjected to ion implantation treatment. The spherical indentation tests in micro and nano-scale and tension test have been performed to study the evolution of local superelastic effect in different volumes of non-implanted and nitrogen ion implanted NiTi alloy. This also included masked NiTi samples, results of nanoindentation test for ion-implanted dose D1, dose D2, and load-penetration curves, etc.

**Yinghua Lin and Yongping Lei (2015)[28]** discussed coarse TiB<sub>2</sub> and NiTi/NiTi<sub>2</sub> particle reinforced titanium matrix composite coatings with part of the network-like structure that have been fabricated by laser cladding. The amount and the size of coarse TiB<sub>2</sub> are decreased and the characteristic of network-like structure gradually became clearer with increasing distance from the surface.

**J.P. Coughlin and J.J. Williams (2009)[132]** also focused on interfacial reactions in model NiTi shape memory alloy fiber-reinforced Sn matrix “smart” composites.

**Stefano Gialanella (2008)[88]** conducted wear tests with a disk-on-block geometry. The block was made of the NiTi alloy, whereas counter face disk materials were AISI M2 high-speed steel and a WC-Co hard metal and found hard metal disks present an extremely low wear rate.

## **2.9 RESEARCH GAPS**

A review of literature brings out the following gaps in the context of NiTi based shape memory alloy, (results are comprised in Table 2.1): -

- Few studies are based on the existing basic actuation parameters and estimation of them for NiTi-based shape memory alloy.
- Limited literature is available which explores the actuation parameters of NiTi-based shape memory alloy with the help of modeling and experimental setup.
- Few studies for NiTi-based fork-lift mechanical equipment are available solely for the manufacturing organizations.
- Few studies are available for the load-carrying capacity of deformed NiTi SMA Wires.
- Limited study for NiTi-based system as solenoid valve (mechanical device) is available solely for the manufacturing organizations.

- Few studies are available for metallurgical and true fatigue properties of deformed NiTi SMA Wires when compared to the same by drawn SMA wires.
- The appropriate methodology is not defined in an organized manner that can be effectively utilized for the selection/improvement of NiTi-based system for shape memory alloys.

Table 2.1 NiTi based SMA's description

Sr. No.	Shape of SMA	Availability of shape	Types of design/ shape analysis	Actuation description	Micro-device (MEMS system)	Mechanical device /equipment
1	Embedded / Composite type	few	many	√	√	not define
2	Coil /helix type	√	few	Few	few	not available
3	Cryofit (coupling / fascinating) type	√	√	√	√	√
4	Gripping / holding type	√	√	√	√	√
5	Thin film type (MEMS based)	many	√	√	√	not define

# **CHAPTER 3**

## **MANUFACTURING AND EXPERIMENTAL SET-UP OF SMA INTELLIGENT HELICAL SPRINGS**

### **3.1 INTRODUCTION**

This chapter specifically focused heat treatment process for manufacturing NiTi-based shape memory alloy intelligent helical springs from drawn conditioned SMA wires. Initially, the description of the material's in which flexinol wires were obtained in terms i.e. sizes, shapes, initial conditions, compositions, and general properties are discussed. Then the preparation of smart intelligent SMA helical springs with different diameters i.e. 1.0mm, 0.5mm, 0.2mm, and 0.1mm based NiTi are also discussed. The flexinol (trade name) converted into a helical spring of the desired length by applying an annealing/normalizing process for constant temperature conditions with the help of restraints wires, clamping wires, fixtures, LM35, multimeter, electronic kit, and DC power supply device, etc. The temperature-elongation relationships may obey mathematical equations for which the actuator may be designed. The designed parameters are also calculated as diameter of spring wire, coil diameter of spring, length of spring, and spring index for the NiTi materials. The experimental set-ups for NiTi-based SMA's helical spring in separated/combined form are discussed. Further, the modified design of helical springs (physical-loading), and the experimental set-up of smart fork-lift are also discussed. For the counter check of spring rates readings of physical loaded helical the 'Spring Load Stiffness Tester' is also mentioned.

### **3.2 MATERIAL DESCRIPTION**

SMA,s are a special type of materials that have a property that enables them to return to a pre-established shape when their temperature is increased from a lower initial condition. It is one of the most frequently used commercial materials to produce SMA. This SMA is a metallic alloy composed of nickel and titanium (in the form of wires), which is used in this study as Nitinol/flexinol.

Descriptions of these are shown in **Table 3.1** and also including the following common points:

- These were prescribed as one-way operating and occupied density i.e.  $6.45\text{g/cm}^3$ . The transformation temperature range of all NiTi-based SMA's lied between  $-200^{\circ}\text{C}$  to  $+150^{\circ}\text{C}$ .
- These SMA's are typically made by the casting process. The vacuum arc melting or induction melting specialized techniques are used as prescribed by the seller.
- The techniques are highly costly and used to keep impurities in the NiTi alloy to a minimum and ensure the metals are well mixed. The ingots are hot rolled into longer sections and then drawn to turn it into wires as mentioned by sellers.
- Standards/ quality manufacturing units are available in the USA, so all wires are purchased from Indian vendors or Indian companies as a vendor.
- Several shapes might be used to obtain smart sensors/actuators, but in present work, these materials are applied for helical shape springs only.

Table 3.1 Nitinol/flexinol wires description

<b>Diameter</b>	<b>Initial condition</b>	<b>Length</b>	<b>Composition</b>
0.004"/0.1mm	Straight annealed	1.0m	49.2% (Ni) – 50.8 % ( Ti)
0.008"/0.2mm	Straight annealed	1.0m	49.2% (Ni) – 50.8 % ( Ti)
0.020"/0.5mm	Straight annealed And soften	10 INCH.	49.2% (Ni) – 50.8 % ( Ti)
0.040"/1.0mm	Straight annealed And soften	10 INCH.	49% (Ni) – 51 % ( Ti)
<b>Other general properties of Nitinol / Flexinol above all mentioned wires</b>			
Melting Point		2370 °F (1300 °C)	
Thermal Expansion Coefficient		$11.0 \times 10^{-6}/^{\circ}\text{C}$ (Austenite)	
Thermal Expansion Coefficient		$6.6 \times 10^{-6}/^{\circ}\text{C}$ (Martensite)	
Specific Heat		0.2 cal/g * °C	
Thermal Conductivity		0.18 W/cm * °C	
Latent Heat of Transformation		1.3 cal/g.	

### 3.3 PREPARATION OF ONE-WAY SMART INTELLIGENT SMA HELICAL SPRINGS

NiTi-based materials having a different composition of nickel and titanium applied here in drawn condition to produce one-way smart intelligent SMA helical springs of diameters such as 1.0mm, 0.5mm, 0.2mm, and 0.1mm respectively with the help of muffle furnace / muffle oven (maximum temperatures 1100°C with working temperatures 1000°C). The muffle furnace's supporting devices such as temperature sensor (digital infrared sensor), and long handle tong/crucible tong were also applied.

Figure 3.1 shows **Muffle Furnace** also known as a retort furnace or laboratory furnace. This laboratory furnace is widely used in scientific experiments i.e. physics labs, material labs, rice laboratories, steel industries, smart material industries paint industries, biotech companies, and small-scale industrial production, etc. Their major applications include general laboratory testing, annealing, normalizing, ash determination, and coal analysis, etc. Its primary attribute was that it has separate combustion and heating chambers. Muffle Furnace is box-type heat treatment equipment commonly used to change physical properties of samples at very high temperatures up to 1600°C. But presented work applied standard model was made with maximum temperature 1100°C with working temperature 1000°C.

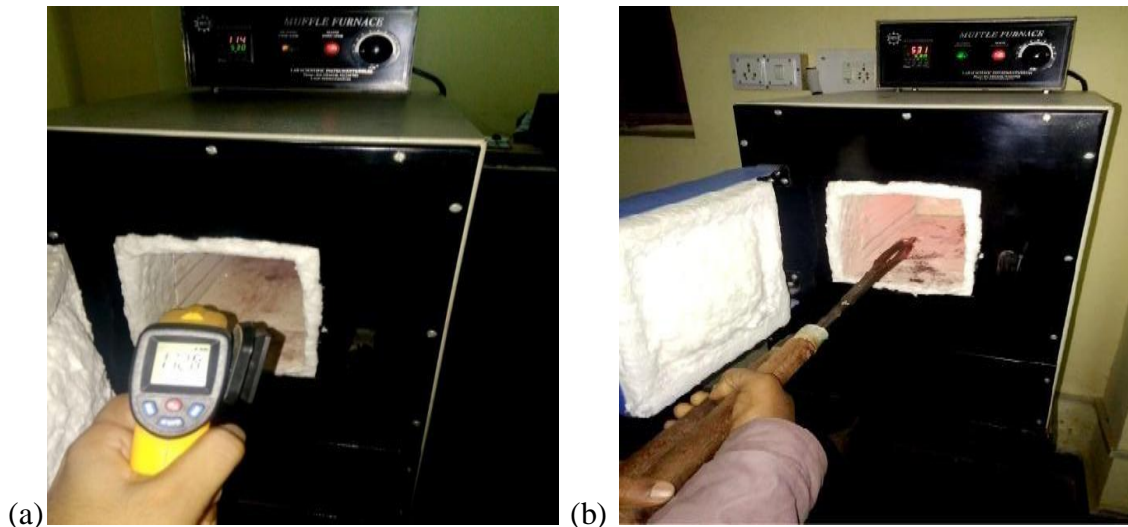


Figure 3.1 Muffle Furnace with (a) digital infrared sensor, (b) handle tong

The following assumptions were also considered during the preparation of one-way smart intelligent SMA helical springs:

- The muffle furnace had the tolerance of  $\pm 5^{\circ}\text{C}$ (max.) during load fluctuations, otherwise, normally  $\pm 2^{\circ}\text{C}$  applied, and muffle voltage regulator is set at  $430^{\circ}\text{C}$ - $550^{\circ}\text{C}$  for 35-45 minutes to made typical helical springs at various stages.
- By this muffle furnace SMA's which having reshaped properties when heated above its critical temperature  $250^{\circ}$ - $630^{\circ}$  for per required desired properties in applications of the material.
- Long handle tong/crucible tong also used for holding the samples before and after heat treatment (HT) processes. These metal tongs with a wooden long handles are a scissor-like tools used to grip/lift hot NiTi specimens instead of holding them directly with hands.
- The Annealing process is applied for 16 hours-24 hours, which alters the microstructure of a NiTi material to change its mechanical or electrical properties after it has been subjected to thermal conditions. Typically, in for 'shaping of SMA alloy' this is used to reduce hardness, increase ductility and help eliminate internal stresses.
- The normalizing process applied for 6 hours – 8 hours if required, which is a heat treatment process used to make NiTi material more ductile and tough after it has been subjected to thermal conditions.

### 3.3.1 Design Parameters statement

SMA's most common form available is wire (drawn conditioned) when compared to other forms it provides the maximum amount of force per cross-sectional area i.e. similar to ribbon form. The length of the SMA wire represents in the terms of stroke and difference in the stain between high temperatures to low temperatures. The bias springs can be formed/ designed by using the stroke to strain ratio in shape memory alloys.

➤ **For drawn wire**, according to José r. Santiago [15]

The length of NiTi-based SMA (wire) is estimated:

$$L = S / \Delta\varepsilon \quad (1.1)$$

Where 'S' represents the stroke parameter in NiTi

And  $\Delta\varepsilon$  is the difference in strain between the low and high operating temperatures.

$$\Delta\varepsilon = \varepsilon_l - \varepsilon_h \quad (1.2)$$

The low-temperature strain is a selected value and as is the case for the high-temperature stress also limits the number of cycles before failure for the actuator. For flexinol, this value can be as high as 8% for a specific cycle; basically, these values are dependant on the type of alloy implemented. From Hooke's Law,

The high-temperature strain:

$$\varepsilon_h = \sigma_h / E_h \quad (1.3)$$

Where 'E<sub>h</sub>' represents Young's Modulus of the material (at the high temperature)

The length increment of the wire at the high temperature becomes:

$$L_i = \varepsilon_h \cdot L \quad (1.4)$$

Now, assuming no two-way training is present in the SMA element the total bias force (or opposite load) required to revert the wire to its martensitic untwined or deformed state can be described as follows:

$$F_r = \sigma_l \cdot A \quad (1.5)$$

Where 'A' is a cross-section area of the wire

➤ **For strip, or ribbon shape**

: A strip shape may provide the same amount of force per cross-sectional area as wire. Among the advantages of using this type of shape is the increased cross-sectional area, which translates to a higher force and an SMA strip can also replace a wire bundle making it more attractive when fastening. The calculation for this type of shape follows that of wire with the only difference being the element area:

$$A = w \cdot h \quad (1.6)$$

The dimensions in the strip element:

$$R_{w-h} = w / h \quad (1.7)$$

R<sub>w-h</sub> represents the strip's width to height ratio. When an SMA has bent the stresses at the surface area of the bent region will be higher than the rest of it. As a result the life of the element is considerably reduced.

Gilbertson [15] recommends the minimum bend radius for a wire:

$$r_{\min} = 50 \cdot d \quad (1.8)$$

In which, 'd' represents the wire diameter and 'r<sub>min</sub>' is the minimum bend radius.



For strip this value is '50' times the height:

$$r_{\min} = 50 \cdot h \quad (1.9)$$

Designing for the lowest possible height, the strip area becomes:

$$A = R_w \cdot h \cdot h^2 \quad (\text{where } A = F_r / \sigma_1) \quad (1.10)$$

Shape memory helical / helix shape offers an increased amount of stroke at the expense of a reduced actuation force. The increased stresses that develop in the wire when setting this form can also potentially reduce its life considerably (spring/helix shape is applied).

### 3.3.2 Preparation of 1.0mm NiTi-based SMA spring

Muffle voltage regulator was set at 530°C for 35 minutes and the NiTi/flexinol wire of 0.040" or 1.0mm to made typical helical with a mean diameter of helical spring 7.2mm and 6 no. of turns. The relation in the composition of this alloy used as 49% (Ni) – 51 % (Ti). The copper critical temperatures range & mild steel critical temperatures range lie between 900- 940°C and 1510-1537°C respectively. So, no issues of heating of copper and mild steel during SMA spring formation were considered. Threaded Screw portion and supporting materials were applied which performed as restraint material, fixtures material, and clamping material as:

**(i) Threaded Screw:** It is shown in Figure 3.2 (a); threads are cut on circumference. The Length of screw Part= 21.6 mm, diameter (d1 = 6.4mm) and diameter (d2 = 8.0mm).

**(ii) End restraints:** It is shown in Figure 3.2 (b); two ends restraint of copper wires were applied. The constrained in the form of a bunch of wires is used and each wire has which diameter = 0.1 mm, When SMA material is processed for annealing, the temperature of it must remain below the critical temperature for phase change of these Ends restraint. These are used left/right side of the screw part. Dimensions of copper wire are following: Length of each wire=13.6mm, No. of wires = 12- 16, the diameter of wire = 0.1mm.

**(iii) Steel Fixture:** Then fixture was used, the material of fixture is mild steel having a high critical temperature above 1510°C, it is made in engineering workshop by lathe machining operation and formed in the form of a sleeve. Then gripping marked on the surface of it. The numbers of gripping mars are two only and at equal -distance measured from ends. Then it is converted into two halves with the help of a cutter. Dimension of Fixture are following:-Length=23.6mm, Inner diameter=3.8mm, Outer diameter= 4.4mm.

(iv) **Clamping Wire:** It is shown in **Figure 3.2 (c)**; the wire used for clamping is also made of copper wire so that SMA material processed for annealing, the temperature of it must remain below the critical temperature for phase change. The diameter of the wire ( $D_w$ ) = 0.8mm and two equal lengths of wire, each value  $L_w = 24.5$ mm. The wire is wound on the thread cuts portion of a screw as shown in figure 3.2 (c) and applied to the supporting material. End restraints are provided before the annealing process.

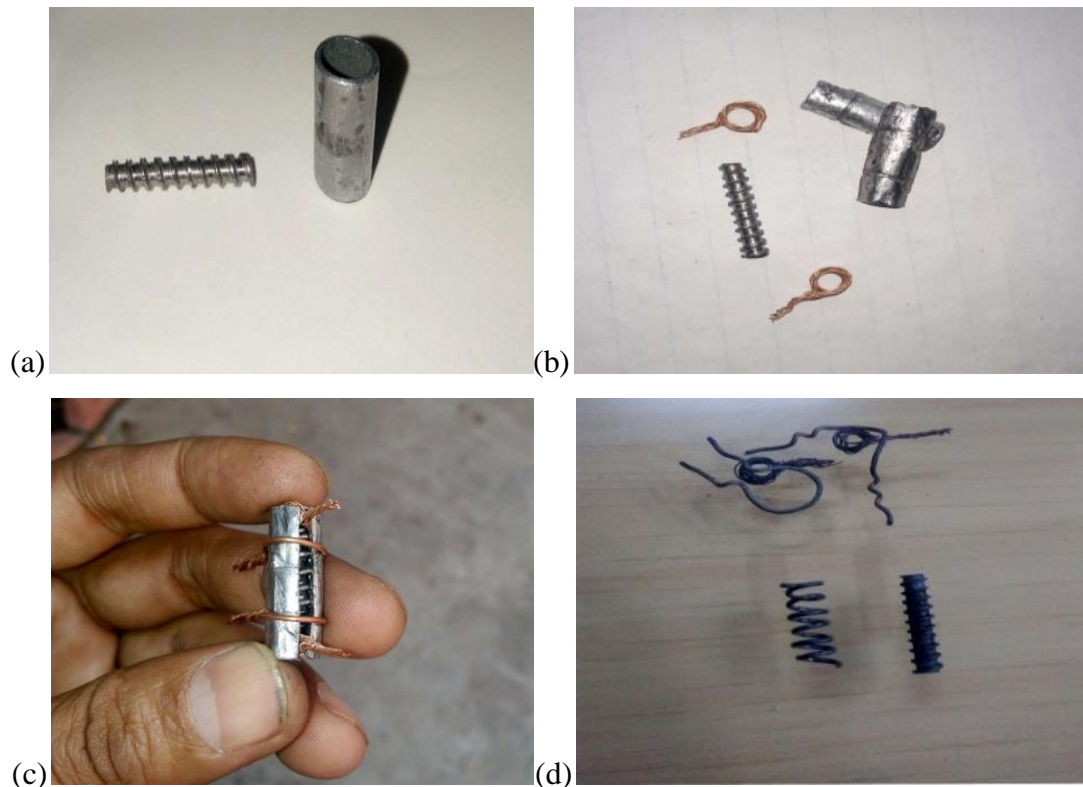


Figure 3.2 Preparation arrangement of 1.0mm SMA involves (a) threaded screw & MS hollow part, (b) end restraints (Cu) & MS fixture, (c) sample before HT processes, and (d) final SMA spring (1.0mm)

### 3.3.2.1 Design helical spring parameters of 1.0mm SMA

The One-way intelligent helical spring of 1.0mm obtained after annealing behaves like a common helical spring but is more ductile with respect to previous material.

So working parameters like forces and stresses must have significant values. The following were the parameters: -

Mean spring coil diameter ( $D_1$ ) = 7.2mm,

Wire diameter ( $d_1$ ) = 1.0 mm,

Number of turns ( $n_1$ ) = 06,

Initial free length of spring ( $L_{initial}$ ) = 21mm.

Spring index ( $c_1$ ) =  $D_1 / d_1 = 7.2 / 1.0 = 7.2$

Spring constant or Stiffness ( $k_1$ ) = Load / unit deflection

$W_1$  or  $F_1$  represents the axial force or load applied,

$x_1$  or  $\delta_1$  represents the extension or deflection in one direction,  $F_1$  or  $W_1$  directly proportional to  $x_1$  or  $\delta_1$ ,

$$k_1 = -F_1/x_1 = -W_1/ \delta_1 \quad (1.11)$$

Correction factor ( $K_1$ ), Wahl correction factor ( $K_{w1}$ ), and shear stress ( $\tau_1$ ) can be calculated for 1.0mm NiTi based shape memory alloy intelligent spring by using the following strength of materials equations (spring expressions) as:

$$\tau = \frac{8.F.D}{\pi d^3} . K = \frac{8.F}{\pi d^3} . C . K \quad (1.12)$$

$$K_w = \frac{4C-1}{4C-4} . K = \frac{0.615}{C} \quad (1.13)$$

In the same manner, another intelligent SMA helical spring was also made for 1.0mm SMA wire.

### 3.3.3 Preparation of 0.5mm NiTi-based SMA spring

The thin flexinol wire of 0.020" or 0.5mm wire was converted into conical spring (helix form) with the help of spring tool, clamping wire, and muffle furnace to know the effect of unique parameters response for its actuation. The relation in the composition of this alloy used as 49.2% (Ni) – 50.8 % (Ti). The process of annealing was done on 0.5mm NiTi wire i.e. SMA wire continuously heated at constant temperature for 45minutes. Then switched-off furnace and specimen remained for 24 hours inside it.

The NiTi wire was wounded upon the threaded provided surface of the spring tool and then clamping wire was used to sustain its position over the NiTi wire as shown in Figure 3.3 (b). The annealing is done by the temperature of muffle furnace for preset-condition by the muffle regulator and the temperature maintained at 550°C.

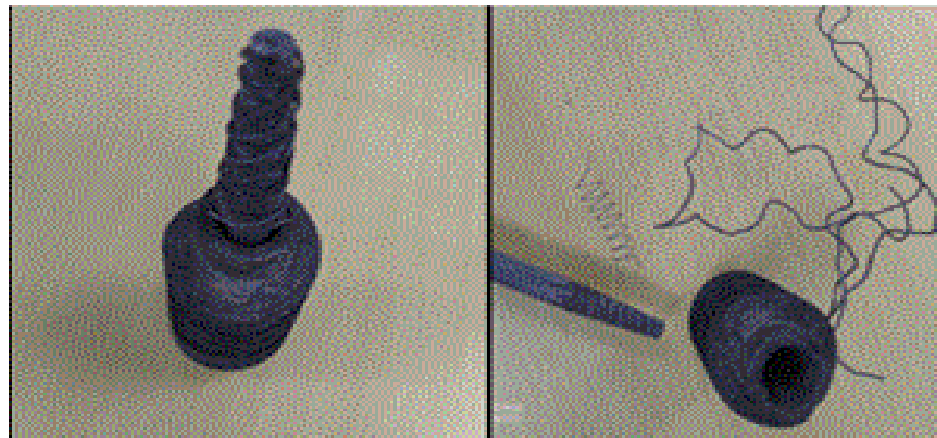


**Fixture-cum-spring tool**

(a)

**Clamping wire (soften MS)**

(b)



**Hollow straight Holder**

(c)

**Final SMA Spring (0.5mm)**

(d)

Figure 3.3 Preparation arrangement of 0.5mm SMA involves (a) fixture-cum-spring tool, (b) clamping wire (soften mild steel), (c) hollow straight holder, and (d) final SMA spring (0.5mm)

### 3.3.3.1 Design helical spring parameters of 0.5mm SMA

The One-way intelligent helical spring of 0.5mm obtained after annealing behaves like a common helical spring but is more ductile with respect to previous material. So working parameters like forces and stresses must have significant values.

The dimensions of 0.5mm NiTi based SMA wire obtained as: Mean coil diameter ( $D_2$ ) = 7.7mm, Inner coil diameter (Apex-End) = 5.5mm, Wire diameter ( $d_2$ ) = 0.5 mm, Number of turns ( $n_2$ ) = 08, Outer coil diameter (Base-End) = 9.8mm.

And initial free length of spring ( $L_{\text{initial}}$ ) = 2.1cm. Spring index ( $c_2$ ) =  $D_2/d_2 = 7.7/0.5 = 1.54$ , Spring constant or Stiffness ( $k_2$ ) = Force or Load / unit deflection,  $W_2$  or  $F_2$  represents the axial force or load applied,

$x_2$  or  $\delta_2$  represents the extension or deflection in one direction,

$F_2$  or  $W_2$  directly proportional to  $x_2$  or  $\delta_2$ ,

$$k_2 = -F_2/x_2 = -W_2/\delta_2 \quad (1.14)$$

Correction factor ( $K_2$ ), Wahl correction factor ( $K_{w2}$ ) and shear stress ( $\tau_2$ ) can be obtained for 0.5mm NiTi based shape memory alloy intelligent spring by using equation 1.12 and equation 1.13 respectively.

### 3.3.4 Preparation of 0.2mm & 0.1mm NiTi-based SMA springs

The thin flexinol wires of 0.004" or 0.1mm and 0.008" or 0.2mm were converted into helical spring (helix form) with the help of spring tool, drill bits, and muffle furnace to know the effect of unique parameters response for its actuation as shown in **Figure 3.4 (b)**. The relation in the composition of this alloys used in both SMA's as 49.2% (Ni) – 50.8 % (Ti).

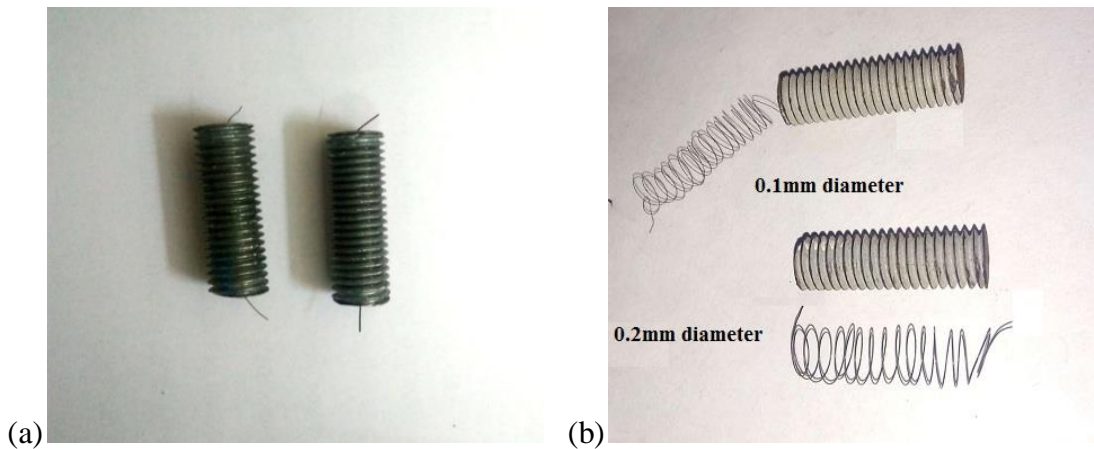


Figure 3.4 Preparation arrangement of 0.2mm and 0.1mm SMA's involves (a) fixture-cum-spring tool (pre-final), and (b) Final SMA's springs of 0.1mm and 0.2mm

: The annealing is done by the temperature of muffle furnace for preset-condition by muffle regulator and the temperature maintained at 530°C. The time of the annealing process of the SMA wires 0.1 & 0.2 was 16 hours. Then the normalizing process was also used by just opening the door of the muffle furnace but the piece was maintained inside of it for up to 6 hours. The preparations of fixture-cum-spring tools or spring tools are done separately in the work.

This tool removed the fixtures, clamping devices, and wrapping wires (detailed theory of fixture-cum-spring tool formation mentioned the same as-referred in ‘chapter 6’). The following working tools are considered during the preparation of one-way smart intelligent SMA helical springs of 0.1mm and 0.2mm as:

**(i) Drill-Machine** (230V/2200rpm) mainly used to drill the mild steel with the holes of different sizes in the center-face side of both the spring tools.

**(ii) Electric cutter** (3000rpm/400W) used with cutter & buffing wheel, The ceramic cutter used here which made of silicon carbide and having 6 inches diameter with a thickness of 1.0mm. The buffing wheel is also made of ceramic material and applied to smoothing a work piece's surfaces.

**(iii) Drill bits** (0.8mm, 0.9mm, 1.0mm, 1.5mm) are cutting tools used to remove material to create holes, almost always of circular cross-section.

The bench-vice (fixed-base), hand threaded tool (external threading for pitch equal to 1.25mm by using die-stock), vernier caliper (digital type), and various general tools used in engineering workshop, etc.

### 3.3.4.1 Design helical springs parameters of 0.2mm and 0.1mm SMA's

This included the mean coil diameter of 0.1mm SMA helical spring = 6.5mm + 0.10mm = 6.6mm, outer coil diameter of it = 6.7mm and inner coil diameter r= 6.5mm. Similarly, mean coil diameter of 0.2mm SMA helical spring = 6.5mm + .02mm = 6.7mm, outer coil diameter of it = 6.9mm and inner coil diameter = 6.5mm.

The dimensions of 0.2mm NiTi based SMA wire obtained as:

Mean coil diameter ( $D_3$ ) = 6.7mm,

Wire diameter ( $d_3$ ) = 0.2 mm,

No. of turns ( $n_3$ ) = 16,

Spring index ( $c_3$ ) =  $D_3/d_3 = 6.7 / 0.2 = 33.5$

Spring constant or Stiffness ( $k_3$ ) = Force or Load / unit deflection

$W_3$  or  $F_3$  represents the axial force or load applied,

$x_3$  or  $\delta_3$  represents the extension or deflection in one direction,

$F_3$  or  $W_3$  directly proportional to  $x_3$  or  $\delta_3$ ,

$$k_3 = -F_3/x_3 = -W_3/ \delta_3 \quad (1.15)$$

Similarly, the dimensions of 0.1mm NiTi based SMA wire obtained as:

Mean coil diameter ( $D_4$ ) = 6.6mm,

Wire diameter ( $d_4$ ) = 0.1 mm,

No. of turns ( $n_4$ ) = 18,

Spring index ( $c_4$ ) =  $D_4/d_4 = 6.6 / 0.1 = 66.0$

Spring constant or Stiffness ( $k_4$ ) = Force or Load / unit deflection

$W_4$  or  $F_4$  represents the axial force or load applied,

$x_4$  or  $\delta_4$  represents the extension or deflection in one direction,

$F_4$  or  $W_4$  directly proportional to  $x_4$  or  $\delta_4$ ,

$$k_4 = -F_4/x_4 = -W_4/ \delta_4 \quad (1.16)$$

Correction factors ( $K_3, K_4$ ), Wahl correction factors ( $K_{w3}, K_{w4}$ ) and shear stress ( $\tau_3, \tau_4$ ) can be calculated for 0.2mm and 0.1mm NiTi based shape memory alloy intelligent springs by using equation 1.12 and equation 1.13 respectively.

### 3.4 ARRANGEMENT/EXPERIMENTAL SETUP

This part of the work used two types of arrangements/experimental set-ups. The first one is in the separated form; all components of the experiment have been divided. The second one is in the combined form in which all components of the experiment have compiled at the common platform but the values of readings obtained for deformed SMA's intelligent NiTi based helical springs were same. Both values of readings have been cross-verified i.e. obtained nearly the same.

(i) **Experimental setup in the separated form:** Different SMA wires (drawn conditioned) were treated at different temperatures as 330°C, 430°C, 530°C, and 550°C for the formation of SMA helical springs. Two wires were discussed: 0.1mm wire and 1.0mm wire which were used for the heat treatment process (annealing/normalizing, if required) i.e. 0.1mm at 330°C, 1.0mm at 430°C, 1.0mm at 530°C, and 0.1mm at 550°C. It includes the temperature sensor i.e LM35 which is one type of transistor having three legs. In this sensor, two ceramic capacitors are attached for the accuracy of volt measurement. The component is used as a temperature sensor in the presented work.

The other main components are included as digital multimeter, power supply (DC), and Electronic kit (used as power point through lead-connectors). The Arrangement or set-up of various main components with temperature sensor is shown in **Figure 3.5**.

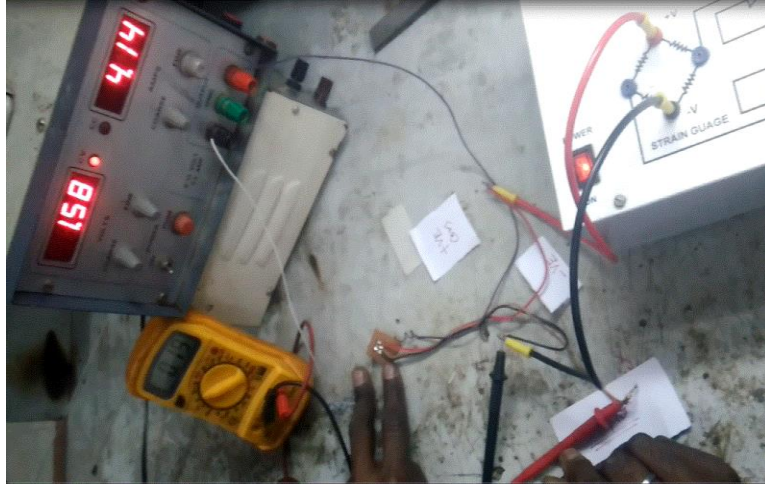


Figure 3.5 Experimental Setup in separated form

**Digital-Multimeter:** It is a standard diagnostic tool for technicians in the electrical/electronic industries. A multimeter has also known as a VOM (volt-ohm-milliammeter) is an electronic measuring instrument that combines several measurement functions in one unit. There are two basic types of multimeters such as digital and analog multimeters but work applied digital-type due to better accuracy in measurements, reduce reading and interpolation errors, to very small changes in input voltages parallax errors are eliminated, auto polarity function to avoid wrong polarity, etc. This digital multimeter is used as a test tool here to measure two electrical values i.e. principally voltage (volts), current (amps) as shown in Figure 3.5.

**DC Power Source:** The power input Voltage = 0-15 volt, Current = 0-5 AMP, three connecting point as +ve terminal, -ve terminal & ground terminal (GND).

**Strain gauge kit or amplifier circuit (operational type):** The load cell had analog to digital converter (ADC) IC from interim in which circuit used digital panel meter to give alphanumerical display as digital panel voltmeter (detailed mentioned same as-referred in 'chapter 5').

**Temperature sensor (LM35):** A temperature sensor LM35 has been used; this sensor comes under semiconductor-type (detailed mentioned same as-referred in 'chapter 5').

**Deformed SMA's:** A shape-memory alloy is an alloy that can be deformed when cold but returns to its pre-deformed (remembered) shape when heated.



It may also be called memory metal, memory alloy, smart metal or smart alloy. The various SMA's have been deformed in this presented work as per requirements such as 0.1mm and 1.0mm.

**(ii) Experimental setup in combined form**

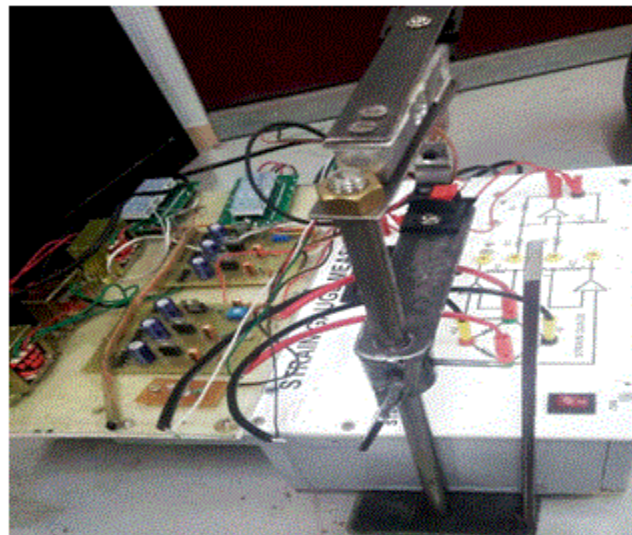
: The experimental setup was used for shape memory alloy NiTi-based helical springs to with help of combination various prepared parts and various arrangements of components which had been implemented in a particular manner so that results or output can be obtained (the detail of this set-up same as-referred in chapter '5').

The main components /parts as shown in **Figure 3.6** included:

- Iron-Stand: base plate with the vertical column, cylindrical rod, adjustable lower plate with locking
- Load Cell (20 Kg)
- Temperature Sensor (LM35)
- Amplifier Circuit (Operational)
- DC Supply (0-15 volt) Resistors(1k-10k)
- Capacitor-1000mf/25v,1mf/63v
- Diode-Electrolytic
- Rectifiers-BridgeIN4007



Deformed NiTi testing approach



Setup or arrangement

Figure 3.6 Experimental Setup in combined form

- 3terminal, Nuts, bolts, washers, scale etc
- Transistors Transformers (Set-down909)
- Inductors (coil/wound)

### 3.5 OBSERVATIONS OF BASIC PARAMETERS FOR VARIOUS CONSTANT TEMPERATURES CONDITIONS

In this experimental work, few NiTi-based actuators were considered for observation. For basic parameters i.e. voltage, temperature, and length of actuator measurements are taken here. Two types of readings are taken for the length of an actuator i.e. expansion to compression and compression to expansion.

Figure 3.6; Initially, NiTi-based wires in the drawn condition in terms of different sizes, shapes, initial conditions, and compositions converted into intelligent helical springs by annealing and normalizing (if required) processes for constant temperature conditions with the help of restraints wires, clamping wires and fixture. Initially, readings obtained are mentioned and the basic parameters included as applied voltages/ DC Supply (V), ( $L_c$ ) length in compression (end to end) or ‘displacement moves’ in downward, ( $L_e$ ) length in elongation (end to end) in upward, ( $W_t$ ) working/actuation temperatures are considered.

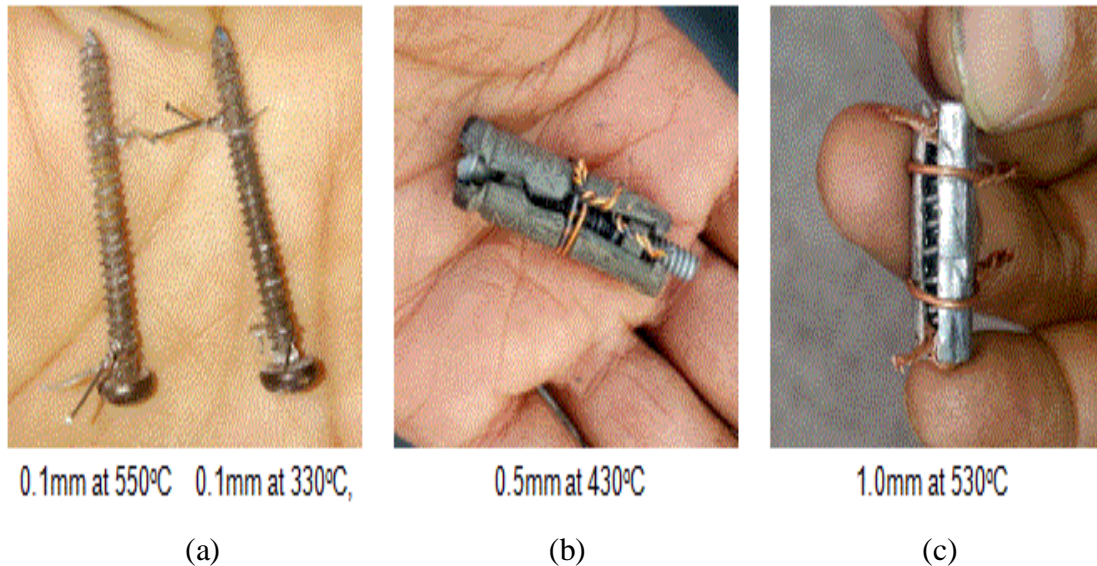


Figure 3.7 Constant temperatures conditions of various NiTi-based includes (a) 0.1mm SMA at 550°C & 0.1mm SMA at 330°C, (b) 0.5mm SMA at 430°C, and (c) 1.0mm SMA at 530 °C

➤ **For 0.5mm SMA at 430 °C**

**From Table 3.2,** shows the temperatures and lengths ( $L_c$ ) in which helical spring / 0.5mm SMA of 34mm length (end to end) in compression to expanded form obtained. When spring was set in compressed form i.e. with an initial length 14.3 mm at room temperature and when DC supply passed with preset voltages, then the temperature of spring start increasing, and following changes were observed in the length of helical spring as can be seen in tabular form.

Table 3.2 Parameters obtained at 430 °C for 0.5mm SMA  
(Compression to expansion)

Temperature in °C	Length ( $L_c$ ) of spring in 'mm'
20	14.3
23.2	16.5
27.3	22.3
30.5	27.7
34.1	31.2
37.5	33.3
40.1	34

Table 3.3 shows DC supply and lengths of spring in which helical spring / 0.5mm SMA of 35.2mm length (end to end) in expansion to compressed form obtained. When spring was set in expanded form i.e. with Initial length 52 mm at room temperature and when DC supply passed with preset voltages the following changes were observed in the length of helical spring as can be seen in tabular form.

Table 3.3 Parameters obtained at 430 °C for 0.5mm SMA (Expansion to compression)

DC Supply in 'Volt'	Length of Spring in 'mm'
0.5	52
1.2	49.4
1.9	45.2
2.3	41.4
2.6	39.1
3.1	37.2
4.1	35.2

**For 1.0mm SMA at 530 °C**

Table 3.4; shows temperatures, voltages, and lengths in which helical spring (1.0mm) SMA of 18.3mm length (end to end) in compression to expanded form obtained. When spring was set in compressed form i.e. with Initial length 5.2 mm at room temperature and when DC supply passed with preset voltages, then the temperature of spring start increasing, and following changes were observed in the length of helical spring as can be seen in tabular form.

Table 3.5; shows temperatures, voltages, and lengths in which helical spring (1.0mm) SMA of 26.3mm length (end to end) in expansion to compressed form obtained. When spring was set in expanded form i.e. with an initial length of 42mm at room temperature and when DC supply passed with preset voltages then the temperature of spring start increasing and following changes was observed in the length of helical spring as can be seen in tabular form.

Table 3.4 Parameters obtained at 530 °C for 1.0mm SMA  
(Compression to expansion)

Sr. No	Temperature in °C (Celsius)	DC Supply in V (Volt)	Length (L <sub>c</sub> ) of Spring in mm (End to End & Linearly )
1	22.4	1.0	5.2
2	25.2	1.5	10.1
3	29.6	2.0	14.2
4	35.1	2.5	16.4
5	40.2	3.0	18.3

Table 3.5 Parameters obtained at 530 °C for 1.0mm SMA  
(Expansion to compression)

Sr. No	Temperature in °C (Celsius)	DC Supply in V (Volt)	Length (L <sub>c</sub> ) of Spring in mm (End to End & Linearly )
1	22.4	1	42
2	25.1	1.5	39.4
3	28.6	2	34.6
4	34.2	2.5	30.2
5	39.2	3	26.3

Table 3.6; shows temperatures, voltages, and lengths in which helical spring (0.1mm) SMA of 19.3mm length (end to end) in expansion to compressed form obtained. When spring was set in expanded form i.e. with an initial length of 36.8mm at room temperature and when DC supply passed with preset voltages then the temperature of spring start increasing and following changes were observed in the length of a helical spring.

Table 3.7 shows temperatures, voltages, and lengths in which helical 0.1mm SMA helical spring of 18.1mm length (end to end) in compression to expanded form is obtained. When spring was set in compressed form i.e. with an initial length of 4.6mm at room temperature and when DC supply passed with preset voltages, then the temperature of spring start increasing, and following changes were observed in the length of helical spring as can be seen in tabular form.

Table 3.6 Parameters obtained at 550 °C for 0.1mm SMA  
(Expansion to compression)

Sr No.	Temperature in °C (Celsius)	DC Supply in V (Volt)	Length of H S in mm (End to End & Linearly )
1	19.6	0.9	36.8
2	23.0	1.3	29.2
3	25.1	1.8	26.4
4	28.9	2.2	23.0
5	34.3	2.6	19.3

Table 3.7 Parameters obtained at 530 °C for 1.0mm SMA  
(Compression to expansion)

Sr No.	Temperature in °C (Celsius)	DC supply in V (Volt)	Length of H Sin mm (End to End & Linearly)
1	20.1	0.8	4.6
2	23.9	1.4	8.8
3	25.2	2.1	12.4
4	29.6	2.5	15.2
5	34.5	2.8	18.1

**For 0.1mm SMA at 330 °C**

No need to find working temperatures and length of an actuator in both cases as compression to expansion or vice versa because NiTi-based helical SMA spring is not properly exactly formed in a helix shape.

**In further work**, a modified design of helical springs (physical-loading) was also implemented. For values of readings of that types of helix shape springs work applied the experimental set-up of a smart fork-lift. The smart fork-lift was implemented for physically loaded helical springs to find spring rates and this set-up is equipped with help of a combination of various prepared parts and various arrangements of components (the detail of this set-up same as referred in chapter ‘8’).

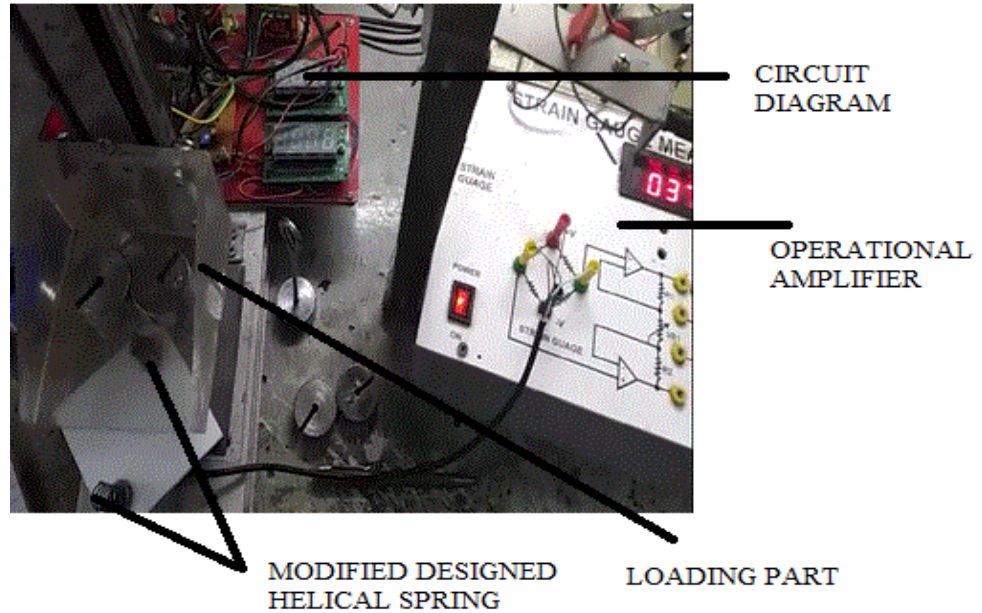


Figure 3.8 Experimental Setup

Figure 3.8 shows the main components/parts included as Bearings (4-pieces), Steel round bar (2-pieces), Load Cell (0-3.0Kg), Temperature Sensor (LM35), Transparent Acrylic Box, Power supply circuit (5V), Pulley and supports (Al-based), Load-Amplifier, Basic electrical-electronic components, Hanging wire (steel), terminals, Allen keys(Hard-steel), Nuts/bolts/washers, digital caliper, scale, etc.

For the counter check of spring rates readings of physically loaded helical springs used **in modified the design of helical springs**, the work also used the ‘Spring Load Stiffness Tester’ (JCBUST YMCA product).

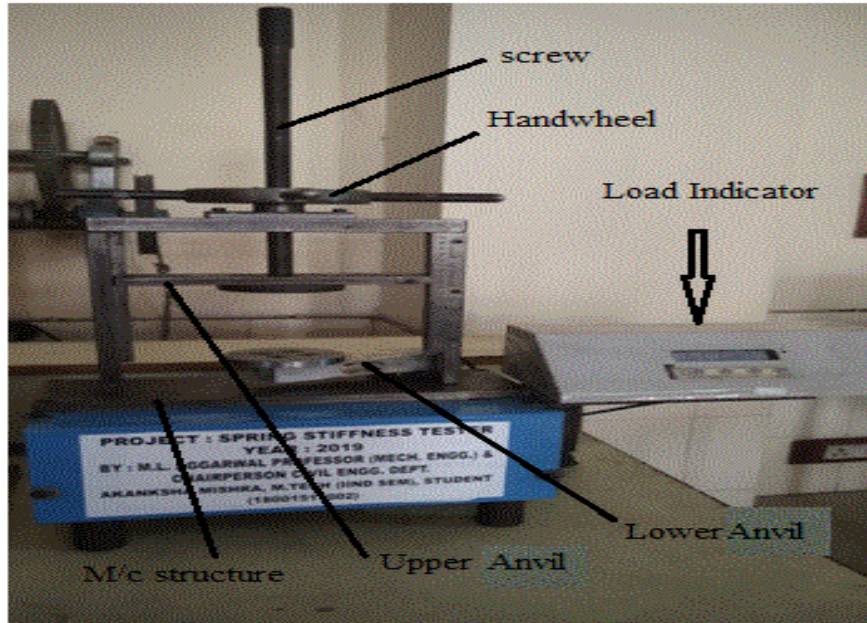


Figure 3.9 (Spring-load stiffness tester)

Figure 3.9 shows the experimental setup is shown (available in JCBUST YMCA) was used for testing the stiffness of spring samples. The spring sample to be tested is fixed between the two anvils, the lower one being fixed and the upper one movable. The upper anvil is moved to adjust the sample using the hand-wheel. The lower anvil is connected to the load cell.

### 3.6 SUMMARY

In the experimental work, flexinol is converted into a helical spring of the desired length by applying an annealing/normalizing process for constant temperature conditions with the help of restraints wires, clamping wires, fixtures, LM35, multimeter, electronic kit, and DC power supply. The description of the material's in which NiTi or flexinol wires were obtained in the drawn condition in terms i.e. sizes, shapes, initial conditions, compositions, and their properties have been discussed. Then the preparation of smart intelligent SMA helical springs one way operated and design helical springs parameters i.e. 1.0mm, 0.5mm, 0.2mm, and 0.1mm based on NiTi/flexinol were discussed. Basic actuation parameters are described on NiTi shape memory effect as the temperatures, actuating currents/voltages, and elongation length in compression & expansion in a shape memory alloy intelligent helical spring actuators.

The results of basic parameters for various constant temperatures conditions i.e. 330°C, 430°C, 530 °C, and 550 °C are obtained as mentioned in Tables 3.2, 3.3, 3.4, 3.5, 3.6, and 3.7 respectively.

The designed parameters have been calculated as the diameter of spring wire, coil diameter of spring, length of spring, and spring index for the NiTi materials by using the design equations for the various NiTi intelligent helical springs (having diameters i.e. 1.0mm, 0.5mm, 0.2mm, and 0.1mm respectively). Various experimental set up for analysis of various parameters have been described. The experimental set-ups for NiTi-based SMA's helical spring in separated form and second one combined form are discussed. For the modified design of helical springs (physical-loading) the experimental set-up of smart fork-lift was also discussed. For the counter check of spring rates readings of physical loaded helical also used the 'Spring Load Stiffness Tester'.



# **CHAPTER 4**

## **ESTIMATION OF VARIOUS PARAMETERS OF SMA INTELLIGENT HELICAL SPRINGS**

### **4.1 INTRODUCTION**

This chapter explores the parameters of shape memory alloy intelligent helical springs such as the temperatures, voltages, and elongations (length in compression and expansion). These springs have the capability to recover its original shape by eliminating residual deformations when subjected to thermo-mechanical stress made suitable for significant mechanical actuators. These actuators further may apply to mechanical equipment/devices. In this chapter the various temperature conditions i.e. 330°C, 430°C, 530°C, and 550°C are applied for exploring basic parameters of smart intelligent NiTi based SMA helical springs as prepared in the previous chapter '3' (NiTi/flexinol wires were obtained in the drawn condition in terms of different sizes, shapes; then intelligent helical springs processed by annealing and normalizing (if required) for various temperature conditions with the help of restraints wires, clamping wires and fixture, LM335 & DC power supply device). NiTi-based smart intelligent SMA helical springs having different wire diameters such as 1.0mm, 0.1mm, 0.5mm, and 0.1mm were set in compressed form and expanded form. The linear variation expressions were observed for preset compression lengths and expansion lengths with different values of voltages. Firstly the variations of temperature and length with respect to the DC source are represented. Secondly, the variations of length and temperature are shown. This chapter also includes a graph between various entities such as a wire in compression to expansion with DC supply, wire in expansion to compression with DC supply, wire in expansion to compression with temperature, and wire in compression to expansion with temperature. The effect on change in lengths of the intelligent helical SMA springs (NiTi-based) due to temperature helped in exploring parameters in terms of linear variation expression, equations & correlations coefficient. This chapter provides insight for manufacturing, design, and applications of shape memory alloy intelligent helical spring actuators.

### **4.2 BASIC PARAMETERS**

The nomenclature of basic parameter defined by various entities applied such as applied voltages =  $V$ , working/actuation temperatures =  $W_t$ , length in compression (end to end) or ‘displacement moves’ in downward =  $L_c$ , and length in elongation (end to end) or ‘displacement moves’ in upward =  $L_e$ , respectively.

### 4.3 EXPERIMENTAL RESULTS AND DISCUSSION

NiTi-based smart intelligent SMA helical springs having different wire diameters such as 1.0mm, 0.1mm, 0.5mm, and 0.1mm were set in compressed form and expanded form which is prepared at various preset temperatures conditioned in chapter ‘3’. The temperature of these forms increasing with the application DC source and the length of deformed intelligent helical spring results are analyzed.

#### 4.3.1 Experimental results and discussion of 1.0mm SMA at 530°C

When 1.0mm SMA helical spring was set in **compressed form**, the length of this deformed spring is considered linearly, and end to end. The DC source values in ‘Volt’, the temperature in ‘Celsius’ and length in ‘mm’ are measured in readings.

Table 4.1 shows an SMA spring (1.0mm) in compressed form i.e. with a length of 5.2mm at room temperature and when a current was passed, the temperature of the spring starts increasing and the length of the deformed intelligent helical spring ( $L_c$ ) increased. For example at an increase of length up to 16.4mm; at this stage, temperature 35.1°C, and voltage 2.5V are obtained.

Table 4.1 SMA spring (1.0mm) in compression to expansion

Variation of linear length with temperature (helical spring)		
Temperature in °C (Celsius)	DC Supply in V (Volt)	Length ( $L_c$ ) of Spring in mm (End to End & Linearly )
22.4	1.0	5.2
25.2	1.5	10.1
29.6	2.0	14.2
35.1	2.5	16.4
40.2	3.0	18.3
45.4	4.0	19.6
47.3	5.0	22.1

Figure 4.1 represents the variation of temperature and length of 1.0mm SMA at 530°C with respect to DC source in compression to expansion. For temperature and length, correlations coefficient values obtained as  $R^2 = 0.917$  and  $R^2 = 0.865$  respectively. It shows the variation of temperature with respect to length for 1.0mm SMA in compression to expansion and equation of model for compressed form obtained as follows with correlations coefficient  $R^2 = 0.931$ .

$$Y_{ce} = 5.649x + 19.13 \quad (4.1)$$

$$Y_{ce} = 2.878x + 9.729 \quad (4.2)$$

$$Y_{cm} = 0.556x - 4.483 \quad (4.3)$$

The equation (4.1) shows voltage supply to temperature with correlations coefficient value = 91.7%, equation (4.2) shows voltage supply to length with correlations coefficient value = 86.5% and equation (4.3) related with compressed model relationship between temperature and length with correlations coefficient value = 93.1% respectively.

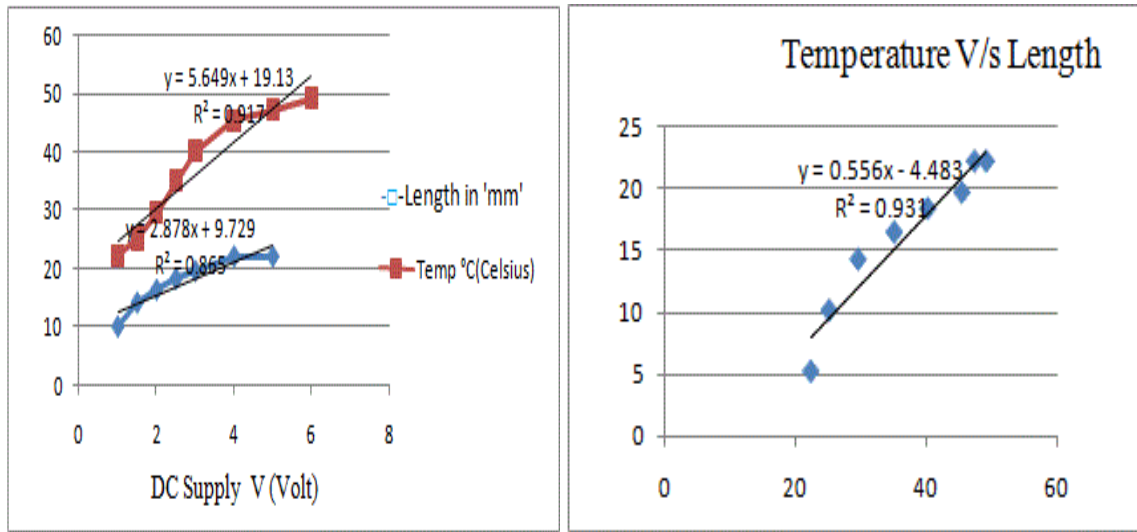


Figure 4.1 Temperature, and length of 1.0mm SMA in compression to expansion

When 1.0mm SMA helical spring was set in **expanded form**, the length of this deformed spring is also considered end to end and linearly. The DC source values in ‘Volt’, the temperature in ‘Celsius’ and length in ‘mm’ are also measured in readings.

Table 4.2 SMA spring (1.0mm) in expanded form i.e. with length 42mm at room temperature; then current was passed, the temperature of spring start increasing and length of deformed intelligent helical spring ( $L_e$ ) decreased. For example, a decrease of length up to 26.3mm; at this stage, temperature 39.2°C, and voltage 3.0V are obtained.

Equation (4.4) shows voltage supply to temperature with correlations coefficient value = 93.3%, equation (4.5) shows voltage supply to length with correlations coefficient value = 84.7%.

Table 4.2 SMA spring (1.0mm) in expansion to compression

Variation of linear length with temperature (helical spring)		
Temperature in °C (Celsius)	DC supply in V (Volt)	Length (L <sub>e</sub> ) of spring in mm (End to End & Linearly)
22.4	1.0	42.0
25.1	1.5	39.4
28.6	2.0	34.6
34.2	2.5	30.2
39.2	3.0	26.3
43.4	4.0	23.2
46.1	5.0	22.1

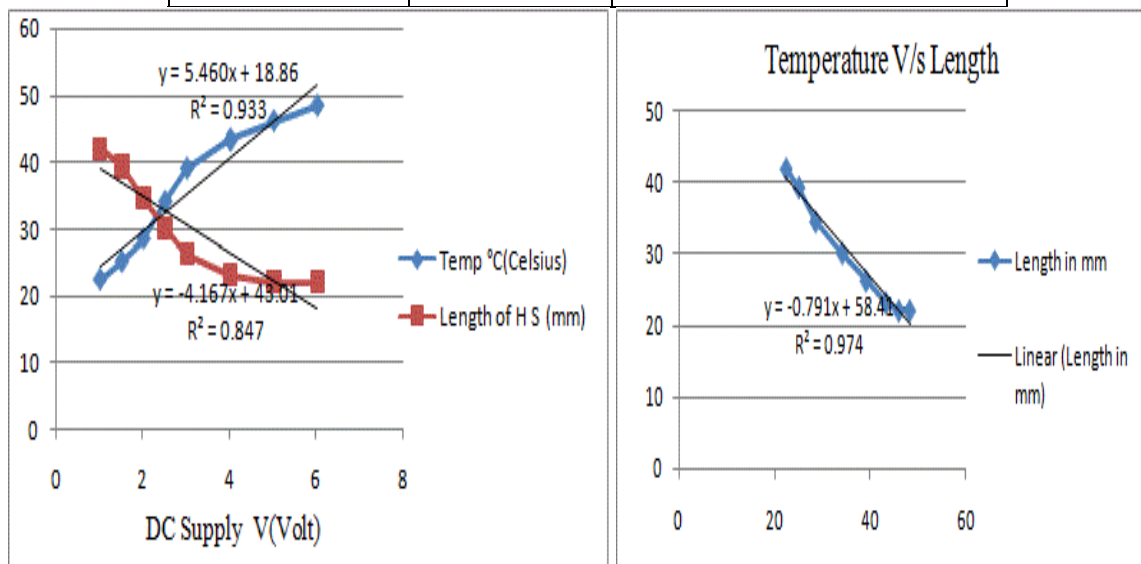


Figure 4.2 Temperature, and length of 1.0mm SMA in expansion to compression And the equation (4.5) related with the expanded model relationship between temperature, and length with correlations coefficient value = 97.4% respectively.

#### 4.3.2 Experimental results and discussion of 0.1mm SMA at 550°C

When 0.1mm SMA helical spring was set in **compressed form**, the length of this deformed spring is considered linearly, and end to end. The DC source values in 'Volt', temperature in 'Celsius' and length in 'mm' are measured in readings.

Table 4.3 shows the SMA spring (0.1mm) in compressed form i.e. with a length of 4.6mm at room temperature and when the current was passed, the temperature of the spring starts increasing and the length of the deformed intelligent helical spring ( $L_c$ ) increased. For example at an increase of length up to 18.1mm; at this stage, temperature 34.5°C, and voltage 2.8V are obtained.

Table 4.3 SMA spring (0.1mm) in compression to expansion

Variation of linear length with temperature (helical spring)		
DC Supply in V(Volt)	Length ( $L_c$ ) of spring in mm (End to End & Linearly )	Temperature in °C (Celsius)
0.8	4.6	20.1
1.4	8.8	23.9
2.1	12.4	25.2
2.8	18.1	34.5
3	19.3	37.2
3.5	19.3	40.1
4.5	19.3	43

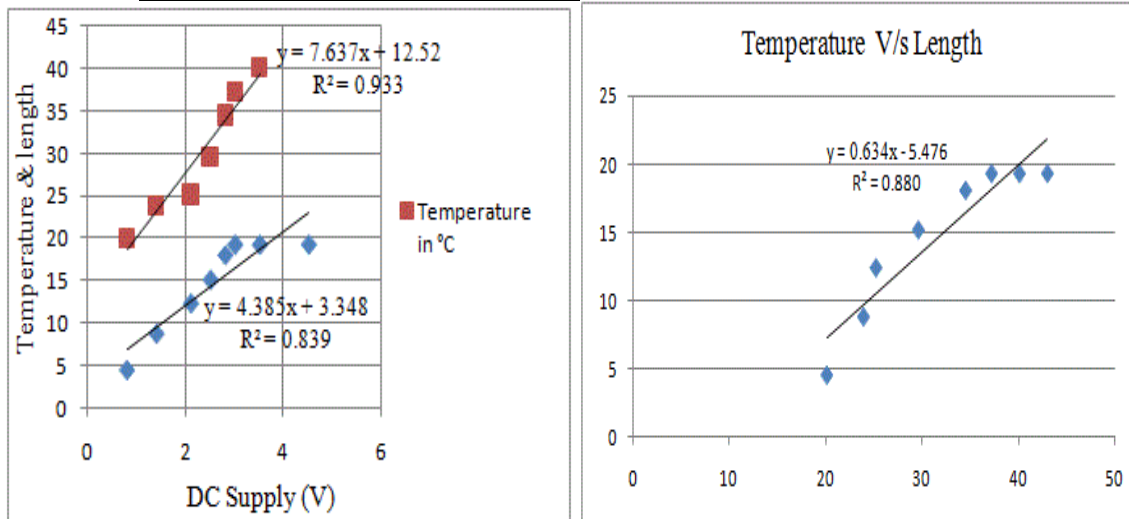


Figure 4.3 Temperature, and length of 0.1mm SMA in compression to expansion

Figure 4.3 represents the variation of temperature and length of 0.1mm SMA at 550oC concerning DC supply in compression to expansion. For temperature and length, correlations coefficient values were obtained as  $R^2 = 0.933$  and  $R^2 = 0.839$  respectively. It also shows the variation of temperature concerning length for 0.1mm SMA in compression to expansion, and equation of model for compressed form obtained as follows with correlations coefficient = 0.880.

$$Y_{ce} = 7.637x + 12.52 \quad (4.7)$$

$$Y_{ce} = 4.385x + 3.348 \quad (4.8)$$

$$Y_{cm} = 0.634x - 5.476 \quad (4.9)$$

The equation (4.7) shows voltage supply to temperature with correlations coefficient value = 93.3%, equation (4.8) shows voltage supply to length with correlations coefficient value = 83.9%, and equation (4.9) related with the expanded model relationship between temperature, and length with correlations coefficient value = 88.0% respectively.

When 0.1mm SMA helical spring was set in **expanded form**, the length of this deformed spring is also considered end to end and linearly. The DC source values in ‘Volt’, the temperature in ‘Celsius’ and length in ‘mm’ are also measured in readings.

Table 4.4 SMA spring (0.1mm) in expansion to compression

Variation of linear length with temperature (helical spring)		
DC Supply in V (Volt)	Temperature in °C (Celsius)	Length (L <sub>e</sub> ) of Spring in mm (End to End & Linearly)
0.9	19.6	36.8
1.3	23.0	29.2
1.8	25.1	26.4
2.2	28.9	23.0
2.6	34.3	19.3
3.5	38.0	19.3
5	40.3	19.3

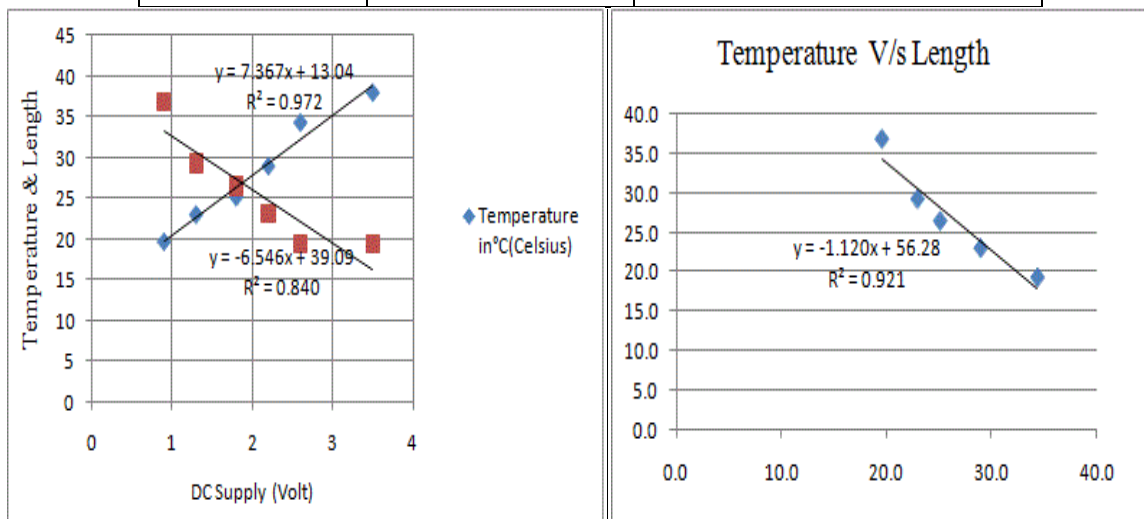


Figure 4.4 Temperature, and length of 0.1mm SMA in expansion to compression

Table 4.4 shows spring was set in expanded form i.e. with length 36.8mm at room temperature; then current was passed, the temperature of spring start increasing and the length of deformed intelligent helical spring ( $L_c$ ) decreased. For example at an increase of length up to 23.0mm; at this stage, temperature 28.9°C, and voltage 2.2V are obtained.

Figure 4.4 represents the variation of temperature and length of 0.1mm SMA at 550°C with respect to DC supply/source for expanded to compression form. For temperature and length, correlations coefficient values obtained as  $R^2 = 0.972$  and  $R^2 = 0.840$  respectively. It also shows the variation of temperature with respect to length for 0.1mm SMA in expansion to compression and the equation of the model for expanded form is as follows with correlations coefficient = 0.921%.

$$Y_{ec} = 7.367x + 13.04 \quad (4.10)$$

$$Y_{ec} = -6.546x + 39.09 \quad (4.11)$$

$$Y_{em} = -1.120 x_s + 56.28 \quad (4.12)$$

The equation (4.10) related with voltage supply to temperature with correlations coefficient value = 97.2%, equation (4.11) related with voltage supply to length with correlations coefficient value = 84.0% and equation (4.12) shows model relation of expansion to compression with correlations coefficient value = 92.1% respectively.

#### 4.3.3 Experimental results and discussion of 0.1mm SMA at 330°C

It is established that working temperatures, and length of actuator for compression to expansion or vice versa (in both cases); NiTi-based helical SMA springs are not exactly formed in helix shapes. So, measurements/readings are not taken here due to error in basic design, or manufacturing.

#### 4.3.4 Experimental results and discussion of 0.5mm SMA at 430°C

When 0.5mm SMA helical spring was set in **compressed form**, the length of this deformed spring is considered linearly, and end to end. The DC source values in ‘Volt’, the temperature in ‘Celsius’ and length in ‘mm’ are measured in readings.

Table 4.5; SMA spring (0.5mm) was set in compressed form i.e. with length 14.3mm at room temperature and when the current was passed, the temperature of spring starts increasing and the length of the deformed intelligent helical spring ( $L_c$ ) increased. For example at an increase of length up to 31.2mm; at this stage, temperature 34.1°C and voltage 2.7V are obtained.

Table 4.5 SMA spring (0.5mm) in compression to expansion

Variation of Helical Spring linear length with temperature		
DC Supply in V (Volt)	Temperature in °C (Celsius)	Length (L <sub>c</sub> ) of spring in mm (End to End & Linearly )
0.3	20	14.3
1.1	23.2	16.5
1.8	27.3	22.3
2.2	30.5	27.7
2.7	34.1	31.2
3	37.5	33.3
4.1	40.1	34
5	44.6	35.2

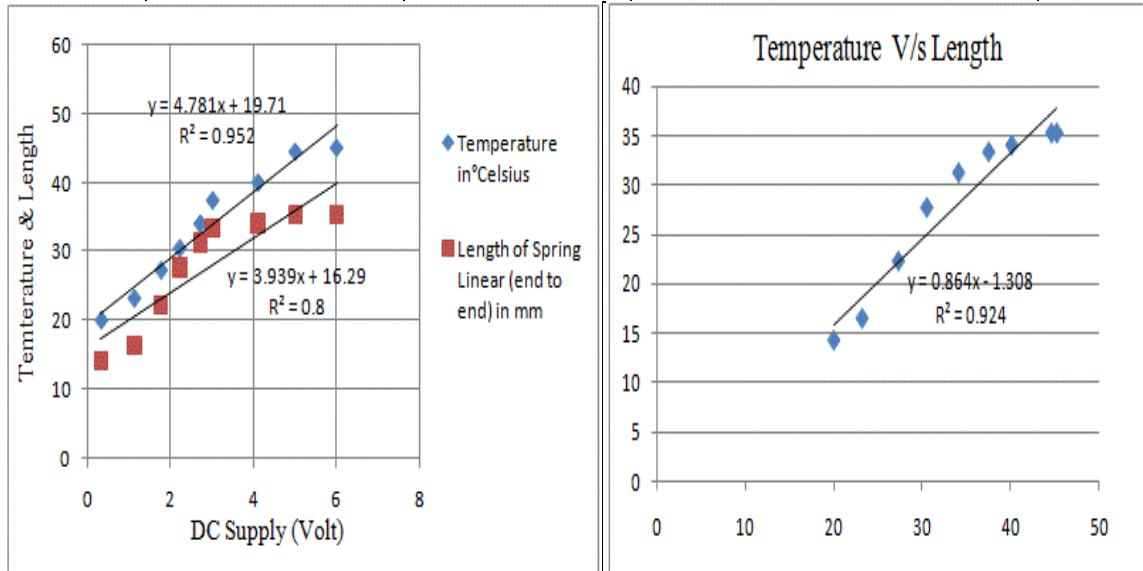


Figure 4.5 Temperature, and length of 0.5mm SMA in compression to expansion

Figure 4.5 represents the variation of temperature and length of 0.5mm SMA at 430°C with respect to DC supply in compression to expansion. For temperature and length, correlations coefficient values obtained as  $R^2=0.952$  and  $R^2=0.80$  respectively.

It shows the variation of temperature with respect to length for 0.5mm SMA in compression to expansion and equation of model for compressed form obtained as follows with correlations coefficient  $R^2=0.924$ .

$$Y_{ce} = 4.781x + 19.71 \quad (4.13)$$

$$Y_{ce} = 3.939x + 16.29 \quad (4.14)$$

$$Y = 0.864x - 1.308 \quad (4.15)$$



The equation (4.13) related with voltage supply to temperature with correlations coefficient value = 95.2%, equation (4.14) related with voltage supply to length with correlations coefficient value=80.0% and equation (4.15) shows model relation of expansion to compression with correlations coefficient value = 92.4% respectively.

When 0.5mm spring was set in **expanded form**, then length of deformed intelligent helical spring ( $L_e$ ) decreased. The DC source values in ‘Volt’, temperature in ‘Celsius’ and length in ‘mm’ are also measured in readings. The length of this deformed spring is also considered end to end, and linearly.

Table 4.6; spring was set in compressed form i.e. with length 52.0mm at room temperature; when the current was passed, the temperature of spring starts increasing, and the length of the deformed intelligent helical spring ( $L_e$ ) decreased. For example at a decrease of the length up to 37.2mm; at this stage, temperature 38.0°C and voltage 3.1V are obtained.

Table 4.6 SMA spring (0.5mm) in expansion to compression

Variation of linear length with temperature (helical spring)		
DC Supply in V(Volt)	Temperature in °C (Celsius)	Length ( $L_e$ ) of spring in mm (End to End & Linearly )
0.5	20.0	52.0
1.2	22.5	49.4
1.9	26.6	45.2
2.3	30.7	41.4
2.6	34.2	39.1
3.1	38.0	37.2
4.1	40.8	35.2
5.4	44.6	35.2

Figure 4.6 represents the variation of temperature and length of 0.5mm SMA at 430°C with respect to DC source for expanded to compression form. For temperature and length, correlations coefficient values obtained as  $R^2 = 0.946$  and  $R^2 = 0.846$  respectively. It also follows the variation of temperature with respect to length for 0.5mm SMA in expansion to compression and equation of model for expanded form obtained as follows with correlations coefficient  $R^2 = 0.957$ .

$$Y_{ec} = 5.451x + 17.77 \quad (4.16)$$

$$Y_{ec} = -3.776x + 51.78 \quad (4.17)$$

$$Y_{em} = -0.714x + 64.88 \quad (4.18)$$

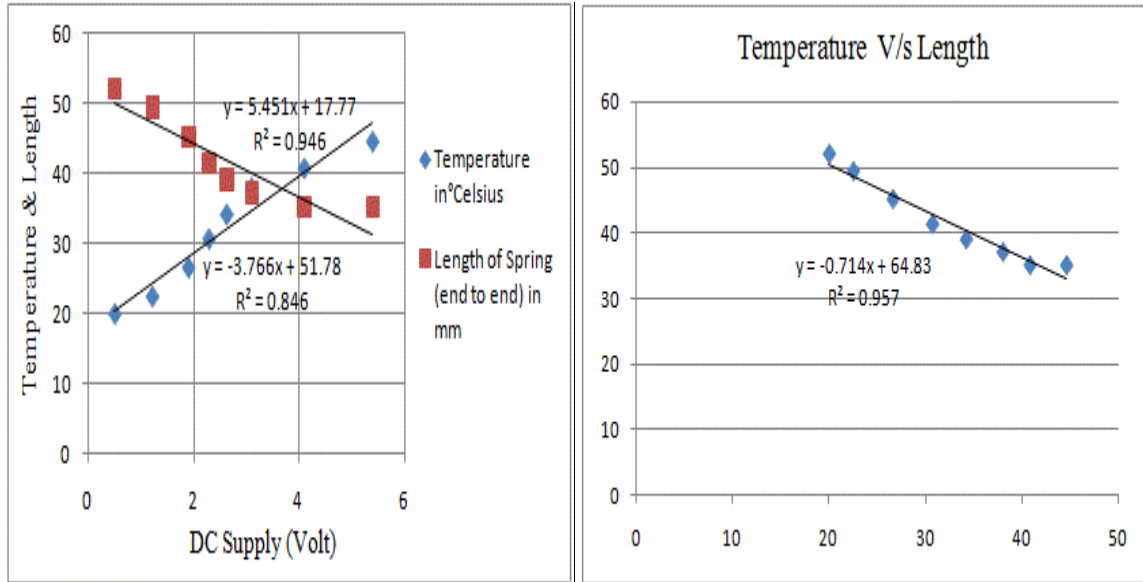


Figure 4.6 Temperature, and length of 0.5mm SMA in expansion to compression

The equation (4.16) shows voltage supply to temperature with correlations coefficient value=94.6% and equation (4.17) shows voltage supply to length with correlations coefficient value=84.6% respectively and equation (4.18) shows expanded model relation with correlations coefficient value=95.7% respectively.

#### 4.4 MODELING OF SMA'S BASED HELICAL SPRINGS ON CONSTANT TEMPERATURE CONDITIONS

The recommended approach of various SMA's having different wire diameters as 0.1mm, 0.5mm, 1.0mm, and 0.1mm can be seen in table 4.7 respectively. Here, effective model equations show the combined effect of compressed and expanded form results as: -

$$Y^I = 0.556x - 4.483 - 0.791x + 58.41 = -0.235x + 53.93 \quad (4.19)$$

$$Y^{II} = 0.634x - 5.476 - 1.120x + 56.28 = -0.486x + 50.80 \quad (4.20)$$

$$\text{And } Y^{III} = 0.864x - 1.308 - 0.714x + 64.88 = 0.150x + 64.57 \quad (4.21)$$

The effective equations 4.19, 4.20 and 4.21 represented for 1.0mm, 0.1mm and 0.5mm SMA's respectively. And correlations coefficients obtained for 1.0mm, 0.1mm and 0.5mm SMA's as under: -

$$\text{Effective model equation for 1.0mm SMA} = (93.1 + 97.4) / 2 = 95.25\%$$

$$\text{Effective model equation for 0.1mm SMA} = (88.0 + 92.1) / 2 = 90.05\%$$

$$\text{Effective model equation for 0.5mm SMA} = (92.4 + 95.7) / 2 = 94.05\%$$

Table 4.7 Observations of 0.1mm, 0.5mm, 1.0mm, and 0.1mm SMA's

Wire Diameter	Initial Condition	Temp (°C)	Formation of helical spring	SME (after deforming)	Recommend approach
0.1mm	Straight annealed	330 <sup>0</sup>	Proper	Reshaped but Not exactly	Less suitable
0.5mm	Straight annealed	430 <sup>0</sup>	Proper	Reshaped	more suitable
1.0mm	Straight annealed And soften	530 <sup>0</sup>	Proper	Reshaped	more suitable
0.1mm	Straight annealed And soften	550 <sup>0</sup>	Proper	Reshaped	suitable

From the results, as shown in **Table 4.7**, linear variation expressions are observed for preset compression length and expansion length with different values of voltages. The effect on change in length of the SMA springs (NiTi based) was observed with respect to temperatures that help to analyze its basic parameters.

#### 4.5 SUMMARY

This chapter explores the parameters such as temperature, length in elongation, length in compression, and current/voltage values in terms of linear expressions. This work helps in the manufacturing and design of shape memory alloy intelligent helical spring actuator. The modeling equations are helpful in the design of intelligent helical spring actuator and can be used for various purposes as launching devices, automation devices, etc. The study is specifically focused on heat treatment process temperatures for manufacturing of NiTi-based shape memory alloy intelligent springs i.e. 330°C, 430°C, 530°C, and 550°C for 1.0mm, 0.1mm, and 0.5mm respectively. This work helps to choose the suitable heat treatment constant temperature condition of NiTi-based SMA's which is applied for the formation of intelligent helical spring actuators for mechanical equipment. This chapter also provides insight for manufacturing, design, and applications of shape memory alloy intelligent helical spring actuators by using the above model equations which having effective correlations coefficient values  $\geq 94.0\%$ .

# CHAPTER 5

## DESIGN OF NiTi SMA FOR ACTUATING HELICAL SPRING

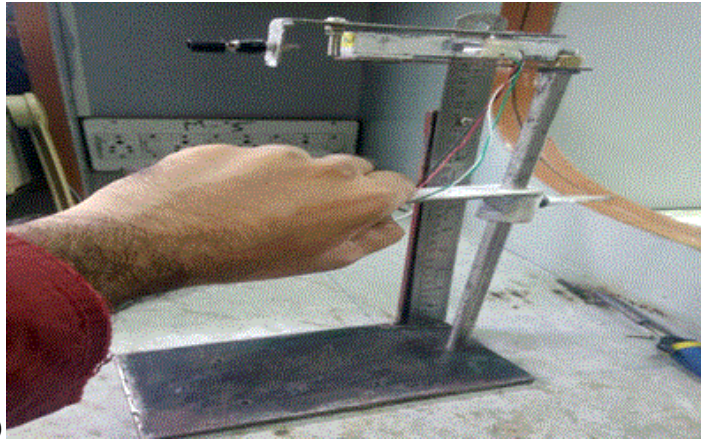
### 5.1 INTRODUCTION

In this chapter, a model has been formulated which can enable the stability of one-way intelligent helical spring SMA by measuring its parameters before implementing it in mechanical equipment. The parameters included in this present work as average scale values, load-cell strain, load capacity, current, working temperature, atmospheric temperature, and applied voltage. Electronic components such as capacitors, registers, PN diodes, transistors, rectifiers, IC7107, and also electrical components such as power supply, inductors, transformers cables, sockets, connectors were used for experimentation. Two temperature sensors were applied, one for SMA wire & the other for accuracy of load-cell. The SMA was first annealed & normalized then formed in an intelligent helical spring by using the ends constrained, fixtures, and clamping wires so that adequate dimensioned helical springs were obtained. In the presented work, 1.0mm NiTi-based one-way intelligent helical spring wire was considered for observations with preset conditions as a small actuator before implementing in a mechanical instrument/equipment. The development of a physical model for a 1.0mm NiTi-based one-way intelligent helical spring in terms of various actuation parameters was also estimated. The investigation objective considered establishing a physical model based on SMA helical springs. This working model be measure NiTi-based helical SMA springs at any predefined condition up to 20Kg.

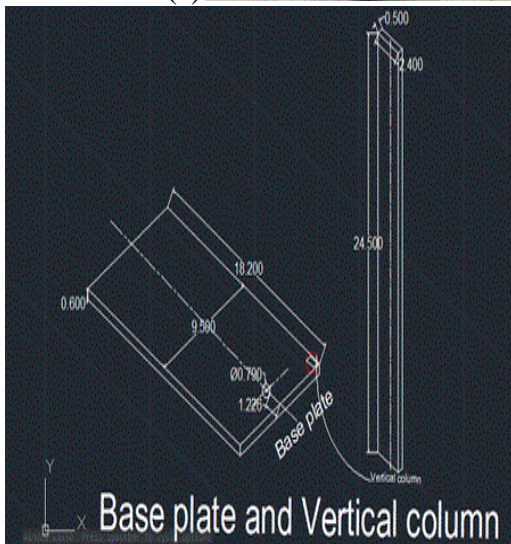
### 5.2 MAIN COMPONENTS/PARTS

The sub-parts included as iron stand, load cell, temperature sensor, amplifier circuit, dc supply, and basic electronic-electrical components.

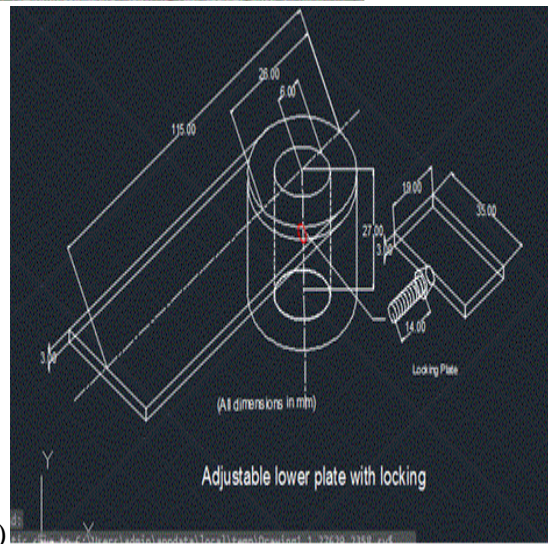
**(I) Iron Stand:** Iron has melting point 2800F, working temperature range of NiTi is very low as compare to Iron. Iron stand in **Figure 5.1(a)** shows the captured photo comprised of sub-parts such as base plate and vertical column, cylindrical rod (vertical type), and adjustable lower plate with locking.



(a)



(b)



(c)

Figure 5.1 Iron Stand (a) captured photo, (b) base plate and vertical column, and (c) adjustable lower plate with locking

**Base plate and vertical column:** It can be seen from **Figure 5.1(b)**, which is made with the help of AutoCAD software of Autodesk Company Version-2017.

Base plate has dimension = 18.2X9.5X0.6,

Where, thickness of plate = 0.6cm,

Width of plate = 9.5 cm,

Length (at which vertical column was welded along it) = 18.2 cm

Hole represents dimension = M7.9X0.375 (in base plate)

Vertical column dimension = 24.5X2.4X0.5

Where, vertical height of column = 24.5cm,

Width of vertical column = 2.4cm,

Thickness of vertical column = 0.5 cm'

Threaded hole diameter = 1.2 cm (in base plate)

(All dimensions are taken in cm, and the tungsten arc welding machine (400Amp) was also applied to weld the vertical column near to the edge of the plate)

**Cylindrical rod (vertical type):** This cylindrical rod of vertical type has been placed on the threaded-hole area of the base plate by simple adequate placing, turning & tightening into them. After proper placing, it should seem to be vertical concerning the base plate. Dimensions included as (all dimensions are taken in cm): -

Length of rod = 30.7 (28+1+1.7),

Where, middle portion of rod = 28 cm,

Threaded portion of the rod on both sides = 1/1.7 cm,

Thread tap dimension up to 0.6 cm (for 1 cm length),

Thread tap dimension up to 1.5cm (for 1.7cm length)

Diameter of middle portion ( $\phi_m$ ) = 1.2 cm,

Dimensions of threaded portion for both sides are M7.9 x1.25 (in which outer diameter ( $\phi_i$ ) = 7.9 mm)

**Adjustable lower plate with locking:** It can be seen from **Figure 5.1(c)**, which is also made with the help of AutoCAD software of Autodesk Company Version-2017.

Dimensions included as (all dimension are taken in cm/mm): -

Cylindrical hollow part of thickness = 0.7 cm,

Length = 2.7cm,

Inner diameter ( $\phi_i$ ) = 1.2 cm,

Outer diameter ( $\phi_o$ ) = 2.6 cm (1.2+2X0.7)

Now, for rectangular thick part dimension = 11.5X2.6X0.3,

Where, hole diameter ( $\phi_h$ ) = 1.2 cm,

Tightened hexagonal nut dimension in mm = M7.9x0.375,

Screw length = 1.4 cm.

Locking plate dimensions = 3.5cmX1.9cmX3mm

(Where '3 mm' represent the thickness of it)

**(II) Load Cell:** The various types of load cells are commercially available such as: -

- Beam-type
- S-Type

- Tension/Compression type
- Cantilever-type
- Straight bar-type etc.

But, this work applied straight bar-type load cell, and sometimes it is also called a strain gauge.

Table 5.1; The Load cell for 0-20 kg of pressure (type-single point) mainly mentioned the measuring range/rated capacity, non-linearity, rated output, gauge factor, recommended excitation voltage, and metal film/metal foil.

Table 5.1 Load cell for 0-20 kg of pressure specifications as-received

Measuring Range or Rated capacity	0 to 20 Kg	Rated-output	'one' m-Volt/Volt
Non Linearity	0.15 % (Factor of safety)	Excitation-voltage	12 Volts
G.F (Gauge factor)	2 to 5	Metal-Film & Metal-Foil	Constantan & Silicon



Figure 5.2 Load Cell

Figure 5.2 shows the without plates straight bar load cell whose ranges from 0-20 kg of pressure (force). It is the initial part for analog to indication whereas an internal process includes amplifier & analog to digital converter.

Load cell(20Kg)  $\xrightarrow{\text{Analog signal}}$  Internal ( $\downarrow\uparrow$  material)  $\xrightarrow{\text{Digital signal}}$  Digital Indicator

[**Note:**'Internal ( $\downarrow\uparrow$  material)' means metal body/alloy-steel of load cell to which strain gauges have been secured]

**(III) Temperature Sensor:** The many types of temperature sensors are available commercially which includes as:-

- RTD's
- Thermocouples (including NTC type and PTC type)
- Semiconductor sensors.

Table 5.2 shows LM-35 specifications which mentioned such as operating range, non-linearity, rated range, self-heating, linear scale factor, material ICs, color, material and connecting points.

Table 5.2 Specifications as-received for temperature sensor (LM35)

Operating-range	4 to 20 volts	Non linearity	$\pm 1/4^\circ\text{Celsius}$
Rated-range	-ve $55^\circ$ to +ve $150^\circ\text{Celsius}$	Self heating	$0.08^\circ\text{Celsius}$
Linear scale factor	+10.0 mV/ $^\circ\text{C}$	Material ICs	Silicon
Color or Body	Black	Connectors points	'3'[A-Volts, B-Output, C-GND]

Figure 5.3 shows two LM-35 temperature sensors are used for open-atmosphere temperature and SMA reading. These come under semiconductor temperature sensors. These semiconductor sensors are classified into different types accordingly like voltage output, current output, digital output, resistance output, silicon, and diode temperature sensors/ICs, etc.

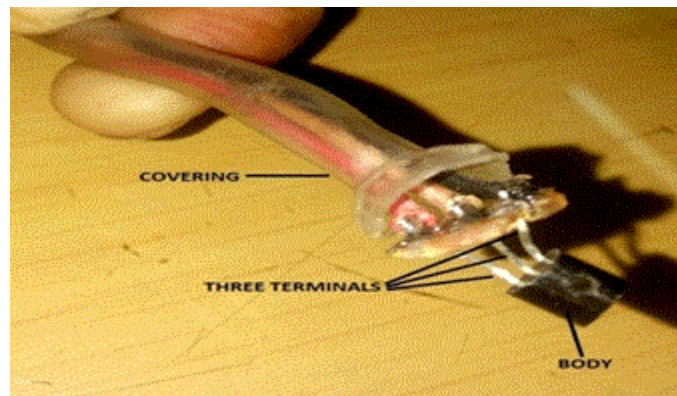


Figure 5.3 Temperature Sensor

**(IV) Amplifier Circuit:** The operational type amplifier circuit is used here which is prepared in the form of a kit as shown in **Figure 5.4**. It includes: -

- a) IC7107 (0 to 2000 V) digital panel meter; seven-segments-display circuit as several seven light-emitting diodes.



b) Analog to digital converter (ADC) IC from interim in which circuit used digital panel meter to give alphanumerical display as digital panel voltmeter.

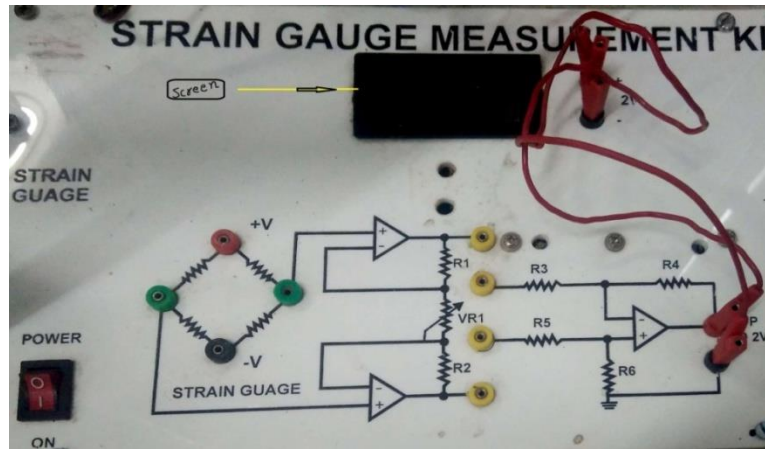


Figure 5.4 Amplifier circuit (Operational type)

**IC:** Integrated circuit (IC-7107) as shown in **Figure 5.5** that consists of the following as:

- seven segments decode
- reference voltage source
- comparator
- display-drives as its internal circuiting

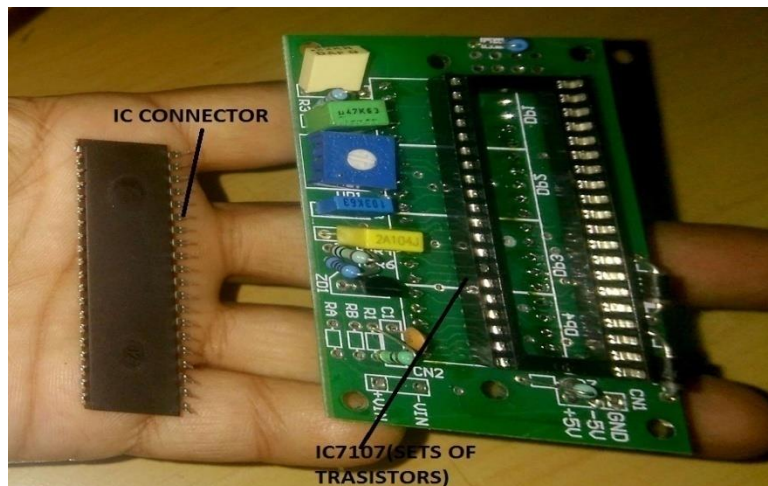


Figure 5.5 IC 7107

**Description of 40 pins (also shown in Figure 5.5):** pin configuration include pin 1 for supply voltage (+) and it provides the operating voltage for the IC, Next 2,3,4,5,6,7 & 8 for 7- segment 4<sup>th</sup> digit which is connected to 7 segment display for displaying the once digit of output value.

9, 10, 11, 12, 13, 14, & 25 for 7-segment 3<sup>rd</sup> digit which is connected to 7- segment for displaying the tenth digit, Next 15, 16, 17, 18, 22, 23 & 25 for 7-segment 2<sup>nd</sup> digit which is connected to 7-segment for displaying the hundredth digit, Next 19 and 20 for 7-segment 1<sup>st</sup> digit in which pins are connected to 7-segment for displaying the thousandth digit and 21 for the ground which connected to the round of the system. Next 26 for supply voltage (-) which provides the negative supply voltage.

Next 27 for signal integrate which is connected to a capacitor and 28, 29 for auto-zero & buff which is connected to capacitor, and resistor network. Next 30, 31 for the common & connected to ground, then next 33, 34 for ref (+) and ref (-) in which capacitor is connected across these pin for neutralizing fluctuations in reference voltage. Next 35, 36 for reference high & reference low which either can supply reference voltage or use internal reference voltage, Next 37 for test pin which not used during operation, next 38, 39, 40 for OSC1, OSC2, OSC3 which use RC network top set the oscillator frequency. It has 3 ½ bit (0-1999) ADC modules with 4 digit 7 segment display driver & analog input voltage is equal to supply voltage. The typical operating frequency = 48 KHz.

Digital output value = 0-1999 (up to 2 volts)

Number of LED = 07 (in segment)

Display = 7 (for segment drive)

Total pin = 40

$$\text{COUNT} = 1000 \times V_{\text{IN}}/V_{\text{REF}} \quad (5.1)$$

In the present work, a dual-slope type simple A/D converter has been used. If we talk about the quantity of A/D converter which included three in numbering, first for the atmospheric temperature sensor, second for wire-temperature sensor and third for strain gauge which directly attached to the load-cell.

**(V) DC Supply:** The power source/ supply are used for finding values of voltages and currents in the intelligent helical springs of different dimension and different heat-treated conditions.

Figure 5.6 shows the DC supply with CV and CC display unit in which CV refers to current, voltage, and CC for current. It also included: -

- (a) Coarse & fine regulating switch
- (b) Power button: On/Off switch (with side fuse)

- (c) Voltage = 0-15 volt
- (d) Current = 0-5 AMP
- (e) '3' connecting point as +ve terminal, -ve terminal & ground terminal.



Figure 5.6 DC supply with CV, and CC display

#### (VI) Basic Components (electronic-electrical)

In this present work, mainly components included as resistors, capacitors, diodes, inductors transistors rectifiers, and transformers. These are described as follows:

**Resistors (1k-10k):** It is the passive electrical component that produces friction in the current flow direction. It means register opposes the flow of electrons. In this work the carbon film resistors have been used which generally having 4-band rather than 5-band or 6-band, and are available in the form of metal film & metal oxide film due to cost priority. The 4-band resistors have four colors which define the value of the register.

**Capacitor (1000mf/25v, 1mf/63v):** The basic component of the electric circuit which stores the energy in an electric field. It measures the value in terms of capacitance i.e. farad (F). In present work the ceramic capacitors have been used which are very cheap & easily available in the market then electrolytic capacitors also have been used as per requirement & necessity of work.

**Diode (Electrolytic):** it is a one-way valve or gate for electricity. It allows the flow of current in one direction. The diode is a semiconductor generally consists of two types of materials like silicon and germanium. In the present work, mostly P-N junction diodes had been used.

**Inductors (coil/wound):** it is a coil or reactor and passive two-terminal electrical components which resist changes in electric current passing through it.

It consists of a conductor such as wire, usually wound in coil or we can say when a length of wire is formed onto a coil, it becomes a basic inductor, when there is current through the coil, a three-dimensional electromagnetic field is created surrounding the coil in all directions.

**Transistors (3-terminal):** It acts as a switch or gate for electronic signals. It consists of trace layers of semiconductors material, and each capable of a current. The type of transistors includes BJT & MOSFET (BJT or bipolar junction such as NPN type or PNP type).

**Rectifiers (Bridge-IN4007):** it is an electrical device that converts Ac to DC with the help of one or two diodes or we can say it as the rectification with the help of semiconductor diodes. There are many possible ways to construct rectifier circuits using diodes. The three types of basic rectifiers circuits such as half-wave rectifier, full wave rectifier, and bridge rectifier.

**Transformers:** Small capacity transformers were used in the present work in digital panel meters.

### **5.3 MATERIAL & MANUFACTURING OF SMA HELICAL SPRING**

The flexinol wire (composition as 49% Nickel and 51% Titanium) of diameter 1.0 mm was used (detailed theory mentioned the same as-referred in 'chapter 3').

The parameters obtained were as: -

- (D) Mean coil Dia = 7.4 mm,
- (d) Wire diameter = 1.0 mm,
- (n) Number of turns = 8,
- (c) Spring index =  $D/d=7.4$ ,
- ( $L_{initial}$ ) Initial free length of spring = 2.5 cm etc.

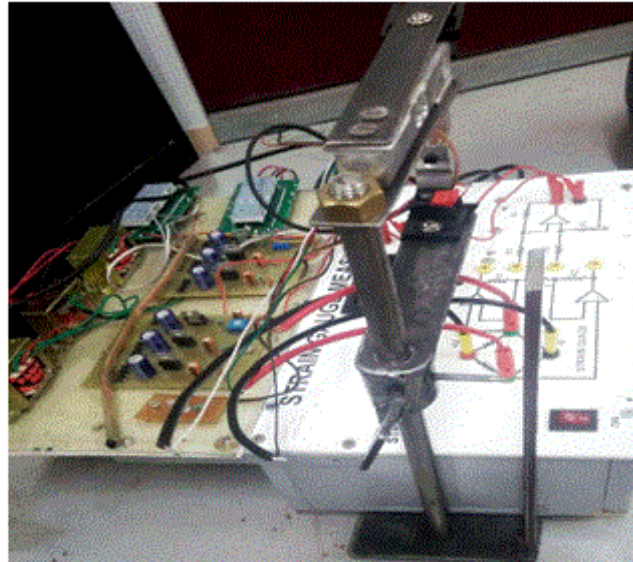
### **5.4 EXPERIMENTAL SETUP AND OBSERVATION DATA**

The Setup involved two observations as the first one to the scale-value calculations, and the second one to experimental observations.

Figure 5.7 shows setup or arrangement which comprised of Iron stand, load cell, temperature sensor, amplifier circuit, DC source and basic electronic-electrical components in a particular manner with help of nuts, screws washers, and engineering workshop tools, soldering gun and TIG welding M/c so that input values can be initiated.



Deformed NiTi testing approach



Setup or arrangement

Figure 5.7 Setup with deformed 0.1mm NiTi testing approach

**5.4.1 Scale-value calculations:** The steel hanger weight was 50gm, which has been used in this work. The slotted weights are also applied.

Table 5.3 shows the slotted weight in ‘gm’, hanging weight in ‘gm’ load-cell strain, atmospheric temperature values in ‘°C’ difference values, and final related value.

**Average relative scale value for 1gm = (Relative Scale I+ Relative Scale II+ Relative Scale III+ Relative Scale IV)/4 = 11.1035**

Table 5.3 Average scale value for 1.0mm NiTi SMA Spring

Sr No .	Slotted weight (gm)	Hanging weight (gm)	Load-Cell Strain	Atm Temperature (°C)	Difference value	Relative scale
1	0	50gm	5	32.3	5	10
2	50	100g	9	32.4	4	11.111
3	100	150	13	32.3	4	11.538
4	150	200	17	32.4	4	11.765
<b>Average relative scale value</b>				<b>11.1035</b>		

**5.4.2 Experimental observations:** The 1.0mm NiTi deformed SMA helical spring is used in above-mentioned arrangements.

Table 5.4 shows the observation data for the deformed 1.0mm NiTi SMA helical spring.

The nomenclatures of all constraints are denoted as:

Preset length of SMA spring = L,

Applied voltage values = V,

Average scale values =  $A_s$  (in terms of strain gauge values),

Values of average currents = I,

Average wire temperature/working SMA temperature values =  $W_t/T$ ,

Atmospheric temperature changed values =  $A_t$ , And Average Load-lifted values =  $L_A$  respectively.

**Spring-load value calculated as: -**

**= Reading of Average load cell strain value (for an applied voltage) X Average relative scale value**

**(Included as first three were nil, 4<sup>th</sup> = 38.5\*11.10, 5<sup>th</sup> = 76\*11.10, 6<sup>th</sup> = 83\*11.10, 7<sup>th</sup> = 90.5\*11.10, 8<sup>th</sup> =110.5\*11.10, 9<sup>th</sup> = 117\*11.10 and 10<sup>th</sup> = 128\*11.10 respectively).**

Table 5.4 Observation data for 1.0mm deformed SMA

Sr. No	Preset Length (L) (cm)	Voltage Applied (V) (volts)	Avg Current in wire (Amp.)	Atm Temp (°C)	Avg Wire Temp (°C)	Avg Load-Cell Strain	Spring-load value (gm)
1	7.5	0.2	0.93	32.9	33.1	0	Nil
2	7.5	0.4	1.81	32.9	33.8	0	Nil
3	7.5	0.6	2.95	33	34.2	0	Nil
4	7.5	0.8	3.87	33	35	38.5	427.35
5	7.5	1	4.995	33	36.25	76	843.6
6	7.5	1.2	6.12	33.1	38	83	921.3
7	7.5	1.4	7.545	33.1	40.2	90.5	1004.55
8	7.5	1.6	8.675	33	48.25	110.5	1226.55
9	7.5	1.8	9.97	33.1	58.5	117	1298.7
10	7.5	2	10.635	33	64.5	128	1420.8

## 5.5 RESULTS AND DISCUSSION

This part of work included minimum value to maximum value relationship, minimum value to maximum value relationship, minimum value to median value relationship; maximum value to median value relationship, resultant stress ( $\tau_{rs}$ ) calculation, and model equations as first model equations, second model equations, and imaginary deflections.

### (i) The minimum value to maximum value relationship for $W_t$ and $A_s$ at voltage (V)

In the presented work, the voltage values are taken in volts, temperature values in  $^{\circ}\text{C}$ , and average load-cell strain or GF value ( $A_s$ ) in mathematical numbers/integers.

Table 5.5 shows the voltage applied (V), average wire temperature ( $W_t$ ), and average load-cell strain or gauge factor ( $A_s$ ) for the minimum value to maximum value relationship. All mentioned values in this are taken from the observations data for 1.0mm deformed SMA.

Table 5.5 Minimum value to Maximum value of  $W_t$ ,  $A_s$

Sr. No.	Voltage (V)	Average Wire Temperature ( $W_t$ ) in $^{\circ}\text{C}$	Average Load-Cell ( $A_s$ )
1	0.8	35.00	38.5
2	1.0	36.25	76.0
3	1.2	38.00	83.0
4	1.4	40.20	90.5
5	1.6	48.25	110.5
6	1.8	58.50	117.0
7	2.0	64.50	128.0

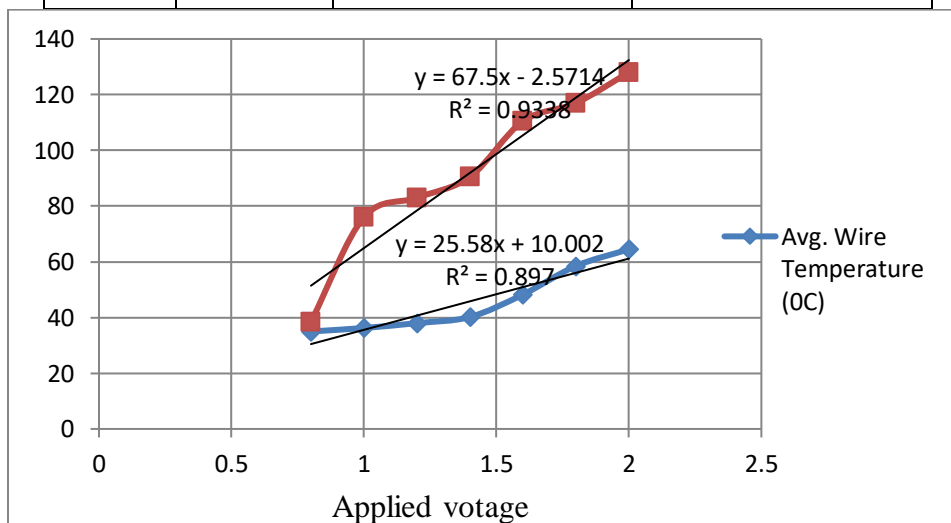


Figure 5.8 Minimum values to maximum value of  $W_t$ ,  $A_s$

Figure 5.8 shows the average load-cell strain or gauge factor ( $A_s$ ) with respect to the applied voltage. Similarly, Average Wire Temperature ( $W_t$ ) is shown with respect to the applied voltage.

**Linear correlations** were obtained as  $R^2 = 0.933$  obtained for  $W_t$  and  $R^2=0.897$  obtained for  $A_s$  from graph where 'R' represents the correlation coefficients. The equations of the model for Minimum value to maximum value relationship obtained as:

$$Y = 67.5x - 2.571 \quad (5.2)$$

$$Y = 25.58x + 10.00 \quad (5.3)$$

Equation (5.2) shows relation for average load-cell strain to applied voltage and equation (5.3) shows relation for average wire temperature to applied voltage respectively.

**(ii) The minimum value to maximum value relationship for  $W_t$  at current (I)**

The current values are taken in ampere, and average load-cell strain or GF value ( $A_s$ ) in mathematical numbers/ integers.

Table 5.6 shows the average current (I) and average load-cell strain or gauge factor ( $A_s$ ) for the minimum value to maximum value relationship. All mentioned values in this are taken from the observations data for 1.0mm deformed SMA.

Table 5.6 Data considered for Average current & GF value

Sr. No.	Average Current (I)	Average Load-Cell Strain
1	3.870	38.5
2	4.995	76.0
3	6.120	83.0
4	7.545	90.5
5	8.675	110.5
6	9.970	117.0
7	10.635	128.0

Figure 5.9 shows the minimum value to maximum value relationship of average currents (I) and average load-cell strain or gauge factor ( $A_s$ ). The values for average currents and average load cell strains are obtained corresponding to applied voltages which are shown graphically.



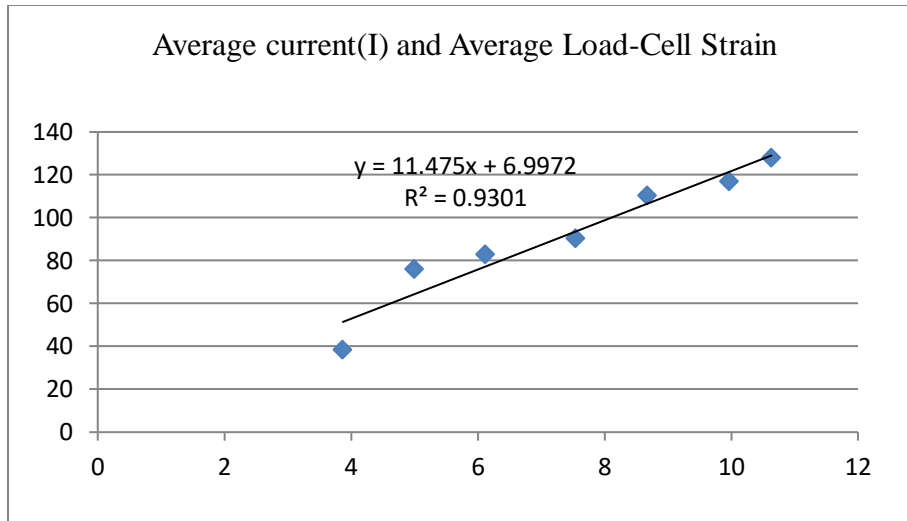


Figure 5.9 Variation of GF values vs. Average currents

**Linear correlations** were obtained as  $R^2 = 0.930$  obtained for  $W_t$  from graph where ‘R’ represents the correlation coefficients. The equations of the model for minimum value to maximum value relationship were obtained  $Y = 11.47x + 6.997$  (5.4)

The equation (5.4) shows the relation for an average load-cell strain to applied current values.

**(iii) The minimum value to maximum value relationship for  $L_s$  at a voltage (V)**

The presented work considered the minimum value to maximum value for Spring-load value and average voltage readings. The Spring-load values are taken in Kg and average voltage readings in volts.

Table 5.7 shows the Spring-load value ( $L_s$ ) and average voltage for the minimum value to maximum value relationship. All mentioned values in this are taken from the observations data for 1.0mm deformed SMA.

Table 5.7 Data considered for voltage and spring-load values

Sr. No.	Average Voltage (V)	Spring-load
1	0.8	0.42735
2	1	0.8436
3	1.2	0.9213
4	1.4	1.00455
5	1.6	1.22655
6	1.8	1.2987
7	2	1.4208

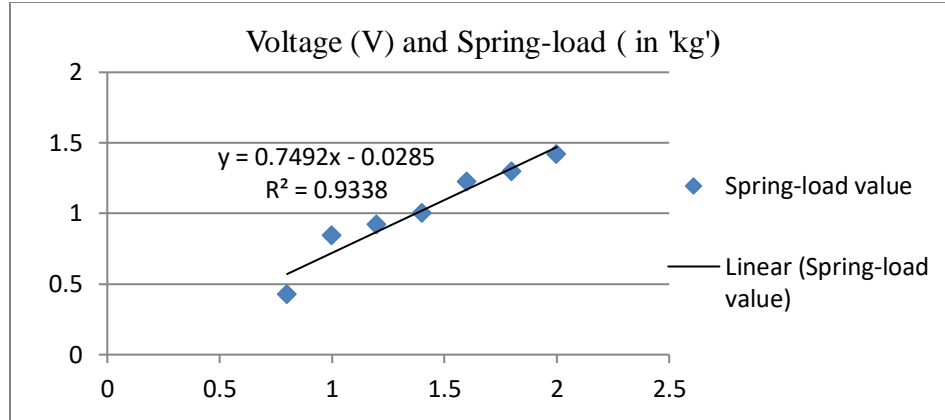


Figure 5.10 Variation of spring load ( $L_s$ ) vs. applied voltage

Figure 5.10 shows the minimum value to maximum value relationship of Spring-load value ( $L_s$ ) and average voltage. The values for Spring-load value obtained corresponding to applied voltages are shown graphically.

**Linear correlations** were obtained as  $R^2 = 0.933$  obtained for  $L_s$  from graph where ‘R’ represents the correlation coefficients. The equations of the model for Minimum value to maximum value relationship obtained as:

$$Y = 0.749x + 0.028 \quad (5.5)$$

The equation (5.5) shows relation for Spring-load values.

**(iv) The minimum value to Median value relationship for  $L_s$  at a voltage (V)**

The work also considered the minimum value to median value relation for Spring-load value and average voltage readings. The Spring-load values are taken in Kg and average voltage readings in volts.

Table 5.8 shows the Spring-load value ( $L_s$ ) and average voltage for the minimum value to median value relationship. Four readings of spring-load values with respect to applied voltage had considered as the median in 7 values from table 5.7 (but these all mentioned values in this are taken from the observations data for 1.0mm deformed SMA)

Table 5.8 Data considered for V &  $W_t$  for minimum to median value

Sr. No.	Voltage (Volts)	Spring-load value ( $W_t$ )
1	0.8	0.42735
2	1	0.8436
3	1.2	0.9213
4	1.4	1.00455

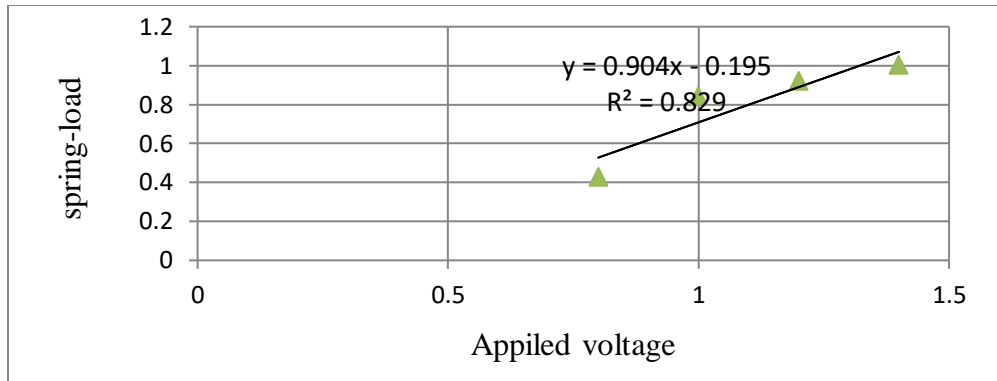


Figure 5.11 Variation of  $W_t$  for minimum to median value

Figure 5.11 shows the minimum value to median value relationship of Spring-load value ( $L_s$ ) and average voltage. The values for Spring-load value obtained corresponding to applied voltages are shown graphically.

**Linear correlations** were obtained as  $R^2=0.829$  obtained for  $L_s$  from the graph where ‘R’ represents the correlation coefficients. The equations of model for Minimum value to median value relationship obtained as:

$$Y = 0.904x - 0.195 \quad (5.6)$$

The equation (5.6) shows relation for Spring-load value to applied voltage values.

**(v) The maximum value to Median value relationship for  $L_s$  at a voltage (V)**

The work also considered the maximum value to median value relation for Spring-load value and average voltage readings. The Spring-load values are taken in Kg and average voltage readings in volts.

Table 5.9 shows the Spring-load value ( $L_s$ ) and average voltage for the maximum value to median value relationship. Four readings of spring-load values with respect to applied voltage had considered as the median in 7 values from table 5.7 (but these all mentioned values are taken from the observations data for 1.0mm deformed SMA)

Table 5.9 Data considered for V &  $W_t$  for maximum to median value

Sr. No.	Voltage (Volts)	Spring-load value ( $L_s$ )
1	2	1.4208
2	1.8	1.2987
3	1.6	1.22655
4	1.4	1.00455

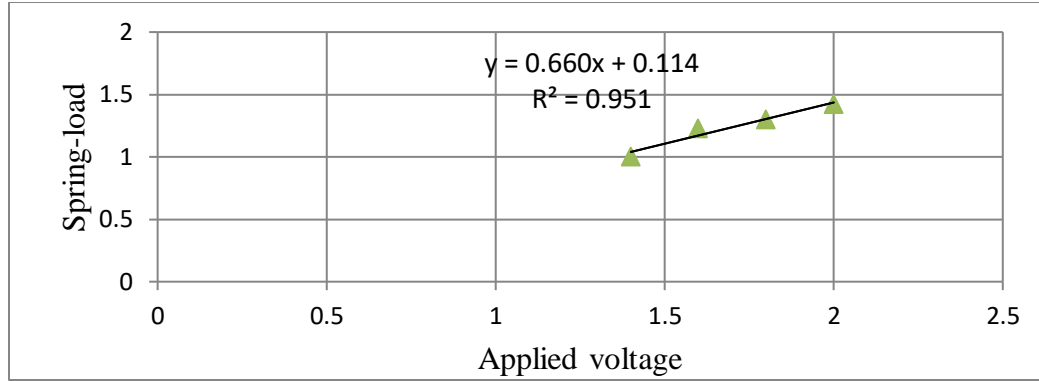


Figure 5.12 Variation of  $W_t$  for maximum to median value

Figure 5.12 shows the Maximum value to median value relationship of Spring-load value ( $L_s$ ) and average voltage. The values for Spring-load value obtained corresponding to applied voltages are shown graphically.

**Linear correlations** were obtained as  $R^2 = 0.951$  obtained for  $L_s$  from graph where ‘R’ represents the correlation coefficients. The equations of model for Maximum value to median value relationship obtained as:

$$Y = 0.660x + 0.114 \quad (5.7)$$

The equation (5.7) shows relation for Spring-load value to applied voltage values.

## 5.6 SUMMARY

The NiTi SMA-based model of helical spring has been formulated which can enable the stability of SMA by measuring its parameters before implementing it in mechanical equipment. Electronic components such as capacitors, registers, PN diodes, transistors, rectifiers, IC7107, and also electrical components such as power supply, inductors, transformers cables, sockets, connectors, etc were used for experimentation. The linear model equations are obtained. In the presented work 1.0mm NiTi-based one-way intelligent helical spring wire was considered for observations with preset conditions. The development of a physical model for 1.0mm NiTi-based one-way intelligent helical spring in terms of various actuation parameters included in this present work as average scale values, load-cell strain, load capacity, current, working temperature, atmospheric temperature, and applied voltage also estimated. This model enables the strength of intelligent helical SMA spring before its practical implementing as an actuator. It also enables the design parameters of a single spring or number of SMA springs with the help of results.

# **CHAPTER 6**

## **LOAD CARRYING CAPACITY OF SMA SPRINGS**

### **6.1 INTRODUCTION**

In this chapter, thin diameter SMA wires which contract like muscles when electrically driven, are described to know the effect parameters as weight or distance gain with instant time response for its actuation. Here, the three springs having a different numbers of turns, different weights and different diameter 0.1mm, 0.2mm, and 0.5mm were prepared with the help of fixture-cum-spring tool. The parameters included such as the wire temperature, scale-load capability response, strain capacity, wire-current, and voltage during working were estimated for intelligent helical SMA spring. The slender 0.1mm and 0.2mm flexinol wires were considered for observation of various parameters during their actuation on a common platform. The common platform was defined by the model already discussed for intelligent helical SMA spring. But 0.5mm flexinol wire discussed with the minor application of 0.5mm SMA-based wire as a simple solenoid valve has been discussed in which SMA-based conical spring in the helix form, was employed. The advantageous purpose of the valve to operate one way and can control the supply of water, oil, liquid fuel, and liquid refrigerant but choked by gravitational force. It can be placed or installed anywhere in a vertical position as per its limitations or reduction of cost. For converting SMA's into intelligent helix shape springs heat treatment process was applied. It involved the following steps: -

- I. Separately Preparation of NiTi based intelligent helical spring (done previously in 'chapter 3')
- II. Practical illustration slender or thin diameter 0.1mm and 0.2mm NiTi SMA wires
- III. Practical application of 0.5mm by Illustrated with A SMA-Based Solenoid Valve

### **6.2 MATERIAL DESCRIPTION**

The one-way shape memory SMA's in the form of NiTi wires of different dimensions have been used with the nominal composition of 49.2% (Ni) – 50.8 % (Ti).

Table 6.1 shows the specifications for 0.1 mm, 0.2mm, and 0.5mm slender wires which were obtained in drawn conditions. The specifications include lengths, diameters, thermal expansion coefficient (austenite), thermal expansion coefficient (martensite), melting point, specific heat, thermal conductivity latent heat of transformation, thermal conductivity, composition, and specific heat.

Table 6.1 Specification as-received for 0.1 mm, 0.2mm and 0.5mm slender wires

Length of wires	1meter, 1meter and 10 INCH.
Diameters	0.004", 0.008" and 0.020" (Flexinol)
Thermal Expansion Coefficient (Austenite)	$11.0 \times 10^{-6}/^{\circ}\text{C}$
Density	$6.45 \text{ g/cm}^3$
Melting Point	2370 °F (1300 °C)
Shapes	Round (for each)
Latent Heat of Transformation	578 cal/g.
Composition	49.2% (Ni) –50.8 %( Ti)
Specific Heat	$0.2 \text{ cal/g} * ^{\circ}\text{C}$
Thermal Conductivity	$0.18 \text{ W/cm} * ^{\circ}\text{C}$

### 6.3 EXPERIMENTATION OF 0.1MM AND 0.2MM NITI-BASED SMA'S

In the following section, 0.1mm and 0.2mm slender wires are described by considering unique parameters as light weights and very small diameters of SMA. The parameters included such as the average wire temperature, average scale-load capability response, average strain capacity, and voltage during working are estimated for intelligent helical SMA spring. There is a focus on the effect of load gain by slender wires with instant time response for its actuation the common platform is applied for loading and unloading conditions as electro-mechanical components actuator model of previous chapter '5'.

### 6.3.1 Preparation of Spring Manufacturing Tools

The preparation applied the mild steel round bar, bench-vice (fixed base), electric cutter, drill m/c, threading tool (1.25mm) and helical spring manufacturing, etc.

(i) **Mild steel round bar:** It can be seen from **Figure 6.1**, mild steel round bar which is made with the help of AutoCAD software of Autodesk Company Version-2017, The dimensions of the round rod are represented as 8mmx120mm in which diameter equal to 8mm and length equal to 120mm.



Figure 6.1 Round bar (Mild steel)

The weight of this used round bar available in kg/feet is also equal to 0.120kg (approx); mild steel round bar can be drilled, cut/welded to suit a huge number of applications as supplier mentioned, and said also supply to clients for a variety of purposes.

(ii) **Bench-Vice:** It is used in the presented work as a holding device with a fixed base. It has jaws to hold the work-piece firmly in place provided. This mechanical device is used to secure an object to allow work to be performed on it.

Vices have two parallel jaws, one fixed and the other movable. Gripping is available in faces of fixed and movable jaws in terms of knurling. This device was used to grip the mild steel round bar and a hand operating threading tool was applied to produce various external threads on the periphery of the round rod.

(iii) **Electric Cutter:** The cutter used in engineering workshops is generally electrical driven and manually operated. The buffing wheel is made of ceramic material and applied to smoothing a work piece's surface using an abrasive.

Technically, polishing referred to processes here that used an abrasive which was glued to the work wheel, while buffing used a loose abrasive applied to the work wheel.

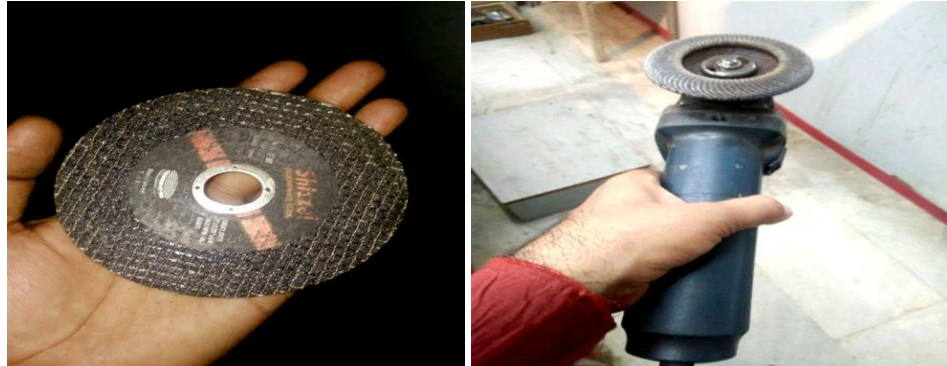


Figure 6.2 Electric cutter with buffing wheel and cutter

Figure 6.2 shows electric cutter with a buffing wheel and cutter in which the ceramic cutter is made of silicon carbide and having 6 inches diameter with a thickness of 1.0mm, and manual operated or hand electric cutter is used which moves with 3000 round in one minute/working supply in terms of power consumed as 400J/s. Here, buffing was used on both sides face of the spring tools and the face of each tool was made right-angled during the working.

**(iv) Drill Machine:** Drilling is a cutting/material removing process that uses various drill bits to cut holes of circular areas/cross-sections in solid materials. A drill is a primary tool used for making round holes or driving fasteners. Drill bits are cutting tools used to remove material to create holes, almost always of circular cross-section.

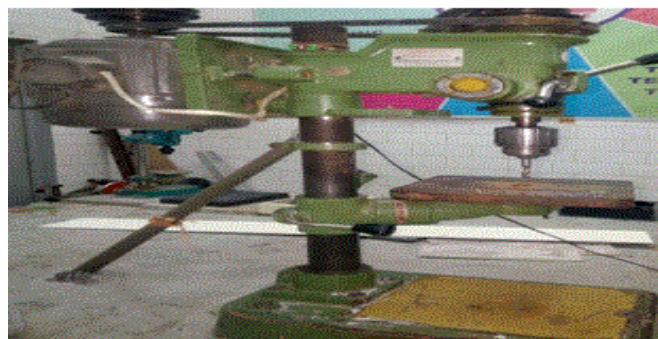


Figure 6.3 Drill Machine (230V/2200rpm)

Figure 6.3 shows the Drill machine is applied here. Drill bits of 0.8, 0.9, 1.0, and 1.5 mm are used here also.

**(v) Threading Tool:** The threading die consists of a cutting body with a chamfer on either side so that it can be applied both-way to acts as a nut with milled-in chip grooves.



The threading die is set in exactly horizontal position on the bevel of the bolt and turned clockwise slowly and with slight pressure from above with right-hand thread. Only when the starting end of the thread is cut and the threading die guides itself.



Figure 6.4 Threading tool

Figure 6.4 shows the threading tool having a pitch equal to 1.25 mm and applied for external thread cutting. This threading tool consists of mainly two parts as first threading die and the second die holder. External threads are made with the help of a threading die or die-stock.

**(vi) Spring Manufacturing:** This is done with the help of pre-final and final spring tools (also called fixture-cum-spring tools). The 0.1mm and 0.2mm slender wires were very soft in condition so easily sets in the provided thread of spring tools but end portions are tightly stretched manually from both sides to obtain accurate SMA helical springs.

Figure 6.5 shows the spring-tools making involves the long threaded part, threaded part of various sizes, drill bits of 0.8, 0.9, 1.0, 1.5mm, fixture-cum-spring tool at pre-final stage, and specimens before heat treatment processes. Two wires of 0.1mm and 0.2mm wrapped over the threaded parts and holes provided in these spring tools.



Long threaded part

(a)

TP of various size

(b)

Drill bits(0.8,0.9,1.0,1.5)

(c)

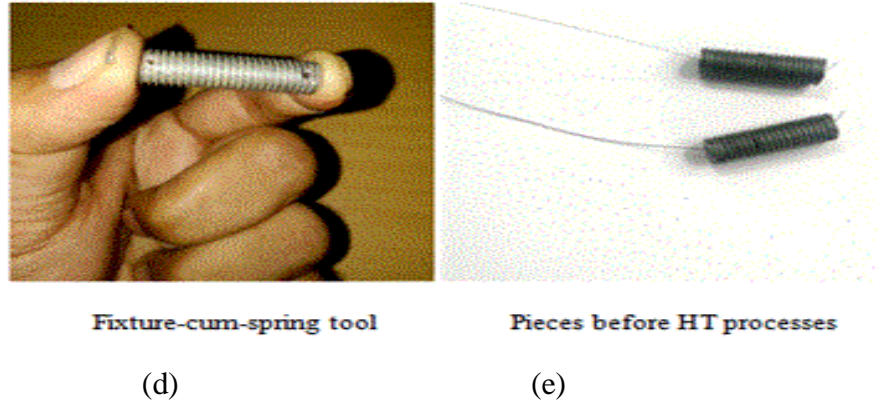


Figure 6.5 Spring-tools making involves (a) long threaded part, (b) TP of various sizes, (c) drill bits of 0.8, 0.9, 1.0, 1.5mm, (d) fixture-cum-spring tool (pre-final), and (e) specimens before HT processes

### 6.3.2 Preparing of SMA Helical Spring Specimens

Flexinol wires are slender or thin diameter types prepared in the form of one-way helical SMA springs to know the effect of unique parameters response for its actuation. The phase transformation of SMA wire varied from 250-630°C. Wires were heated here above to their critical temperature as per required properties in strain recovery rate for the applications in form of mechanics actuators (helical springs) to generate force or displacement. The infrared temperature sensor is applied here to measure the value of temperature. The annealing was done by the temperature of muffle furnace for preset-condition by muffle regulator and the temperature maintained at 530°C for 45 minutes.

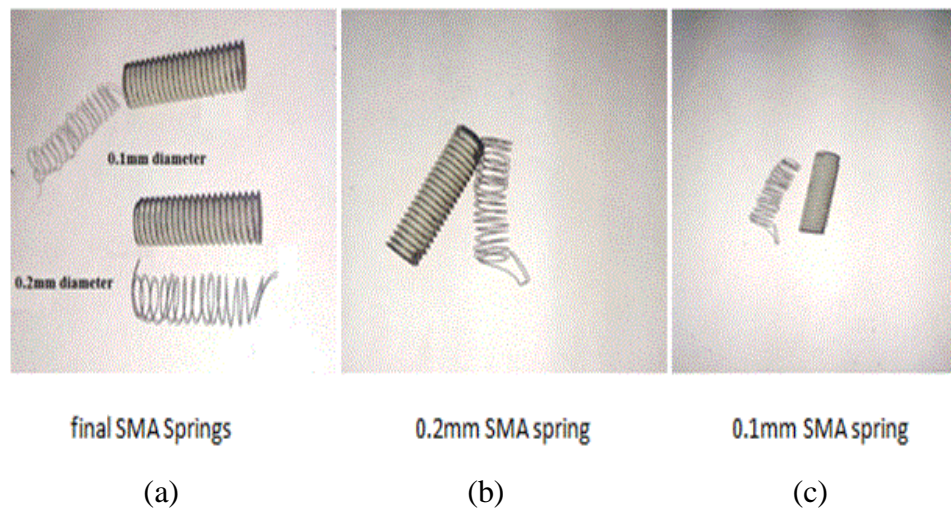


Figure 6.6 Preparation of one-way helical SMA springs includes, (a) combined final SMA springs, (b) 0.2mm SMA spring, and (c) 0.1mm SMA spring

Although tolerance of  $\pm 2^\circ$  was also considered due to the fluctuation exists by auto cut supply for an instant of time with the help of regular. The time of the annealing process of the SMA wires 0.1 & 0.2 was 16 hours. Then the normalizing process was also used by just opening the door of the muffle furnace but the piece was maintained inside of it up to 6 hours.

Figure 6.6 shows the preparation of one-way helical SMA springs included combined final SMA springs, 0.2mm SMA spring, and 0.1mm SMA spring. The final SMA springs dimensions were obtained as mean coil diameter of 0.1mm SMA helical spring =  $6.5\text{mm} + 0.10\text{mm} = 6.6\text{mm}$ , outer coil diameter of =  $6.7\text{mm}$  and inner coil diameter =  $6.5\text{mm}$ . Similarly, Mean coil diameter of 0.2mm SMA helical spring =  $6.5\text{mm} + .02\text{mm} = 6.7\text{mm}$ , outer coil diameter =  $6.9\text{mm}$  and inner coil diameter =  $6.5\text{mm}$  respectively. The number of turns of SMA wire for 0.1mm (diameter)/0.2 (diameter) were also obtained as 18mm, and 16mm respectively. (So, spring index of 0.1 SMA  $D_1/d_1 = 6.6/0.1 = 66.0$ , and spring index of 0.2 SMA  $D_2/d_2 = 6.7/0.2 = 33.5$ )

### 6.3.3 Experimental Observation

First the average scale value in term strain for the weight (in gm) and then discussed the behavior of both the 0.2mm and 0.1mm wires during their actuation.

**6.3.3.1 Average Scale value:** Steel hanger and steel slotted weights are applied here. The steel hanger weight and slotted weights of each piece were obtained as 50gm respectively. The total 200gm weight has been applied.

Table 6.2 shows the slotted weight in ‘gm’, hanging weight in ‘gm’ load-cell strain, atmospheric temperature values in ‘°C’ difference values, and final related value. The Average scale-value has been evaluated (applied the previous chapter ‘5’ actuator model) as:

Initial value strain for load-cell = 0

Average Strain value of hanger = 12

Average Strain value of first weight (for 100gm) = 11.5

Average Strain value of second weight (for 150gm) = 12.5

Average Strain value of last weight (for 200gm) = 12.5

Average Strain value for 50gm ( $48.5/4 = 12.125$ )

**Average relative scale value for 1gm = (Relative Scale I+ Relative Scale II+ Relative Scale III+ Relative Scale IV)/4 = 0.239** i.e. shown in table 6.2

Table 6.2 Average scale value for ‘One’ gram of wires

Sr No	Slotted weight (gm)	Hanging weight (gm)	Load cell Strain	Temp (°C)	Difference	Relative scale
1	0	50gm	12	29	12	0.24
2	50	100g	23.5	29.2	11.5	0.235
3	100	150	36	29	12.5	0.24
4	150	200	48.5	29.1	12.5	0.243
<b>Average relative scale value (0.239)</b>						

**6.3.3.2 Observation data during actuation of 0.1mm SMA spring:** The work applied the previous chapter ‘5’ actuator model to loading or unloading conditions.

Figure 6.7 shows the SMA (0.1mm) testing approach in which this NiTi SMA helical spring was firstly considered in a deformed state for analysis in which one end had attached with socket terminal like previously (chapter ‘5’).

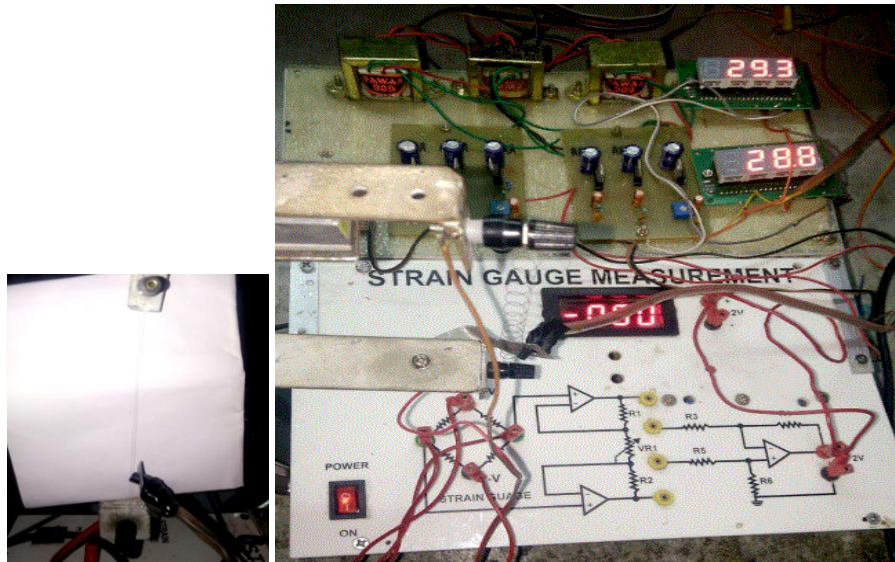


Figure 6.7 SMA (0.1mm) testing approach

The spring-load value is evaluated here with the help of the average scale value by multiplying it, for example as ‘2’ is a strain obtained shown in table 6.3.

Then value of  $L_s$ (spring load value) =  $2 \times 0.239 = 0.478$ . Similarly, all values were evaluated. The various actuation-parameters were obtained as mentioned in **table 6.3 for 0.1mm SMA**.

**6.3.3.3 Observation data during actuation of 0.2mm SMA helical spring:** Similarly, It can be seen from **Figure 6.8** that 0.2mm NiTi SMA helical spring was secondly considered in a deformed state for analysis.

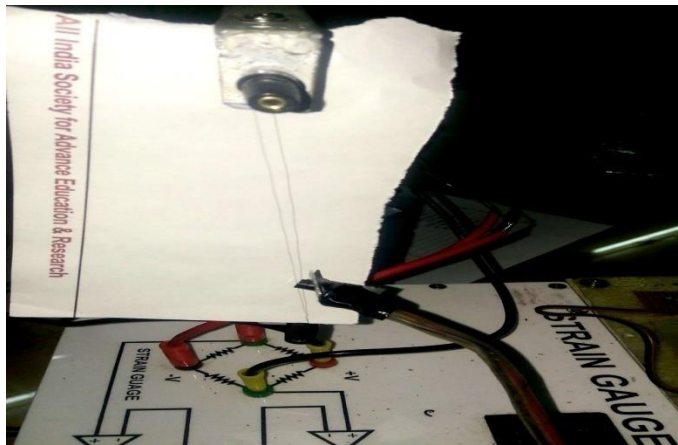


Figure 6.8 SMA (0.2mm) testing approach

The spring-load value was also evaluated here with the help of the average scale value by multiplying it, for example as '9.5' is a strain in table 4 then the value of  $L_s$  (spring load value) =  $9.5 \times 0.239 = 2.271$ .

Similarly, all values were evaluated. The various actuation-parameters were obtained as mentioned in **table 6.4 for 0.2mm SMA**.

For the accuracy of the result, the preset length of both SMA's, sets at 14.5cm. The nomenclatures of all constraints are denoted as: -

Preset length of SMA spring =  $L$ ,

Applied voltage values =  $V$ ,

Average scale values =  $A_s$  (in terms of strain gauge values)

Values of average currents =  $I_A$ ,

Average wire temperature/working SMA temperature values =  $T_A$ ,

Atmospheric temperature changed values =  $A_t$ ,

And Spring-load =  $L_s$  respectively.

Table 6.3 Observation data obtained for 0.1mm SMA

<b>Sr. No.</b>	<b>Length (cm)</b>	<b>Voltage (Volts)</b>	<b>Average Current in wire (Ampere)</b>	<b>Temperature (Atmospheric) ( °C )</b>	<b>Average Wire Temp ( °C )</b>	<b>Average Load-Cell Strain (As)</b>	<b>Spring-load (L<sub>s</sub>) (gm)</b>
1	14.5	0.5	0	29	29	0	Nil
2	14.5	1	0.04	29.1	30.4	0	Nil
3	14.5	1.6	0.04	29.8	31.2	2	0.478
4	14.5	2	0.07	29.7	32.5	4	0.956
5	14.5	3	0.07	30.2	33.2	4	0.956
6	14.5	5	0.07	30.1	34.1	4	0.956
7	14.5	7.8	0.07	30.7	35.5	4	0.956
8	14.5	9.2	0.07	30.4	38.9	4	0.956

Table 6.4 Observation data obtained for 0.2mm SMA

<b>Sr. No.</b>	<b>Length (cm)</b>	<b>Voltage (Volts)</b>	<b>Average Current in wire (Ampere)</b>	<b>Temperature (Atmospheric) (°C)</b>	<b>Average Wire Temp (°C)</b>	<b>Average Load-Cell Strain (A<sub>s</sub>)</b>	<b>Spring-load ( L<sub>s</sub>) (gm)</b>
1	14.5	0.5	0.03	29	29.1	0	Nil
2	14.5	1.0	0.9	29.1	31.4	9.5	2.271
3	14.5	1.6	2.0	29.8	32.8	21	6.91
4	14.5	2	2.7	29.7	34.5	29.5	7.05
5	14.5	3	3.2	30.2	35.2	34.5	8.25
6	14.5	5	3.2	30.1	36.7	34.5	8.25
7	14.5	7.8	3.2	30.7	39.5	34.5	8.25
8	14.5	9.2	3.2	30.4	42.9	34.5	8.25

### 6.3.4 Results for 0.1mm and 0.2mm SMA's

#### For 0.1mm SMA,

The Preset length of 14.5cm measured between the two terminals of the physical model also known as the free length of 0.1mm NiTi-based helical SMA spring is a deformed condition. Table 6.5 shows the data considered for 0.1mm SMA in which various parameters such as V, I<sub>A</sub>, T<sub>A</sub>, and L<sub>S</sub> are represented by the applied voltage, average current in wire, average wire temperature, and spring load respectively. These variables/parameters are taken from table 6.3 for the graphical analysis. So, the only '6' readings are considered and nil values are (column/row) eliminated or not applied.

Table 6.5 Data considered for 0.1mm SMA

Sr. No.	Voltage Applied (Volts)	Avg Current in wire (I <sub>A</sub> ) (Amp.)	Avg Wire Temp. ( T <sub>A</sub> ) (°C )	Spring-load (L <sub>S</sub> ) (gm)
1	1.6	0.04	31.2	0.478
2	2	0.07	32.5	0.956
3	3	0.07	33.2	0.956
4	5	0.07	34.1	0.956
5	7.8	0.07	35.5	0.956
6	9.2	0.07	38.9	0.956

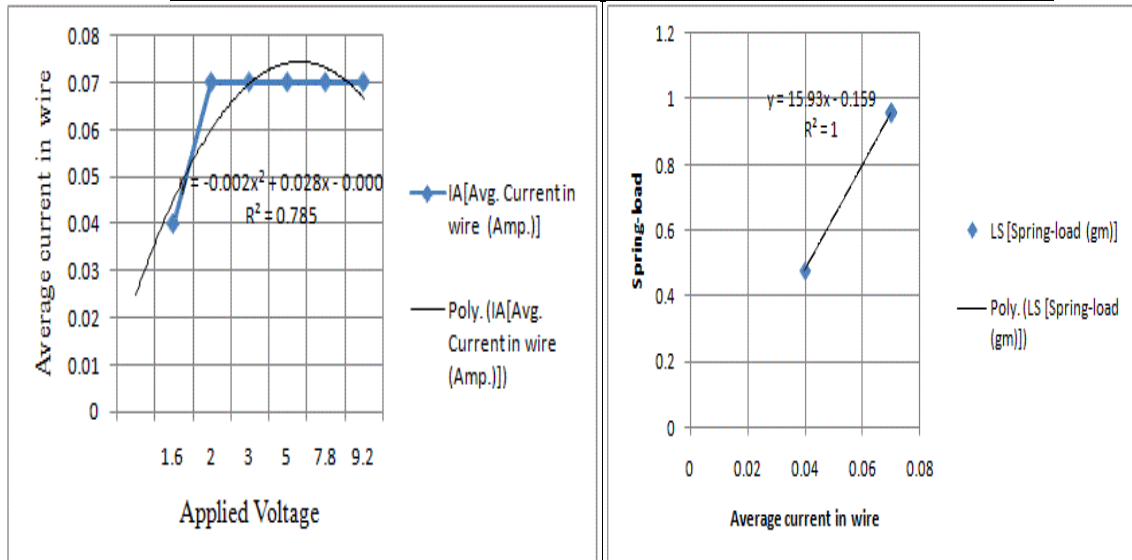


Figure 6.9 Variations of I<sub>A</sub> & V, and I<sub>A</sub>, & L<sub>S</sub> for 0.1mm SMA



Figure 6.9 shows the variation of average current ( $I_A$ ) and average applied voltage (V); then a variation of average current ( $I_A$ ) with respect to spring load ( $L_S$ ) for 0.1mm SMA. The first one the polynomial correlation is obtained as  $R^2 = 0.785$  for average current with respect to an applied average applied voltage, then the second one the polynomial correlation is obtained as  $R^2 = 1$  for average current with respect to spring load. Here, ‘R’ represents the values of correlation coefficients.

$$Y = -0.002x^2 + 0.028x - 0.00 \quad (6.1)$$

$$Y = -15.93x - 0.159 \quad (6.2)$$

The equation (6.1) related with the polynomial correlation coefficients value = 78.5% between  $I_A$  & V. Similarly the equation (6.2) related with the polynomial correlation coefficients value = 100 % between  $I_A$  &  $L_S$  (means values are not changed for 0.1mm SMA)

**For 0.2mm SMA,**

The preset length of 14.5cm measured between the two terminals of the physical-model also known as free length of 0.2mm NiTi-based helical SMA spring is obtained in deformed condition.

Table 6.6 shows the data considered for 0.2mm SMA in which various parameters such as V,  $I_A$ ,  $T_A$ , and  $L_S$  are represented by the applied voltage, average current in a wire, average wire temperature, and spring load respectively. These variables/parameters are taken from table 6.4 for the graphical analysis. So, the only ‘6’ readings are considered and nil values are (column/row) eliminated or not applied.

Table 6.6 Data considered for 0.2mm SMA

Sr. No.	Voltage Applied (Volts)	Avg Current in wire ( $I_A$ ) (Ampere)	Avg Wire Temp ( $T_A$ ) ( $^{\circ}C$ )	Spring-load ( $L_S$ ) (gm)
1	0.5	0.03	29.1	0
2	1	0.9	31.4	2.271
3	1.6	2	32.8	6.91
4	2	2.7	34.5	7.05
5	3	3.2	35.2	8.25
6	5	3.2	36.7	8.25
7	7.8	3.2	39.5	8.25
8	9.2	3.2	42.9	8.25

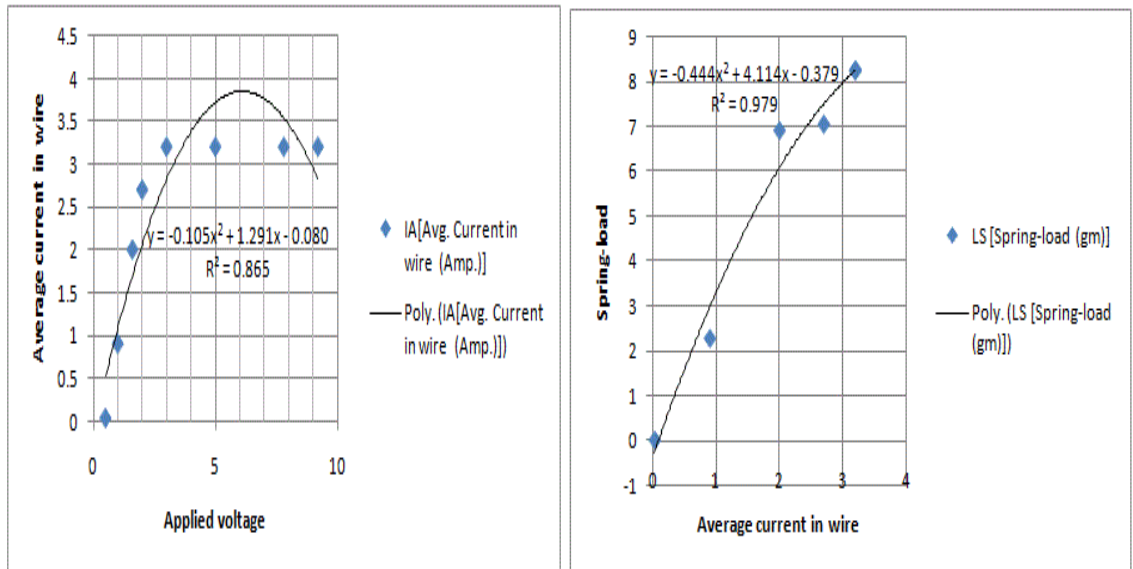


Figure 6.10 Variations of  $I_A$  &  $V$ , and  $I_A$  &  $L_S$  for 0.2mm SMA

Figure 6.10 shows the variation of average current ( $I_A$ ) and average applied voltage ( $V$ ); then a variation of average current ( $I_A$ ) with respect to spring load ( $L_S$ ) for 0.2mm SMA. The first one the polynomial correlation is obtained as  $R^2 = 0.856$  for average current with respect to an applied average applied voltage then the second one the polynomial correlation is obtained as  $R^2 = 0.979$  for average current with respect to spring load. Here, ‘R’ represents the values of correlation coefficients.

$$Y = -0.105x^2 + 1.291x - 0.080 \quad (6.3)$$

$$Y = -0.444x^2 + 4.114x - 0.379 \quad (6.4)$$

The equation (6.3) related with the polynomial correlation coefficients value = 85.6% between  $I_A$  &  $V$ . Similarly the equation (6.2) related with the polynomial correlation coefficients value = 97.9% between  $I_A$  &  $L_S$  (means values are changed up to some extent for 0.2mm SMA)

#### 6.4 ILLUSTRATION WITH 0.5 SMA-BASED SOLENOID VALVE

Application of 0.5mm SMA-based as a simple solenoid valve conical spring in the helix form (conical spring) was employed. The advantageous purpose of the valve to one way operated and can control the supply water, oil, liquid fuel, and liquid refrigerant but choked by gravitational force/self-weight.

So, It placed or installed anywhere in a vertical position as per its limitations. The advantageous purpose of the valve is to operate in one direction and control the supply of water, oil, liquid fuel, and liquid refrigerant but choked by gravitational force/self-weight. This solenoid valve can be called a micro-electro-mechanical system (MEMS) because it is the integration of mechanical elements, sensors, actuators, etc, and fulfilled small-scale precious requirements with high accuracy and precision. The actuation parameters included average strain capacity, average running temperature avg. scale-load capability and wire-current and voltage during actuation were evaluated.

#### 6.4.1 Main Components

The solenoid valve is comprised of the spring tool, clamping wire, acrylic box, core parts (Fixed cylindrical part and sliding part), Muffle furnace, temperature sensors, polystyrene foam sheets, thin plywood sheet and DPM's and basic electric-electronic parts. The main components are as follows:

**(i) Acrylic box:** It can be seen from **Figure 6.11**, which is made with the help of AutoCAD software of Autodesk Company Version-2017,

It includes a base plate having dimensions: 84.9mmx83.6mmx5mm, a top plate having dimensions: 84.9mmx83.6mmx5mm, two side plates and each having dimensions: 75.8mmx83.6mmx5mm. The base plate had a hole of 24.5mm diameter which was centrally placed. Two small acrylic rough plates were also placed on the base plate for the support which can be seen in the original pictorial view.

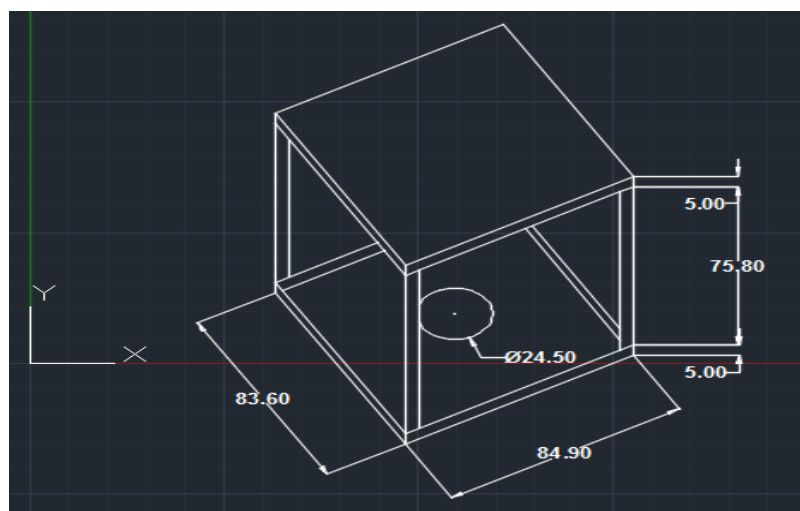


Figure 6.11 Acrylic box

**(ii) Core parts:** The core parts consist of two parts, the first one i.e. fixed cylindrical part, and the second part i.e. sliding part as shown in **Figure 6.12**. The fixed cylindrical was a hollow cylindrical section of stainless steel having an outside diameter: 24.5mm, inside diameter = 22.5mm, height = 60.0mm, and thickness = 1.0mm respectively. The sliding part was a 'cylindrical specimen' which having a significant weight equal to 80gm. The dimensions included as height: 31.5mm, outside diameter: 24.0mm, inside diameter: 22.0mm, and thickness 1.0mm respectively. The sliding part having a plastic wide knob (with hole), was used for one end connections of NiTi-based SMA spring.



Figure 6.12: Sliding part

**(iii) Muffle furnace:** A muffle oven is a one-type furnace in which the subject material is isolated from the fuel and inside coating made of glass wool. It is managed by the digital voltage regulator.

**(iv) Plywood sheet:** Plywood is a material manufactured from thin layers or "plies" of wood veneer that are glued together with adjacent layers or plywood referred to as wood panels made of multi-layered veneer, bonded together with glue. (Wood grain rotated up to 90 degrees to one another). These thin layers also called plies are glued together in alternating, perpendicular directions to create a cross-graining pattern.

**(v) Temperature Sensor (LM35):** Two LM35 temperature sensors have been applied.

**(vi) DPM:** two digital panel meters with amplifier circuit (Operational type) and 5 volts supply output has been applied.

#### **6.4.2 Wire Spring (0.5mm SMA)**

The thin flexinol wire of 0.5mm wire was converted into a conical spring (helix form) with the help of a spring tool, clamping wire, and muffle furnace to know the effect of unique parameters response for its actuation. The relation in the composition of this alloy as 49.2% (Ni) – 50.8 % (Ti) and phase transformation of SMA wire varies from 250-630°C. The wire was heated here above to its critical temperature as per required properties in strain recover rate for the applications in form of mechanics actuators to generate force or displacement. We have also used an infrared temperature sensor for better accuracy in results.

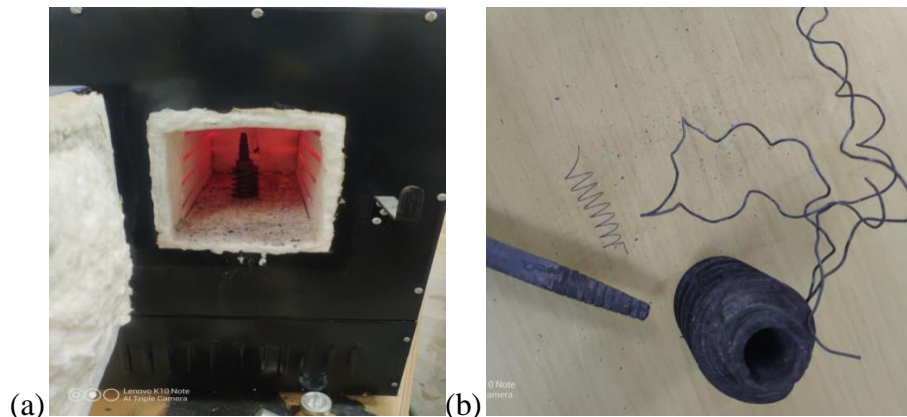


Figure 6.13 SMA spring showing (a) muffle furnace, and (b) fixture holder

Figure 6.13 shows the final SMA spring which showing the muffle furnace, and fixture holder. The fixture holder has been also applied for constant heating of SMA and placed inside the furnace. The NiTi wire was wound upon the threaded provided surface of the spring tool and then clamping wire was used to sustain its position over the NiTi wire. The annealing is done by the temperature of muffle furnace for preset-condition by muffle regulator, and the temperature maintained at 550°C.

Although tolerance of  $\pm 2^\circ$  was also considered due to the fluctuation exists by auto cut supply for an instant of time with the help of regular. The process of annealing was done on 0.5mm NiTi wire. It means SMA wire continuously heated at 550° C (constant temperature) for 45minutes then switched-off furnace and specimen remained for 24 hours inside it.

The dimensions are obtained as:

The number of turns of NiTi SMA wire for 0.5mm diameter was obtained as ‘8’, and mean coil diameter of 0.5mm SMA helical spring = 7.7mm respectively.

Outer coil diameter of it = 9.8mm (base-end) and inner coil diameter = 5.5mm (apex-end) and the spring Index of 0.5mm NiTi SMA-based spring  $\frac{D_1}{d_1} = 7.7/0.5 = 1.54$  respectively.

### 6.4.3 Solenoid Valve Based On 0.5mm SMA

Figure 10.14 represent's a solenoid valve. This solenoid valve can be called a micro-electro-mechanical system (MEMS) because it is the integration of mechanical elements, sensors, actuators, electronics, etc.

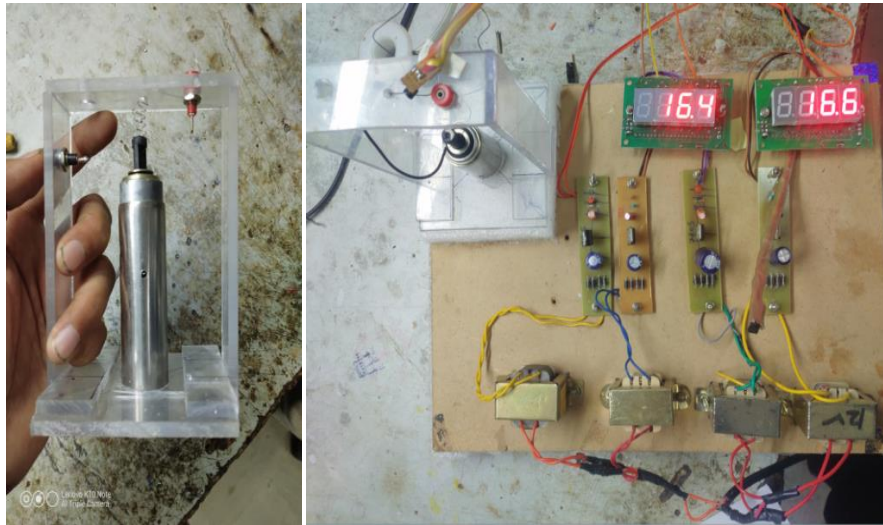


Figure 6.14 A simple solenoid valve 0.5mm SMA-based

Table 6.7 Observation data for 0.5mm SMA-based

Sr No	Voltage (V)	Average current (Ia)	Average Wire Temp (Tavg)	Atm Temp (Ta)	Measured load (gm)	Sliding displacement (Xs)
1	0.8	0	16.9	18.8	80	0
2	1.2	0.03	18.9	18.9	80	0
3	1.64	0.08	20.6	19	80	0
4	1.99	0.09	24.4	18.9	80	0
5	2.4	2.1	29.2	19	80	12.5mm
7	2.8	3.6	30.2	18.9	80	12.5mm

Figure 6.14 shows a simple solenoid valve 0.5mm SMA-based in which temperature sensors, polystyrene foam sheets, thin plywood sheets and DPM's and basic electric-electronic parts are shown.

Table 6.7 shows observation data for 0.5mm SMA-based in which average wire temperature ( $T_{avg}$ ), applied voltage ( $v$ ), average current ( $I_a$ ), atmospheric temperature ( $T_a$ ), measured load (gm), and sliding displacement ( $X_s$ ) are represented in tabular form.

#### 6.4.4 Results for 0.1mm SMA

The variation of average current ( $I_a$ ) and average wire temperature ( $T_{avg}$ ) readings are obtained correspondingly to the applied voltage ( $V$ ) or we can say that value of DC source/ supply readings.

Figure 6.15 shows Variations of  $V$ ,  $I_a$ , and  $T_{avg}$  in which green sketch in the graph represents the variation of average wire temperature ( $T_{avg}$ ), blue sketch in the graph represents the variation of voltage ( $V$ ), red sketch in graph represents the variation of average current ( $I_a$ ).

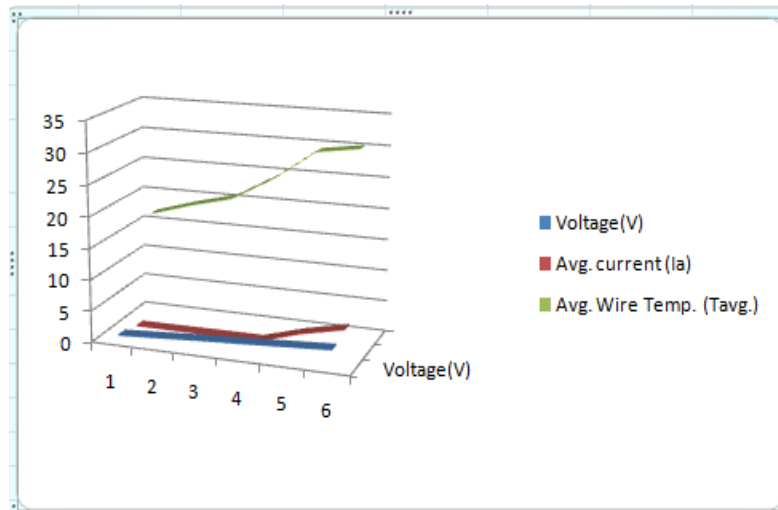


Figure 6.15 Variations of  $V$ ,  $I_a$ , and  $T_{avg}$ .

Figure 6.16 shows the variation of  $I_a$  &  $V$ ,  $T_{avg}$ , and  $I_a$  for 0.5mm NiTi-based SMA conical spring. The first one for the average current ( $I_a$ ) with respect to applied voltage ( $V$ ), and the second one is average wire temperature ( $T_{avg}$ ) concerning average current ( $I_a$ ).

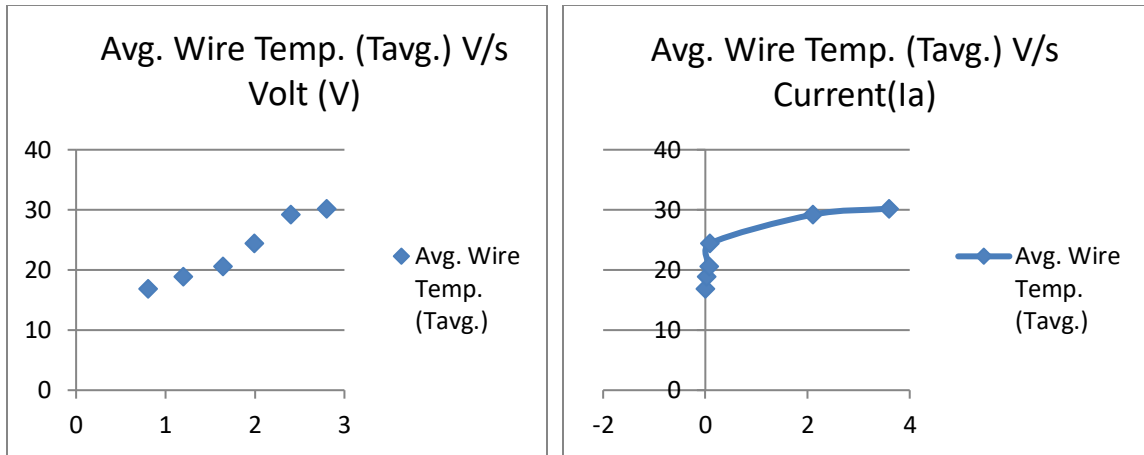


Figure 6.16 variations of  $I_a$  &  $V$ , and  $T_{avg}$  &  $I_a$  for 0.5mm SMA

The load measurement for the sliding specimen was obtained from the outside equal to 80gm and the displacement taken by the NiTi based equally to 12.5mm at the initial voltage of 2.4 (V), initial current 2.1( $I_a$ ) respectively.

## 6.5 SUMMARY

It is evident from experimental results that 0.1mm SMA-based intelligent helical spring having negligible load capacity ( $< 1\text{gm}$ ) under the effect of temperature change by using DC power supply. But the 0.2 SMA-based intelligent having a significant value of load capacity under the effect of temperature change by using DC source or DC power supply. Other points include the initials voltage value (V) obtained was higher in actuation of 0.1mm SMA than 0.2mm SMA and average current value ( $I_A$ ) of 0.1mm SMA obtained smaller as compared to 0.2mm SMA. Temperatures responses were smooth for both slender wires as they increased by increasing the power supply/voltage. This work may help researchers regarding the estimation of load capacity of NiTi-based SMA's wire at various diameters. An illustrative application of 0.5mm SMA as a simple solenoid valve has been discussed in which SMA-based conical spring in the helix form was employed. The obtained results shows that displacement has taken by the NiTi-based SMA equal to 12.5mm at the initial voltage of 2.4(V), and at initial current 2.1( $I_a$ ) respectively. The advantageous purpose of the valve is to one way operated using NiTi-based SMA thin wire and can control the supply of water, oil, liquid fuel, and liquid refrigerant but choked by gravitational force/self-weight.



# **CHAPTER 7**

## **SMART FORK-LIFT ACTUATOR USING NiTi**

### **ONE WAY HELICAL SPRING**

#### **7.1 INTRODUCTION**

In this chapter, a smart fork-lift and its stability are discussed using NiTi intelligent helical spring, for low load applications. The one-way effect and quick-responded actuation were considered for NiTi-based intelligent helical spring in smart Fork-Lift.

The system model is mainly based on the following:

- comprised of bearings
- aluminum wheel
- temperature sensor
- load cell
- DPM's
- DC Supply unit
- channel rods
- Basic electric-electronic components etc.

The annealing/normalizing processes are used for NiTi-based intelligent SMA spring. The thin flexinol wire of 1.0mm wire was considered for observations as a small actuator. A concept of a low-cost, light-weight, compact, and highly portable smart fork-lift is discussed for NiTi intelligent helical spring. It involved the following steps:

- I. Separately Preparation of NiTi based intelligent helical spring (done previously)
- II. Model preparation
- III. Practical illustration

Basically, it is considered as a major application of low load equipment based on NiTi intelligent spring.

#### **7.2 MODEL PREPARATION**

The model of a smart fork-Lift comprised of the following main sub-parts as:

##### **7.2.1 Bearings**

Bearings are machine elements that constrain relative movement to the desired motion and reduce rubbing/friction between moving elements.

Table 7.1 shows the specification for stainless steel bearings in which outer diameter/bore diameter, enclosure, contact angle, slot depth, number of balls, bearing material, weight per piece, width are presented. The given table shows the specification of one bearing in which ball material is made of alloy steel.

Table 7.1 Specification as-received for bearings

Bore-Diameter	17mm/7.5mm	Enclosure	one-shield
Contact-angle	10 <sup>0</sup> -25 <sup>0</sup>	Bearing-Material type	alloy steel
Slot-depth	1.5mm	Weight per piece	40gm
Number of Balls	9	Width	8mm



Figure 7.1 Alloy steel 4-bearings

Figure 7.1 shows Alloy steel 4-bearing in which 9 balls in numbers for each bearing.

The usually stainless steel, alloy steel, and ceramic material balls can be used in present work for the desired objective, but alloy steel balls are used here. Applied bearing balls are special highly spherical/smooth in performance with negligible friction coefficient.

### 7.2.2 Steel Round Bar

The metric stainless steel/steel round bar of grade 316 is applied here. The steel round rods including the following points as:

- Non-standard sizes in both metric and imperial with a wide variety of grades
- Simple grades are including as 303, 316, 321, 420, and 431
- Coefficient of friction between rod and balls of bearing is considered as negligible

- Contact angle between rod and balls of bearing is also considered that lie in the range of  $10^{\circ}$ - $25^{\circ}$ .



Figure 7.2 Stainless steel round rods

Figure 7.2 shows the stainless steel round rods of grade 316 (metric) in which a height of scale equal to 30cm is used.

### 7.2.3 Channels

It was a commonly used iron material, easily available commercially. Iron-channel has a U-shaped cross-section with two narrower sides at right angles to a broader one. It is cheap and obtained at in black color. The basic color was not black but it was painted to avoid rusting otherwise it can get at less price up to Rs.70/-. The dimension of the vertical channel is used as:

Length of vertical channel = 30cm,

Thickness of vertical channel = 3.25mm,

Width of vertical channel = 4.2cm, respectively



Figure 7.3 Channels (Fe/Al)

Figure 7.3 shows the two channels which are made of Fe and Al. The aluminum channel is applied as a horizontal-base and positioned horizontally. The dimension of the horizontal channel is used as:

Length of horizontal channel = 32.6cm,

Thickness of horizontal channel = 1.0mm (in end faces)

Width of horizontal channel = 11.4cm, respectively.

#### **7.2.4 Helical compression spring**

Two helical compression springs (mainly helix shape) have been used which are made of spring steel material. These steels are made of generally high-carbon-steel with very high yield strength, and low-alloy-manganese.



Figure 7.4 Compression springs of spring steel

Figure 7.4 shows two compression springs made of spring steel material. The dimensions of each spring as:

The thickness of helical compression spring = 1.25mm,

Pitch of helical compression spring = 6.75mm,

Free length of helical compression spring = 35.0mm,

Number of Active coil = 04,

And total number of coil = 08, respectively.

#### **7.2.5 Load Cell**

The load cell is a transducer that converts force or load into an electrical signal. A load cell consists of a metallic element that is introduced to a change through tension as pulling apart or compression as pushing together forces.

The strain gauges that sense this change by deflections which are the metallic foil patterns. These are insulated and mounted to the interior of the load cell with proprietary adhesives

Table 7.2 Specification as-received for load cell

Capacity (rated)	0 to 3.0 Kg	Output(rated)	1 m volt/volt
Non linearity	0.15 % (for safety)	Excitation-voltage	12 V
Gauge-factor	2 to 5	Metal-film and Metal-foil	Constantan and Silicon



Figure 7.5 Load cell

Table 7.2 shows specifications for the ht-sensor which included rated capacity, rated output, nonlinearity, recommended excitation voltage, gauge factor, and metal film.

Figure 7.5 shows load cell is placed position for rated capacity 0-3.0Kg, the conversion of force is achieved electrical signals by measuring the physical deformation of the internal strain gauge.

### 7.2.6 Temperature Sensor

The LM35 temperature sensors series are precision integrated circuits that provide output voltage; linearly proportional to the Celsius temperature.

Figure 7.6 shows Temperature sensor LM35 (with small Al-plate) for which digital panel meter (DPM) has been made to converts (analog to digital) signal with the help of different types of registers, different types of capacitors, diode, amplifier, transistors, and transformer, etc.

(Specification for temperature sensor LM35 same as applied in chapter ‘5’)



Figure 7.6: Temperature sensor LM35 (with small Al-plate)

### 7.2.7 Transparent acrylic box

The transparent acrylic box is applied, and used poly-methyl-methacrylate/PMMA materials.

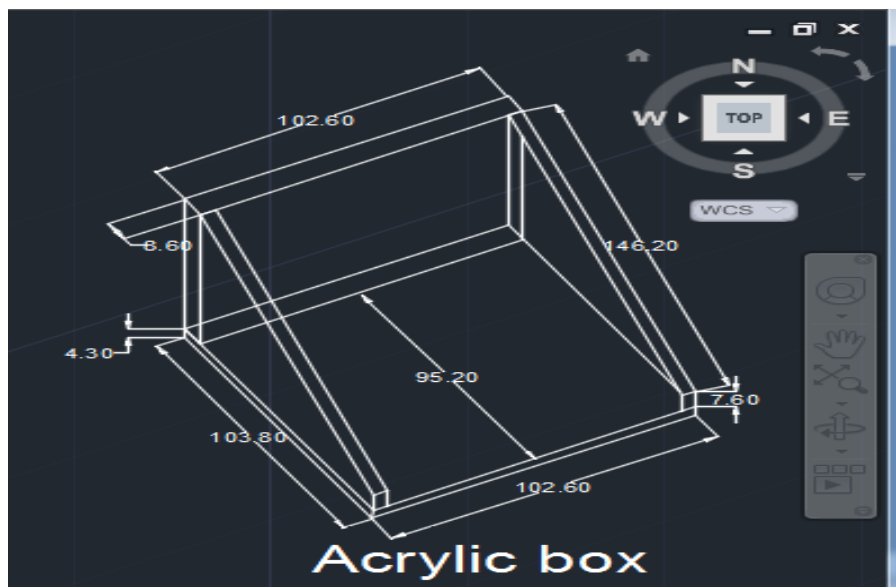


Figure 7.7 acrylic box

Figure 7.7 shows the acrylic box which is sketched by AutoCAD (software version-2017). The dimensions of open-type transparent acrylic box are used as:

Bottom base sheet base thickness of sheet = 4.30mm,

Length of sheet = 102.60mm,

Width of sheet = 95.20mm i.e. (102.60x95.20x4.30).

**For Back vertical face sheet** (is made by combining of two acrylic sheets of the same configuration and also act as a cube): -

The vertical height of sheet face = 63.80mm,

The thickness of vertical sheet = 8.60mm,

Length of vertical sheet = 102.60mm i.e. (102.60x63.80x8.60).

**For side acrylic sheet** ((made of two sheets act as trapeziums):

Parallel sides as small side=7.60mm,

Large side=63.80mm and non-parallel sides as one side= 95.20mm,

Other side=146.20mm, respectively.

### 7.2.8 Power Supply Circuit

The power supply circuit is applied here, in which various equipment in each power supply circuit are included as:

Three regulator-7805(fixed types),

Three sets of capacitors in which each set having again three capacitors configuration as one set of 25V/2200mF configuration,

The second set of 63V/1mF configuration,

And the third set of 0.1mF configuration, respectively.

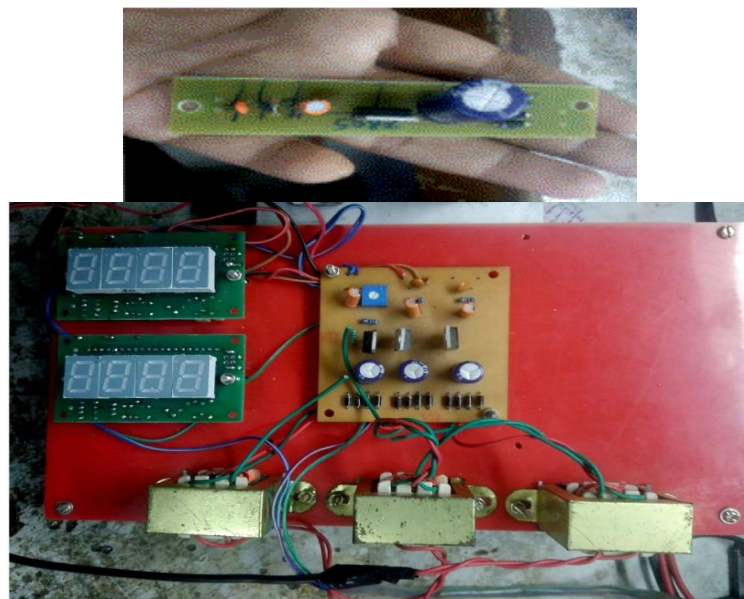


Figure 7.8 Power supply circuits

Figure 7.8 shows the three power supply circuits which are applied; one for the atmospheric temperature sensor, second for DPM-I, and third for DPM-II. Each circuit consists of sets of four diodes of IN4007.

### 7.2.9 Load-Amplifier circuit with DPM

High performance and low-power consuming integrated circuit is applied here i.e. (IC) 7107 which consists of seven segments decodes, reference voltage source, comparator & display drives as its internal circuiting, and description of 40 pins. It includes:

Digital output value = 0-1999 (up to 2 volts),

Drive display = 7 segment drive,

Number of pin = 40,

Number of LED in segment = 07.

(IC 7107 having the same description of 40 pins as- applied in chapter '5')

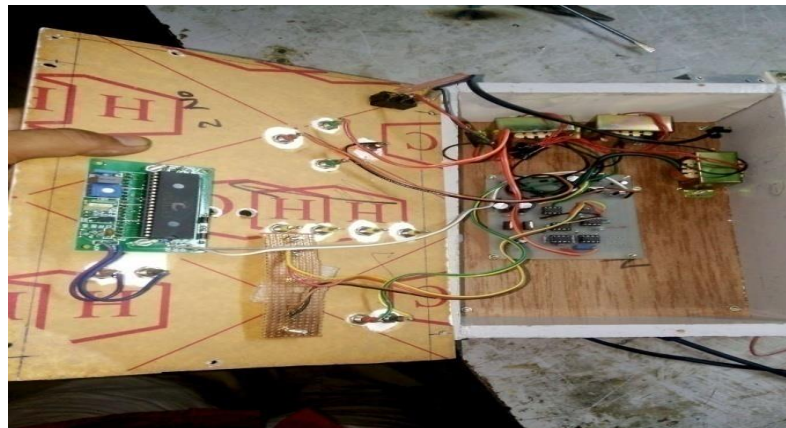


Figure 7.9 Operational amplifier circuits with the digital panel meter

Figure 7.9 shows operational amplifier circuits with digital panel meter which is one type of analog to a digital circuit. It is an operational amplifier circuit with a digital panel meter.

### 7.2.10 Pulley & Supports

The materials of aluminum are used for pulley and support components here.

(Because of light-weight, high-strength/dimensional accuracy/robustness)





Figure 7.10 Pulley and supports

Figure 7.10 shows pulley and supports in which aluminum pulley used is a wheel on the steel bearing which fixed onto a threaded that supports movement and change of direction of a steel-wire and transfer of load between SMA and acrylic box. The dimension of pulley and support is used as: -

Pulley Diameter = 37.20mm,

Thickness = 10.0mm,

Groove size includes as centered slot depth = 1.5mm,

And centered slot width = 3.0mm, respectively.

The dimension of supports (channel- type) is used as:

The total length of each support = 56.50mm,

The thickness of each support = 2.50mm.

The dimension of screw and nuts is used as: -

Bore diameter of screw = 8.0mm,

Pitch of screw = 1.25mm,

Final length remaining after cutting = 41.50mm

Bore diameter of each nut = 8.0mm (for 4-nuts),

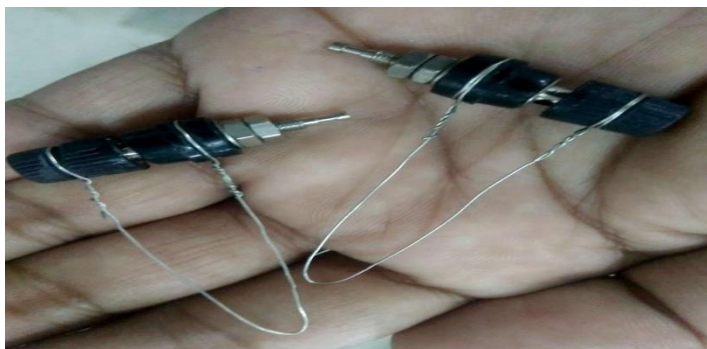
Pitch of each nut = 1.25mm,

And outer diameter of each nut = 12.50mm.

The hexagonal nuts and channel types supports are also used for further fixing of this component.

### 7.2.11 Socket Terminal-Connectors

The load-carrying specimens are also used here as socket terminal connectors. These are connected by the end of the SMA helical spring in which one remained in a fixed position and the other remains in an adjustable position.



### Figure 7.11 Socket terminal connectors

Figure 7.11 shows socket terminal connectors; they (specimens) are used to carry the lifted-weight in this presented forklift. Surfaces of each terminal are grooved by triangular files at two positions on the periphery so that the steel wires could be wound up for the hanging purpose.

#### 7.2.12 Additional Components

**Hanging wire:** A steel wire made of steel in the form of a cylindrical shape with a circular cross-section was applied in this work. Steel wire-gauges come in various standard sizes, as expressed in terms of a gauge number. Steel wires can be made in square, hexagonal, flattened rectangular or other cross-sections, either for decorative purposes or for technical purposes. This was flexible having enough strength to bear the mechanical load up to 10-12kg.

**Multimeter:** A digital type multimeter is used as a volt-ohm-millimeter/measuring instrument (electronic) that combines several measurement functions in one unit.

**Allen keys:** The "Allen" name is a registered trademark, originated by the Allen Manufacturing Company of Hartford, Connecticut circa 1910. Allen keys (hard-steel) or L keys are usually L-shaped tools consisting of a rod having a hexagonal cross-section which is used to turn an Allen screw with a hexagonal recess in the head.

**Digital caliper:** A digital caliper (stainless steel) consists of four jaws was applied. The two upper jaws are used for measuring the internal distances and two lower jaws for measuring the internal distances of objects.

**Hot-air gun:** This air gun (2000W) was used to avoid the heating of wires in temperature sensors.

Other additional parts used/applied such as DC supply (15V/5A), Ruler-scale (steel/30cm). Basic electrical-electronic components are applied as:

- Resistors (1k-10k),
- Capacitors (1000mf/25v, 1mf/63v),
- Diode (Electrolytic),
- Inductors (coil/wound),
- Transistors (3terminal-based),
- Bridge rectifiers (IN4007),

- Transformers (Set-down909)

### 7.3 MATERIAL AND SMA HELICAL SPRING

The 1.0mm NiTi/flexinol (49% Nickel and 51% Titanium) wire with straight annealed and softens conditioned applied manufacturing of SMA helical spring is involved following points as: -

- Used the threaded screw
- End restraints
- Mild steel fixture with copper clamping wire
- Muffle furnace is utilized for the tolerance of  $\pm 5^{\circ}\text{C}$  (muffle voltage regulator preset at  $530^{\circ}\text{C}$  for 45 minutes to form a typical helical spring)
- A mean coil diameter of 7.4 mm
- ‘8’ number of turns the annealing process was firstly applied by switch off the muffle furnace
- Normalized for 6 hours; opening of muffle furnace gate, and removing the helical spring after 24 hours.

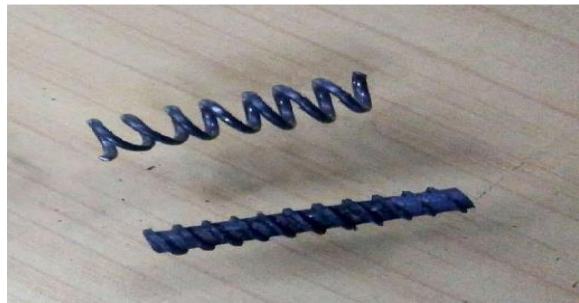


Figure 7.12 Final 0.040" NiTi-based SMA helical spring

Figure 7.12 shows final 0.040" NiTi-based SMA helical spring, the parameters of 1.0mm NiTi is obtained as:

(D) Mean coil diameter = 7.4 mm,

(d) Wire diameter = 1.0 mm, (n),

Number of turns = 8,

(c) Spring index =  $D/d = 7.4$ ,

( $L_{\text{initial}}$ ) Initial free length of spring = 2.5 cm, respectively.

(These are the basic parameters, it,s related detailed of manufacturing is presented in ‘chapter 3’ in terms of threaded screw/end restraints/steel fixture/clamping wire)

## 7.4 EXPERIMENTAL SETUP

The preset length of 1.0mm SMA helical spring wire is used here.

Figure 7.13 shows a smart fork-lift setup in which deformed 9.8cm SMA length is applied. The testing approach includes the 1.0mm SMA helical spring is attached with two socket terminals. Although one socket terminal is maintained fixed on vertically placed iron-channel and this socket so tightened that not be tilted during the loading or unloading of NiTi-based helical spring. Then the other end of NiTi SMA is attached with another socket terminal which is maintained in freely condition such that its position is movable with respect to the fixed socket terminal.

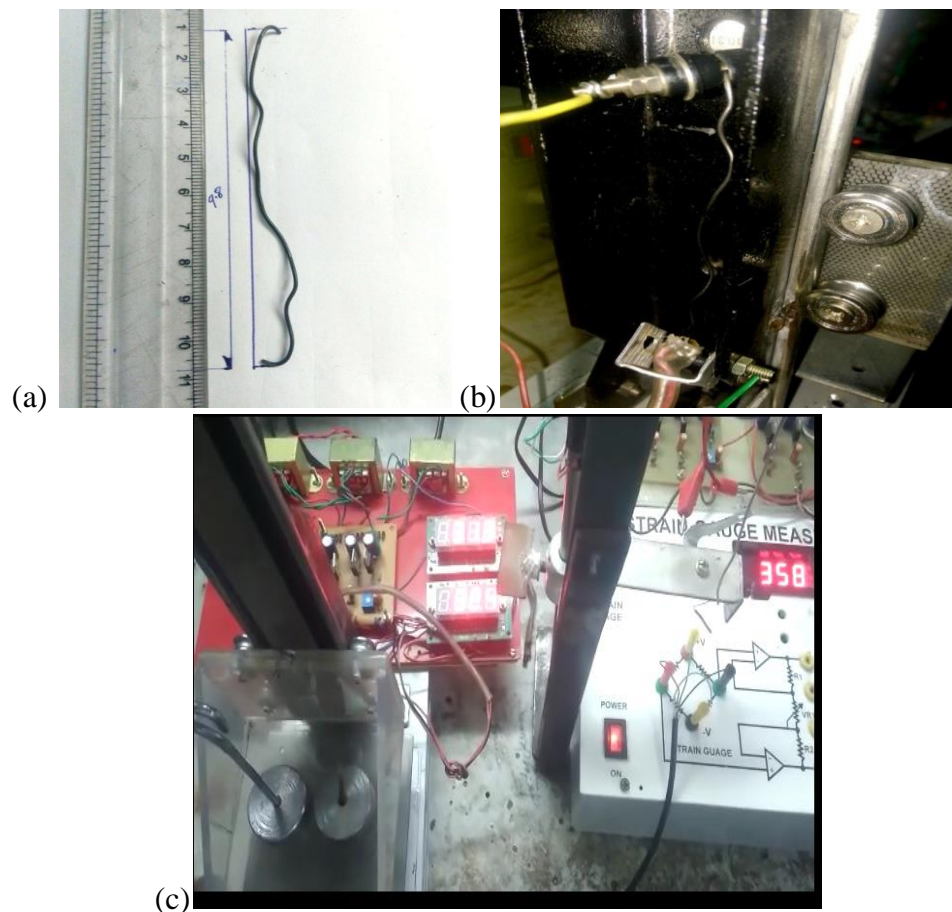


Figure 7.13 Smart fork-lift setup included (a) deformed 9.8cm SMA, (b) SMA testing approach and (c) fork-lift testing equipment

Temperature sensor LM35 is attached with the zigzag backward face side of the iron-channel. The operational amplifier with a digital panel meter is connected to the load cell.

Two helical compression springs are used which are made of spring steel material placed on the load-cell platform. Three 5-V DC power supplies are employed in the presented smart fork-lift as: -

- One for the Temperature sensor LM35 for atmospheric-temperature,
- Second for digital panel meter First
- And third for another digital panel meter.

The SMA sensor is connected with one digital panel meter at which the SMA temperature is received.

## 7.5 RESULTS AND DISCUSSION

### 7.5.1 Scale-value calculation:

The total 200gm weight has been applied.

Table 7.3 Average scale value of 1gm for 0.040" NiTi-based SMA Spring

Sr No.	Weight of Acrylic box (gm)	Load-Cell Strain	Atmospheric Temperature (°C)	Difference	Relative scale
1	0	290	28.9	290	0
2	100	462	29	172	0.581
3	200	636	28.9	174	0.578
Avg. scale value		0.579			

Table 7.3 shows the Average scale value of 1gm for 0.040" NiTi-based SMA spring that included the weight of the acrylic box, load-cell strain, atmospheric temperature, difference values, and related scale. **The average scale value for weight is obtained as “1gm = 0.579”.**

### 7.5.2 Experimental data

The 0.1mm NiTi deformed SMA helical spring is used here; ends are connected to socket terminals. One socket terminal is maintained in a fixed position on the vertically placed iron channel such that it will not be tilt during the loading/unloading. The length of 9.8cm for the SMA helical spring wire represents the vertical length of spring.

Table 7.4 shows observation data for 1.0 mm NiTi SMA Spring that included the values of preset length of SMA spring = L, applied voltage values = V, average scale values =  $A_s$  (in terms of strain gauge values), And average spring-load values =  $L_s$ .

Table 7.4 Observation data for 1.0 mm NiTi SMA Spring

Sr. No.	Preset- Length (L) (cm)	Voltage Applied (V) (volts)	Avg Current in wire ( $I_A$ ) (Amp.)	Temp ( Atmospheric ) ( $A_T$ ) ( $^{\circ}C$ )	Avg Wire Temp ( $W_T$ ) ( $^{\circ}C$ )	Vertical scale Reading (mm)	Avg Load-lifted ( $L_A$ ) (cm)	Avg Load-Cell	Spring-load (gm)
1	9.8	0	0	28.9	29	17.6	0	810	470
2	9.8	1	0.42	28.9	29.4	17.2	0.4	0	0
3	9.8	2	0.8	29	30.6	16	1.6	0	0
4	9.8	2.5	1.6	29	31.8	14.9	2.7	0	0
5	9.8	3	3.2	28.9	33.2	13.4	4.2	0	0
6	9.8	3.5	4.3	28.9	34.1	11.1	6.5	0	0
7	9.8	4	5.1	29	35.75	10.3	7.3	0	0
8	9.8	4.5	5.7	29.1	37.5	10.3	7.3	0	0
9	9.8	5	6.3	29	39.8	10.3	7.3	0	0

And Values of average currents =  $I_A$ , Average wire temperature or working SMA temperature values =  $W_T$ , Atmospheric temperature changed values =  $A_T$ , average load-lifted ( $L_A$ ) respectively.

Figure 7.14 shows the core constraints of smart fork-lift which are used mostly in observations included as average wire temperature ( $W_T$ ), average load-lifted ( $L_A$ ), average currents ( $I_A$ ), and applied voltage ( $V$ ). These core constraints of smart fork-lift have been represented graphically by using the values from table 7.4.

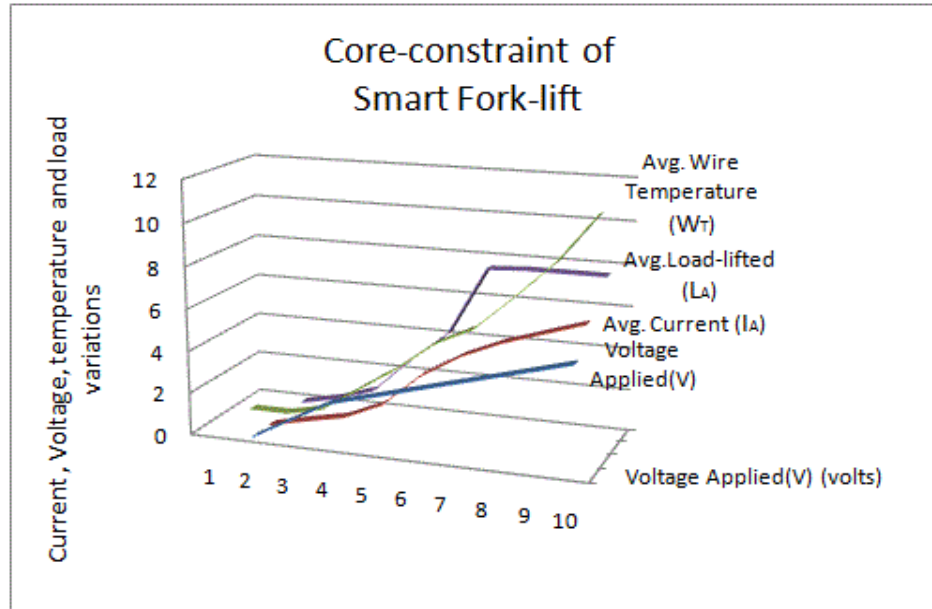


Figure 7.14 Core constraints of smart fork-lift

If we consider core-constraint as the average load lifted with respect to average applied voltage then intermediate values effect of applied voltage is discussed.

Figure 7.15 shows graph between average loads lifted and voltage applied represented by intermediate values of voltage applied. It showed the maximum actuation of SMA and also told that up to 4.0V applied voltage; load is full lifted (no need to apply voltage further voltage as loss of energy)

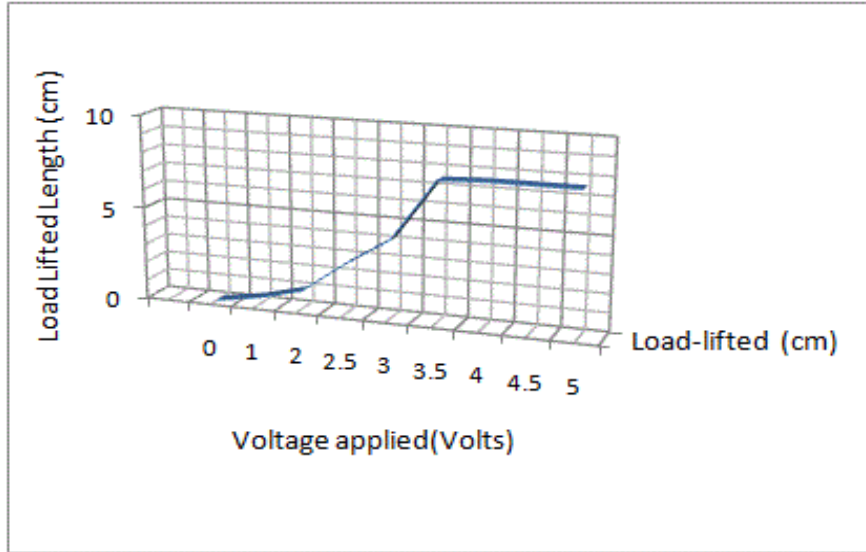


Figure 7.15: Load lifted vs. Voltage applied

Figure 7.16 shows the graph Load lifted with respect to working SMA. Two equations of relationship are obtained. Firstly, the linear relationship of load lifted values ( $L_A$ ) with respect to working SMA temperature values ( $W_T$ ) is as follows with correlations coefficient = 90.6 %. Secondly, the polynomial relationship of load lifted values ( $L_A$ ) with respect to working SMA temperature values ( $W_T$ ) [29<sup>o</sup>C, 29.4<sup>o</sup>C, 30.6<sup>o</sup>C, 31.8<sup>o</sup>C, 33.2<sup>o</sup>C, 34.1<sup>o</sup>C, 35.75<sup>o</sup>C, 37.5<sup>o</sup>C and 39.8<sup>o</sup>C respectively] is as follows with correlations coefficient = 91.9 %. Here, correlation coefficient are obtained as  $R^2 = 0.906$  for linear relationship and  $R^2 = 0.919$  for polynomial relationship respectively.

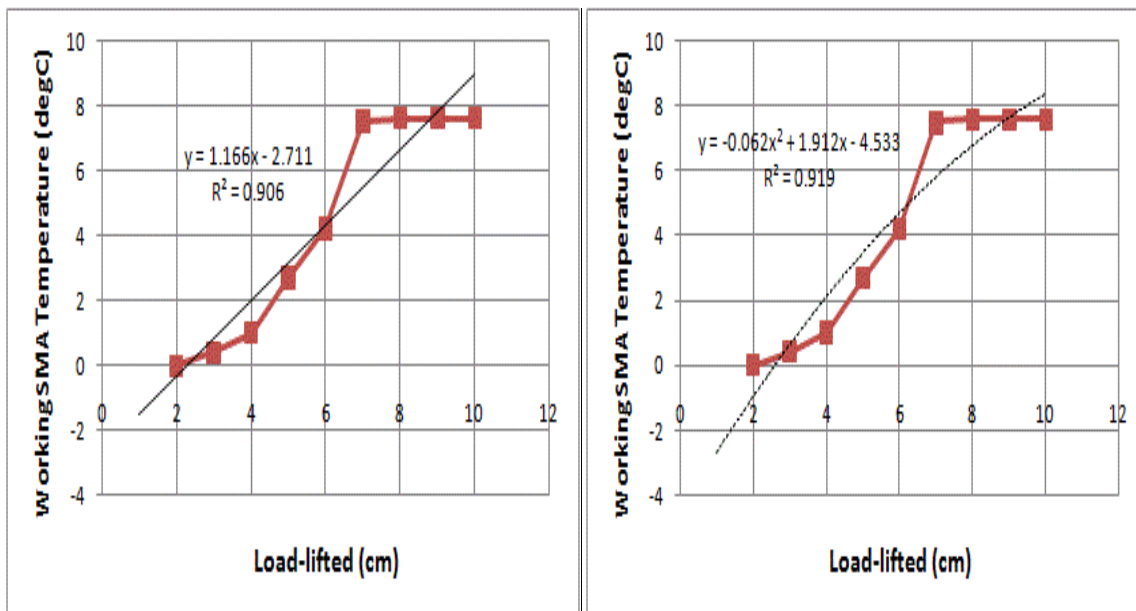




Figure 7.16 Load lifted vs. working SMA temperatures

$$Y = 1.166x - 2.711 \quad (7.1)$$

$$Y = -0.062x^2 + 1.912x - 4.533 \quad (7.2)$$

The mentioned model equations described the behavior of small scale smart fork-lift with respect to 1.0mm NiTi-based shape memory alloy spring.

## 7.6 SUMMARY

This Smart fork-lift actuator using SMA provides a new method (by replacing hydraulic-based, pneumatic pressure-based, gearing, and pulley-based systems for cost-effective light load applications). Increasing voltage showed the higher actuation of SMA. In the end region of voltage increment, a little bit lesser actuation of SMA was observed. The graph between average loads lifted and voltage applied is represented by intermediate values of the voltage applied. It showed the maximum actuation of SMA and also told that up to 4.0V applied voltage; the load is fully lifted (no need to apply voltage further voltage as loss of energy). A high correlation exists with correlation coefficient  $R^2 = 0.906$ . This work will support researchers in developing a thermo-mechanical system of small-scale fork-lift using NiTi metallic materials.

# **CHAPTER: 8**

## **STABILITY AND STIFFNESS ANALYSIS OF HELICAL SPRINGS**

### **8.1 INTRODUCTION**

This chapter presents the behavior of helical compression springs which are applied in a smart forklift. The cylindrical and conical shape helical springs are used here as storage devices in which stability is defined in terms of load gains, evaluation of spring rates, and deflections. Spring rates ( $k$ ) of both springs were compared. These prepared springs are also known as coil springs which regain its original form and position when distorted by the loaded in smart fork-lift apparatus. These springs are developed by applying the heat treatment and quenching processes on the galvanized spring steel material by using the threaded shape fixtures.

These springs worked as mechanical devices are typically used to bear the lifting load which differed here greatly in strength and in size depending on changing its parameters. Both, the cylindrical and conical shapes are made of helically coiled wires with constant clearance between the active coils and able to absorb external counter-acting loads applied against each other in their axis. One-direction deformation in axial format is applied.

### **8.2 PURPOSE**

The purpose to introduce is as follows

- To checks which physical-loaded spring has better spring rate ( $k$ ) i.e. conical (helix type) compression spring / cylindrical helical type compression spring.
- How to prepare the samples of the physical-loaded conical (helix type) compression spring and cylindrical helical compression spring.
- To check the deflection and bearing load for different free lengths in conical (helix type) compression spring/cylindrical helical type compression spring.
- To find the actual load with the help of a strain gauge kit used in forklift for both springs.

### **8.3 MATERIAL AND SPECIFICATIONS**

The manufacturing of cylindrical/conical helical springs in the present work included; a hard drawn carbon steel ASTM A227 wire as shown in **Table 8.1**.

Table 8.1 Composition of spring steel ASTM A227 wire

Carbon (C)	0.60 to 0.85%	Phosphorous (P)	0.04% (max)
Manganese (Mn)	0.30 to 0.85 % (max)	Sulphur (S)	0.05% (max)
Silicon (Si)	0.15 to 0.35%	Colour/Dia	Blacky grey/1.0mm

The specifications of cylindrical tool-fixture and conical tool-fixture springs that have been used for evaluation are given below as: -

(For Conical)

Diameter of Round rod = 12.00mm,

Total Length of conical tool-fixture = 113.00mm,

Unthreaded length = 42.75mm,

Threaded length =  $113.00 - 72.50 = 40.50$ mm,

The angle of teeth cutting on lath M/C =  $2.5^0$ , respectively.

(For Helical)

Diameter of Round rod = 12.00mm,

Total Length of helical tool-fixture = 88.50mm,

Unthreaded length = 42.75mm,

Threaded length =  $88.00 - 42.75 = 45.25$ mm,

The angle of teeth cutting on lath M/c =  $2.5^0$ , respectively.

## 8.4 MANUFACTURING OF HELICAL AND CONICAL SHAPED HELICAL SPRINGS

The following steps are applied:

### STEP-I

**8.4.1 Tempering process for spring steel wire:** The tempering process is applied here in which heating the spring steel wire up to  $650^0\text{C}$  for 10 minutes and then slowly cooled inside the furnace.

Figure 8.1 shows the tempering of wire in which A227 GR-II material is used for spring steel. Other sustaining parts included a muffle furnace (230V/AC/1100<sup>0</sup>C), infrared temperature sensor-based thermometer (digital/leaser type).



Figure 8.1 Tempering of wire

#### STEP-II

**8.4.2 Fixture-cum-spring tool making:** Mild steel rods which were easily obtained from the institutional engineering workshop were used to making the fixture-cum-spring tools. Figure 8.2 shows two fixture-cum-spring-tools and these are prepared on advance lathe M/c. For making these fixtures, presented work applied round bar billets (mild steel-2pieces), drill bit (2.0mm), and drill-machine (230V/2200rpm) also.



Figure 8.2 Fixture- cum-spring-tools

#### STEP-III

**8.4.3 Steel wire-wrapping and clamping:** The wrapping of steel wire is applied here for fixtures. The spring manufacturing tools used as fixtures and clamping wire (Galvanized Mild steel) were applied on tool-fixtures as shown in **Figure 8.3**.



Figure 8.3 wrapping steel wire

#### STEP-IV

**8.4.4 Heating the Steel wire at 860<sup>0</sup>C (solid-phase critical heating):** Solid phase critical heating means heating the steel wire at a specific temperature for 15-20 minutes. **Figure 8.4** shows the muffle furnace operating position at 860<sup>0</sup>C.



Figure 8.4 Muffle Furnace operating at 860<sup>0</sup>C

#### STEP-V

**8.4.5 Quenching process (oil-dip tool-fixtures with springs):** Quenched steel is generally not used directly here, it is used after tempering, and quench oil serves two primary functions. Quenching and tempering are processes applied that strengthen and harden materials like steel and other iron-based alloys.



Figure 8.5 Oil-dip tool-fixtures with springs (after quenching)

Figure 8.5 shows oil-dip tool-fixtures with springs (after quenching). Castrol quenching oil is applied here as a cooling medium.

#### STEP-VI

**8.4.6 Separation of spring from tool-fixture:** The spring is separated from tool-fixtures manually; cylindrical and conical shape helical springs are obtained.

Figure 8.5 shows the separation of spring included clamping wires, cylindrical shape helical and conical shape helical springs which are represented after their formation.

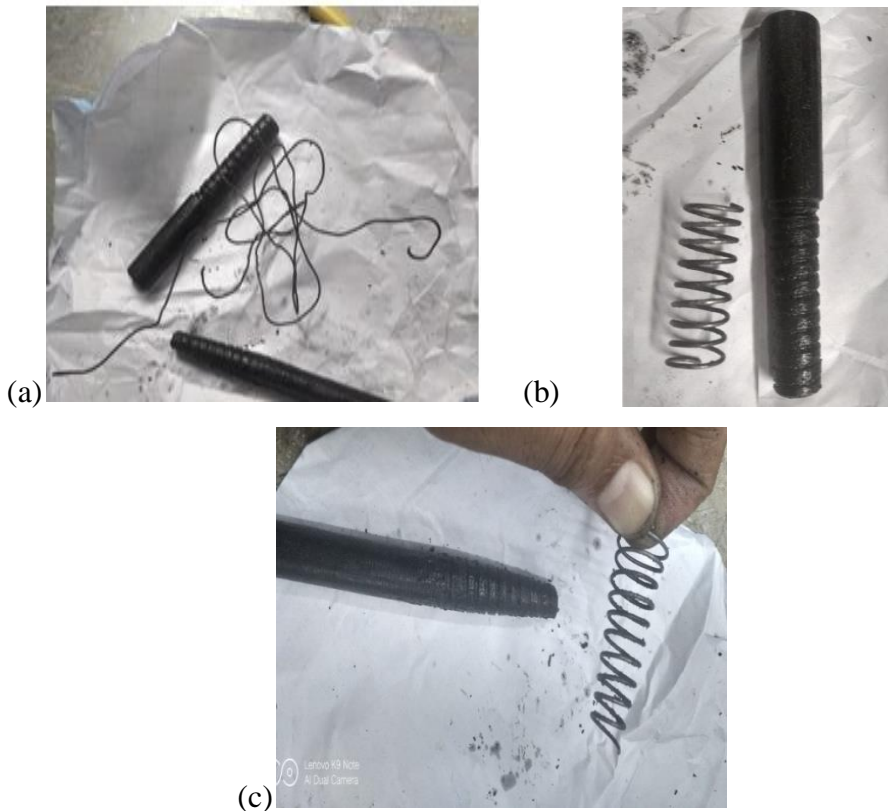


Figure 8.6 Separation of spring included (a) clamping wires, (b) cylindrical shape helical spring, and (c) conical shape helical spring

#### STEP-VII

**8.4.7 Pre-Final and Final specimens:** The formation of specimens that were applied for loading gains, spring rate, and deflections can be seen in **Figure 8.7**.

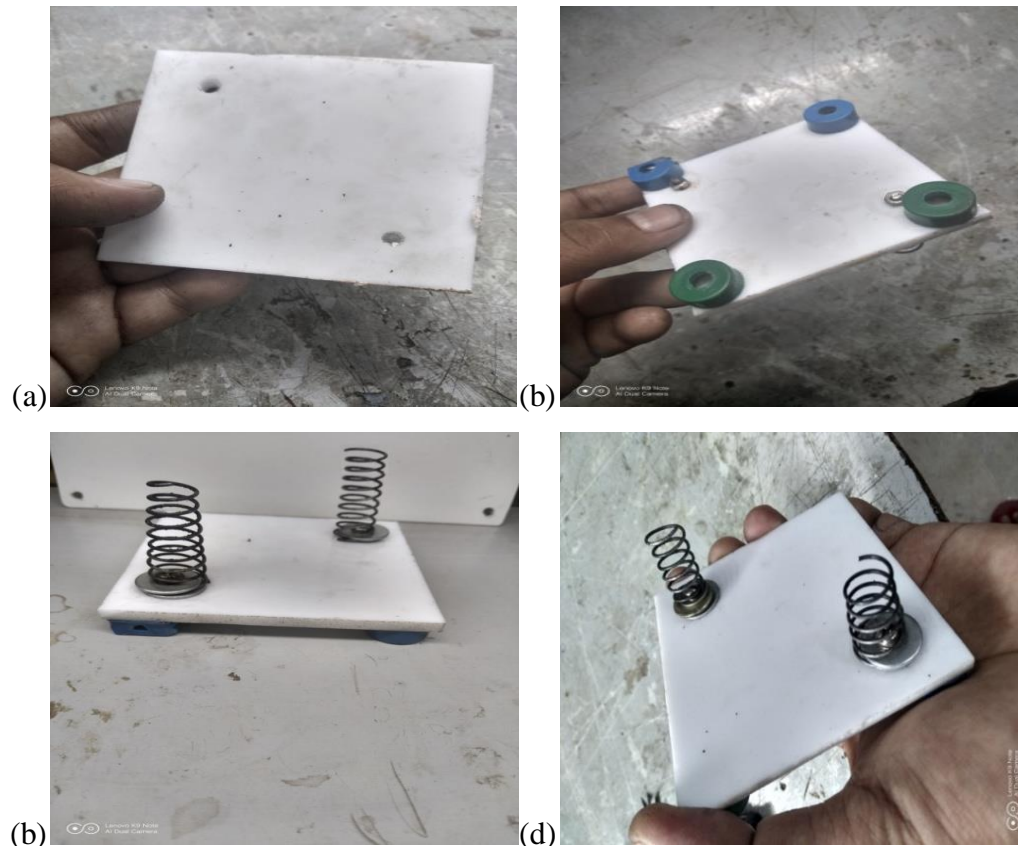


Figure 8.7 Pre-final and final specimens (a) for acrylic base, (b) for ‘four’ supports, (c) for initial specimens, and (d) for final specimens

### 8.5. EXPERIMENTAL SETUP AND OBSERVATION

The analog signal is directly measured by the quantities or physical signal here. Digital signals only have two states. For digital is referred to binary states i.e. 0 and 1. ADC provides a link between the analog world of transducers and the digital world of signals processing/data handling.

Figure 8.8 shows ADC based amplifier circuit with a smart fork-lift loading box. The amplifier circuit behaves as a strain gauge measuring kit in the experimental setup here.

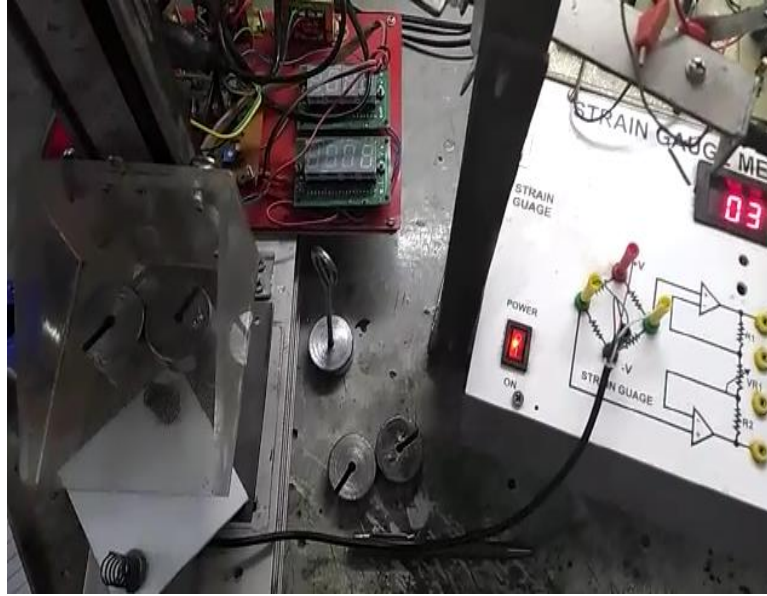


Figure 8.8 ADC based amplifier circuit, and smart fork-lift loading box

**8.5.1 Average scale-value:** The scale values are calculated with the help of an acrylic box of smart fork-lift and steel slotted weights. The steel hanger weight of 100gm has not been used in this work.

Table 8.2 Average scale value i.e. '1' reading of strain equal to '10.512gm'

Sr No	Weight of Acrylic box (gm)	Average Load-Cell Strain	Temp (Atm) (°C)	Difference	Relative scale
1	0	17.5	25.2	0	0
2	100	27	26	9.5	10.526
3	200	36.5	25.1	19	10.526
4	300	46	26.1	28.5	10.526
5	400	55	25.9	37.5	10.666
6	650	80.5	25.6	63	10.317
<b>Average scale value</b>			<b>10.512</b>		

Table 8.2 shows the weight of an acrylic box, GF, and related values. The weight of the acrylic box is obtained i.e.183.96gm.



**8.5.2 Stage First:** This stage is applied for the initial specimen; the weight of the spring holder and acrylic box calculate by the load cell of the smart fork-lift is attached to the strain measurement kit with the help of terminals. The spring rate ( $k$ ) is calculated here for cylindrical and conical springs. The parameters for stage first are used in cylindrical/conical as shown in **Table 8.3**.

**Here, the data were obtained in Table 8.4 and Table 8.5 for cylindrical and conical spring of wire size ( $d=1.0\text{mm}$ ).**

Table 8.3 Parameters for stage first (cylindrical/conical)

Parameters	Cylindrical Spring	Conical Spring
Type of End	Plain End	Plain End
Wire Diameter ( $d$ )	1.0mm	1.0mm
Outer Diameter ( $D_o$ )	12mm	14.3mm (Base end) 6.5mm (Apex end) 12mm (mean dia)
Pitch ( $p$ )	3.8.mm	3.8mm
Free Length ( $L_f$ )	34.8mm	34.8mm
Total Coils ( $N^T$ )	10	10
Active Coil ( $N$ )	8	8

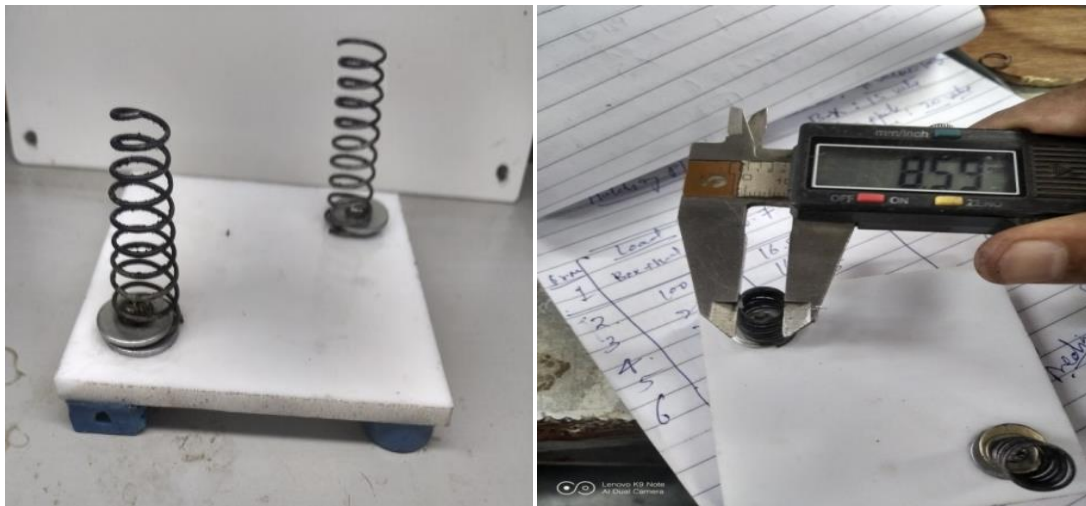


Figure 8.9 specimens for first stage

Table 8.4 shows observation data for stage first for conical shape helical spring. This represented the various values of vertical scale/deflections and average load-strains (which were further applied). The other observations included the weight of the acrylic box, the weight of the spring holder, spring-loaded values, and atmospheric temperatures. In the mentioned data first value of vertical scale is obtained as 'Zero' value concerning negligible spring-loaded value. Both, the weight of the acrylic box and the weight of the spring holder are fixed and load is applied gradually up to 650gm. The vertical scale obtained for cylindrical shape helical spring of wire size ( $d = 1.0\text{mm}$ ) i.e. 3.0mm, 3.9mm, 4.7mm, 5.4mm, 6.0mm, and 7.6mm correspondingly to average load-strains.

Table 8.5 shows observation data for stage first for cylindrical shape helical spring. This represented the various values of vertical scale/ deflections and average load-strains (which also further applied). The other observation parameters included the weight of the acrylic box, the weight of the spring holder, spring-loaded values, and atmospheric temperatures. In the mentioned data first value of vertical scale is obtained as 'Zero' value concerning negligible spring-loaded value. Both, the weight of the acrylic box and the weight of the spring holder are fixed, and load is also applied gradually up to 650gm. The vertical scale obtained for conical shape helical spring of wire size ( $d = 1.0\text{mm}$ ) i.e. 2.46mm, 3.60mm, 4.7mm, 5.7mm, 6.81mm, and 9.62mm correspondingly to average load-strains. Table 8.4 Data obtained for stage first (conical shape helical spring)

Sr. No.	Weight of Acrylic box (gm)	Weight of spring holder (gm)	load applied (gm)	Vertical scale reading (mm)	Average Load-Cell Strain	Temp (Atm) ( $^{\circ}\text{C}$ )	spring load (conical )	Spring Rate (K)
1	0	31.53	0	0	3	25	0	0
2	183.96	31.53	0	3.0	20.5	25.7	215.49	71.83
3	183.96	31.53	100	3.9	29.5	25.2	315.49	80.89
4	183.96	31.53	200	4.7	40	26	415.49	88.40
5	183.96	31.53	300	5.4	51	25.1	515.49	95.46
6	183.96	31.53	400	6.0	61	26.1	615.49	102.58
7	183.96	31.53	650	7.6	71	25.9	865.49	113.88

Table 8.5 Data obtained for stage first (cylindrical shape helical spring)

Sr. No.	Weight of Acrylic box (gm)	Weight of spring holder (gm)	load applied (gm)	Vertical scale reading (mm)	Average Load-Cell Strain	Temp (Atm) (°C)	spring load (helical )	Spring Rate (K)
1	0	31.53	0	0	3	25.9	0	0
2	183.96	31.53	0	3.6	20.5	25.1	215.49	59.86
3	183.96	31.53	100	4.8	29.5	26.1	315.49	65.72
4	183.96	31.53	200	5.9	40	26	415.49	70.42
5	183.96	31.53	300	6.9	51	25.1	515.49	74.70
6	183.96	31.53	400	7.8	61	25.6	615.49	78.90
7	183.96	31.53	650	8.6	71	25.5	865.49	100.63

**8.5.3 Stage second:** This stage is applied for the final specimen in which the weight of the spring holder and acrylic box calculate by the load cell of a smart fork-lift that is attached to the strain measurement kit with the help of terminals. The spring rate (k) is calculated here for cylindrical and conical springs. The parameters for stage second are used in cylindrical/ conical as shown in **Table 8.3**.

**Here, the data was obtained in Table 8.7 and Table 8.8 for cylindrical helical and conical spring of wire size (d=1.0mm) respectively, but different in numbers of turns and free lengths.**

Table 8.7 shows observation data for stage first for cylindrical shape helical spring. This represented the various values of vertical scale/ deflections and average load-strains (which were further applied). The other observation parameters included the weight of the acrylic box, the weight of the spring holder, spring-loaded values, and atmospheric temperatures.

In the mentioned data, first value of vertical scale is obtained as 'Zero' value concerning negligible spring-loaded value. Both, the weight of the acrylic box and the weight of the spring holder are fixed (load is applied gradually up to 650gm).

Table 8.6 Parameters for stage second (cylindrical/conical)

Parameters	Cylindrical Spring	Conical Spring
Type of End	Plain End	Plain End
Wire Diameter (d)	1.0mm	1.0mm
Outer Diameter (D <sub>o</sub> )	12mm	14.3mm (Base end) 8.6mm (Apex end) 13.2mm (mean dia)
Pitch (p)	6.8mm	6.8mm
Free Length (L <sub>f</sub> )	24.39mm	19.80mm
Total Coils (N <sup>T</sup> )	7	6
Active Coil (N)	5	4



Figure 8.10 Final specimens for second stage observations

The vertical scale obtained for cylindrical shape helical spring of wire size ( $d = 1.0\text{mm}$ ) i.e. 2.06mm, 3.01mm, 4.0mm, 4.92mm, 5.78mm, and 8.30mm correspondingly to average load-strains.

Table 8.8 shows observation data for stage first for conical shape helical spring. This represented the various values of vertical scale/deflections, and average load-strains (which also further applied). The other observation parameters included the weight of the acrylic box, the weight of the spring holder, spring-loaded values, and atmospheric temperatures.

Table 8.7 Data obtained for second stage (cylindrical shape helical spring)

Sr. No.	Weight of Acrylic box (gm)	Weight of spring holder (gm)	load applied (gm)	Vertical scale reading (mm)	Average Load-Cell Strain	Temp (Atm) ( <sup>0</sup> C)	spring load (helical )	Spring Rate ( K )
1	0	31.53	0	0	3	25	0	0
2	183.96	31.53	0	1.8	20.5	25.7	215.49	119.72
3	183.96	31.53	100	2.6	29.5	25.2	315.49	121.34
4	183.96	31.53	200	3.3	40	26	415.49	125.90
5	183.96	31.53	300	3.9	51	25.1	515.49	132.17
6	183.96	31.53	400	4.45	61	26.1	615.49	138.31
7	183.96	31.53	650	4.95	71	25.9	865.49	174.84

Table 8.8 Data obtained for second stage (conical shape helical spring)

Sr No	Weight of Acrylic box (gm)	Weight of spring holder (gm)	load applied (gm)	Vertical scale reading (mm)	Average Load-Cell Strain	Temp (Atm) ( <sup>0</sup> C)	spring load (conical )	Spring Rate ( K )
1	0	31.53	0	0	3	25.9	0	0
2	183.96	31.53	0	1.6	20.5	25.1	215.49	134.68
3	183.96	31.53	100	2.3	29.5	26.1	315.49	137.17
4	183.96	31.53	200	2.95	40	26	415.49	140.84
5	183.96	31.53	300	3.56	51	25.1	515.49	144.80
6	183.96	31.53	400	4.14	61	25.6	615.49	148.67
7	183.96	31.536	650	4.66	71	25.5	865.49	185.72

In the mentioned data first value of vertical scale is obtained as ‘Zero’ value concerning negligible spring-loaded value. The weight of the acrylic box & the weight of the spring holder are fixed, and load is applied gradually up to 650gm. The vertical scale was obtained for conical shape helical spring of wire size (d = 1.0mm) i.e. 2.44mm, 3.50mm, 4.71mm, 5.85mm, 6.90mm, and 9.72mm correspondingly to average load-strains.

## 8.6 RESULTS AND DISCUSSION

Here, spring rates (k) of both stages are discussed by analytical calculations in which average load-strains values were changed into the spring-loaded values. The spring rates (k) for physical-loaded helical compression springs according to the properties of spring in the strength of materials as:-

$$F = K.X \quad (8.1)$$

Where 'F' represents forces or loads,

K → spring rate

X → linear extension / deflection

### 8.6.1 Stage first analysis for conical spring and helical spring

Table 8.9 shows the spring rate ( $K_c$ ) of conical spring for stage first in which vertical scale reading, spring-loaded values, and spring rate are included. For example: At 8.4 reading of vertical scale the 103.035 spring rate is obtained.

Figure 8.11 shows a graph between vertical scale reading or deflection and load variation for conical spring. The spring rate ( $K_c$ ) of conical spring is obtained linearly with regression coefficient ( $R^2$ ) = 0.96. The equation of spring-loaded value concerning vertical scale reading is as follows with correlations coefficient = 96.0 %.

$$Y = 121.4x - 55.93 \quad (8.2)$$

Table 8.9 Spring Rate ( $K_c$ ) of conical spring for stage first

Vertical scale reading(mm)	Spring loaded value(conical)	Spring Rate ( $K_c$ )
2.05	215.496	105.120
3.00	315.496	105.165
3.90	415.496	106.537
4.90	515.496	105.203
5.80	615.496	106.12
8.40	865.496	103.035

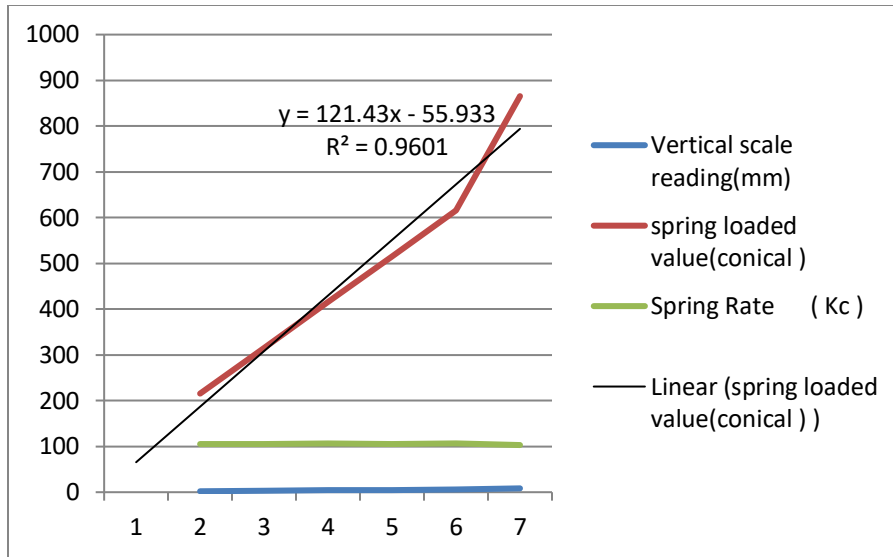


Figure 8.11 Vertical scale reading or deflection vs. load variation for conical spring  
(stage first)

Table 8.10 shows the spring rate ( $K_h$ ) of helical spring for stage first in which vertical scale reading, spring-loaded values, and spring rate are included. For example: At 9.62 reading of vertical scale the 89.968 spring rate is obtained.

Figure 8.12 shows a graph between vertical scale reading or deflection and load variation for conical spring. The spring rate ( $K_h$ ) of helical spring is obtained linearly with regression coefficient ( $R^2$ ) = 0.98.5 Equation of spring-loaded value concerning vertical scale reading is as follows with correlations coefficient = 98.5 %.

$$Y = 13.39x^2 + 0.892x + 176.2 \quad (8.3)$$

Table 8.10 Spring Rate of helical spring for stage first

Vertical scale reading(mm)	Spring loaded value(helical)	Spring Rate ( $K_h$ )
2.46	215.496	87.600
3.60	315.496	87.637
4.70	415.496	88.403
5.70	515.496	90.437
6.81	615.496	90.381
9.62	865.496	89.968

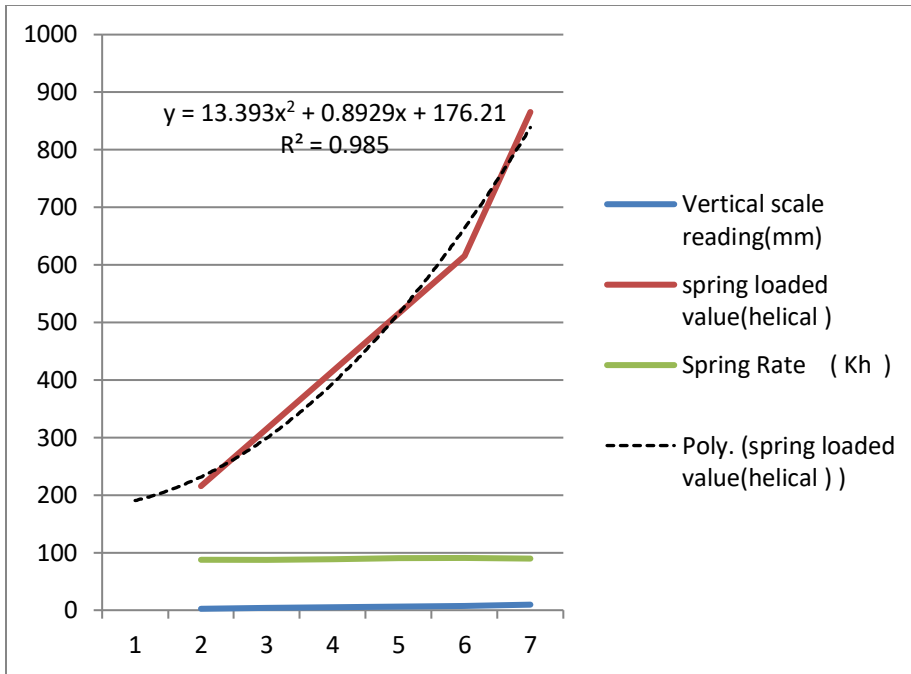


Figure 8.12 Vertical scale reading or Deflection vs. load variation for helical spring  
(stage first)

### 8.6.2 Stage second analysis for conical and helical springs

Table 8.11 shows the spring rate ( $K_h$ ) of conical spring for stage first in which vertical scale reading, spring-loaded values, and spring rate are included. For example: At 8.30 reading of vertical scale the 104.276 spring rate is obtained.

Figure 8.13 shows a graph between vertical scale reading or deflection and load variation for helical spring. The spring rate ( $K_h$ ) of helical spring is obtained linearly with regression coefficient ( $R^2$ ) = 0.99 Equation of spring-loaded value concerning vertical scale reading is as follows with correlations coefficient = 99.0 %.

$$Y = 104.7x + 0.505 \quad (8.4)$$

Table 8.11 Spring Rate of conical spring for stage second



Vertical scale reading(mm)	Spring loaded value(conical )	Spring Rate ( K <sub>c</sub> )
2.06	215.496	104.609
3.01	315.496	104.815
4.00	415.496	103.874
4.92	515.496	104.775
5.78	615.496	106.487
8.30	865.496	104.276

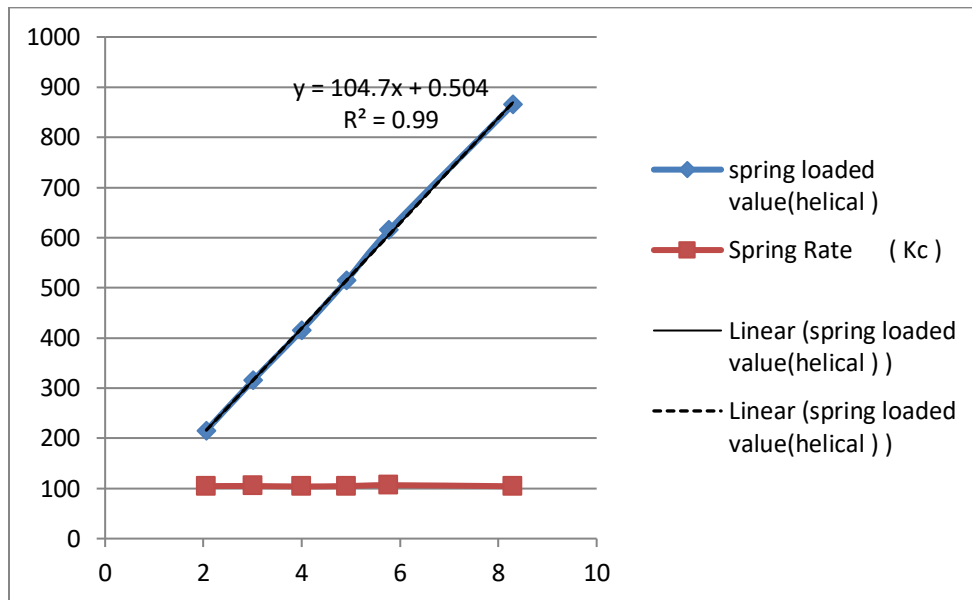


Figure 8.13 Spring Load vs. vertical scale for conical spring (stage second)

Table 8.12 shows the spring rate ( $K_h$ ) of helical spring for stage first in which vertical scale reading, spring-loaded values, and spring rate are included. For example: At 9.72 reading of vertical scale the 89.042 spring rate is obtained.

Figure 8.14 shows the graph between vertical scale reading or deflection and load variation for helical spring. The spring rate ( $K_h$ ) of helical spring is obtained linearly with regression coefficient ( $R^2$ ) = 0.98.5 Equation of spring-loaded value concerning vertical scale reading is as follows with correlations coefficient = 98.5 %.

$$Y=13.39x^2 -25.89x +188.7 \quad (8.5)$$

Table 8.12 Spring Rate ( $K_h$ ) of helical spring for stage second

Vertical scale reading (mm)	Spring loaded value (helical )	Spring Rate ( $K_h$ )
2.44	215.496	88.318
3.50	315.496	90.141
4.71	415.496	88.215
5.85	515.496	88.573
6.90	615.496	89.202
9.72	865.496	89.042

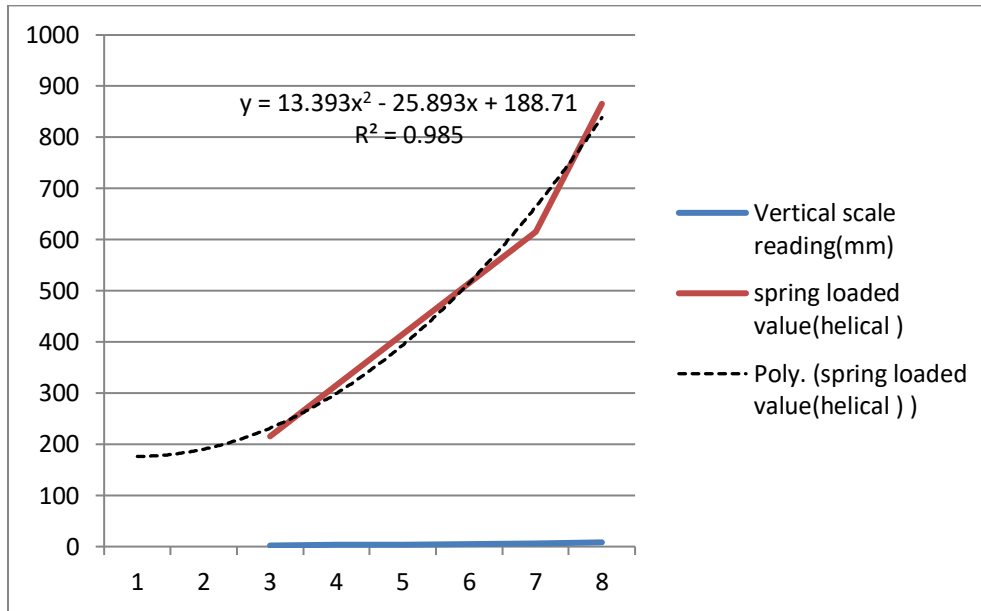


Figure 8.14 Vertical scale reading or deflection vs. load variation for helical spring (stage second)

**Combined spring rate variation** in first and second stages for conical spring and helical springs

Figure 8.15 shows the combined spring rate for conical spring/helical spring in the initial stage/second respectively here. The equations 8.2, 8.3, 8.4, and 8.5 can be used for the stability of helical and conical springs in design.

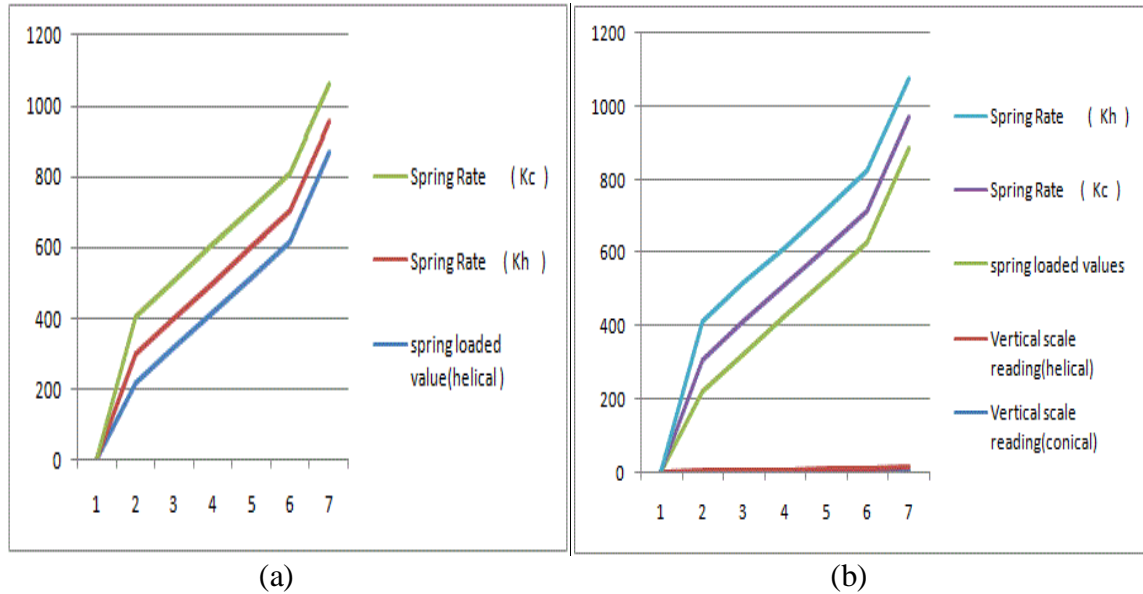


Figure 8.15 combined spring rate variation for (a) Initial/stage first, and (b) stage second. And the stability of conical spring as compared to helical spring was found higher. Table 8.4, 8.5, 8.7, and 8.8 helps for stiffness analysis.

### 8.7 SUMMARY

From experimental results, the spring rate ( $k$ ) is obtained higher for conical helical compression spring than that cylindrical helical compression spring. The stability of conical spring founded higher spring as compared to helical spring. The initial samples of the helical/conical springs are showed the conical spring taken large deflection for the same free lengths in comparison to helical springs. The final samples of the helical and conical springs are showed the conical spring has taken less deflection and bear a large load for the shorter free lengths in comparison to the helical spring for different active coils (four numbers of active coils for conical spring and five numbers of active coils of helical spring were considered). The loads are also calculated with the help of a strain gauge-kit used in the forklift for every spring. Load versus deflection response is obtained also better for conical about cylindrical spring. The equations 8.2, 8.3, 8.4, and 8.5 can be used for stability, and tables 8.4, 8.5, 8.7, and 8.8 helps for stiffness analysis.

## CHAPTER 9

### FATIGUE DESIGN OF HELICAL SPRINGS

#### 9.1 INTRODUCTION

Spring is a resilient member capable of providing large elastic deformation. The applications involved as to applying forces and controlling motion in brakes and clutches, measuring forces as in the case of a spring balance, storing energy as in the case of springs used in watches and toys, and many more at high levels as a shock absorber in railways, automobile industries, etc. Mechanical springs are used in machine designs to exert force, provide flexibility, and store or absorb energy. This chapter will give an overview of the design, non-linear type simulation, and safe fatigue for helical compression springs. Absorption and subsequent release of the external loads come in a form of elastic energy and, due to their material and design; springs tend to return to their initial length when unloaded. In the present work, the design of spring steel (51CrV4) and alloy steel but fatigue test was performed on alloy steel at different load with the help of Solidworks software (Version-2017).

#### 9.2 DESIGN OF HELICAL SPRINGS OF VARIOUS POSITIONING

A “Modify” window should pop up, allowing us to make any necessary changes. One of the benefits of creating a helix this way is that the path followed does not have to be straight i.e. helix can be modified to include arcs due to the number of springs.

Table 9.1 Units for solid model

Unit system	SI (MKS)
Length/ Displacement	mm
Temperature	Kelvin
Angular velocity	Rad/sec
Pressure/Stress	N/m <sup>2</sup>

**Dimensions of Each Spring:** The following dimensions of each spring is used as: -

Thickness of helical compression spring = 1.25mm,

Mean coil diameter = 10mm,

Pitch of helical compression spring = 6.75mm,

Free length of helical compression spring = 35.0mm,

Numbers of Active coil = 04 and a total number of coil = 08, respectively.

Outline of a solid sketch of helical compression springs used as:-

- Start button of software 'Solidworks'(version-2017)
- Make one circle of mean diameter =10mm
- Go to Insert---> Curve ---> Helix.
- Select the Circle and adjust the parameters Pitch=6.75.mm, No of revolution=08 and helix angle =  $7^0$  (must be less than  $10^0$ ).
- Now select a plane normal to helix path.
- Go to feature tab select with 'Sweep' command.
- To do this, select "Path," under "Sweep" in the feature tree and click on the "Edit Sketch" option

#### **Design description:**

The work needs to create a circle that will define the mean diameter of spring, let's go to sketch and select the plane, select the circle to define the mean diameter of spring = 10mm. now go to features, curves, helix, and spiral, there is three option to a create curve as pitch and revolution, height and pitch. A spiral is a different shape, not a helix shape. So sticks with height and pitch option; select height = 35mm as defined by the free length of spring and pitch = 6.75mm (also select the start angle =  $0^0$ ). Further two options are available as clockwise or counterclockwise then select the second option. Now, the exit command is used then the curve is obtained on the screen. Further, define wire diameter of spring = 10mm, create another sketch at the right plane, go to circle, put the wire diameter = 1.25mm, then peer center point of the circle with the curve, now it is fully defined, now go-to features for the swept boss, select the profile and select the curve as the path. This is an ideal spring having the same pitch throughout its length. Work needs more contact areas at the ends of spring and needs less pitch at the ends and more pitch in the middle of spring. Work edit it and go to helix, edit feature and will create the variable pitch option, then expand it, work can change the height, pitch, revolution derived by the height and pitch and the diameter put initially pitch = 3mm and wire diameter = 1.25 up to height = 5mm. this is done for another end for the same pitch.

Also, create cuts at the ends of spring just to make them more physical spring, go to cut extrude through at both ends at the middle (20mm). The added material of springs applied, first one spring-steel (51CrV4), and second one alloy-steel.

The base plate at which the spring is rested is selected as mild steel. The dimensions of the base plate are chosen as 70mmx70mmx5mm. This is done similarly for each helical compression spring. If there are two springs then done two times or three springs done three times. Design of two or three helical springs on the same mild steel resting platform is taken with respect to centre of gravity of the plate.

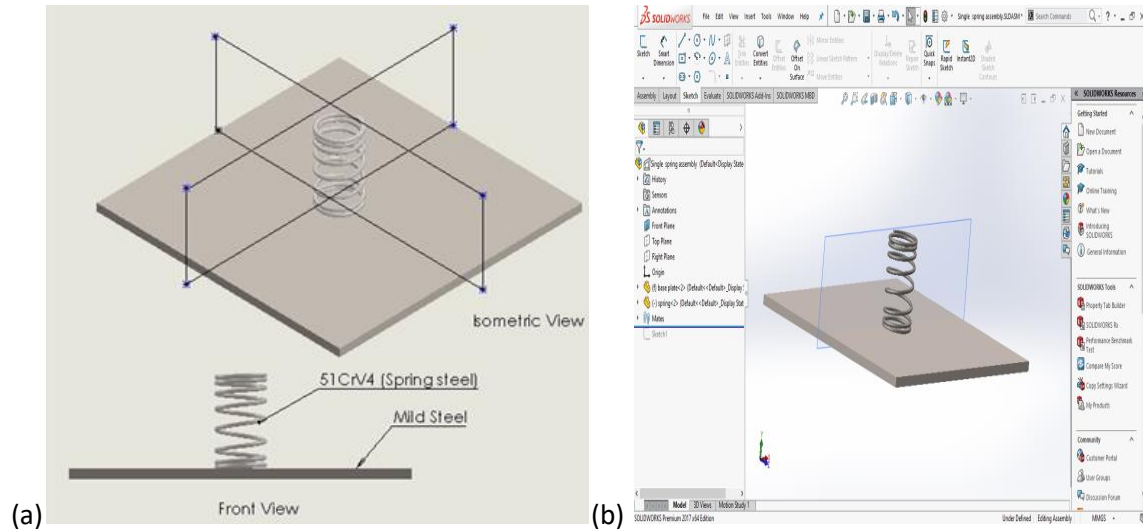


Figure 9.1: single helical (a) single spring steel, and (b) single alloy-steel

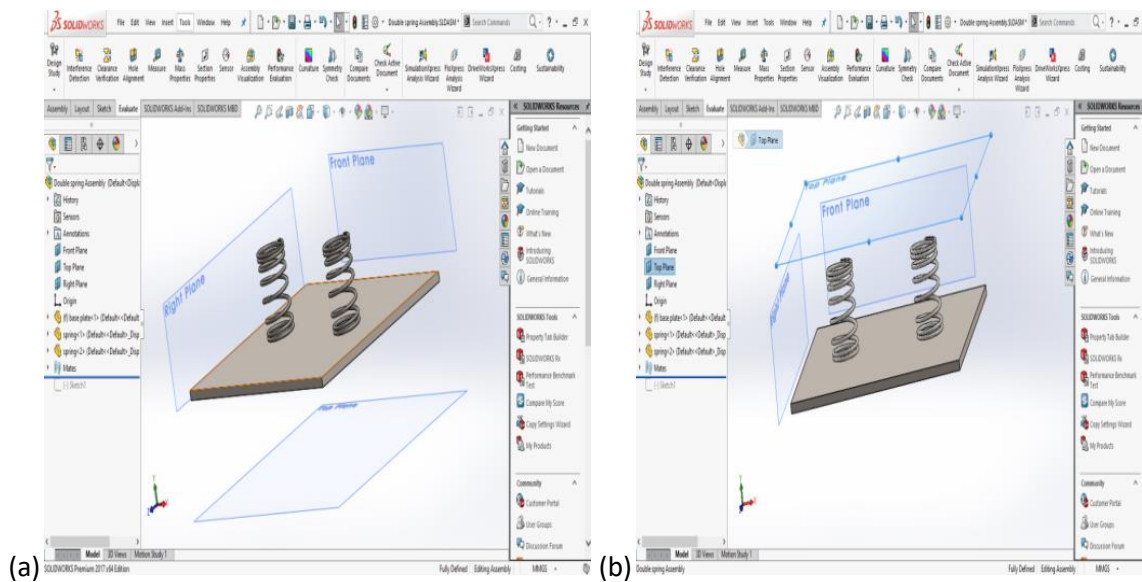


Figure 9.2 dual helical (a) alloy-steel springs and, (b) spring steel springs

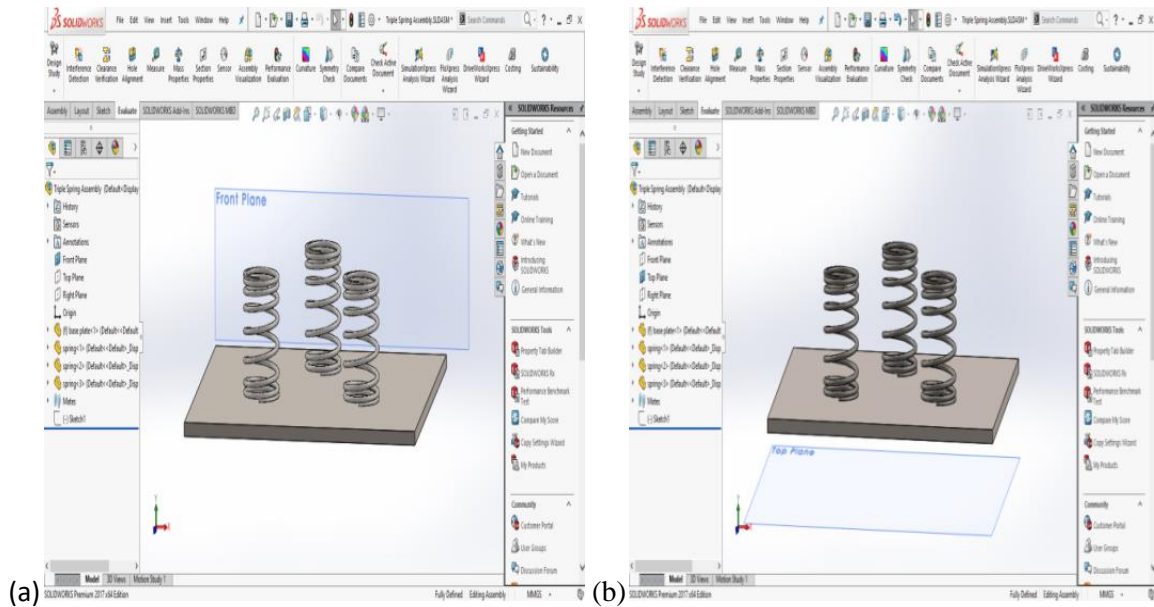


Figure 9.3 triple helical (a) spring steel springs, and (b) alloy-steel springs

Figure 9.1 shows single helical springs of spring-steel and alloy-steel materials in which design of them done by using Solidworks software (Version-2017). The design of a single helical spring using spring-steel material placed at the centroid of the resting plate was made of mild steel as can be seen in figure 9.1(a). Similarly, the design of a single helical spring using alloy-steel material placed at the centroid of resting plate which was also made of mild steel that can be seen in figure 9.1(b).

Figure 9.2 shows dual helical springs of spring-steel and alloy-steel in which design them done by using Solidworks software (Version-2017). The helical double springs rested on the same platform at an equal distance from the centroid of it. The distance from each spring from the centroid of the plate was taken as  $L/2 = B/2 = 70/2 = 35\text{mm}$  and  $L/4 = B/4 = 17.5\text{mm}$ . The design of dual helical springs using spring-steel the material at the same plate was made of mild steel as can be seen in figure 9.2(a). Similarly, the design of dual helical springs using alloy-steel material at the same plate was also made of mild steel as can be seen in figure 9.2(b).

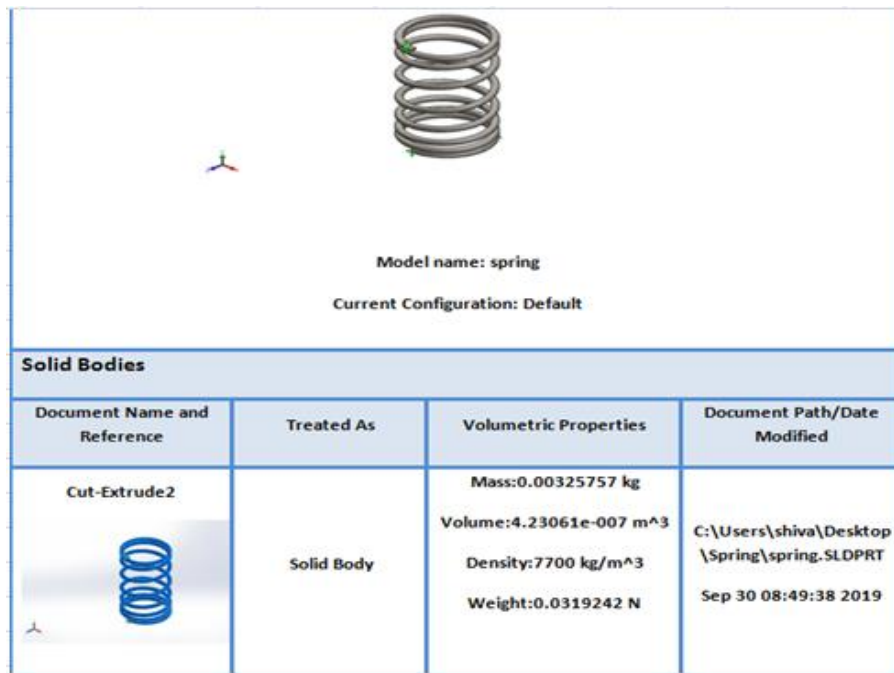
Figure 9.3 shows triple-helical springs of spring-steel and alloy-steel in which design them done by using Solidworks software (Version-2017). The helical double springs rested on the same platform at an equal distance from the centroid of it.

The distance from each spring from the centroid of the plate taken as 24.75mm (because by using triangular geometry in which distance of the centroid from each helical spring is taken as  $[(17.5)^2 + (1.75)^2]^{1/2} = 24.75\text{mm}$  where  $L/4 = B/4 = 17.5$ ). The design of triple-helical springs using spring-steel material at the same plate was made of mild steel as can be seen in figure 9.3(a). Similarly, the design of dual helical springs using alloy-steel material at same plate which was also made of mild steel as can be seen in figure 9.3(b).

### 9.3 SIMULATION OF HELICAL SPRING

The detailed description of the simulation included the model information with assumptions, material properties, loads and fixtures, contact information, mesh information, resultant Forces and finally study results.

#### 9.3.1 Model information with assumptions



Solid Bodies			
Document Name and Reference	Treated As	Volumetric Properties	Document Path/Date Modified
Cut-Extrude2	Solid Body	Mass:0.00325757 kg Volume:4.23061e-007 m <sup>3</sup> Density:7700 kg/m <sup>3</sup> Weight:0.0319242 N	C:\Users\shiva\Desktop\Spring\spring.SLDPRT Sep 30 08:49:38 2019

Figure 9.4 Model Information

Helical spring treated as solid body; all units are taken in SI (MKS) as mentioned in Table 9.1 as units for the solid model. The model name here used as spring can be seen in **Figure 9.4** and various values of mass, volume, weight, and density are represented.

#### 9.3.2 Material properties

The various properties of helical springs are mentioned here for the simulation result.



Table 9.2 Material Properties

Model type:	Linear Elastic Isotropic
Default failure criterion:	Max von Mises Stress
Yield strength:	6.20422e+008 N/m <sup>2</sup>
Tensile strength:	7.23826e+008 N/m <sup>2</sup>
Elastic modulus:	2.1e+011 N/m <sup>2</sup>
Poisson's ratio:	0.28
Mass density:	7700 kg/m <sup>3</sup>
Shear modulus:	7.9e+010 N/m <sup>2</sup>
Thermal expansion coefficient:	1.3e-005 /Kelvin

Table 9.2 shows material properties in which values of model type, default failure criterion, yield strength, tensile strength, elastic modulus, Poisson’s ratio, mass density, shear modulus, and thermal expansion coefficient are provided.

### 9.3.3 Loads and Fixtures

The Loads and Fixtures are mentioned here for the result of simulation in helical spring.


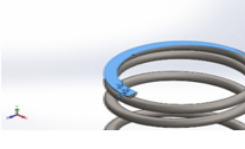
Fixture name	Fixture Image	Fixture Details		
Fixed-1		Entities: 1 face(s) Type: Fixed Geometry		
<b>Resultant Forces</b>				
<b>Components</b>	<b>X</b>	<b>Y</b>	<b>Z</b>	<b>Resultant</b>
Reaction force(N)	-0.000168052	0.27388	-0.00170772	0.273886
Reaction Moment(N.m)	0	0	0	0
On Flat Faces-1		Entities: 1 face(s) Type: On Flat Faces Translation: 0, 0, 20 Units: mm		
<b>Resultant Forces</b>				
<b>Components</b>	<b>X</b>	<b>Y</b>	<b>Z</b>	<b>Resultant</b>
Reaction force(N)	0.000167855	-0.273873	0.00170792	0.273878
Reaction Moment(N.m)	0	0	0	0

Figure 9.5 Loads and Fixtures

Figure 9.5 shows fixture name, fixture image, fixture detail as entities (face), fixed geometry, resultant forces as components, reaction forces, reaction moment in all three directions.

### 9.3.4 Contact Information

These mentioned **contact, contact image, contact properties mainly.**


Contact	Contact Image	Contact Properties		
Contact Set-1		Type: No Penetration contact pair Entites: 1 face(s) (Self-Contact) Advanced: Surface to surface		
Contact/Friction force				
Components	X	Y	Z	Resultant
Contact Force(N)	-2.5806E-015	4.012E-014	6.4889E-015	4.0724E-014

Figure 9.6 Contact Information

Figure 9.6 shows contact information in which contact as set 1, contact image as helical, contact properties as type, entities, advanced. This also included the contact/friction force as components (x, y, z, resultant), force in ‘Newton’ along with all three directions.

### 9.3.5 Mesh information

This provides the mesh criteria with mesh information details.

Table 9.3 Mesh information

Mesh criteria		Mesh information - Details	
Mesh type	Solid Mesh	Total Nodes	73925
Mesher Used:	Curvature-based mesh	Total Elements	42104
Jacobian points	4 Points	Maximum Aspect Ratio	17.111
Maximum element size	10 mm	% of elements with Aspect Ratio < 3	99.7
Minimum element size	0.5 mm	% of elements with Aspect Ratio > 10	0.00475
Mesh Quality Plot	High	% of distorted elements(Jacobian)	0
		Time to complete mesh(hh:mm:ss):	0:00:06

Table 9.3: represents mesh information mesh type as solid mesh, curvature-based mesh, jacobian points as 4 points, maximum element size as 10mm, minimum element size as 0.5mm, mesh quality as high, total nodes = 73925, total elements = 42104, maximum aspect ratio = 17.111, % of element with aspect ratio < 3 = 99.7, % of an element with aspect ratio > 10 = 0.00475, % of distorted of an element and time of complete mesh.

### 9.3.6 RESULTANT OF SIMULATION

Here two tables also included the first one for Reaction forces and thesecond one for Reaction Moments for the helical spring. Table 9.4 shows reaction forces in which values of selection sets with resultant are provided in all three directions. Similarity Table 9.5 shows reaction moments in which values of selection sets with resultant are provided in all three directions (mostly ‘Zero’ values are considered).

Table 9.4 Reaction forces

Selection set	Units	Sum X	Sum Y	Sum Z	Resultant
Entire Model	N	-1.82532e-007	7.68643e-006	2.01908e-007	7.69124e-006

Table 9.5 Reaction Moments

Selection set	Units	Sum X	Sum Y	Sum Z	Resultant
Entire Model	N.m	0	0	0	0

Figure 9.7: shows the simulation result in which the Reaction forces includes the selection set, units of measurement, summation in X, Y, and Z individually, then resultant of selection or entire model.

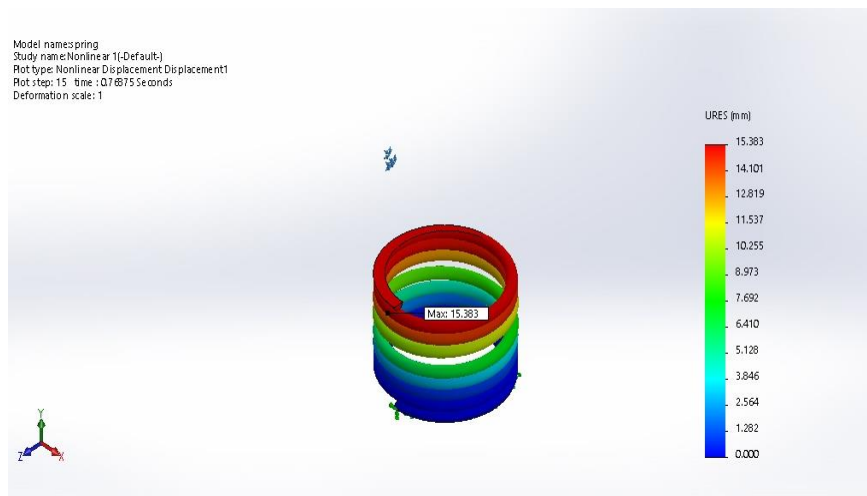


Figure 9.7 Simulation result

## 9.4 RESULTS AND DISCUSSION

The stiffness is defined as the load per unit deflection in order to take into account the effect of direct shear and change in coil curvature a stress factor

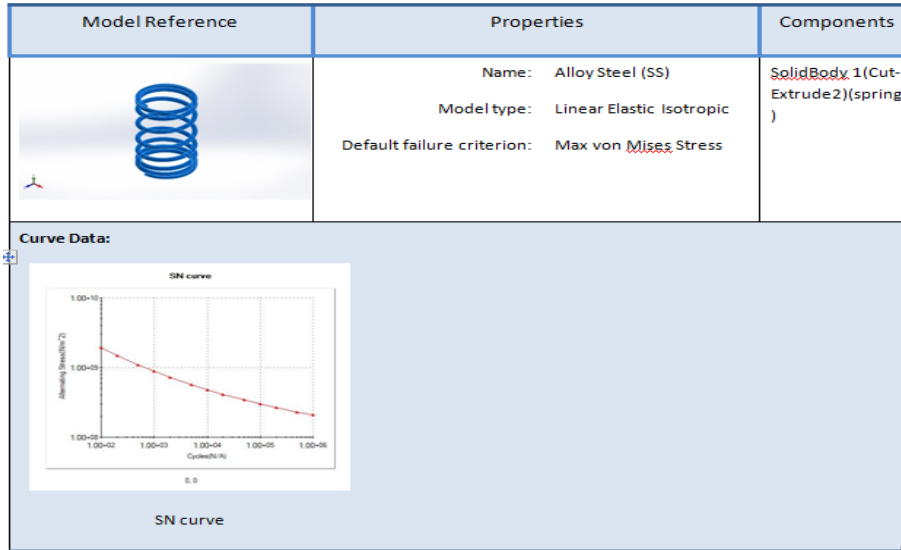


Figure 9.8 Material properties with model reference

Figure 9.8 shows material properties with model reference in which model reference properties as alloy steel (ss), linear elastic isotropic, Max von mises stress and components as solid body 1(cut-extrude 2) also mentioned.

Table 9.6 Loading Options

Event Name	No. of cycles	Loading Type	Study Association		
Event-1	1000	Fully Reversed (LR=-1)	Study name	Scale Factor	Step
			Nonlinear 1	1	1
Event-2	500000	Fully Reversed (LR=-1)	Study name	Scale Factor	Step
			Nonlinear 1	1	1
Event-3	50000	Fully Reversed (LR=-1)	Study name	Scale Factor	Step
			Nonlinear 1	1	1
Event-4	200000	Fully Reversed (LR=-1)	Study name	Scale Factor	Step
			Nonlinear 1	1	1

Table 9.6 shows Loading Options in which Loading options were divided into the four numbers of events as Event-1, Event-2, Event-3, and Event-4. It also included a number of cycles, loading type with study name, scale factor & step.

➤ **Study results are shown in Figure 9.9**

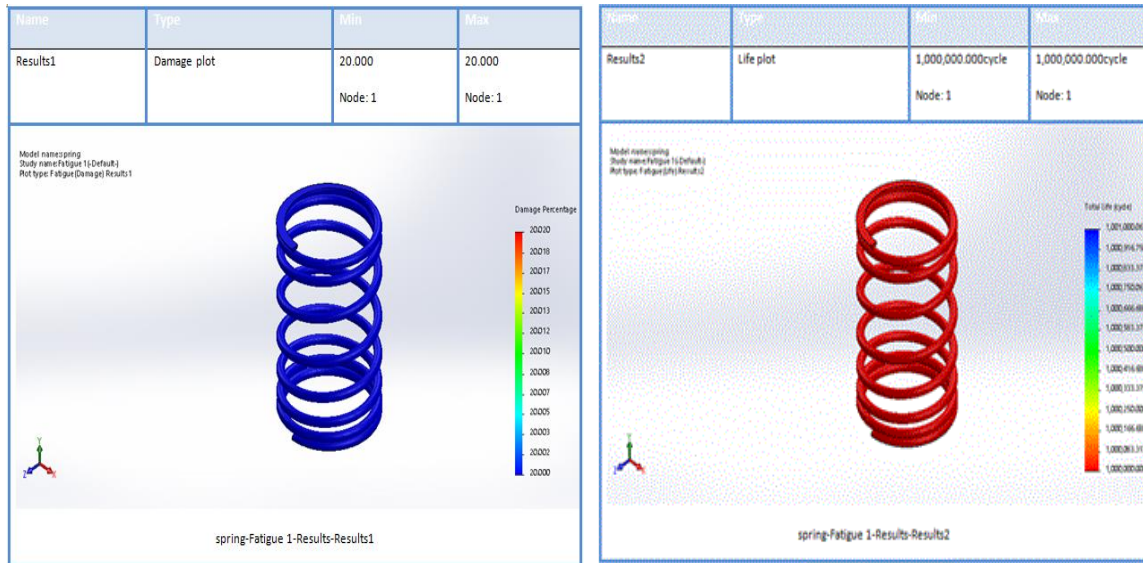


Figure 9.9 Study results (First and Second)

Figure 9.9 shows the first study results, and second study results, the blue color spring represents the first study result in which spring fatigue results are shown. It included damage plot (safe zone considered), maximum cycles, minimum cycles, and damage percentage. Similarly, red color spring represents the second study (safe zone considered), the result in which spring fatigue results are shown. This result also included damage plot maximum cycles, minimum cycles, and damage percentage.

## 9.5 SUMMARY

The design of spring steel (51CrV4) and alloy steel springs were done at centre of the resting plate which was made of mild steel for the single spring, dual springs, and triple springs by Solidworks software (Version-2017). The fatigue tests were performed on alloy steel at different loads with the help of Solidworks software. Before the fatigue analysis, the results of the Non-linear simulation analysis were also included through this software. The detailed description of the simulation included the model information with assumptions, material properties, loads and fixtures, contact information, mesh information, resultant forces, and finally study results. The fatigue results start from 5N, 20N, 50N, and 100N are discussed. First and Second study results provide damage plot, maximum cycles, minimum cycles, and damage percentage.

# **CHAPTER 10**

## **METALLURGICAL & FATIGUE PROPERTIES OF SMA WIRES**

### **10.1 INTRODUCTION**

In this chapter, metallurgical & mechanical fatigue properties of NiTi-based SMA wires or flexinol wires are presented which had different diameters. In metallurgical behavior; 0.1mm (Straight annealed), 0.2mm (Straight annealed), 0.5mm (Straight annealed and soften), and 1.0mm (Straight annealed and soften) round wires shaped have been analyzed (before/after the SMA intelligent helical). A mechanical fatigue test was performed also for slender wires only. The purpose of metallurgical properties is to checks the internal micro-structural or metallurgical behaviors of four SMA wires for one conditional position (drawn) to another condition position (actuator) which is mainly discussed. It helps to understand the significant changed effect of Ni and Ti elements positioning of both in Nitinol/flexinol and also the purpose of fatigue properties to checks true-fatigue or mechanical fatigue property of slender SMA wires i.e. 0.1mm, 0.2mm respectively. For metallurgical arrangement for specimens of SMA's wires in which tablet, camera, microscope, lens, cables, and wires are employed. For mechanical fatigue arrangement (directly used) for testing included separate eccentric-loads/dead weights, bearing & its housing assembly, driver, AC motor weight hanger assembly, bearing spindle/shaft, digital counter and cut-off switch, and end grippers. The two specimens (mild steel pieces with NiTi SMA Wires) as one for 0.1mm SMA, and the other for 0.2mm SMA also prepared.

### **10.2 METALLURGICAL PROPERTY**

Metallurgical property involves the physical and chemical behavior of metallic elements, their inter-metallic compounds, and their mixtures or alloy. We have considered here micro-structural behavior only the small pieces of four NiTi-based SMA wires of 0.1mm, 0.5mm, 0.2mm, and 0.1mm. The two specimens of mild steel were prepared in which these wires are placed and fixed.

First specimens for drawn condition before implementation as an actuator of all four wires as received from the purchaser and the second specimen for intelligent helical springs (after implementation as an actuator). It included:-

- Preparation of NiTi-based SMA's specimens
- Polishing of specimens of NiTi-based SMA's
- Etching Process
- Microstructures of SMA's wires

### 10.2.1. Preparation of SMA's specimens

For the preparation of SMA's specimens fixing and insertion of four NiTi-based SMA's wires of diameters 0.1mm, 0.5mm, 0.2mm, and 0.1mm within the two mild steel pieces (having rectangular in cross-sections) on one preferred side of the face by applying 'm-seal' and 'Araldite' as an epoxy adhesive in holes provided on the specimens are discussed. This work also used the drilling machine and drill bits of different sizes (0.8mm, 0.9mm, 1.0mm, and 1.5mm). So, the mainly applied tools/machine/material includes; two mild steel pieces (with rectangular cross-section bar (0.110kg/feet)), a hand-punch tool, drilling machine (230V/2200rpm), drill bits (0.8mm, 0.9mm, 1.0mm and 1.5mm), electric cutter (with buffer and ceramic cutter (3000rpm/400W)), epoxy adhesive (standard), and wire stripper.

**10.2.1.1 Two Mild steel pieces (rectangular cross-section bars (0.160kg/feet)/(0.140kg/feet)):** The weight of this used bars having lower grade-A479 (as prescribed by local city seller) presented in kg/feet also equal to 0.160kg/feet and 0.140kg/feet (approx.) up to the 120mm or 12cm length. .

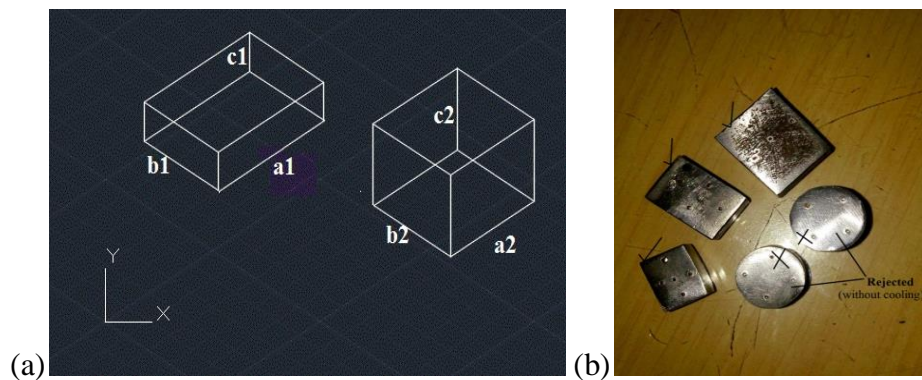


Figure 10.1 Two steel pieces (a) AutoCAD drawing, and (b) Actual images

Figure 10.1 shows two steel pieces in which first by AutoCAD Drawing and the second by the actual captured image. The drawing's made with the help of AutoCAD software of Autodesk Company Version-2017. The dimensions of the first mild steel piece having a rectangular cross-section are represented as 14mmx13mmx11.5mm ( $a_1 \times b_1 \times c_1$ ) in which NiTi-based SMA's wires portion are to be placed after implementing as an actuator or intelligent spring. Similarly, the dimensions of the second mild steel piece having rectangular cross-section are represented as 24.5mmx18mmx6.5mm ( $a_2 \times b_2 \times c_2$ ) in which NiTi-based SMA's wires portion are to be placed before implementing as an actuator, or intelligent spring (drawn condition). Captured image shows three damaged pieces due to cutting behave as a heat treatment process and drill bits failed on working with these pieces.

**10.2.1.2 Epoxy adhesive (standard):** For the fixing and placing of portions of NiTi-based SMA's into the respective holes, we applied 'm-seal' and 'Araldite' as epoxy adhesives. Here, primarily M-seal epoxy adhesives applied to covered deep holes-sections and then secondary were applied Araldite epoxy adhesives.

**M-seal Epoxy Adhesive (Primarily):** M-seal used for multi-purpose sealant with various applications as sealing, joining, fixing, and building. Its versatility and ease of application make it commonly used across multiple industry segments, as well as households to fill gaps, cracks and plug leaks in pipes and joints (variety of materials including metals, rubber, wood, glass, asbestos, porcelain, and plastic). Mainly M-seal applied here for the fixing of NiTi-based SMA's wires portions into the mild steel. The procedure included as taken an M-seal pack removed resin base and hardener out of packs. Taken equal amount of resin base and hardener and mixed resin base and hardener with each other until it forms a uniform color. Used this mixture, and filled it in between the SMA and mild steel hole to ensure the maximum gap.

**Araldite Epoxy Adhesive:** Araldite is used here as high-performance/heavy-duty, durable epoxy adhesive sets by the interaction of a resin with a hardener. Araldite joints are concerned with waterproof/stress-proof/heat-proof, non-corrosive/non-toxic, and resistant to most chemicals. It was available in a different pack but used the most common pack containing two different tubes, one for the resin, and the other for the hardener.

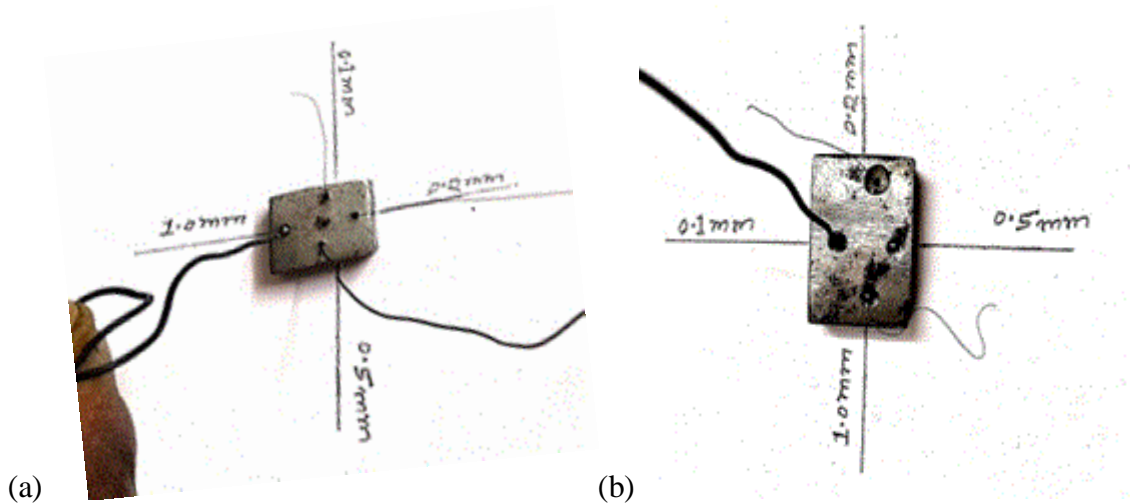


Then filled again over the gap between mild steel pieces and NiTi wires portions SMA's specimens, and left for overnight/eight hours (at least) for better strength. This is used here as a secondary epoxy adhesive after the M-seal and mixed the resin and hardener with each other until it forms uniform color.

**10.2.1.3 Other tools/materials:** It included as hand-punch tool (hard-metallically), drill bits of 0.8mm, 0.9mm, 1.0mm, and 1.5mm sizes, drilling m/c (230v/2200rpm), electric cutter (3000rpm/400w), ball peen hammer /metallic hammer and chisel-peen hammer (all having hemispherical type peen), steel ruler scale, vernier caliper (simple) and digital vernier caliper (least counts 0.2 mm or 0.02 cm), vernier height gauge, v-block, bench-vice (fixed base), buffering wheel, wire strippers (red for soft cutting and light-gray for hard cutting), '4' niti or sma's wire-portions in drawn conditioned (having ' $\phi$ ' equals 0.1, 0.2, 0.5, and 1.5, all dimensions in mm), '4' NiTi or SMA's wire-portions after implementing as an actuators/smart intelligent springs (having ' $\phi$ ' equals 0.1, 0.2, 0.5, and 1.5, all dimensions in mm).

**10.2.1.4 Pre-Final & Final SMA's specimens**

Figure 10.2 shows four pre-final & final SMA's specimens as SMA's specimen before implementing as an actuators/drawn conditioned, SMA's specimen after implementing as an actuators/smart intelligent springs, final specimens with SMA's wire pieces, and separated final SMA's specimens. This also shows the remaining pieces four NiTi-based SMA's wires of diameters 0.1mm, 0.5mm, 0.2mm, and 0.1mm after epoxy adhesives and cutting.



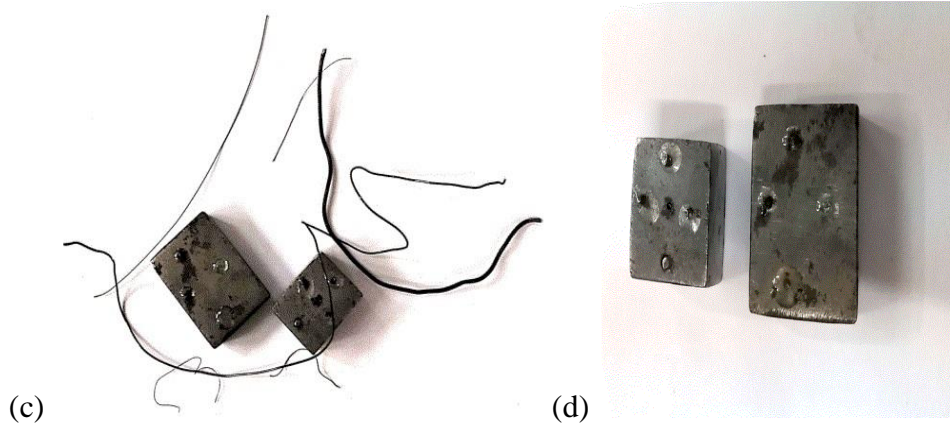


Figure 10.2 (a) SMA's specimen before implementing as an actuators/drawn conditioned, (b) SMA's specimen after implementing as an actuators/smart intelligent springs, (c) Final specimens with SMA's wire pieces and, (d) Separated final SMA's specimens

### 10.2.2 Polishing of specimens of SMA's

For smoothing a work-piece's surfaces, polishing of specimens of SMA's applied here with the help of various hand files, emery papers having different grit size and polishing machine (metallurgical double disc polishing machine having rubbing or chemical action). The polishing processes were done for the purpose to enhance the appearance of specimens of SMA's, preventing contamination of specimens of SMA's, removing oxidation in specimens of SMA's, and creating a reflective surface of specimens of SMA's. Mainly the polishing applied for examination of a NiTi-based SMA's microstructures under a microscope to create flat and defect-free surfaces.

**10.2.2.1 Hand Files:** A hand file also called a hand tool used to remove fine amounts of material from a work-piece. Hand files were used in the workshop to smooth rough surfaces. They were available in common jobs used in woodworking, metalworking, etc.



Figure 10.3 Work-pieces after Hand Files (fine & coarse)

Figure 10.3 shows two mild steel pieces with fine/coarse finish by hand files in which these hand files are made of a case hardened steel bar of different cross-sections as rectangular, triangular.

**10.2.2.2 Emery paper:** Emery papers or polishing paper rated on the average grit size which is glued to the backing. The common grit sizes are commercially available for coarse to fine finish, medium to a fine finish, and fine to micro/very fine (CF, MF, FM). For coarse to fine finish size varies as 40, 46, 54, 60-100), for medium to fine finish 100-180, and for fine to micro/very fine 180-280.

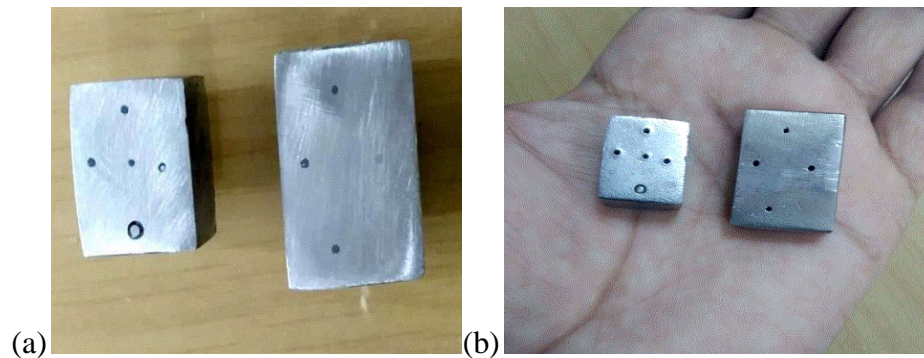


Figure 10.4 (a) after emery paper up to '100-180'grit size, and (b) after emery paper up to '180-280'grit size

Figure 10.4 shows two mild steel pieces after emery paperwork up to '100-180'grit size and up to '180-280'grit size. The presented work had applied 80, 120, and 280 grid sizes. The emery papers were used to smooth metal and take off rust. These were made of silicon carbide and aluminum oxide as workable-side.

**10.2.2.3 Polishing machine:** The polishing process was used for creating a smooth and shiny surface by rubbing it or using a chemical action, leaving a surface with a significant specular reflection (by using Aluminum Oxides ( $Al_2O_3$ ) white pieces mixed with water). It applied the velvet polishing cloth, aluminum oxide ( $Al_2O_3$ ) metallurgical double disc polishing machine.

**The polishing machine process involved a metallurgical double disc polishing machine in which water-container, velvet polishing cloth, and aluminum oxide ( $Al_2O_3$ ) also included.**

**Metallurgical double disc polishing machine:** Independent motor for each disc powered by high torque 1/2 hp motor.

It has a water faucet and stainless steel sink with a smooth drainage system. It has a variable speed system operated manually by the handle. It has a gunmetal disc of diameter 200 mm with a locking ring to hold the cloth or emery paper. It covered load speed of ranges 350-1200 r/min, voltage-220V, and powder coated surface treatment.

**Velvet polishing cloth:** Normally the metallographic polishing cloth is commercially called velvet polishing cloth. Polishing is a more aggressive process while buffing is less harsh, which leads to a smoother, brighter finish. The front side of it very soft portion compared to the backside. The thickness of the cloth was 0.25mm and the color was red used in round-shape The most common metallographic abrasive used in cloth is silicon carbide as pressure-sensitive adhesive (PSA).

**Aluminum Oxide (Al<sub>2</sub>O<sub>3</sub>):** It was typically used for achieving a fine lapped finish on softer materials prior to polishing for the mild steel/specimens of SMA's. This was used in pieces with water which dissolved completely and had a white appearance. (Glue no. 250mm)

#### **Images of the polishing part (applied)**

(This included the six images as hand files, emery papers, aluminum oxide, velvet cloth, polishing machine, and polished piece)



### 10.2.3 Etching Process

The etching process is applied here to cut into the unprotected parts of NiTi-based specimens of SMA's surfaces by using an etching reagent. The final specimens of SMA's dipped in a bath of etching reagent (mixture of distilled water and chemical-acids. The etching reagent is technically called the etchant or mordant (French for "biting"). In modern manufacturing, other chemicals may be used on other types of material chemical etching in which high precision subtractive manufacturing process involved that used baths of temperature-regulated etching chemicals to selectively remove material to produce high precision metal parts in any desired shape.

**10.2.3.1 Preparation of Etching reagent:** It included the mixture of distilled water, nitric acid, and hydrochloric acid hydrofluoric acid, so-called as final etching reagent. Then this final etching reagent was further applied on the NiTi-based specimens of SMA's surfaces. The glass test tube and gradual cylinder were used for accurate quantities of measurements.

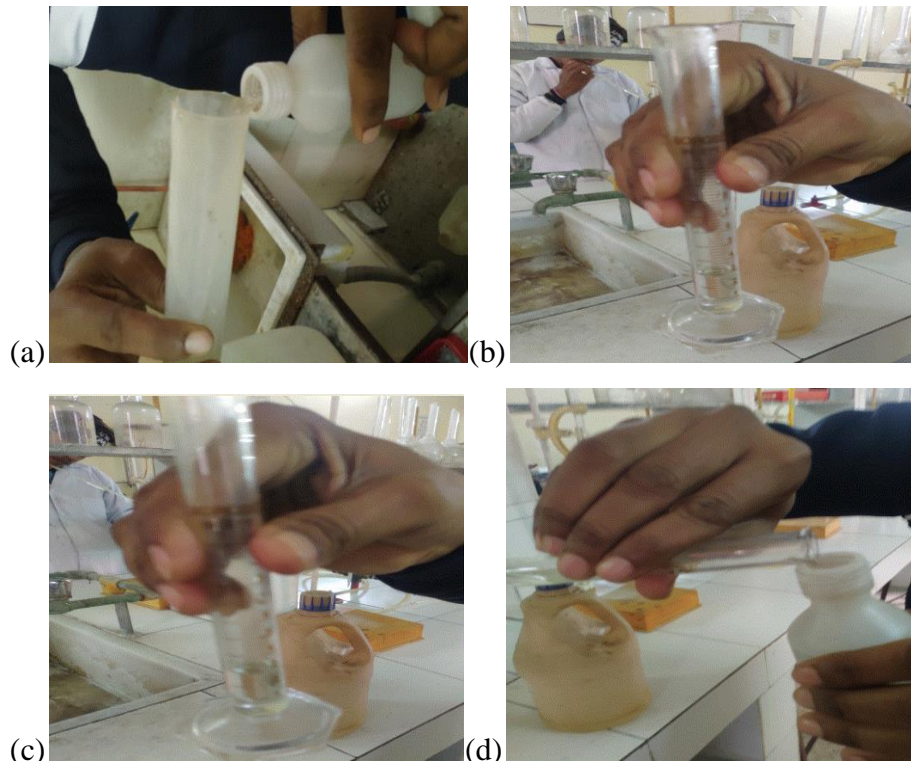


Figure 10.5 (a) distilled-water (95ml), (b) nitric acid (2.5ml), (c) hydrochloric acid (1.5ml), and (d) hydrofluoric acid (1.0ml)

Figure 10.5 shows three chemicals as nitric acid with the quantity of 2.5ml, hydrochloric acid with the quantity of 1.5ml, hydrofluoric acid with quantity of 1.0ml, and distilled water with the quantity of 95ml. The final quantity of etching reagent had obtained 100ml (quantity was reduced in proportion as per the minimum requirement of etching reagent).

- The final etching reagent had spread over both NiTi-based SMA's specimens surfaces which were placed nearer to each other for 15-20 minutes as shown in **Figure 10.6** and covered with tissue paper to avoid rusting then specimens were used to microstructure studies

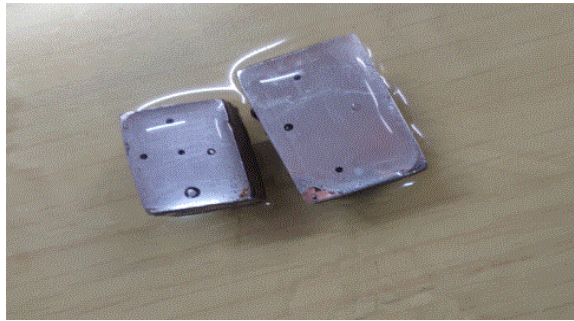


Figure 10.6 NiTi-based SMA's specimens (after etching reagent)

#### 10.2.4. Microstructures of SMA's wires

Microstructure referred to the very small-scale structures of a material in which NiTi-based SMA's wires of prepared specimen's surfaces are revealed by an optical microscope above 25× magnification. In this work, optical microscope image of 200x magnification had been considered. Examination of the microstructure of NiTi-based SMA's wires material provided information used to determine if the structural parameters are within certain specifications. The analysis results were used as a criterion for acceptance or rejection. The micro-structural examinations were generally performed by using optical or scanning electron microscopes to magnify features of NiTi wires under analysis. The amount or size of these features can be measured, quantified, and compared to acceptance criteria. These examinations are often used in failure analysis to help identify the type of material in question and determine if the material received the proper processing treatments. Metallurgical examinations may evaluate in terms of the extent of carburization and decarburization, extent of inter-granular attack or corrosion, extent of grain size, and volume fraction of various phases or second phase particles in prepared SMA specimens.

#### 10.2.4.1 Arrangement /setup for Specimens of SMA's wires

For finding the microstructures of NiTi/Flexinol wires, basically by the microscope which attached to camera and tablet with the help of cables and wires as can be seen arrangement. In metallurgical behavior; 0.1mm (Straight annealed), 0.2mm (Straight annealed), 0.5mm (Straight annealed and soften), and 1.0mm (Straight annealed and soften) round wires shaped have been analyzed before and after the SMA intelligent helical.

- Tablet
- Camera(HD ready)
- Microscope
- Two lens(Interior 10x, outer 20x)
- Cables and wires
- Two Specimens



Figure 10.7 Arrangement /setup for Specimens of SMA's wires  
(Showing scanning electron microscope)

the microstructures of all NiTi-based SMA's or flexinol wires portions which applied before implementing as an actuators/drawn conditioned and after implementing as an actuators/smart intelligent springs.

Figure 10.7 shows arrangement/setup for specimens of SMA's wires in which tablet, camera, microscope, lens, cables, and wires are included (this arrangement/setup for capturing the images of the specimen used in HD-ready format, and working as a scanning electron microscope).

#### 10.2.4.2 Final Microstructures of SMA's wires

The microscopic images of NiTi-based SMA wires presented by scanning electron microscope which having lens of maximum 200x magnification that can be seen in **Figure 10.8.**

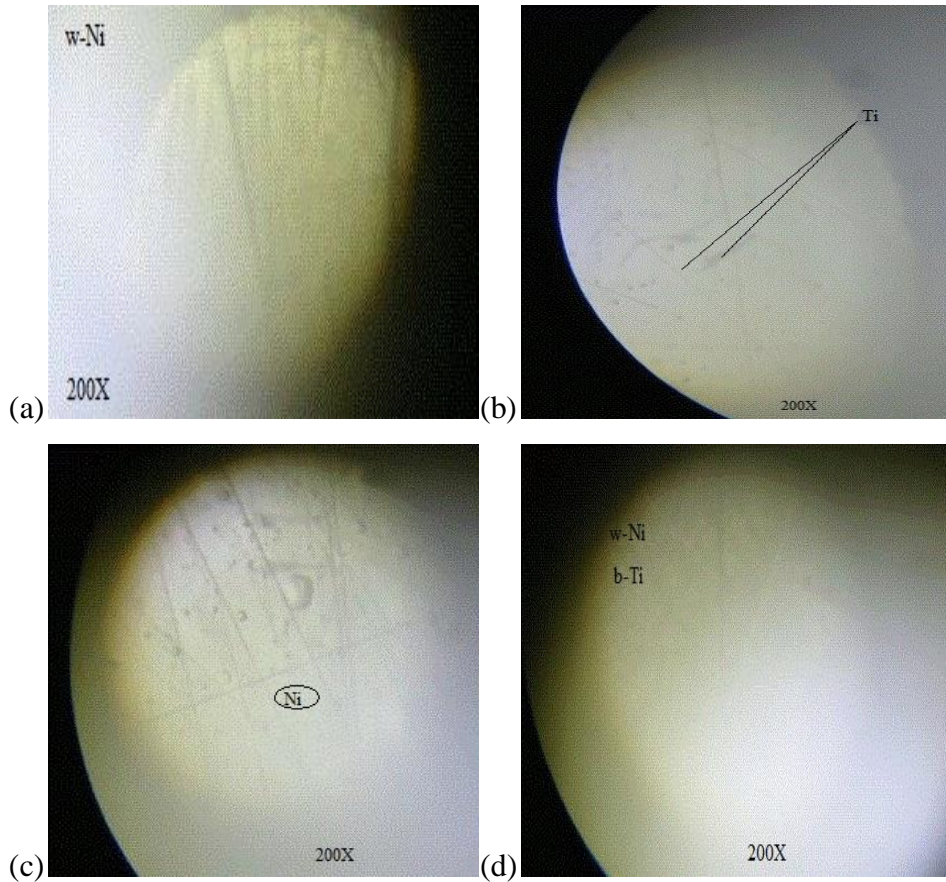


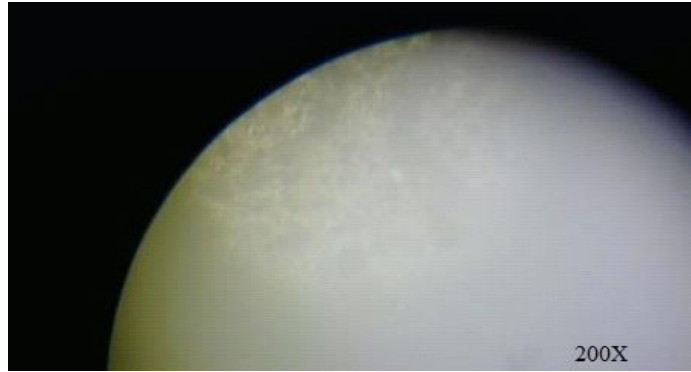
Figure 10.8 (a) 0.2mm wire (B/200X), (b) 0.2mm wire (A/200X), (c) 0.5mm wire (B/200X), (d) 0.5mm wire (A/200X)

Slender SMA wires (having less/negligible load-capability) include the microstructures of 0.2mm drawn condition (before implementation) and actuator (after implementation). The SMA wires (having load-capability) include the microstructures of 0.5mm drawn condition (before implementation) and actuator (after implementation). Basically capital letters 'A' and 'B' abbreviations referred to after and before words here.

#### **Other images of metallurgy**

It included the Specimen of Mild steel-200X (outside-region of SMA's), 1.0mm wire (B/200X), 1.0mm wire (A/200X), 1.0mm wire (B/200X), and 0.1mm wire (A/200X).

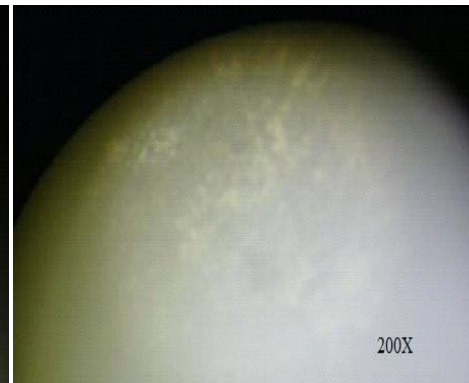




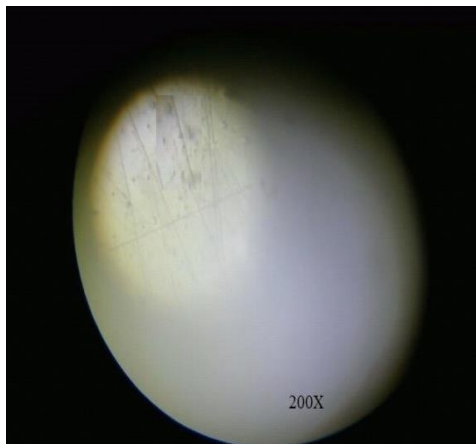
Specimen of Mild steel-200X (outside-region of SMA's)



1.0mm wire (B/200X)



1.0mm wire (A/200X)



1.0mm wire (B/200X)



0.1mm wire (A/200X)

### 10.3 MECHANICAL FATIGUE OR TRUE-FATIGUE PROPERTY

Fatigue testing was performed by applying cyclic loading to a structure. Basically, it depends on the stress amplitude and the frequency of applied loads, fatigue failure of SMA wires can occur by two means, thermal fatigue failure, and mechanical fatigue failure.

But considered n mechanical fatigue in which the tendency of a material to fracture by means of progressive brittle cracking under repeated alternating or cyclic stresses of intensity considerably below the normal strength. The eccentric loading was used for 500gm, 1000gm, 1500gm, and 3000gm respectively. It included:-

- Preparation of specimens with slender SMA wires
- Final fatigue tests

### **10.3.1 Preparation of specimens with slender SMA wires**

It involved the holing and screwing of two NiTi-based slender SMA wires of 0.1mm and 0.2mm within the mild steel pieces (having cylindrical cross-sections) on centering face sides are discussed. This work also used the drilling machine and drill bits of different sizes. Two specimens of mild steel were prepared to have a cylindrical shape by using the engineering workshop tools, and machines. So, the mainly applied tools/machine/material includes two mild steel pieces (cylindrical cross-section), lathe machine (center lathe), buffering wheel (wire-based), drilling machine (230v/2200rpm) & drill-bits (2.0mm/3.4mm), electric cutter (3000rpm/400w), bench-vice (fixed base), tap holder and metric tap (millimeter-thread) and pipe wrench.

**10.3.1.1 Lathe machine (Center lathe):** The various types of lathes are available in industries/workshops such as speed lathes, Metal lathes, bench lathes, capstan lathes, engine/center lathes, tool room lathes, turret lathes, and special purpose lathes, etc. But, center or engine lathe (horizontal) type used here to perform the operations mainly like turning, facing and centering the two mild pieces that can be seen in figure 10.9. The lathe worked as a machine tool which holds the mild steel work-piece between two rigid, and strong supports called centers or chuck (three-jaw).

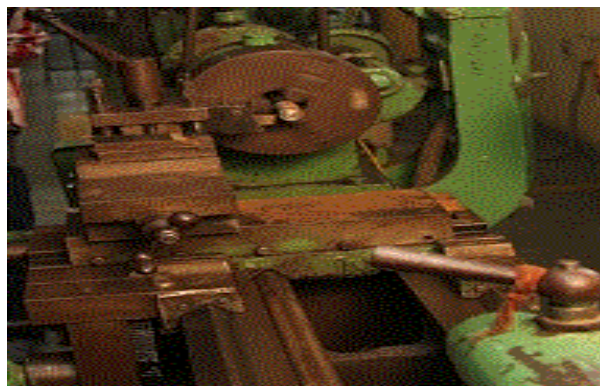


Figure 10.9 Center Lathe (Horizontal bed type)

Figure 10.9 shows the horizontal bed type center lathe machine. This lathe rotated the work-piece about the centerline of these two parts or we can say machined the mild steel pieces between its headstock and tailstock centers. This engine lathe machine having '6' feet length of bed consist of a basic part such as base, headstock, tool post, three-jaw chuck, tail stock, main drive, and carriage.

**10.3.1.2 Buffering wheel:** A wire brush or buffering wheel is also used here as a surface polishing/ finishing tool for the mild steel pieces. The steel used is generally a medium to high carbon variety and very hard and springy, other wire brushes feature bristles made from stainless steel or brass depending upon the types of applications.



Figure 10.10 Buffering wheel (wire based)

Figure 10.10 shows wire-based buffering wheel/wire brush in which brush bristles are made of high-speed steel wires. Buffering process used to shine two mild steel pieces. This work referred to polishing process which used abrasive belt finishing.

**10.3.1.3: Other tools/materials:** It included as a pipe wrench (14 inches length) Electric cutter (3000rpm/400W), Drilling M/c (230V/2200rpm) and Drill-bits (2.0mm/ 3.4mm), Bench-vice (Fixed Base), Tap holder, Metric tap (millimeter-thread), Ball-peen hammer /Metallic hammer, Steel Ruler scale, vernier caliper (simple) and Digital vernier caliper (least counts 0.2 mm), Prick punch, '2' NiTi based SMA's wire-portions (length of each wire i.e.72mm) in drawn conditioned ( having ' $\phi$ ' equals 0.1 and 0.2, all dimensions in mm), '2' NiTi based SMA's wire-portions after implementing as an actuators/smart intelligent springs (having ' $\phi$ ' equals 0.1 and 0.2, all dimensions in mm), drill-bit tightening keys, screwdrivers, and wrenches.

**10.3.1.4 Pre-Final & Final SMA-based specimens:** Pre-final specimens referred to mild steel pieces without positioning of SMA wires in provided holes through screwing that can be seen in **Figures 10.11 (a) and 10.11(b)**. Final SMA-based specimens referred to mild steel pieces positioned with SMA wires in provided holes through screwing. Two holes were provided with each mild steel piece i.e. 2.0mm, 3.4mm and each mild steel piece having dimensions as size of axis face hole = 2.00mm, diameter ( $\phi$ ) = 10mm and length = 30.5mm respectively.

**Images of pre-final & final SMA-based specimens**

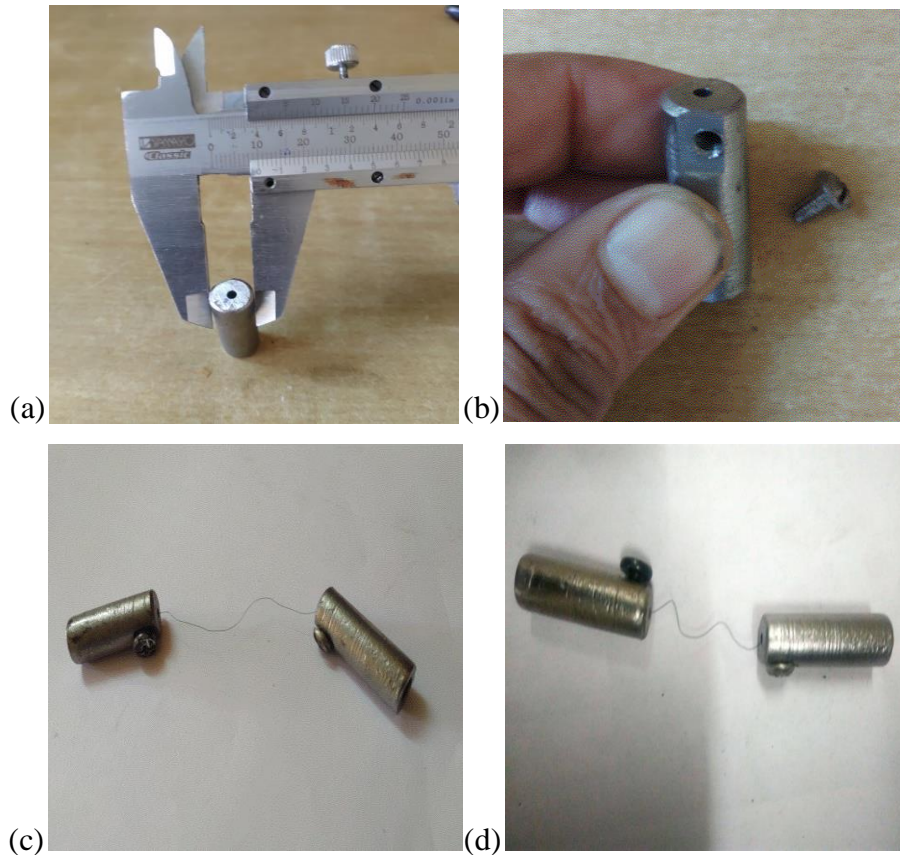


Figure 10.11 a) mild steel piece with axis face hole (2.00mm), (b) mild steel piece with turning side hole (3.4mm, tap size i.e. m4x0.75), (c) final SMA-based specimens with 0.1mm NiTi wire, and (d) final SMA-based specimens with 0.2mm NiTi wire

**10.3.2 Arrangement /Set-up for Specimens of Slender SMA wires**

SMA materials fatigue is also a phenomenon where structures failed when subjected to a cyclic load. True-fatigue testing as the process of progressive localized permanent structural change occurring in a material subjected to fluctuations.

There are several common testing in which two common types included fatigue load controlled high cycle that associated with loads in the elastic regime and strain-controlled low cycle fatigue that involve plastic deformations. Fatigue is the most common source behind failures of mechanical structures.



Specimen testing approach



Fatigue testing machine

Figure 10.12 Arrangement /setup for Specimens of Slender SMA wires (showing fatigue testing machine and specimen testing approach)

Figure 10.12 shows arrangement/etup for Specimens of Slender SMA wires. The fatigue testing machine is applied and specimen testing approaches in which Eccentric-Loads are used for specimens of slender SMA wires/ NiTi SMA-materials. The Set-up of fatigue testing included separate eccentric-loads/ dead weights, bearing and its housing assembly, driver, AC motor weight hanger assembly, bearing spindle/shaft, digital counter and cut-off switch, and end gripper as shown in specimen testing approach. The two the specimens (mild steel pieces with NiTi SMA Wires) as one for 0.1mm SMA and the other for 0.2mm SMA also used as shown in figures 10.11 (c) and 10.11(d).

Fatigue testing presented here to failure in response to alternating loads (as opposed to monotonic straining). The fluctuating stresses and strains at some point or points may culminate in cracks initiation or fracture after a sufficient number of cycles.

### 10.3.3 Results and discussion

Instead of measuring the resistance to fatigue failure in NiTi wire through an upper limit to strain, the typical measure of fatigue failure of NiTi wires referred to resistances which were expressed in terms of numbers of cycles with respect to eccentric loads.

The fatigue testing involved the two loading points and NiTi wire specimen exist at initial load point/bearing housing, whole method discussed as:

NiTi wire ( $\pm$ )

Bearing Housing  $\rightarrow$   $\downarrow$   $\rightarrow$  Bearing-housing  $\rightarrow$   $\downarrow$   $\rightarrow$  Flexible coupling  $\rightarrow$  High-Load (Load)

Speed motor  $\rightarrow$  Counter

For the number of cycles; are given/required in an application that can be safely endured by the NiTi SMA-materials.

Table 10.1 shows observation result for mechanical fatigue/true-fatigue testing approach in which Eccentric-Loads are applied for specimens of slender SMA wires/ NiTi SMA-materials. This included the diameter, length, condition drawn/heat treatment, profile, eccentric-load, no. of cycles, and status (where SA  $\rightarrow$  Straight annealed, HT  $\rightarrow$  Heat treated)

Table 10.1 Observation data for mechanical fatigue/true-fatigue

Diameter (D)	Length (L)	Condition Drawn/HT	Profile	Eccentric-Load (gm)	Number of Cycles (S)	Status
0.1mm	72mm	SA	round	1500	10,522(>10,000)	Not failed
0.2mm	72mm	SA	round	1500	10,346 (>10,000)	Not failed
0.1mm	72mm	HT	round	3000	89829 (<10,000)	Failed
0.2mm	72mm	HT	round	3000	10,128 (>10,000)	Not failed

Eccentric-Load of 500gm /1000gm also applied for NiTi SMA- materials but did not fail due to NiTi SMA- materials having high strength in most of concern mechanical properties. So, fatigue properties checked in slender SMA wires at various eccentric-loads i.e. 1500gm and 3000gm that can be seen in table 10.1. In the presented work, eccentric loads (S) and a number of cycles (N) had considered to failure of the specimen. Figure 10.13 represents graph a between eccentric-load and number of cycles with wire diameters (D) in which linear condition is considered and 0.1mm NiTi SMA wire diameter not failed at the Eccentric-Load up to 1500gm. But it failed at 3000gm with the numbers of cycles 89829 < 10,000.

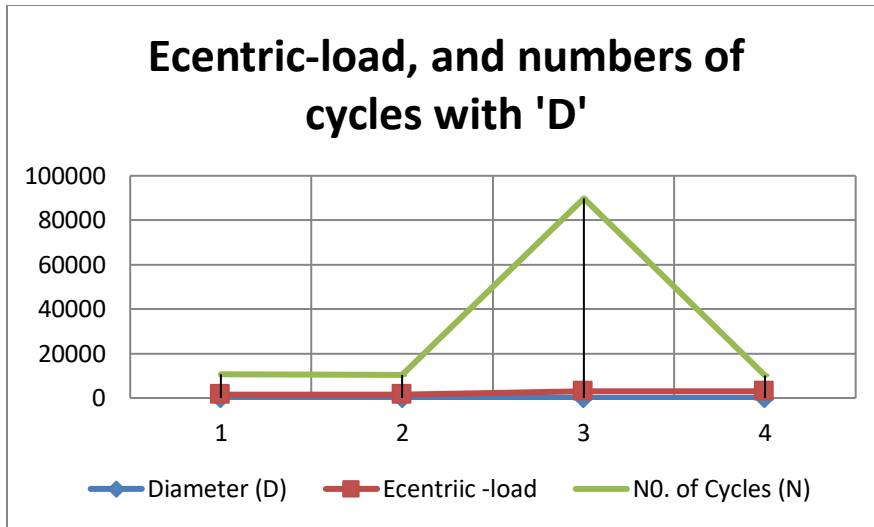


Figure 10.13 Eccentric-load, and numbers of cycles with ‘D’

Figure 10.14 represents a graph between eccentric-load and the number of cycles in which the relation of the polynomial condition is mentioned. The blue-line shows the application of Eccentric-Load and red curve shows the peak of numbers of cycles.

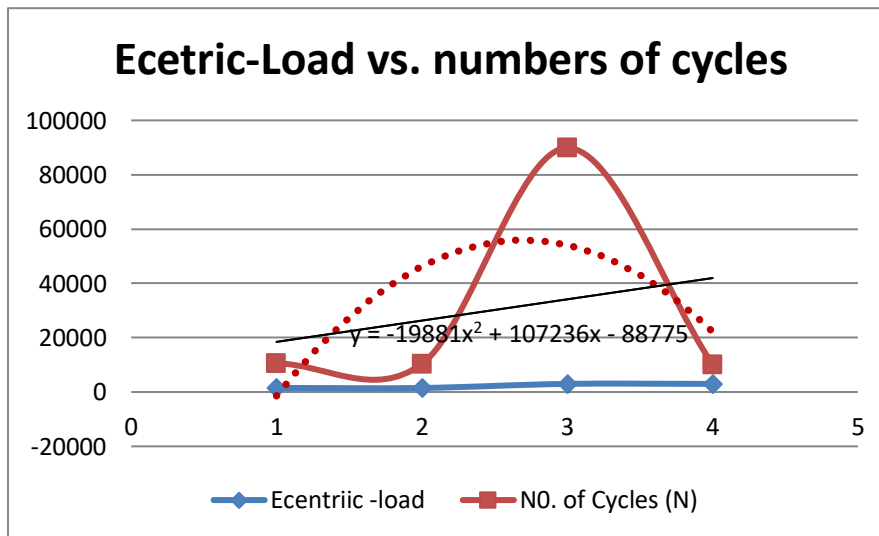


Figure 10.14 Eccentric-load vs. Number of Cycles

**Modeling equations in terms of Numbers of cycles (N)** is as follows (dependable to failure)

$$Y = 7830.x + 10631 \quad (10.1)$$

$$Y = -19881x^2 + 10723x - 88775 \quad (10.2)$$

Equation 10.1 represented in terms of Numbers of cycles (N) for linear condition and equation 10.2 represented in terms of Numbers of cycles (N) for polynomial condition.

At Eccentric-Load of 3000gm, 0.1mm NiTi SMA- materials failed. In general, for low cycle fatigue in terms of plastic and elastic deformation required a small numbers of cycles ( $N < 10^5$ ) for high loads and high cycle fatigue in terms of elastic deformation required large numbers of cycles ( $N > 10^5$ ) for low loads.

#### **10.4 SUMMARY**

Microstructures of slender 0.2 SMA wire (before implementation) having rough darks lines but microstructures of slender 0.2 SMA wire (after implementation) having fine darks lines and spots at a significant distance. Similarly, microstructures of slender 0.1 SMA wire (drawn conditioned) also having rough darks lines, spots but microstructures of slender 0.1 SMA wire (after implementation) having fine darks lines and spots at a significant distance. Similarly, microstructures of 0.5 SMA wire (before implementation) having rough darks lines but microstructures of slender 0.2 SMA wires (after implementation) having fine darks lines and spots at a significant distance but microstructures of 1.0mm SMA wires (before implementation) having mixed rough spot in both images before and after implementation.

Both (0.1mm & 0.2mm) NiTi-based SMA's having good fatigue strength property as not failed at eccentric-loads of 1500gm. 0.2mm NiTi-based SMA's having good fatigue strength property as not failed at eccentric-loads of 3000gm but 0.1mm failed at eccentric-loads of 3000gm. Finally from the results, the NiTi or flexinol wires founded there is no true yield strength but rather an eccentric loads were required.



# CHAPTER 11

## CONCLUSIONS AND SCOPE FOR FUTURE WORK

### 11.1 RESULTS AND DISCUSSION

Based on the research gaps identified in the available literature and all objectives of this work; both are tried to accomplish accordingly/systematically. Firstly, the manufacturing and arrangement of the experimental set-up of smart intelligent NiTi-based helical SMA spring from deformed SMA-wires i.e. 0.1, 0.2mm, 0.5mm, and 1.0mm SMA are done. Various models have been formulated for one way intelligent helical SMA spring by measuring its parameters before implementing it in mechanical equipment/devices. Load-carrying capacities of 0.1, 0.2, and 1.0mm NiTi SMA's were also found.

The various parameters included as average scale values ( $A_S$ ) in terms of strain gauge values, average wire temperature values ( $W_T$ ), average spring-load values ( $L_S$ ), values of average currents ( $I_A$ ), the atmospheric temperature changed values ( $A_T$ ) and applied voltage values ( $V$ ) were estimated at various stages for NiTi-based intelligent helical SMA spring.

This work included the illustrative application of 0.5mm SMA as a simple solenoid valve. The design of spring steel (51CrV4) and alloy steel springs were done at the center of the plate (motionless, and made of mild steel for the helical springs by applying SolidWorks Software; Version-2017). The fatigue tests were performed on alloy steel at different loads and the results of the non-linear simulation analysis were analyzed. Illustrative application smart fork-lift actuator using NiTi one-way helical spring has been discussed. The stability and stiffness of physical-loaded helical compression springs have been analyzed.

Finally, the metallurgical and mechanical fatigue properties of slender NiTi SMA Wires have been discussed in the present thesis. Some important results are described as: -

❖ **Heat treatment at temperature 530°C is a more suitable temperature for reshaping of initial conditioned-based NiTi SMA Wires into smart intelligent SMA helical springs.**

The study is specifically focused on heat treatment process temperatures for manufacturing of NiTi-based shape memory alloy intelligent springs i.e. 330°C, 430°C, 530°C, and 550°C for 1.0mm, 0.1mm, and 0.5mm respectively. This work helps to choose the suitable heat treatment temperature condition of NiTi-based SMA's before implementing as an actuator for mechanical device/equipment. This chapter explores the parameters such as average working temperature, length in elongation, length in compression, and current or voltage values in terms of linear expressions. The maximum value of the effective correlation coefficient is obtained as 95.25% for 1.0mm NiTi SMA helical spring. Table 11.1 shows the conclusions based on the test results.

Table 11.1 Observations of 0.1mm, 0.5mm, 1.0mm, and 0.1mm SMA's

<b>Wire Diameter</b>	<b>Initial Condition</b>	<b>Temp (°C)</b>	<b>Effective correlation coefficient</b>	<b>SME (after deforming)</b>	<b>Recommend approach</b>
0.1mm	Straight annealed	330 <sup>0</sup>	Nil	Reshaped but Not exactly	Less suitable
0.5mm	Straight annealed	430 <sup>0</sup>	94.05%	Reshaped	more suitable
1.0mm	Straight annealed And soften	530 <sup>0</sup>	95.25%	Reshaped	more suitable
0.1mm	Straight annealed And soften	550 <sup>0</sup>	90.05%	Reshaped	suitable

❖ **NiTi-based SMA model of helical spring has been formulated which can enable the stability of SMA by measuring its parameters before implementing in mechanical device/equipment.**

The study also published research work in the field of NiTi-based SMA modeling. The various working parameters of 1.0mm NiTi based intelligent helical spring were obtained during the practical illustration as average scale values( $A_S$ ) in terms of strain gauge values, average spring-load values( $L_S$ ), values of average currents( $I_A$ ), average wire temperature values( $W_T$ ), the atmospheric temperature changed values( $A_T$ ) and applied voltage values( $V$ ) for the preset length of SMA spring. The linear model equations are obtained.

❖ **Developed mechanical device (small scale): a simple solenoid valve 0.5mm SMA based**

The study published research work in the field application of NiTi-based shape memory alloys. Results are discussed in which SMA Conical Spring in the helix form was employed. The obtained results show that displacement has taken by the NiTi-based equally to 12.5mm at the initial voltage of 2.4(V) and initial current 2.1(Ia) respectively. The advantageous purpose of the valve is to operate one way and can control the supply water, oil, liquid fuel, and liquid refrigerant but choked by gravitational force/self-weight.

❖ **Load-carrying capacities of 0.1mm, 0.2mm, and 1.0mm NiTi SMA wires**

The study published research work in the field NiTi-based shape memory alloys. Tables 11.2, 11.3, and 11.4 show the conclusions based on the test results. It is evident from experimental results that 0.1mm SMA/intelligent helical spring having negligible load capacity (< 1gm) under the effect of temperature change by using DC power supply, But the 0.2 SMA-based intelligent having a significant value of load capacity under the effect of temperature change by using DC source. The temperatures responses were smooth for both slender wires as they increased by increasing the power supply/voltage. The maximum load taken by intelligent helical SMA spring during the experiment at 2.0V was obtained as 1420.80gm or 1.4208Kg. The NiTi-based SMA's of 0.2mm SMA spring was obtained very small load capacity (<10 gm).

Table 11.2 Observation data obtained for 0.1mm SMA

<b>Sr. No.</b>	<b>Preset-Length (cm)</b>	<b>Voltage Applied (Volts)</b>	<b>Avg Current in wire (Ampere)</b>	<b>(Atm) Temperature (°C)</b>	<b>Avg Wire Temp (°C)</b>	<b>Avg Load-Cell Strain (A<sub>s</sub>)</b>	<b>Spring-Load (L<sub>s</sub>) (gm)</b>
1	14.5	0.5	0	29	29	0	Nil
2	14.5	1	0.04	29.1	30.4	0	Nil
3	14.5	1.6	0.04	29.8	31.2	2	0.478
4	14.5	2	0.07	29.7	32.5	4	0.956
5	14.5	3	0.07	30.2	33.2	4	0.956
6	14.5	5	0.07	30.1	34.1	4	0.956
7	14.5	7.8	0.07	30.7	35.5	4	0.956
8	14.5	9.2	0.07	30.4	38.9	4	0.956

Table 11.3 Observation data obtained for 0.2mm SMA

<b>Sr. No.</b>	<b>Preset-Length (cm)</b>	<b>Voltage Applied (Volts)</b>	<b>Avg Current in wire (Ampere)</b>	<b>(Atm) Temperature (°C)</b>	<b>Avg Wire Temp (°C)</b>	<b>Avg Load-Cell Strain (As)</b>	<b>Spring-Load (L<sub>s</sub>) (gm)</b>
1	14.5	0.5	0.03	29	29.1	0	Nil
2	14.5	1.0	0.9	29.1	31.4	9.5	2.271
3	14.5	1.6	2.0	29.8	32.8	21	6.91
4	14.5	2	2.7	29.7	34.5	29.5	7.05
5	14.5	3	3.2	30.2	35.2	34.5	8.25
6	14.5	5	3.2	30.1	36.7	34.5	8.25
7	14.5	7.8	3.2	30.7	39.5	34.5	8.25
8	14.5	9.2	3.2	30.4	42.9	34.5	8.25

Table 11.4 Observation data obtained for 1.0mm SMA

Sr. No.	Preset-Length (cm)	Voltage Applied (volts)	Avg Current in wire (Ampere)	(Atm) Temperature (°C)	Avg Wire Temp (°C)	Avg Load-Cell Strain (As)	Spring-Load ( L <sub>s</sub> ) (gm)
1	7.5	0.2	0.93	32.9	33.1	0	Nil
2	7.5	0.4	1.81	32.9	33.8	0	Nil
3	7.5	0.6	2.95	33	34.2	0	Nil
4	7.5	0.8	3.87	33	35	38.5	427.35
5	7.5	1	4.995	33	36.25	76	843.6
6	7.5	1.2	6.12	33.1	38	83	921.3
7	7.5	1.4	7.545	33.1	40.2	90.5	1004.55
8	7.5	1.6	8.675	33	48.25	110.5	1226.55
9	7.5	1.8	9.97	33.1	58.5	117	1298.7
10	7.5	2	10.635	33	64.5	128	1420.8

❖ **Combined average currents variations for 0.1mm and 0.2mm intelligent helical SMA springs concerning applied voltage (V)**

The various working parameters of intelligent helical SMA spring were obtained during the practical illustration as applied voltages (V), average scale values, spring-load values, average currents ( $I_A$ ), working temperatures, and the atmospheric temperature. The average currents ( $I_A$ ) changed concerning applied voltage (V) for 0.1mm intelligent helical SMA spring and 0.2mm intelligent helical SMA spring were represented graphically. Temperatures response was smooth for the both slender-wires as it increased by increasing the power supply/voltage. Figure 11.1 shows the conclusions based on the test results.

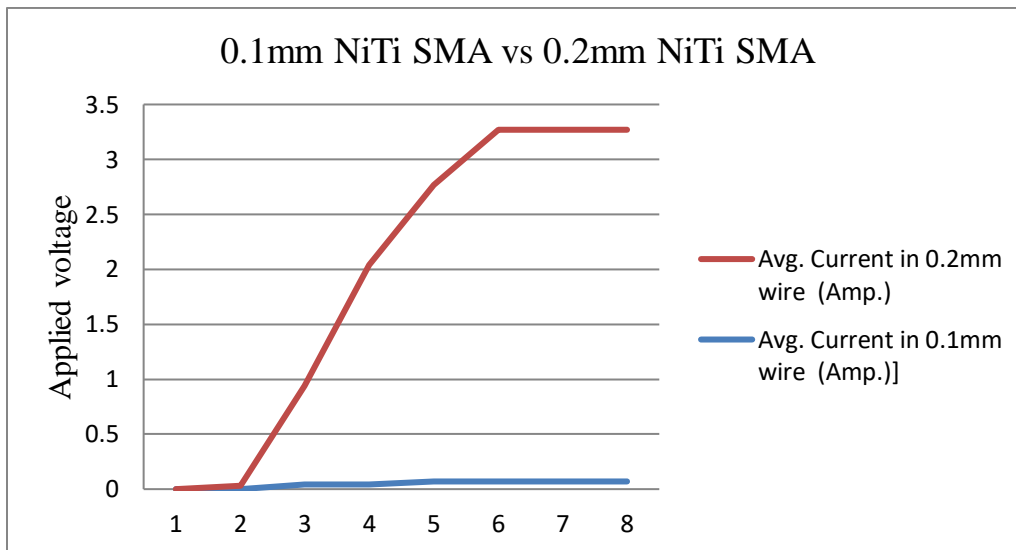


Figure 11.1 Combined average currents ( $I_A$ ) variations with applied voltage (V)

❖ **Simulation and Fatigue design results are estimated for spring steel (51CrV4)/alloy steel materials**

The design of spring steel (51CrV4) and alloy steel springs were done at the centre of the plate (motionless, and made of mild steel for the helical springs by SolidWorks Software; Version-2017). The fatigue tests were performed on the alloy steel at different loads. The results of Non-linear simulation analysis were also included. The detailed description of simulation as the model information with assumptions, material properties, loads and fixtures, contact information, mesh information, and resultant forces. Figure 11.2 shows fatigue results started from 5N, 20N, 50N, and 100N. These results provided damage plots, maximum cycles, minimum cycles, and damage percentages.

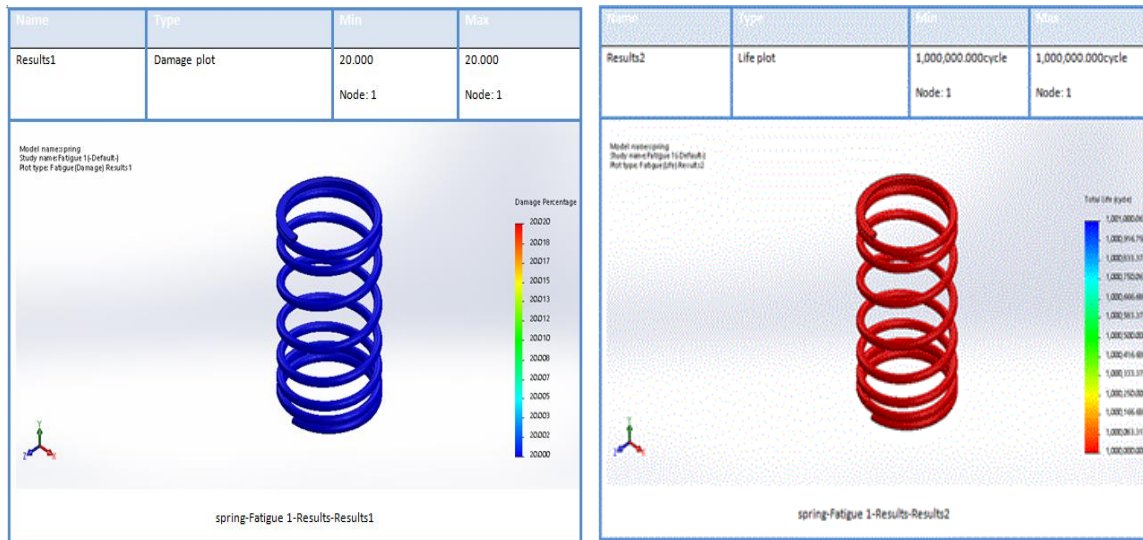


Figure 11.2 Fatigue results

❖ **Developed mechanical instrument (small scale): a smart forklift (1.0mm NiTi-based one-way helical spring)**

A smart forklift actuator using SMA provides a new method (by replacing hydraulic/pneumatic-pressure/gearing/pulley based systems) for cost-effective light load applications. The polynomial relationship of load lifted values ( $L_A$ ) concerning working SMA temperature values ( $W_T$ ) is as follows with correlations coefficient = 91.9 %. The study published research work in the field application of NiTi-based shape memory alloys.

❖ **Spring rates are estimated for conical and helical compression springs**

The experimental result in Table 11.5, Table 11.6 shows; the spring rates ( $k$ ) are obtained higher for conical helical compression spring than cylindrical helical compression spring. So, the stability of conical spring as compared to helical spring is obtained higher. The initial samples of the helical and conical springs are showed that the conical spring has taken large deflection for the same free lengths in comparison to the helical spring. The final sample of the helical and conical springs is showed that the conical spring has taken less deflection and bear large loads. The studied published research work in the field of manufacturing and stability of physical loaded helical compression springs.



Table 11.5 Observation data for conical shape helical spring

Sr. No.	Weight of Acrylic box (gm)	Weight of spring holder (gm)	load applied (gm)	Vertical scale reading (mm)	Avg Load-Cell Strain	Atm Temp ( $^{\circ}$ C)	spring loaded value (conical )	Spring Rate ( $K_c$ )
1	nil	31.536	nil	nil	3	25	nil	nil
2	183.96	31.536	nil	3.0	20.5	25.7	215.496	71.832
3	183.96	31.536	100	3.9	29.5	25.2	315.496	80.89641
4	183.96	31.536	200	4.7	40	26	415.496	88.4034
5	183.96	31.536	300	5.4	51	25.1	515.496	95.46222
6	183.96	31.536	400	6.0	61	26.1	615.496	102.5827
7	183.96	31.536	650	7.6	71	25.9	865.496	113.8811

Table 11.6 Observation data for cylindrical shape helical spring

Sr. No.	Weight of Acrylic box (gm)	Weight of spring holder (gm)	load applied (gm)	Vertical scale reading (mm)	Avg Load-Cell Strain	Atm Temp ( $^{\circ}$ C)	spring loaded value (helical )	Spring Rate ( $K_h$ )
1	nil	31.536	nil	nil	3	25.9	nil	nil
2	183.96	31.536	nil	3.6	20.5	25.1	215.496	59.86
3	183.96	31.536	100	4.8	29.5	26.1	315.496	65.72833
4	183.96	31.536	200	5.9	40	26	415.496	70.42305
5	183.96	31.536	300	6.9	51	25.1	515.496	74.70957
6	183.96	31.536	400	7.8	61	25.6	615.496	78.90974
7	183.96	31.536	650	8.6	71	25.5	865.496	100.6391

❖ **Analysis of metallurgical properties of 0.1 and 0.2mm NiTi SMA wires**

Microstructures of slender 0.2 SMA wire (before implementation) having rough darks lines but microstructures of slender 0.2 SMA wire (after implementation) having fine darks lines and spots at a significant distance.

Microstructures of slender 0.1 SMA wire (drawn conditioned) also having rough darks lines, spots but microstructures of slender 0.1 SMA wire (after implementation) having fine darks lines and spots at a significant distance. Figure 11.3 shows the conclusions based on the test results.

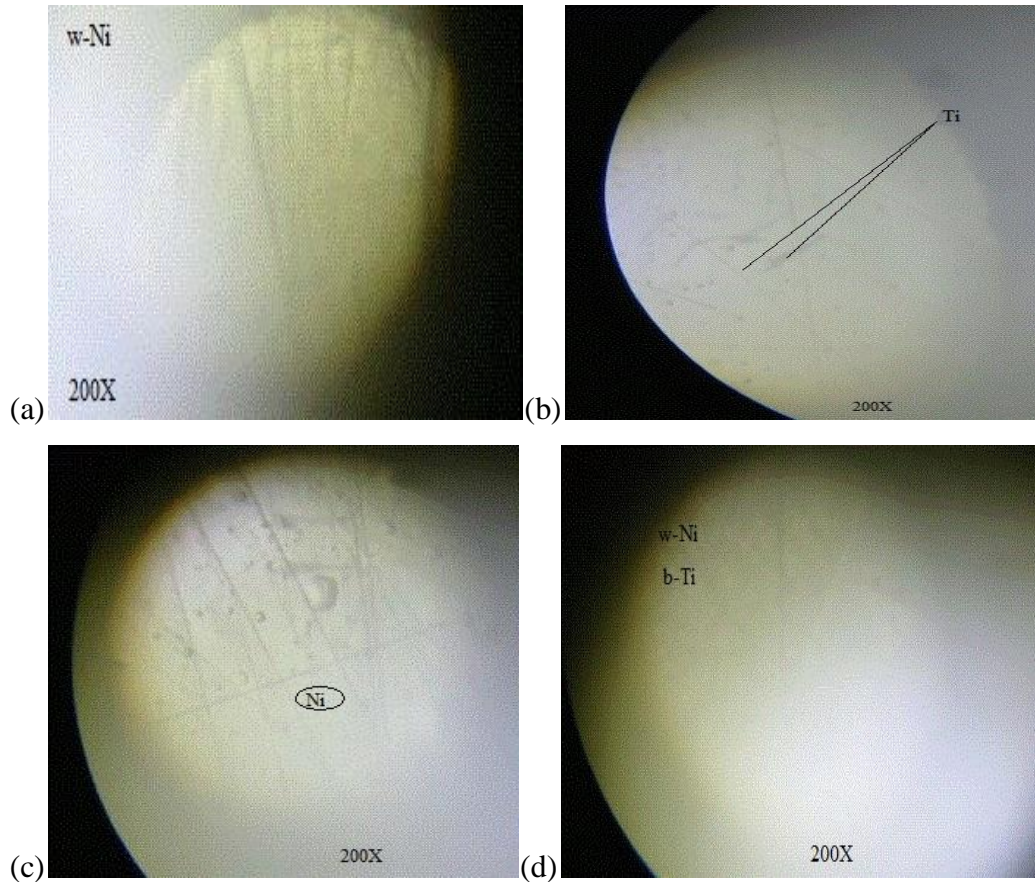


Figure 11.3 (i) 0.2mm wire (B/200X), (ii) 0.2mm wire (A/200X), (iii) 0.5mm wire (B/200X), and (iv) 0.5mm wire (A/200X)

❖ **Mechanical fatigue/True-fatigue results are estimated for 0.1 and 0.2mm NiTi SMA wires**

0.1mm and 0.2mm NiTi-based SMA wires having good fatigue strength property as not failed at eccentric-loads of 1500gm. 0.2mm NiTi-based SMA's having good fatigue strength property as not failed at eccentric-loads of 3000gm but 0.1mm failed at eccentric-loads of 3000gm. Finally from the results, the NiTi/flexinol wires founded there is no true yield strength but rather eccentric loads were required. Table 11.7 shows the conclusions based on the test results.

Table 11.7 Observation data for fatigue results

Diameter (D)	Length (L)	Condition Drawn/HT	Profile	Eccentric-Load (gm)	Number of Cycles (S)	Status
0.1mm	72mm	SA	round	1500	10,522(>10,000)	Not failed
0.2mm	72mm	SA	round	1500	10,346 (>10,000)	Not failed
0.1mm	72mm	HT	round	3000	89829 (<10,000)	Failed
0.2mm	72mm	HT	round	3000	10,128 (>10,000)	Not failed

## 11.2 CONCLUSIONS

- ❖ The present research provides various models for helical springs based on experimental work. The models can be used for the design of shape memory alloy based on NiTi helical springs.
- ❖ A design of instruments and calculation of various parameters for shape memory alloy helical springs are presented, specifically for the testing of various actuation parameters at various levels.
- ❖ 0.1mm SMA-based intelligent helical spring having negligible load capacity under the effect of temperature change. For slender wire 0.1mm SMA; based on NiTi having higher initial voltage values (V) than 0.2mm SMA in case of their actuation.
- ❖ The initial voltage values (V) were higher but average current values ( $I_A$ ) were very small in actuation of 0.1mm intelligent helical SMA spring than 0.2mm intelligent helical SMA spring.
- ❖ The maximum load taken by 1.0mm intelligent helical SMA spring during the experiment at 2.0V was obtained as 1.4208Kg, much higher as compared to SMA's 0.2mm SMA spring load capacity which was very small (<10 gm).

- ❖ Smart fork-lift equipment, based on NiTi SMA Spring provides a new concept by replacing hydraulic, pneumatic, gearing, pulley-based systems, and other actuators in low load applications. This type of actuator may reduce the higher cost of comparative other equipment.
- ❖ A conical compression spring having a higher value of spring rate than a cylindrical compression spring for the same mean coil diameter. A conical spring provides higher comfort for the same height.
- ❖ A correlation exists between change in spring length with temperature during compression and tension of SMA helical spring. This can be used in the design of actuators.
- ❖ A small diameter SMA spring can take a higher load (100%-400%) as compared with a conventional spring. It is due to the fact the load application is temperature dependant.
- ❖ An overview design, non-linear type simulation, and safe fatigue life was found for helical compression springs used in smart fork-lift using CAD analysis.
- ❖ Small scale NiTi-based equipment as a simple solenoid valve one-way operated suggested specifically controlling the supply of water, oil, liquid fuel/liquid refrigerant, and choked by gravitational force.
- ❖ An overview mechanical fatigue properties of NiTi-based alloy tested in a safe range (both, 0.1mm & 0.2mm); having a better fatigue strength property as not failed at prescribed eccentric-loads.
- ❖ Experimental results show that spring rate ( $k$ ) is obtained higher for conical helical compression spring than that for a cylindrical helical compression spring. The stability of conical spring as compared to a helical spring is obtained higher.

- ❖ An overview of metallurgical properties of alloy wires (NiTi-based) were examined by their microstructures (before and after implementation).

### **11.3 LIMITATIONS AND SCOPE FOR FUTURE WORK**

#### **Limitations:**

Though a lot of efforts have been made in this research work to ensure the quality enabled factors of different stages of NiTi based shape memory alloy but this research is not free from the limitations. The limitations of the present work are as follows:

- The findings of the present work are not corroborated for the actual practical settings.
- The developed mechanical small device: a simple solenoid valve (0.5mm NiTi SMA) based frame-work depends upon the opinion of experts and it may have some element of bias.
- The developed mechanical small instrument; a smart fork-lift (1.0mm NiTi SMA based one-way helical spring) based framework depends upon the opinion of experts and it may have some element of bias.
- Development of model equations for permanent function becomes problematic because of the combinatorial approach, particularly when variables are large in number. This requires the development of computer software.

#### **Scope for Future Work:**

Some work may be carried out in the future and the present work can be extended in the following directions:

- The instrument/smart forklift can be developed at a small scale for the same or other different types of shape memory alloys.
- A solenoid valve based on NiTi can be developed for various fields of engineering as aeronautical engineering, pharmaceutical engineering, biomedical engineering, etc.
- The fatigue life test developed for different stages of NiTi-based shape memory alloy can be statistically tested.
- A comprehensive questionnaire-based survey can be carried out to know the impact of the identified modified actuation factors in the SMA's manufacturing organizations.

## REFERENCES

- [1] Mohammad H. Elahinia, Mahdi Hashemi and Majid Tabesh, manufacturing and processing of NiTi implants: a review, progress in materials science, Elsevier, 57, 911-946, 2012.
- [2] Saurabh. S. Kawate, Chethan. K. N, Laxmikant G Keni, innovation and recent trends in shape memory alloy: a review, international journal of engineering & technology, 7, 2172-2177, 2018.
- [3] [https://en.wikipedia.org/wiki/Shape-memory\\_alloy/Nickel\\_titanium](https://en.wikipedia.org/wiki/Shape-memory_alloy/Nickel_titanium)
- [4] Yongqing Fu, Hejun Du and Weimin Huang, TiNi-based thin films in MEMS applications: a review, Elsevier, 395-408, 2004.
- [5] Ricardo Alexandre, Amar de Aguiar and Marcelo Savi, SMA helical springs: modeling, simulation and experimental analysis, Brazilian society of mechanical sci. and engg., January, 2009.  
(<https://www.researchgate.net/publication/242163391>)
- [6] P. Sittner and L. Heller,  $B2 \rightleftharpoons B19^I \rightleftharpoons B2^T$  martensitic transformation as a mechanism of plastic deformation of NiTi, shape memory superelasticity, Springer, 5, 383-396, 2019.  
(<https://doi.org/10.1007/s40830-019-00250-5>)
- [7] Nicole Latrice Harris Odum, the characterization of thin film nickel titanium shape memory alloys, doctor of philosophy dissertation, Materials Engineering Department, Auburn University, Alabama, 2010.
- [8] Cimprič Darjan, Shape memory alloys, Univerza v Ljubljani, January, 2007.  
(<https://www.yumpu.com/en/document/view/17852376>)
- [9] Je-sung Koh, design of shape memory alloy coil spring actuator for improving performance in cyclic actuation, department of mechanical engineering, Ajou University, Korea, 2018.
- [10] Daniela tarnita, D. N. tarnita and N. Bizdoaca, properties and medical applications of shape memory alloys: review, Romanian journal of morphology and embryology, 50, 15–21, 2009.
- [11] Rohit Patil, Nandini Patra and Abhinav Sharma, design and development of peristaltic soft robot using SMA actuators with different control strategies, Materials sci. and engg., IOP Conf. Series, 390, 2018.

(<https://doi.org/10.1088/1757-899X/390/1/012044>)

- [12] Md. Amri Zainal, Shafishuhaza Sahlan and Md. Sultan Mohamed Ali, micromachined shape-memory-alloy microactuators and their application in biomedical devices, *Micromachines*, 68, 79-901, 2015.
- [13] Mehrshad Mehrpouya and Hossein Cheraghi Bidsorkhi, MEMS applications of NiTi based shape memory alloys: A review, *micro and nanosystem*, 8, 79-81, 2016.
- [14] Piyas Chowdhury, frontiers of theoretical research on shape memory alloys: a general overview, *Shap. Mem. Superelasticity*(Springer), 4, 26-40, 2018.
- [15] José r. Santiago Anadón, large force shape memory alloy linear actuator, doctor of philosophy dissertation, University of Florida, United states, 2002.
- [16] Danish Mahmood Baitab, Dayang Laila Abang and Haji Abdul Majid, A review of techniques for embedding shape memory alloy (SMA) wires in smart woven composites, *IJET (UAE) journal*, 7, 129-136, 2018.
- [17] Sam Bakhtiari, NiTi-based shape memory alloys beyond the shape memory effect and superelasticity, doctor of philosophy dissertation, Western University, Australia, 2019.
- [18] Sundara sathiyar, Vikram singh and Rajesh V, gripper actuator using shape memory alloy spring, *international journal of scientific research and publications*, 8, 1-3, 2015.
- [19] Pierre-Antoine Gédouin, Laurent Pino, Shabnam Arbab Chirani, R-phase shape memory alloy helical spring based actuators: modeling and experiments, 289, 65-76, 2019. ([www.researchgate.net/pub/331412508](http://www.researchgate.net/pub/331412508))
- [20] SC Mishra, applications of shape memory alloys: a review, *STM-journals*, vol. 2, Issue 2, 2015.
- [21] E. Hornbogen, ausforming of NiTi, *journal of materials science*, Ruhr-Uni., Bochum, Germany, 34, 599-606, 1999.
- [22] Supriya rahul burgul and Atul.p.kulkarni, fatigue analysis for helical compression spring for determining design alternatives for enhanced life and performance, *IJTRE*, , Issue 7, vol. 2, 1070-1078, 2015.
- [23] Niranjan Singh, General Review of Mechanical springs used in automobiles suspension system, *IJAERS*, 3(1), 115-122, Dec.2013.

- [24] Goran Vukelica and Marino Bricib, failure analysis of a motor vehicle coil spring, European Conference on Fracture (ECF21, Catania, Italy), Elsevier, pp.2944-2950, 20-24 June, 2016.
- [25] M. Tazarv and M.S. Alam, shape memory alloy for bridge columns, Eleventh U.S. National Conference on Earthquake Engineering, California, June 25-29, 2018.
- [26] M Kabla, E Ben-David and D Shilo, novels shape memory alloy microactuator for large in-plane strokes and forces, Smart Mater. Struct., IOP Science, 25, 075020 (8pp), 2016.  
(<http://iopscience.iop.org/0964-1726/25/7/075020>)
- [27] Samuel de Oliveira, Simplício Arnaud da and Silva Rebecca Casimiro de Souza, prediction of elastic strength coil of shape memory alloy using recursive neural network, 23rd ABCM International Congress of Mechanical Engineering, Brazil, December 6-11, 2015.
- [28] Yinghua Lin and Yongping Lei, Mechanical properties and toughening mechanism of TiB<sub>2</sub> / NiTi reinforced titanium matrix composite, Materials and design, Elsevier, 80, 82-88, 2015.
- [29] Ronak b chaudhari and Dr. l.g.navale, Effect of change in parameters like material, wire diameter, pitch on fatigue life of helical spring used in stamping machine, IJSRD, vol.5, issue 4, pp.1561-1567, 2017.
- [30] Iqra Zubair Awan and Abdul Qadeer Khan, fascinating shape memory alloys, Chem. Sci. journal, france, 40, 1-23, 2018.
- [31] Satbeer Singh Bhatia and Ajeet Bergaley, analysis of the design of helical compression spring to study the behaviour of steel an composites used as spring materials, international journal of engineering sciences & research technology, 3(8), 576-583, 2014. (<https://www.academia.edu/search>)
- [32] Taemin Byun, Tae Soo Bae and Kwon Hee Kim, analysis on biomechanical characteristics of SMA fixation grip for femoral fractures, advanced science and tech. letters, Korea, 141, 19-25, 2016.
- [33] Hyuk-Soo Han, Dae-Ha Kim and Seung-Baik Kang, The use of a ti-ni shape memory alloy ring bone fixator, Seoul National University, Korea, 4, 231-235, 2011.



- [34] Rinaldo Puff, Marcos Giovanni Dropa de Bortoli & Raul Bosco Jr, fatigue analysis of helical suspension springs for reciprocating compressors, ICE Conference, Purdue University, July 12-15, 2010.
- [35] Vishal Chaudhari and Prof. G. V. R. S.Rao, structural analysis of helical compression spring, IJSRSET, Issue 4, vol.2, pp.2394-4099, 2016.
- [36] Sam Bakhtiari, NiTi-based shape memory alloys beyond the shape memory effect and superelasticity, doctor of philosophy dissertation, University of Western Australia, January, 2019.
- [37] R. M. Satava and S. B. Jones, smart materials, devices, and structures implications for surgical practice, Surgical Endoscopy, Springer, 10, 871-874, 1996.
- [38] Pedro Nunes and Paulo Silva Lobo, influence of the SMA constitutive model on the response of structures, 2nd International conference on structural integrity, Elsevier, 5, 187-194, 2017.
- [39] G. Machado, H. Louche and T. Alonso, superelastic cellular niti tube-based materials: fabrication, experiments and modeling, materials and design journal, Elsevier, 65, 212-220, 2015.
- [40] Saidjafarzoda Ilhom, Laser-induced recoverable surface patterning on Ni50Ti50 SMAs, Western Kentucky University press, Masters (2018).  
([https://uknowledge.uky.edu/Theses & Specialist Projects/Paper 3052](https://uknowledge.uky.edu/Theses%20&%20Specialist%20Projects/Paper%203052))
- [41] Saidjafarzoda Ilhom, "Formation of two-way shape memory effect in NiTi alloy using pulsed laser irradiation," western kentucky university, publications/49, 2018  
([https://uknowledge.uky.edu/me\\_facpub/49](https://uknowledge.uky.edu/me_facpub/49)).
- [42] T. Ikeda, analytical investigation of strain loading frequency effect on stress-strain-temperature relationship of SMA, department of aerospace engineering, nagoya university, japan, Arch. Mech., 67, 4, 275-291, 2015.
- [43] Yousef Payandeh, Fodil Meraghni and Etienne Patoor, study of the martensitic transformation in NiTi–epoxy smart composite, materials and design, Elsevier, 39, 104–110, 2012.
- [44] M.J. Mahtabi, Nima Shamsaei and Benjamin Rutherford, Mean strain effects on the fatigue behavior of superelastic Nitinol alloys, Fatigue design conference (6<sup>th</sup>), 133, 646-654, 2015.

(<https://www.sciencedirect.com/search>)

[45] Francesca Berti, Lorenza Petrini and Andrea Spagnoli, A discussion about multi-axial fatigue criteria for NiTiNol cardiovascular devices, ECF22-Loading and Environmental effects on Structural Integrity, Elsevier, 13, 813-818, 2016.

[46] Bashir S. Shariat, Yinong Liu and Gerard Rio, Hystoelastic deformation behaviour of geometrically graded NiTi SMAs, material and design journal, Elsevier, 50, 879-885, 2013.

[47] O. Tyc, J. Pilch and P. Sittner, fatigue of superelastic NiTi wires with different plateau strain, Elsevier, procedia structural integrity 2, 1489-1496, 2016.

[48] S. Kucharski, N. Levintant-Zayonts and J. Luckner, Mechanical response of nitrogen ion implanted NiTi shape memory alloy, Materials and Design journal, Elsevier, 56, 671-679, 2015.

[49] Gajendra singh rathore and Upendra kumar joshi, fatigue stress analysis of helical compression spring: a review, international journal of emerging trends in engineering and development, Issue 3, vol.2, 2013.

[50] E. Hornbogen, thermo-mechanical fatigue of shape memory alloys (review), Ruhr-University, Bochum, Germany, 39, 385-399, 2004.

[51] Claire Morin, a comprehensive approach for fatigue analysis of SMAs, materials and structures in mechanics, thesis,ENSTA-Paristech, 2011.

(<https://pastel.archives-ouvertes.fr/pastel-00608205>)

[52] Noshirwaan aibada and Siddhant sundaram, review of studies on helical compression springs with a perspective of material, methods and failure, IJMET, Issue 3, vol.9, pp.936-945, 2018.

[53] A Hadi, A Yousefi-Koma and M Elahinia, a SMA spring-based actuator with stiffness and position controllability, proceedings of the institution of mechanical engineers, journal of systems and control engineering, 7, 902-917, 2011.  
(<http://pii.sagepub.com/content/225/7/902>)

[54] Andrea Spaggiari, Igor Spinella, and Eugenio Dragoni, design of a telescopic linear actuator based on hollow shape memory springs, journal of materials engineering and performance, 20, 489-496, 2011.

- [55] R. B. Barjibhe and Dr. Bimlesh Kumar, vibration control of cantilever beam using SMA springs in series, international research journal of engineering and technology, 2, 1790-1793, 2015.
- [56] Mohammad Mahdi Kheirikhah, Samaneh Rabiee and Mohammad Ehsan Edalat, a review of shape memory alloy actuators in robotics, RoboCup, Springer, 206-217, 2011.
- [57] Amin Jamalimehr and Hossein Ravanbakhsh, investigation of dog-bone geometry for simple tensile test of pseudoelastic shape memory alloys, Iran J. Sci Technol, Springer, October, 2016.
- [58] Zahra Khalid and Azhar Ali Bangash, canine retraction using closed nickel titanium coil spring and an elastic module, journal of the college of physicians and surgeons, 28, 695-698, 2018.
- [59] Luciano G. Machado, SMAs for vibration isolation and damping, doctor of philosophy dissertation, Texas A&M University, 2007.
- [60] Yanhong Ma and Qicheng Zhang, a novel smart rotor support with SMA metal rubber for high temperatures and variable amplitude vibrations, school of energy and power engineering, Beihang University, China, 2014. (<http://dx.doi.org/10.1088/0964-1726/23/12/125016>)
- [61] Mohammad H. Elahinia, Hashem Ashrafioun and Mehdi Ahmadian, a temperature-based controller for a shape memory alloy actuator, journal of vibration and acoustics, 127, 285-291, 2015.
- [62] Bethany Gordon, shape memory alloy fiber-reinforced mortar, University of Virginia, MATS-UTC USRP, July, 2015.
- [63] M. Bocciolone and M. Carnevale, application of martensitic SMA alloys as passive dampers of GERP laminated composites, national research council CNR, Italy, 23, 34-46, 2013.
- [64] Mojtaba Nasr-Esfahani and Reza Ebrahimi-Kahrizsangi, bonding strength, hardness and bioactivity of nano bioglass-titania nano composite coating on NiTi nails, Bentham Science Pub. Ltd., 7, 568-575, 2011.
- [65] Kin-Tak Lau and Alik Wai-Lik Chan, debond induced by strain recovery of an embedded NiTi wire at NiTi / epoxy interface, Elsevier, 23, 265-270, 2002.

- [66] Rameshwar S. Ingalkar, rehabilitation of buildings and bridges by using shape memory alloys, international journal of civil engineering research, 5, 163-168, 2014.
- [67] J.M. McNaney, V. Imbeni and Y. Jung, an experimental study of the superelastic effect in a shape-memory Nitinol alloy under biaxial loading, mechanics of materials, Elsevier, 35, 969-986, 2003.
- [68] Vishal.B.Wani and Ajay.D.Patil, review paper on shape memory alloy actuators for fire alarm, S.S.B.T College of engg. & tech., Jalgaon. NLPP, December, 2008.
- [69] Vaibhav chaturvedi and Rituparna datta, design and analysis of a vibration isolation system based on four-bar mechanism integrated with SMA wire, IEEE, Electronic ISBN: 978-1-4799-3010-4 , 257-262, 2014.
- [70] Huilong Hou, Mark W. Horn and Reginald F. Hamilton, biased target ion beam deposition and nanoskiving for fabricating NiTi alloy nanowires, Springer, 2,330-336, 2016.
- [71] H. Fischer, B. Vogel and W. Pfleging, flexible distal tip made of nitinol (NiTi) for a steerable endoscopic camera system, Elsevier, A273-75, 780-783, 1999.
- [72] Girolamo Costanza and Maria Elisa Tata, SMAs for aerospace, recent developments, and new applications: a short review, MDPI-materials, April, 2020. (www.mdpi.com/journal/materials)
- [73] G. Song, N. Ma and H. N. Li, applications of shape memory alloys in civil structures, Engineering Structures, Elsevier, 28, 1266-1274, 2006.
- [74] Jaronie Mohd Jani, design optimization of shape memory alloy linear actuator applications, doctor of philosophy dissertation, School of aerospace, mech. and mfg. engg., RMIT University, Australia, 2016.
- [75] Jaronie Mohd Jani, Martin Leary and Aleksandar Subic, A review of shape memory alloy research, applications and opportunities, materials and design journal, Elsevier, 56, 1078-1113, 2014.
- [76] Dieter Stoeckel, shape memory actuators for automotive applications materials & design journal, vol. 11 no.6, 302-307, 1990.  
(<https://www.sciencedirect.com/science/article/abs/pii/026130699090013>)

- [77] Xiaoyong Zhang, Xiaojun Yan and Qiaolong Yang, design and experimental validation of compact, quick-response SMA separation device, Transactions of the ASME, vol. 136, January, 2014.
- [78] H. B. Pawar and D.D. Desale, optimization of three wheeler front suspension coil spring, 2<sup>nd</sup> International conference on materials manufacturing and design engineering, Elsevier, 20, 428-433, 2018.
- [79] P. K. Kumar and D. C. Lagoudas, introduction to shape memory alloys, Springer science, March, 2008.  
(<http://dx.doi.org/10.1007/978-0-387-47685-8>)
- [80] C. Laureanda, One-way and Two-way SME: thermo–mechanical characterization of NiTi wires, doctor of philosophy dissertation, University of Pavia, Italy, 2008.  
(<https://www.pdfsemanticscholar.org>)
- [81] Rosario Pecora, Generoso Iannuzzo and Massimo Riccio, actuator device based on SMA, and a wing flap assembly fitted with such an actuator device, United States Patent (US-8, 348, 201, B2), January, 2013.
- [82] Ranjith Pillai Ra, Murali G and Gopal M, modeling and simulation of a SMA spring actuated flexible parallel manipulator, international conference on robotics and smart mfg., Elsevier, 133, 895-904, 2018.
- [83] Esuff Khan and Sivakumar M. Srinivasan, a new approach to the design of helical SMA spring actuators, SMR, Hindawi publishing corporation, 5 (pages), 2011.  
(<http://dx.doi.org/10.1155/2011/167195>)
- [84] Young Pyo Lee and Byungkyu Kim, locomotive mechanism design and fabrication of biomimetic micro robot using SMA, International conference on robotics & automation, IEEE, 5007-5012, April, 2004.
- [85] Sangbae Kim and Elliot Hawkes, micro artificial muscle fiber using NiTi spring for soft robotics, International conference on intelligent robots and systems, IEEE, 2009.  
(<https://ieeexplore.ieee.org/doc/5354178>)
- [86] Ehsan Tarkesh Esfahani and Mohammad H. Elahinia, developing an adaptive controller for a shape memory alloy walking assistive device, Journal of vibration and control, April, 2010.  
(<http://jvc.sagepub.com>, dio: 10.1177/1077546309344163)

- [87] Zariff Ch. and Mohammad Hailat, aluminum-based composites reinforced with sic particles and NiTi fibers, journal materials science, Springer, 46, 1945-1955, 2011.
- [88] Stefano Gialanella and Gloria Ischia, phase composition and wear behavior of NiTi alloys, journal materials science, Springer, 43, 1701-1710, 2008.
- [89] S. Hahn and M. F. X. Wagner, challenges during microstructural analysis and mechanical testing of small-scale pseudoelastic NiTi structures, Springer, 2,171-179, 2016.
- [90] Michele Guida and Andrea Sellitto, analysis of the impact dynamics of SMA hybrid composites for advanced applications, MDPI-materials, January, 2019. ([www.mdpi.com/journal/materials](http://www.mdpi.com/journal/materials))
- [91] Shivananda Pai Mizar, thermomechanical characterization of nitinol and nitinol based structures using aces methodology, PhD-dissertation, Worcester polytechnic institute Dec, 2005. (<https://digital.wpi.edu>)
- [92] Yingying Zhu, Haizhen Wang and Zhiyong Gao, a stress-induced martensitic transformation in aged Ti<sub>49</sub>Ni<sub>51</sub> alloy after high-velocity impact, MDPI-materials, June, 2016. ([www.mdpi.com/journal/materials](http://www.mdpi.com/journal/materials))
- [93] Vinicius Piccirillo and Jose Manoel Balthazar, a nonlinear and chaotic non-ideal vibrating system with SMA, journal of theoretical and applied mechanics, 46, 597-620, 2008.
- [94] Sergio Puértolas and José M Pérez-García, design of splints based on the NiTi alloy for the correction of joint deformities in the fingers, Biomedical engineering online, 49, 2010, (<http://www.biomedical-engineering-online.com/content/9/1/49>)
- [95] Yutaka Toi, Jong-Bin Lee and Minoru Taya, FEA of superelastic, large deformation behavior of SMA helical springs, computers and structures journal, Elsevier, 82, 1685-1693, 2004.
- [96] Donatello Cardone and Salvatore Sofia, experimental evaluation of a device prototype based on shape memory alloys for the retrofit of historical buildings, Journal of materials engineering and performance, 21, 2719-2728, 2012.

- [97] S. Ballandras, M. Calin and S. Zissi, microstereolithography and shape memory alloy for the fabrication of miniaturized actuators, *Journal of sensors and actuators*, Elsevier, 62, 741-747, 1997.
- [98] Mauro dolce and Roberto marnetto, passive seismic devices based on shape memory alloys, 12WCEE, January, 2000.  
(<https://www.researchgate.net/publication/228357179>)
- [99] H. Asadi, Y. Kiani and M. Shakeri, exact solution for nonlinear thermal stability of hybrid laminated composite timoshenko beams reinforced with SMA fibers, *Composite Structures journal*, Elsevier, 108, 811-822, 2014.
- [100] Luana B. Pe'rtile and Patri'cia M. S. Silva, In vivo human electrochemical properties of a NiTi-based alloy (Nitinol) used for minimally invasive implants, *Journal of biomedical materials research*, 1072-0178, May, 2008. ([www.interscience.wiley.com](http://www.interscience.wiley.com))
- [101] Nubailah Abd Hamid and Azmi Ibrahim, pseudo elastic and self-healing cyclic properties of smart NiTi SMA for seismic mitigation, *Materials Science and Engg (IOP Conf. Series)*, 431, 2018.  
(<http://dx.doi.org/10.1088/1757-899X/431/7/072012>)
- [102] Ahmed M. El Kady and Ahmed E. Mahfouz, mechanical design of an anthropomorphic prosthetic hand for SMA actuation, 5th Cairo International biomedical engineering conf., Cairo, Egypt, Dec., 2010.
- [103] Alaa AbuZaiter and Marwan Nafea, micromanipulator based on integrated SMA Bimorph actuators, 40th micro & nano engg. Conference, September, 2014.  
(<https://www.researchgate.net/publication/322937046>)
- [104] A. Banerjee and B. Bhattacharya, optimum discrete location of SMA for enhanced actuation of a compliant link, *Journal of mechanical design*, vol. 132, February 2010.  
(<http://www.asme.org/search>)
- [105] K.C. Munasinghe and B.G.C.T. Bowatta, new mems based micro-gripper using SMA for micro level object manipulation and assembling, IEEE, 2016.  
(<https://ieeexplore.ieee.org/doc/978-1-5090-0645-8/16>)
- [106] I. Dutta, D. Pan and B.S. Majumdar, role of SMA reinforcements on strain evolution in lead-free solder joints, *Journal of electronic materials*, 35, 1902-1913, 2006.

- [107] Nagahiko Shinjo and Geoffrey W. Swain, use of a SMA (NiTi) for the design of an oscillatory propulsion system, *Journal of oceanic engineering, IEEE*, 29, 750-755, 2004.
- [108] Yuchen Chen, Xing Shen, Jiefeng LI, and Jinjin Chen, nonlinear hysteresis identification and compensation based on the discrete preisach model of an aircraft morphing wing device manipulated by an SMA actuator, *Chinese journal of aeronautics*, 32, 1040-1050, 2019.
- [109] Han Zhang and Etienne Burdet, robotic micro-assembly of scaffold/cell constructs with a SMA gripper, *International conference on robotics & automation, IEEE*, May, 2002.  
(<https://ieeexplore.ieee.org/doc./0-7803-7272-7/02>)
- [110] N. Grassi and C. Cipolla, validity of shape memory NiTi colon-ring biodynamix colonring, *Edizioni Internazionali (CIC)*, Vol. 33, pp. 194-198, May, 2012.
- [111] Y.Q. Fu, J.K. Luo and A.J. Flewitt, thin film shape memory alloys and microactuators, *Int. J. computational materials science and surface engineering*, 2, 208-226, 2009.
- [112] M Parlinska, H. Clech and J.A. Balta, adaptive composites with embedded shape memory alloys, *EDP Phy. Sciences Journal, France*, 4, 197-204, 2000.
- [113] Xi Wang, crystallization and martensitic transformation behavior of NiTi SMA thin films, doctor of philosophy dissertation, The School of Engineering and Applied Sciences, Harvard University, Cambridge, 2007.
- [114] Christoph Bechtold and Rodrigo Lima, method for fabricating miniaturized NiTi self-expandable thin film devices with increased radiopacity, *Shape Memory Superelasticity, Springer*, 2, 391-398, 2016.
- [115] Christoph Bechtold and Christoph Chluba, fabrication and characterization of freestanding NiTi based thin film materials for shape memory micro-actuator applications, *Shape Memory Superelasticity, Springer*, 5, 327-335, 2019.
- [116] Donghai Qiu and Sébastien Seguy, tuned nonlinear energy sink with conical spring: design theory and sensitivity analysis, *Journal of mechanical design, American Society of Mechanical Engineers*, 140, 2018. (<https://hal.insa-toulouse.fr/hal-01819561/document>)



- [117] H. Asadi and M. Bodaghi, on the free vibration of thermally pre/post-buckled shear deformable SMA hybrid composite beams, *Journal of aerospace science and technology*, Elsevier, 31, 73-86, 2013.
- [118] Youli Zhu, Yanli Wang and Yuanlin Huang, failure analysis of a helical compression spring for a heavy vehicle's suspension system, *case studies in engineering failure analysis*, Elsevier, vol.2, 169–173, 2014.
- [119] Rahul M. Gupta and Bhushan C. Bissa, heat transfer enhancement and friction factor analysis in tube using conical spring insert, *international journal of research in engg. and tech.*, 4, 253-260, 2015.
- [120] Pratik Sharma and Ganesh Kondhalkar, design and analysis of conical spring for performance enhancement of mirror assembly using hybrid approach, *international research journal of engineering and technology*, 5, 808-813, 2018.
- [121] Nicholas G. Garafolo and Rachel J. Collard, performance mapping of an aluminum-Nitinol composite vibrating beam, *Journal of mechanical design and vibration*, 5, 27-36, 2017.
- [122] J A Balta, F Bosia and V Michaud, smart composites with embedded SMA actuators and fibre bragg grating sensors: activation and control, *journal of smart materials and structures*, 14, 457-465, 2005.  
(<https://stacks.iop.org/SMS/14/457>)
- [123] Gangbing Song and Brian Kelly, active position control of a shape memory alloy wire actuated composite beam, IOP publishing, March, 1999.  
(<https://iopscience.iop.org/article/10.1088/0964-1726/9/5/316>)
- [124] Romulo Pierre Batista Dos Reis, vibration attenuation in an epoxy smart composite beam with embedded NiTi shape memory wires, *Materials Science Forum*, 643, 7-13, 2010.
- [125] Shahabeddin Ahmadi and Kiran Jacob, shape memory alloy film damping for smart miniature systems, *international journal of smart and nano materials*, Taylor & Francis, 9, 199-215, 2018.
- [126] T. Shahrabi and S. Sanjabi, extremely high pitting resistance of NiTi SMA thin film in simulated body fluids, *Materials Letters*, Springer, 62, 2791-2794, 2008.

- [127] C. Chluba and H. Ossmer, ultra-low fatigue quaternary TiNi-based films for elastocaloric cooling, *Shape Memory Superelasticity*, Springer, 2, 95-103, 2016.
- [128] Shuyong Jiang and Junbo Yu, investigation on deformation mechanisms of NiTi SMA tube under radial loading, *MPDI*, 268, 2017.  
(<http://dx.doi.org/10.3390/met7070268>)
- [129] S. Hahn and A. Schulze, thin NiTi films deposited on graphene substrates, *Shape Memory Superelasticity*, Springer, 3, 1-8, 2017.
- [130] Xiang Chen and Adam Hehr, deformation mechanisms in NiTi-Al composites fabricated by ultrasonic additive manufacturing, *Shape Memory Superelasticity*, Springer, 1, 294-309, 2015.
- [131] Bing Yang and Zheng Luo, high damping of lightweight TiNi-Ti<sub>2</sub>Ni shape memory composites for wide temperature range usage, *Journal of materials engineering and performance (ASM International)*, 26, 4970-4976, 2017.
- [132] J.P. Coughlin and J.J. Williams, interfacial reactions in model NiTi shape memory alloy fiber-reinforced Sn matrix “smart” composites, *Metallurgical And Materials Transactions A*, 40A, 176-184, 2009.
- [133] A R Sadeghi and H Mostajabodaveh, effects of milling and heat treatment on the synthesis of NiTi powders, *Journal of Wuhan University of Technology*, 32, 1156-1162, 2017.
- [134] Ying Zhao and Minoru Taya, study on energy absorbing composite structure made of concentric NiTi spring and porous NiTi, *International Journal of Solids and Structures*, 43, 2497-2512, 2006.
- [135] C.P. Kealey and S.A. Whelan, in vitro hemocompatibility of thin film Nitinol in stenotic flow conditions, *Journal of Biomaterials*, Elsevier, 31, 8864-8871, 2010.
- [136] Francisco M. Braz Fernandes and Rui Martins, structural characterization of NiTi film shape memory alloys, sensors and actuators, *Elsevier*, 99, 55-58, 2002.
- [137] Christoph Bechtold and Rodrigo Lima de Miranda, method for fabricating miniaturized NiTi self-expandable thin film devices with increased radiopacity, *Shap. Mem. Superelasticity(ASM International)*, 2, 391-398, 2016.
- [138] David Rigberg and Allan Tulloch, thin-film nitinol (NiTi): a feasibility study for a novel aortic stent graft material, *Journal of Vascular Surgery*, 50, 375-380, 2009.

- [139] Chavan Madhura, Narendra Naukudkar and S. B. Kumbhar, design and development of robot gripper: shape memory alloy approach, industrial engg. journal, 3, 19-25, 2017.
- [140] Jan Schrooten, Ve´ronique Michaud and John Parthenios, progress on composites with embedded SMA wires, special issue on smart materials-fundamentals and applications, Materials Transactions, 43, 961-973, 2002.
- [141] Z.W. Zhong and S.Y. Chan, Investigation of a gripping device actuated by shape memory alloy wire, sensors and actuators (A 136), Elsevier, 335-340, 2007.
- [142] Shane J. Yates and Alexander L. Kalamkarov, experimental study of helical SMA actuators: effects of design and operating parameters on thermal transients and stroke, MDPI-materials, 3, 123-149, 2013.

## **BRIEF PROFILE OF THE RESEARCH SCHOLAR**

Suresh kumar completed his B.Tech (Mechanical Engineering) in First Division from Kurukshetra University in 2004 and M.Tech (Manufacturing Technology & Automation) in First Division with Honours from YMCAIE, Faridabad-Maharishi Dayanand University, Rohtak in 2008. He is a Ph.D. student under the guidance of Dr. M. L. Aggarwal and Dr. Lakhwinder Singh in the Department of Mechanical Engineering, YMCA University of Science and Technology, Faridabad. Presently he is working as an Assistant Professor in the Department of Mechanical Engineering, Institute of Engineering (IET), Alwar (Rajasthan) from 2018. He is having more than 10 years of teaching and 2 years of industrial experience. His research areas of interest are design, manufacturing, automation. He has published more than 10 papers in the International, National Journal and presented papers in prestigious conferences in India.



## LIST OF PUBLICATIONS OUT OF THESIS

### (i) List of Published papers

S. No.	Title of paper along with volume, Issue No, year of publication	Publisher	Impact factor	Referred or Non Referred	Remarks
1.	Finite analysis of open coil helical springs, Volume 8, Issue 3, 2015	Invertis journal of science and Technologies Published by Indian journals	---	Referred	
2.	Stress evaluation technique-cum-physical model for intelligent helical SMA spring, Volume 8, Issue 12, December 2019	International Journal of Engineering Research & Technology	-	Referred	
3.	Design & correlation of SMA intelligent helical spring by differing the cons. temp. and diameter for a mechanical actuator, Volume 8, Issue 3, March 2019	Universal Review	---	Referred	UGC
4.	A simple solenoid valve SMA-based, Volume 6, Issue 6, June 2019	Journal of Emerging Tech. and Innovative Researches	---	Referred	UGC
5.	Stability of physically-loaded helical springs used in smart fork lift, Vol. 9, Issue 2, Dec. 2019	Blue Eyes Intelligence Engineering and Sciences Publication	---	Referred	
6.	The effect of slender-wires diameters intelligent helical springs, Vol. 5, Issue 11, Nov. 2020	International Journal of Modern Science and Technology		Referred	
7.	Reduced weight and cost in Smart Fork-Lift using NiTi one way helical spring, ISSN(P): 2249-6890; ISSN(E): 2249-8001 Vol. 10, Issue 1, Feb 2020, 483-498	International Journal of Mechanical and Production Engineering Research and Development	---	Referred	SCOPUS

**(ii) List of conferences Papers**

<b>S. No.</b>	<b>Title of paper along with volume, Issue No, year of publication</b>	<b>Publisher</b>	<b>Impact factor</b>	<b>Referred or Non Referred</b>	<b>Remarks</b>
1.	Review of composite helical spring analysis with ansys product software, 28-29 March, 2014	International conference on data acquisition, transfer, processing and management, Lingaya's University (India)	Not Mentioned	---	
2.	Design of shape memory alloy intelligent helical Spring for a mechanical actuator, 3-4 June, 2018	International conference on materials, applied physics and engineering (ICMAE), Indore (India)	Not Mentioned	---	

## Appendix A

Table 1-1 detail information about the phases seen during the shape memory effect and Figure 1-1 represents a schematic showing the relationship between the crystal structure microstructure of Ni-Ti [7].

Table 1-1

Phase	Structure	Lattice Parameters	Where seen
<b>B19'</b> (Martensite)	Monoclinic	a=0.2898 nm b=0.4108 nm c=0.4646 nm $\beta=97.78^\circ$	NiTi alloys quenched from B2 parent phase (evident via surface relief)
<b>R</b>	Trigonal	a=0.738 nm c=0.532 nm	In Ti-47Ni-3Fe; Ni-rich NiTi; NiTi if cold worked and annealed
<b>B19</b> (Martensite)	Orthorhombic	a=0.2881 nm b=0.4279 nm c=0.4514 nm	50Ti-(50-x)Ni-(x)Cu If $5 \leq x \leq 7.5$
<b>B2 (Austenite)</b>	Cubic	a=0.3015 nm	

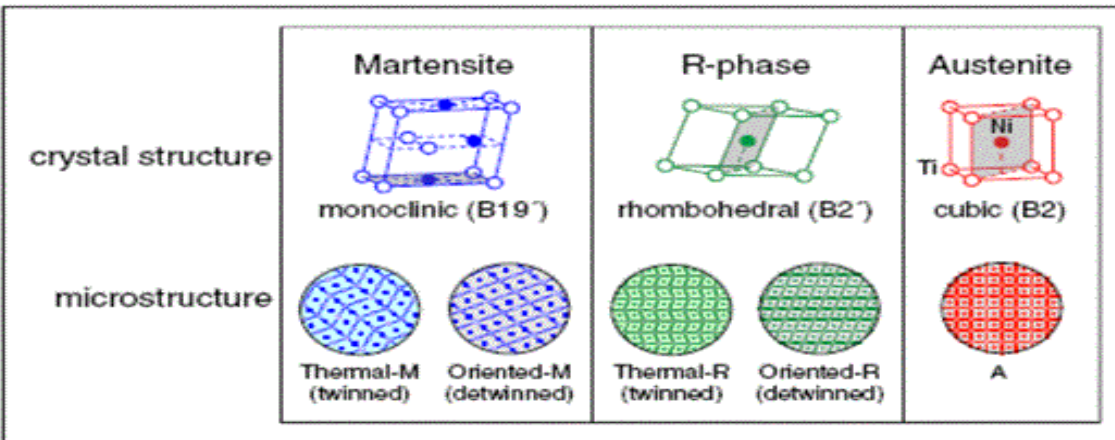


Figure 1-1

## Appendix B

Table 2-2 represents the commercial Ni-Ti physical properties under which the exact values of properties are mentioned [79].

Table 2-2

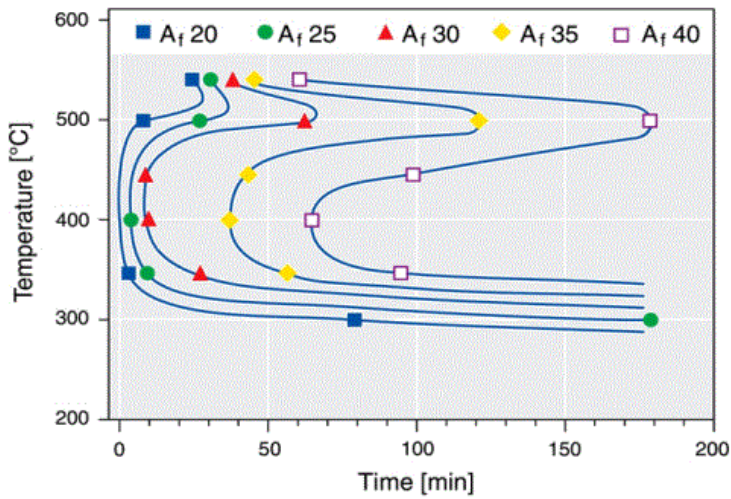
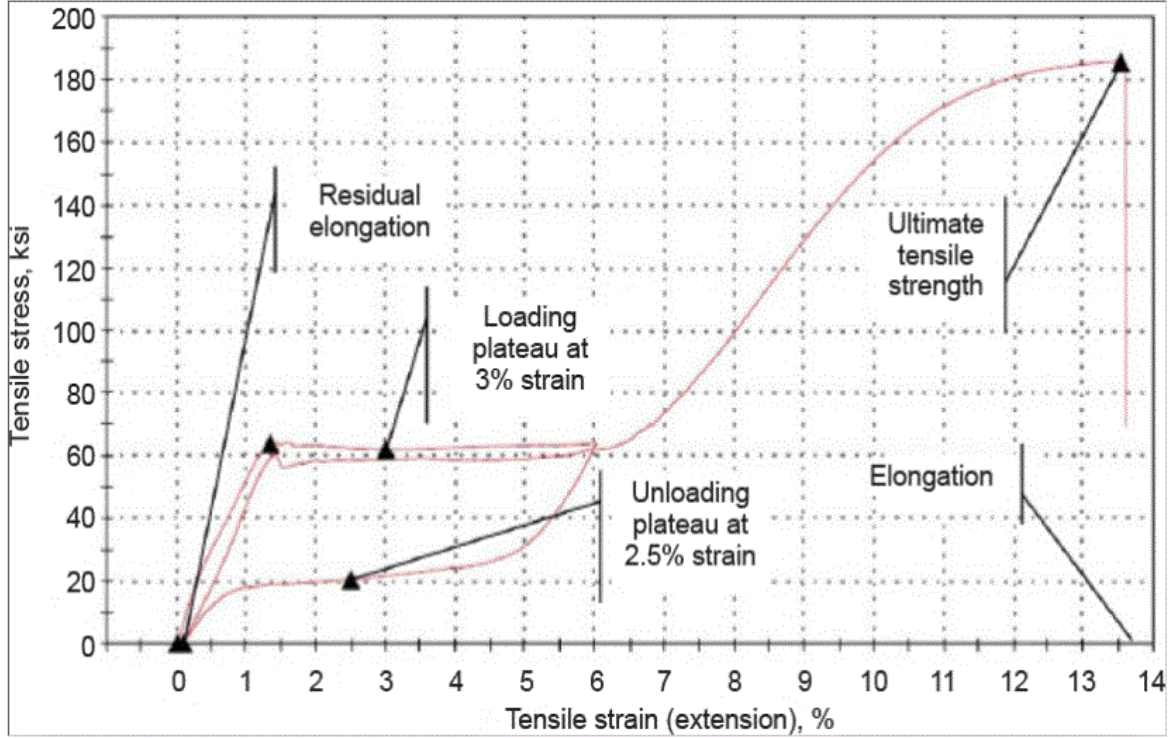
Property	Symbol	Units	Value	
			Martensite	Austenite
Corrosion Resistance	-	-	Similar to 300 series SS or Ti-alloy	
Density	$\rho_0$	kg/m <sup>3</sup>	6450-6500	
Electrical Resistivity (approx.)	$\rho_R$	$\mu\Omega$ cm	76-80	82-100
Specific Heat Capacity	c	J/kg K	836.8	836.8
Thermal Conductivity	k	W/m K	8.6-10	18
Thermal Expansion Coefficient	$\alpha$	m/m K <sup>-1</sup>	$6.6 \times 10^{-6}$	$11.0 \times 10^{-6}$
Ultimate Tensile Strength	$\sigma_{UTS}$	MPa	895 (Fully annealed)/1900 (Hardened)	
Young's Modulus (approx.)	E	GPa	28-41	75-83
Yield Strength	$\sigma_Y$	MPa	70-140	195-690
Poisson's Ratio	$\nu$	-	0.33	
Magnetic Susceptibility	$\chi$	$\mu\text{emu g}$	2.5	3.8

Density	6.45 gm/cm <sup>3</sup>	0.23 lb/in <sup>3</sup>
Thermal Conductivity	10 W/m <sup>o</sup> K	5.78 Btu/hr ft <sup>o</sup> F
Specific Heat	322 j/kg <sup>o</sup> K	0.08 Btu/lb <sup>o</sup> F
Latent Heat	24,200 J/kg	10.4 Btu/lb
Ultimate Tensile Strength	750-960 Mpa	110-140 ksi
Elongation to Failure	15.5%	15.5 %
Yield Strength (Austenite)	560 Mpa	80 ksi
Young's Modulus (Austenite)	75 Gpa	11 Mpsi
Yield Strength (Martensite)	100 Mpa	15 ksi



# Appendix C

Tensile stress-strain relationship of Ni-Ti shape memory alloy with conventional TTT diagram (technology.matthey.com)



Conventional time-temperature-transformation (TTT) diagram for NiTi wire with initial A<sub>f</sub> = 11 °C

Figure 2-2

## Appendix D

Table 3-3 represents the Standard VIM / VAR Table for Ni-Ti shape memory alloys (Robertson et al. study).

Table 3-3

Element, w/o	Current Study		Robertson et al. Study				
	Standard VIM-VAR		Standard VAR	Standard VIM-VAR	Standard VIM	Process Optimized VIM-VAR	High-Purity VAR
	Ingot 1	Ingot 2	Tube	Tube	Tube	Tube	Tube
Nickel	55.90	55.93	55.83	55.89	55.8	55.98	56.1
Titanium	Balance	Balance	Balance	Balance	Balance	Balance	Balance
C	0.0272	0.0283	0.0020	0.0268	0.0330	0.0269	0.0020
Cr	0.0004	0.0002	0.0050	<0.0100	0.004	0.0100	0.0050
Co	0.0009	0.0009	0.0050	<0.0100	0.003	0.0100	0.03
Cu	0.0004	0.0004	0.0050	<0.0100	0.0010	0.0100	0.0050
H	<0.0050	<0.0050	0.0015	0.0008	0.0011	0.0007	0.0008
Fe	0.0068	0.0066	0.0050	0.0062	0.011	0.011	0.0063
Nb	0.0001	0.0001	0.0050	<0.0100	0.0010	0.0100	0.0050
N	0.0005	0.0012	NR	NR	NR	NR	NR
O	0.0152	0.0238	NR	NR	NR	NR	NR
N+O	0.0157	0.0250	0.0274	0.0197	0.041	0.026	0.0063
Transformation Temperature <sup>a</sup> , A <sub>s</sub> , °C	-4	-3	-19	-10	-1	-9	-9
Maximum non-metallic inclusion length, μm	9	15	38	17	7	19	15
Area fraction, %	0.74	0.75	1.25	1.1	0.7	1.18	0.46

<sup>a</sup>Measured by differential scanning calorimetry (DSC) in accordance with ASTM F2004.<sup>12</sup>